HYDRO-STRUCTURAL DESIGN ASPECTS OF ARTICULATED TOWERS

by

SHUKAI WU, BSc

Submitted as a Thesis for The Degree of Doctor of Philosophy, Department of Naval Architecture and Ocean Engineering, University of Glasgow.

Great Britain
May, 1987

ProQuest LLC.
789 East Eisenhower Parkway
P.O. Box 1346
Ann Arbor, MI 48106 – 1346

DECLARATION

Except where reference is made to the work of others, this thesis is believed to be original.

DEDICATION

To my parents

ACKNOWLEDGEMENT

I am deeply indebted to Professor D Faulkner, Head of Department, for allowing me to carry out this research and for his constructive guidance.

My true gratitude also goes to Dr R C McGregor, my supervisor, for his supervision, very useful discussions and suggestions and for his encouragement.

In addition, I am sincerely grateful to Mr N S Miller, a former Senior Lecturer in the Department, Drs A Incecik and N Bose, Lecturers in the Department, for their generous help in many ways and stimulating discussions. Also to Dr A M Ferguson, Superintendent of the Hydrodynamics Laboratory, for his help, especially in making the tank testing facilities available.

I wish to express my thanks and appreciation to Mr E Peters for his great patience and care in typing my thesis. Also to all the teaching, research staff and technicians in the Hydrodynamics Laboratory for their help and contributions towards making my research work possible.

Finally, I am indebted forever to my parents and friends at home in China for their continuous encouragement and support.

CHAPTER HEADINGS

CONTENTS

SUMMARY

In this Thesis an investigation is presented into the performance of stand-alone articulated tower structures under different environmental loadings. An engineering approach is taken in analysing those design aspects, mainly associated with the dynamic response and structural strength of such structures. This enables the present analysis procedure to be applied to real design practice.

Firstly, various aspects of the environmental conditions and the environmental loadings are reviewed. The major sources of the environmental loading include harmonic waves, low frequency wave drift, fluctuating winds and current.

Secondly, the effect of the variation of those parameters defining the environmental loadings on the structural motion and internal sectional forces etc, of a monolithic single articulated tower is investigated. Conclusions are drawn regarding the selection of the values of those parameters.

Thirdly, the effect of those parameters defining the geometrical dimensions of an articulated tower structure on its motion response, internal sectional forces and stability etc, is examined in detail. This is aimed at optimising the geometry of the articulated tower. Articulated tower structures of hybrid form, using lattices, are also studied in comparison with their equivalent monolithic form.

Fourthly, studies were carried out on the viability of some of major assumptions made in the present work. They are associated

with the non-linear interaction between an articulated tower and the environment and the rigid body mode vibration motion of the structure.

Structural strength calculations for stiffened large diameter thin shell cylinders are presented, based on the DnV Rules, which are computerised. A structural weight optimisation is performed using a non-linear programming technique. This provides a useful means of assessing the structural strength for the design of articulated tower structures.

Finally, model tests have been carried out and comparisons between the theoretical predictions and the model test measurements are presented.

NOMENCLATURE

A	Column cross sectional area.
$\bar{A}$	The solid cross sectional area of a column.
A_{ef}	Effective solid sectional area associated with ℓ_{ef} of stiffened cylinders.
A_i	Cross sectional area of the ith column ($i = 1,2,...N$), $A_i = \pi D_i^2/4$ and D_i^2 for a column of circular and square cross sections, respectively.
$A_{r,s}$	Cross sectional area of ring frame or stringer.
a_x	Horizontal acceleration at the middle deck level of an articulated tower.
b	Flange width.
C	Speed of wave propagation.
C_a	Added virtual mass coefficient.
C_d	Drag coefficient.
C_{da}	Wind drag coefficient.
C_{da1}	C_{da} for the deck.
C_{da2}	C_{da} for the above water part of the upper column.
C_ℓ	Linearised damping.
$C_{\ell d}$	Linearised viscous damping.
C_m	Added mass coefficient, $C_a = C_m + 1$.
C_n	Non-linear damping.
C_s	Structural damping.
$C_s(\omega)$	Wave drift coefficient.
D	Characteristic column cross sectional dimension, taken as the radius for circular cylinders and width for a column of a rectangular section.
D_i	Diameter or characteristic cross sectional dimension of the ith column.
d	Water depth.
E	Young's modulus.
$\vec{e}$	Unit vector along an arbitrarily oriented cylinder with coordinates (e_x, e_y, e_z).

F Horizontal force in general.

$F(\vec{X})$ Penalty function.

$F_{\ell}^{(i)}(t)$ Linearised surge wave force on the ith column of an articulated tower with inertia and drag components $F_{\ell d}^{(i)}(t)$ and $F_{\ell i}^{(i)}(t)$, respectively.

F_s Amplitude of the internal sectional shear force along an articulated tower in waves, $F_s(z,t)$.

F_{1v} Heaving force on a vertically submerged cylinder in waves, amplitude of the heaving force $F_{1v}(z,t)$.

F_{js} Surge force due to mean wave drift (j = 2), mean wind drag (j = 3) and steady current (j = 4).

f Frequency in Hz.

$f(\vec{X})$ Objective function

f_{ℓ} Oscillating frequency of vortex shedding due to steady current.

f_y Yielding stress.

f_j Surge force per unit length on a vertically oriented column due to harmonic waves (j = 1), slowly varying wave drift (j = 2) and fluctuating wind (j = 3), with the force acting normally to the column axis.

$G(\omega)$ Gain function or response amplitude operator.

g Gravitational acceleration, $g = 9.8064 m/s^2$.

g_a Expected minimum air gap between the deck and the wave crest, g_a = 3m is taken here.

$g_i(\vec{X})$ Inequality constraints.

H Wave height.

H_b Breaking wave height.

H_s Significant wave height.

H_w Orbital width of the wave particle motion.

h Length of web cross section.

h_c Deck clearance from the MWL.

h_{cb} Distance between the CB and the articulated joint in the intact condition.

h'_{cb} Distance between the CB and he articulated joint in the free floating condition.

h_{cg} Distance between the CG and the articulated joint in the intact condition.

h_{dg} Height of the centre of deck payload above the MWL.

$h_i(\vec{X})$ Equality constraints.

I Second moment of inertia of the column cross section.

$\bar{I}_{\ell a}, I_{\ell a}$ The first and second moments of inertia of the added hydrodynamic mass.

$\bar{I}^{(i)}_{\ell a}, I^{(i)}_{\ell a}$ First and second moments of inertia of the added hydrodynamic mass of a column segment cut out of the ith column of an articulated tower.

$\bar{I}_s, I_s$ First and second moments of inertia of the structural mass.

$\bar{I}^{(i)}_s, I^{(i)}_s$ First and second moments of inertia of the structural mass of a column segment cut out of the ith column of an articulated tower about the y' axis.

$I_m(z)$ Distributed second mass moment of inertia.

I_p, I_q Second moment of inertia of a stiffener cross sectional area about its two principal axes, respectively.

I_x, I_y Second moment of inertia of a column cross sectional area about its two principal axes, respectively.

i Integer as a sub- and superscript, except where otherwise stated, indicating the ith column of an articulated tower, $i = 1,2\ldots,N_e$.

j_d Integer number defined such that $z_{j_d} < d < z_{j_d+1}$.

j_1, j_2 Total number of lumped mass located between z_{1i} and z_{2i}.

$[K]$ Global stiffness matrix.

K_ℓ Time independent restoring stiffness component due to gravitational force and hydrostatic buoyancy.

$K^{(i)}_\ell$ Restoring stiffness due to the static axial force component along the length of the ith column.

$K_{\ell min}$ Minimum of K_ℓ.

$K_{\ell o}$ Specified K_ℓ according to $K_{\ell o} = M_{3s}/\theta_{mwo}$.

K_t Time dependent restoring stiffness component due to the heaving force along an articulated tower structure.

$[K^e]$ Element bending stiffness matrix.

$[K^e_\sigma]$ Element geometrical stiffness matrix.

k Wave number.

L Characteristic length, distance between bulkheads of thin shell cylinders (in Chapter 3), length scale in a gusty wind velocity spectrum.

$L_c(\omega)$ Length of the equivalent lever arm in calculating the pitch moment of the wave drift force on a submerged column in waves, with $L_{ci}(\omega)$ being that of the ith column of an articulated tower.

L_i Length of the ith column of an articulated tower.

L_o Length of a lattice structure.

L_s Submergence depth of the buoyancy chamber.

ℓ Ring frame spacing, length of a single bay of a lattice (in Chapter 9).

ℓ_{ef} Effective ring frame spacing of stiffened cylinders.

$\ell_j/r_j/t_{r_j}$ Length/radius/shell thickness of the main frames (j = 6), horizontal lateral bracings (j = 7), lateral diagonal bracings (j = 8), horizontal diagonal bracings (j = 9), spatial diagonal bracings (j = 10) and the riser (j = 11), ith respect to a single bay.

M Bending moment with two components M_x, M_y (in Chapter 3).

$[M^e]$ Element mass matrix.

$[M]$ Global mass matrix.

$M_\ell(t)$ Pitch moment of linearised surge wave force on an articulated tower, with drag component of $M_{\ell_d}(t)$ and inertia component $M_{\ell_i}(t)$.

$M_\ell^{(i)}(t)$ Pitch moment of the surge wave force on the ith column of an articulated tower, with drag component $M_{\ell_d}^{(i)}(t)$ and inertia component $M_{\ell_i}^{(i)}(t)$.

M_b Amplitude of the internal sectional bending moment along an articulated tower in waves.

M_q Lumped mass located at $z = z_q$ on an articulated tower.

M_{js} Pitch moment of the mean wave drift force (j = 2), drag force due to mean wind velocity (j = 3) or drag force due to steady current (j = 4).

N Axial tension.

N_e Number of column elements (including lattices) composing an articulated tower.

n Number of stiffeners between bulkheads or along the circumference of a cylinder (in Chapter 3), total number of nodes (in Chapter 4).

n_b Number of bays dividing the length of a lattice structure.

n_d Number of deck storeys.

n_f Number of main frames (legs) of a lattice structure.

n_t Number of members (bracings plus main frames) within a single bay of a lattice structure.

P Lateral pressure.

$p(z,t)$ Dynamic pressure in waves.

R Characteristic radius, $R = D/2$, mean radius (in Chapter 3).

R_i Characteristic radius of the ith column, $R_i = D_i/2$.

$\vec{r}, \dot{\vec{r}}, \ddot{\vec{r}}$ Radial displacement, velocity and acceleration vectors.

r_5 Radius of the circle along the circumference of which the main frames of the lattice are located.

S Strouhal number (in Chapters 2 and 9).

$S_w(\omega)$ Energy spectrum of the fluctuating wind velocity component.

$S_\eta(\omega)$ Energy spectrum of the wave height.

$S_j(\omega)$ Angular displacement spectrum of an articulated tower due to random waves ($j = 1$), slowly varying wave drift ($j = 2$), or gusty wind.

$S_{jm}(\omega)$ Pitch moment spectrum of the surge force on an articulated tower due to random waves ($j = 1$), slowly varying wave drift ($j=2$), or gusty wind ($j=3$)

s Stringer spacing.

T Wave period, torsional moment (in Chapter 3).

$[T^e]$ Transformation matrix between local and global coordinate systems.

$T(z,t)$ Axial force along an articulated tower, $T(z,t) = T_s(z) + T_d(z,t)$, with $T_s(z)$ being the time dependent component and $T_d(z,t)$ being the time varying axial force due to dynamic pressure.

$T_{d1}(z,t)$ Time varying axial force component due to the free surface elevation of waves.

$T_{d2}(z,t)$ Time varying axial force component due to the dynamic pressure.

$T_s(z_1)$ Static component of the axial force on the articulated joint.

T_z Average zero-up-crossing wave period.

t Time, shell thickness.

$\bar{t}$ Equivalent shell thickness of stiffened cylinders taking into account the structural weight of the stiffeners.

t_i Shell thickness of the ith column of an articulated tower.

$\bar{t}_i$ Equivalent shell thickness of the ith column of an articulated tower.

t_f Flange thickness.

t_m Minimum shell thickness, excluding corrosion.

t_w Web thickness.

$\vec{U}_n$ Normal wave particle velocity to an arbitrarily oriented column with components (U_{nx}, U_{ny}, U_{nz}).

U_x, U_z Wave particle velocity components in horizontal and vertical directions, respectively.

$\dot{U}_x, \dot{U}_z$ Wave particle acceleration components in the horizontal and vertical directions, respectively.

V Shear force with components V_x, V_y (in Chapter 3).

V_c Current velocity with two components: V_{ct}, the tidal driven component and V_{cw}, the wind driven component.

V_i Buoyancy of the ith column of an articulated tower structure.

$\bar{V}_s$ Volume of the ballast chamber obtained under the condition that $L_1 = 0.0$, $\alpha_2 = 1.0$, $\rho_2 = 2.5 t/m^3$ and $T_s(z_1) = 0.0$.

$V_w, \bar{V}_w, V_w'$ Instantaneous wind velocity, mean wind velocity component and gusty wind velocity component, respectively, $V_w = \bar{V}_w + V_w'$.

$\bar{V}_{w1hr}$ One hour mean wind velocity.

$\bar{V}_{w1hr10}$ $\bar{V}_{w1hr}$ measured at 10m above the water surface.

$\bar{V}_{ws}$ Sustained wind velocity.

$\bar{V}_{ws10}$ $\bar{V}_{ws}$ measured at 10m above the water surface.

V_Σ Total buoyancy.

W_o Deck payload.

W_{si} Structural material weight of the ith column of an articulated tower.

$W_{\Sigma s}$ Total structural material weight, $W_{\Sigma s} = \Sigma\ W_{si}$.

W_{bi} Ballasting material weight inside the ith column.

W_{Σ} Total weight of an articulated tower.

$\vec{X}$ Free variable vector.

(x,y,z) Cartisan coordinates system.

y' Axis through point $P_o(x_o,y_o,z_o)$ in (x,y,z) coordinates system and parallel to the y axis.

z_i Vertical coordinate, $i = 1,2...,N_e,N_e + 1$, with z_i and z_{i+1} defining the position of the ith column element.

z_{1i},z_{2i} Vertical coordinates of the bottom and top ends of a vertically oriented column segment cut out of the ith column of an articulated tower, $i = 1,2...,N_e$.

Gusty factor accounting for the averaging time period of the mean wind velocity.

α_i Diameter/length ratio of the ith column, $\alpha_i = D_i/L_i$.

α_r Ratio of r_5/r_6.

α_{vw} Ratio between the deck space and deck payload in m^3/t.

β Exponent of the mean wind velocity profile above the water surface.

β_m Ratio between the total structural mass and that of all the bracings with respect of a single bay.

β_o Ratio of $\theta_{mwo}/\theta_{\Sigma}$ with θ_{Σ} given in equation (8.1).

β_1 Taper angle of a frustrum buoyancy chamber.

δ $\delta = h_{cb} - h_{cg}$, the distance between the CB and the CG.

ζ Damping ratio.

η Free wave surface elevation.

κ Sea surface roughness ratio.

$\theta(t)$ Angular displacement of an articulated tower structure in regular waves.

$\bar{\theta}$ Amplitude of $\theta(t)$.

θ_{mwo} Specified θ_3, the static tilt angle under the mean wind loading.

θ_{Σ} Total of the extreme angular displacement expected during the life time of an articulated tower structure.

$\theta_{\Sigma d}$ Component of θ_{Σ} due to harmonic waves, slowly varying wave drift and gusty wind, together.

$\theta_{\Sigma s}$ Component of θ_{Σ} due to mean wave drift, mean wind and steady current.

θ_j Angular displacement of an articulated tower structure due tomean wave drift loading ($j = 2$), mean wind loading ($j = 3$), or steady current loading ($j = 4$).

λ Wave length.

ν Poisson's ratio

π $\pi = 3.1415926$

ρ_a Density of the atmosphere, $\rho_a = 1.025 kg/m^3$.

ρ_w Sea water density, $\rho_w = 1027 kg/m^3$.

ρ_i Density of the ballasting material enclosed inside the ith column of an articulated tower structure.

ρ_{si} Material density of the ith column shell.

σ_j rms angular displacement of an articulated tower structure due to random wave loading ($j = 1$), slowly varying wave drift loading ($j = 2$), or gusty wind loading ($j = 3$).

σ_s rms internal sectional shear force along an articulated tower structure due to random wave loading.

σ_b rms internal sectional bending moment along an articulated tower structure due to random wave loading.

σ_{zn} Direct stress due to axial force.

σ_{zm} Direct stress due to bending.

σ_{θ} Circumferential stress due to lateral pressure.

σ_{1x} rms horizontal acceleration at the middle deck level of an articulated tower in random waves.

τ_{zv} Shear stress due to shear force.

τ_{zt} Shear stress due to torsion.

Φ Incident wave velocity potential

ω Circular frequency.

ω_i Natural frequency of the ith flexural mode vibration motion, $i = 1,2,...$

ω_n Natural frequency of RBMV motion.

Ba.C	Ballast chamber.
B.C.	Buoyancy chamber.
BS5500	British Standards: 5500.
CB	Centre of buoyancy.
CG	Centre of gravity.
E.C.	Extension column.
FMV	Flexural motion vibration.
HAT	Hybrid single articulated tower.
L.C./L.L	Lower column/lower lattice.
MAT	Monolithic single articulated tower.
MWL	Mean water level.
OSC	Orthogonally stiffened cylinder.
RAO	Response amplitude operator.
RBMV	Rigid body mode vibration.
RSC	Ring stiffened cylinder.
rms	Root mean square.
SSC	Stringer stiffened cylinder.
U.C/U.L	Upper column/upper lattice.

CHAPTER 1

FEATURES AND POTENTIAL APPLICATIONS OF VARIOUS TYPES OF ARTICULATED TOWER SYSTEMS

1. INTRODUCTION

1.1 Features of Articulated Tower Systems

The present work deals with practical design aspects of stand-alone single articulated tower structures, one of the group of structures classified as compliant structures. An articulated tower structure can be categorised in different ways as outlined in fig. 1.4.

Geometrically, the structure can be of the form of a single cylindrical column or composite cylindrical columns with different diameters, or of lattice type, or even a hybrid structure. The geometry varies with water depth, environmental conditions, deck payloads and the function of the structure. In addition, the above factors also heavily influence the criteria, in terms of structural responses, economics, safety, construction, inspection and maintenance of the structure, against which it is designed.

A sketch of a typical monolithic single articulated tower (MAT) structure which is composed of several columns of different diameters is shown in fig. 1.1. Furthermore, a hybrid articulated tower (HAT) can be of three different forms as is shown in fig. 1.2.

The basic principle of the structure, by its definition, is that its compliancy allows it to move dynamically with the ocean waves unlike the conventional fixed platforms which resist the wave excitation statically. As the result of the compliant motion the wave force transfer into the structure is reduced.

1.2. Potential Applications

Various potential applications of different types of articulated towers could be envisaged. For example, the stand-alone structure can be used as a flare tower, service tower associated to sub-sea wells (for well control, maintenance and replacement of the sub-sea production systems, etc), loading and offloading station, storage buoy and a production platform. It can also be used in connection with floating production, storage and offloading (FPSO) systems with semi-submersibles and/or surface vessels as a riser column and single leg mooring such as a single anchor leg mooring (SALM) system, single anchor leg storage (SALS) system and yoke tower [1,2]

1.3. Market Demands

The realisation of the above potential applications of articulated tower structures obviously depends on the future of the offshore industry and the future of offshore oilfield development. A brief look at the outlook in this area is necessary.

The future of offshore industry is directly related to the amount of recoverable reserves of hydrocarbons offshore. Its forecasting is fraught with uncertainty yet there are some optimistic

references [3] which indicate that the bulk of future potential hydrocarbons will be made offshore. A considerable amount will be within the continental shelf regions in water depths not exceeding 200m, while the rest of the reserves will be in deep water and in the polar region. Some other references [4] to [8], forecast the trends of future oilfield discovery, discussed the problems related to the future oilfield development and the possible solution to the problems.

The model based forecast [4] indicates that the size of oilfield decreases as the oil province becomes more mature and that the largest fields are discovered early in the life of the basin. This applies to oil and gas field sizes in a mature basin. The fundamental issue of the small field development is the economic viability. This is primarily influenced by the reserves, capital cost, development programme and the consequent rate of return.

This particular problem for small oil field development, together with those related to deep water oilfield development will render the conventional fixed platforms out-of-date and will urge viable new concepts to be sought as, on the one hand, the conventional fixed platforms are not competitive in small oilfields compared with some other concepts such as articulated loading/production systems. On the other hand, in deep waters the dynamic amplification of the first order wave force becomes increasingly unacceptable due to the sharply decreased structural stiffness, the increase of which gives rise to heavy penalties such as the tendency to excessive structural dimensions (and structural weight) with related economic and technical installation problems.

There are several alternative structural concepts currently

under serious and extensive investigation. Among them are those based on the use of articulated structures, either stand-alone or connected with other systems. For the time being, attention will be concentrated on the use of stand-alone articulated towers or articulated towers connected with a FPSO system such as riser columns and single leg mooring to the FPSO systems.

2. A STATE-OF-ART REVIEW OF ARTICULATED TOWER DESIGN

2.1. Existing Applications

Limited use of articulated tower structures has been made for the last decade or so. The first prototype articulated tower, ELFOCEAN, was installed in 100m of water in the Bay of Biscay in 1968 [1]. It was operational for three years during which time extensive tests confirmed the suitability of the concept for a range of applications.

The North Sea launched a new generation of single point mooring (SPM) in the mid-1970s. Since then articulated towers have been used as loading terminals and flare towers in the North Sea. Table 1.1 gives a list of articulated structures installed in the North Sea. Most of them are made of steel. Maureen field articulated loading platform (ALP) is the only concrete structure. The water depths are around 100m to 160m. The ALP currently in service in the Statfjord C is 196m long overall and is probably the largest articulated structure commissioned to date. Figure 1.3 shows some of the existing articulated tower structures used as loading platforms.

Elsewhere worldwide, the structure has not been so popular. However, FPSO systems based on the use of articulated columns such as

SALM or SALS have been matching up with the North Sea, as shown also in Table 1.1, particularly the Hondo field floating production system is anchored by a double articulated column. Together with other types of single point mooring (SPM) systems it is estimated [31] that there are about 400 in service, worldwide.

Over the past fifteen years or so considerable success has been achieved during the design, construction, installation and operation period among the above structures. Some experience and benefits over the use of articulated tower structures have been gained. However, not all the existing applications have enjoyed unmitigated success and the North Sea environment has been particularly tough on offshore loading systems from the beginning. They were considered to be a quick way to bring a field on stream and gain the benefits of early cash flow but this aim has not always been achieved.

The conventional single point mooring proved adequate in the early days of North Sea development in the southern sector but once production moved north and deeper and new designs were required, they suffered all kinds of teething problems [9].

Two of the earliest 'new' designs - those of Auk and Beryl - were delayed in start-up for some months. Before production was scheduled to begin, the Auk system began sinking on station. This had to be arrested by pumping polystyrene pellets into the buoyancy chamber which was filling up through a malfunctioning valve. Even after this, in severe storms in December 1975, it dragged its anchors. In the same storms a more dramatic event occurred when release of the locking pin securing the Beryl tower at its base was apparently

accidentally triggered and the tower floated free in the North Sea for a few days and was reinstalled later in June 1976.

The Thistle field ALP was also installed late but its troubles were only just beginning. In January 1979, after the tower was found to be riding unnaturally high in the water, inspection showed that it had become detached from the lower section at the upper universal joint. Further problems occurred during the January storms in 1983. The tower broke free from its moorings and drifted towards Norway. By this time the system was operating only as a stand-by and since the operator, BRITOIL, had definitely committed itself to the pipeline export route and the tower was finally abandoned in February 1984. In addition, the Statfjord A (an ALP) was towed to Norway for repair and overhaul, due to a crack in the support column, in 1984 and Beryl ALP was abandoned early in 1986.

Despite a series of early mishaps and accidents which often delayed on-stream dates and ruined quick cash flow schemes, operators have often continued to prefer offshore loading to pipelines.

2.2. Previous Work - A Review of Available Literature

Extensive work, both theoretical research and model tests, has been carried out on the behaviour of articulated tower structures fulfilling different functions. Some in-situ measurement has also been made [11]. Attention has been paid to the understanding of the performance of articulated tower structures in response to environment loads as well as to the economics in future marginal and deep-water oilfield development. Consequently, a certain amount of literature, as well as model test data, is available on stand-alone articulated towers.

Kirk et al investigated the rigid body dynamic response of both single and double articulated tower structures under the excitation of non-linear waves and currents in the time domain [12,13] and in the frequency domain [14]. From the time domain analysis it is concluded that the tower, when subject to the exciting forces, undergoes a complex swirling trajectory motion and that the maximum response of the tower occurs when the waves and currents are in the same direction. It is also concluded that the complex swirl motion of the tower may give rise to special problems in respect of tanker hook-up operations and the wear and maintenance of the articulated joint.

In the frequency domain random analysis, the non-linear damping term is linearised. The results are related to the 100 year storm of H_s = 15m. It is eventually concluded that the influence of the drag force in the high frequency range is negligible in comparison with the inertia force but significant in limiting the slow drift resonant motion and the slowly varying resonant motions of articulated towers can cause a considerable increase in the bending moment due to deck weight, etc.

The effect of vortex shedding on the motion of articulated towers in waves was investigated by Chakrabarti [15] and transverse motion was found coupled with the motion in the wave direction.

An articulated tower with a single flexible column of uniform cross-section was analysed theoretically by Eatock-Taylor and Drake [16]. The tower was excited harmonically by regular waves and the hydrodynamic forces were calculated by means of a complete wave diffraction and radiation analysis. The column is idealised by

Euler-Bernoulli beam theory. Vibrations of the first three modes were studied. The theoretical results for a double articulated column were successfully compared with experimental data from a model test in random waves. Some important conclusions were drawn that the magnitude of the resonant rigid body response was relatively insensitive to the ratio of the structural to displaced mass; that the hydrodynamic damping at the rigid body resonant frequency was in all cases low and is between 1-10% of the critical for the first flexural mode; that the magnitude of the response at the first flexural resonance was roughly proportional to the reciprocal of the resonant frequency (the degree of approximation improving with an increase in frequency) and that between the rigid body and first flexural resonance there was a cancellation frequency for each response (displacement, shear, moment, etc).

Drake and Eatock-Taylor [17] also investigated the drift of single column articulated towers using potential flow theory. The column dimension was assumed to be large compared with the orbital disturbance of waves. Two distinctive approaches in calculating the drift force, namely the near and far field approaches [18,21], were formulated, with identical expressions derived for the mean drift force and moment from both approaches, except for a buoyancy term. It was shown that the drift force on the tower structure, although of second order in magnitude, could excite pitch response of first order as the articulated tower was designed to have a low natural frequency in the tilt mode relative to wave frequencies. The calculation of mean drift forces on articulated tower structures oscillating in a wave tank taking into account the effect of the parallel walls of the tank, was presented by Eatock Taylor and Tung elsewhere [22] together with limited experimental results.

Full scale measured motions of a North Sea articulated loading platform have been presented by Spidsoe [11]. Three periods of separate sampling under the wind and wave excitations were made. The analysis of the recording indicated that the platform was sensitive to aerodynamic loading caused by turbulent wind which seemed linearly interactive with the hydrodynamic loading. The effect of vortex shedding was observed but it was not very important. Non-linear interaction between low frequency motions caused by wind and wave forces was also observed.

For concrete articulated towers, some results from theoretical prediction as well as from Test-Conat model tests were presented in reference [10].

In addition, certain model tests were carried out over the last few years [23,27]. Among these, reference [23] was based on concrete models of different geometry. Others were based on a single model, either concrete or steel. Most of them were carried out in waves only, either regular, random, or both, except in references [25,26], where they were carried out under waves, wind and current. The model is either a stand-alone articulated tower or one connected to a moored tanker. These are summarised below.

Model structures of different geometry were tested in NMI [23] in random waves only by simulating Jonswap and ITTC spectra with different significant wave heights and wave periods. Response to harmonic and subharmonic waves, shear force and heaving force on the articulated joint were measured. They were compared with results from theoretical calculations. Good agreement between theory and the model

test was achieved.

The model test was based on a Type I hybrid articulated tower structure [27], as shown in fig. 1.2 and was carried out in regular and irregular waves. The measurements included horizontal motion at the top of the model, shear force and heaving force on the articulated joint. The theoretical predictions were based on Morison's equation and linear wave theory. Three different sets of drag and added mass coefficients were used: constant coefficients, coefficients selected from experimental data of oscillating flow past stationary cylinders and calculated coefficients, based on the diffraction theory. Comparisons were also presented between the model test and theoretical predictions. The conclusions drawn are:

a. Horizontal motion and shear forces on the joint are insensitive to variation of drag coefficient. There is good correlation between the model test and theoretical predictions. The best results were achieved with calculated added mass coefficients from diffraction theory. At high frequencies, however, a model test tends to give rise to higher results of horizontal motion than theoretical predictions, which is attributed to the diffraction effect.

b. The heaving force correlates poorly in all cases; measured results were lower than theoretically predicted.

The articulated tower model in reference [24] was tested alone, as well as when connected with a moored tanker and semi-submersible in head and beam seas, respectively. The model test was carried out in regular waves and, in the main, irregular waves simulating the Pierson-Moskowitz (P-M) spectrum. The model detail is

presented together with results obtained from model testing and from theoretical predictions which were subsequently compared. The results included angular response to harmonic waves and subharmonic waves (slowly varying wave drift), shear force and heaving force on the articulated joint in harmonic waves. Theoretical predictions were based on Morison's equation using linear wave theory for harmonic waves and Pinkster's formula [28] for subharmonic waves. Satisfactory correlations were achieved for the stand-alone model.

Elsewhere [25], a model test of an articulated tower model was carried out, either when the model was stand-alone or connected with a moored tanker. The conditions simulated in model testing included irregular waves, wind and current. The theoretical prediction in reference [25] is based on the time domain simulation. Problems associated with model testing in relation to full scale calculation was discussed, due to the difference in Reynolds Number, R_e. Vortex shedding was reported to be observed. No model details are available, however. The conclusions drawn do not appear to be substantial.

3. THE BACKGROUND OF THE PRESENT WORK, ITS AIM AND APPROACH

Existing applications of an articulated tower, together with limited theoretical predictions and model testing have, to a large extent, demonstrated their feasibility technically, functionally and economically although the price has been high over the penalty of the naivity and immaturity of some early stage applications. Very little literature is, however, available in relation to the comprehensive understanding of the structural behaviour and in the form of design guidance, in respect of some aspects which are fundamental to any systematic conceptual design appraisal. This is because:-

a. Design data for the existing applications and from their full scale measurements are not available, mostly for commercial reasons presumably.

b. There is not enough work done to address, fully and clearly, some or all of those aspects directed to guide the practical design of articulated tower systems.

c. Some of the models used to describe the idealised structure are highly mathematical for theoretical formulations but far from reality and subsequently the results and conclusions cannot be credited completely for practical design purposes, apart from the tedious analysis.

d. Attention is not adequately paid to some of the aspects of the structure-environment interactions which are of secondary importance and are often neglected in the conventional fixed offshore structure design.

In addition, occasions are often encountered in the preliminary design stage for which techniques are need, not for the final design evaluations but for the estimations of fundamental parameters with which a rough general appraisal of a particular design proposal can be made at the first attempt. In this case, it is clearly desirable to have simple and quickly accessible tools available. It is with the above background that the present work was carried out.

The aims of the present study are as follows:

a. To contribute to the understanding of the behaviour of stand-alone single articulated towers, in particular with those aspects fundamental to the conceptual design.

b. To judge the performance of the tower on technical, functional and economic grounds, with the functional performance in particular, and assess the feasibility of the tower for future offshore marginal and deep water oilfield development.

c. To find a simplified analysis procedure to provide a first-shot approximation of engineering accuracy oriented towards being used in real design practice.

d. To generate practical design data on the basis of which the general design guidances are to be outlined.

The emphasis will be on c. and d. In doing so, attempts will be made to take an engineering approach to the problem and to keep in line with available design codes and standards recommended by the classification societies. Environmental conditions specific to the North Sea will be adopted.

The dynamic analysis was carried out in the frequency domain. In order to perform the dynamic analysis in the frequency domain the following assumptions were made:-

a. The structural system and the structure-environment interactions are linear.

b. The motion of the structure is dynamically stable.

c. The motion of the structure is dominated by the rigid body mode vibration (RBMV) and the contribution from the flexural mode vibrations (FMV) is negligible.

The first assumption has the following implications:

a. the characteristics of the structural system are linear,

b. the linear wave theory is valid,

c. the motion amplitude of the structure is small,

d. the drag effect of the wave force is small compared with the inertia effect so that the non-linear drag force can at least be linearised and,

e. the different sources of external excitations, mainly due to winds, wave and current, act on the structure independently and coincide in direction.

This assumption simplifies the problem of dynamic response greatly because, instead of having to approach the problem in the time domain, frequency domain solutions can be attempted. The time saving is clearly significant. The second assumption has no real impact on the simplification and implies that the possibility of structural dynamic instability can be neglected in the initial design but should be considered for the final analysis. The last assumption also makes some contributions to the simplifications of the problem as it renders the structural system to one degree-of-freedom, which would otherwise make finite element analysis necessary.

Both theoretical calculations and model testing were done. In terms of content, these may be divided into five parts:

a. modelling of the environment and the structure-environment interactions,

b. conceptual design and structural strength estimations,

c. validation of the fundamental assumptions, theoretically and experimentally,

d. parametric studies and geometrical optimisation,

e. important conclusions and recommendations on further studies.

3.1 Modelling of the Environment and the Structure Environment Interactions

This part includes the modelling of the environment, the environmental forces, motion and structural response of the articulated towers, due to the structure-environment interactions.

The environmental forces include wind, waves, current, earthquakes and etc, etc. For the present study only the first three aspects are considered. These are normally the major source of environmental loading acting on structures.

The wind is defined by its velocity, direction and duration. The velocity is composed of two components: the mean velocity component, which is a function of the height above the sea surface and averaging time period and the fluctuating differential velocity component, which is largely independent of the height above the sea surface and is often assumed to form a Gaussian process so that it can be represented in terms of wind velocity spectrum. Two wind velocity spectra, namely, Davenport and Harris spectra were used.

Linear wave theory was used to describe the regular waves which can be defined uniquely by the wave height and wave period. Also, the waves were assumed to be long crested to discount their directionality. Wave energy spectra were used to describe the wave frequency content of irregular waves in a short term sea state over a storm, which is often assumed to be ergodic and stationary. The severity of a sea state is represented by the significant wave height and zero-up-crossing period which are, in general, related to the wind velocity, duration and/or the distance over which the wind blows (fetch). Four commonly used wave spectra were utilised in this study, namely, Bretschneider, ITTC, Jonswap and ISSC wave spectra.

The current was assumed to be steady and is defined in terms of its velocity and direction. The velocity was composed of two components: the tidal driven velocity, which was modelled as constant along the water depth and wind driven velocity, the distribution of which extends only a little below the sea surface. Linear decay was assumed down to 50m below the sea surface [55].

In the process of structure-environment interaction, forces are exerted on the structure due to relative motion. The interactive forces due to wind, waves and current are all modelled individually in the form of Morison's equation on the basis that the structural cross sectional dimensions are small compared with wave lengths of practical significance. In particular, the interactive drag force in Morison's equation is linearised in calculating the linear dynamic response due to harmonic waves. The second order wave drift force, due to subharmonic waves, is calculated using Pinkster's formula [28]. By assuming that the second order wave force decays at a rate of the

square of the rate at which the kinematics of harmonic waves decay, the pitch moment of the second order wave drift force is calculated. They are all expressed in terms of drift coefficient $C_s(\omega)$ and wave spectrum, where ω is the wave frequency. Owing to lack of data on $C_s(\omega)$ for submerged cylinders, $C_s(\omega)$ is approximated by:-

$$C_s(\omega) = \begin{cases} 0.65\ D\omega^2/g & \text{if } 0 < D\omega^2/g \leqslant 1.0 \\ 0.65 & \text{otherwise} \end{cases}$$

The concept of design environmental conditions which are taken to be the worst environmental conditions which are expected to occur during the lifetime of the offshore structure is used to calculate the extreme environmental loading. These conditions are determined so as to have a probability of occurrence of once in 100 years. It is also assumed that the worst wind, wave and current occur at the same time and in the same direction. In addition, less severe short term environmental conditions, say, 12 times a year, are often defined to represent the operational environmental conditions, which are the most severe conditions under which the structure can remain operational. All the above mentioned are detailed in Chapter 2.

Regarding the RBMV motion of an articulated tower as a generalised single degree-of-freedom system, static and dynamic structural responses are carried out. The static response is due to mean wind loading, steady current loading, mean wave drift loading and lateral offset of deck payload. The dynamic response is to due to dynamic wind loading, harmonic wave loading and slowly varying wave drift loading. The dynamic response to harmonic waves is carried in the frequency domain. These calculations are detailed in Chapter 5 for monolithic articulated tower structures and in Chapter 9 for hybrid articulated towers. In addition, the internal sectional forces,

namely, the shear force and bending moment along the structure due to harmonic wave were also calculated.

Model tests were carried out in regular waves for the purpose of validating the linear dynamic response analysis. The pitch moment of the articulated tower as well as the shear force and heaving force on the articulated joint were measured and were subsequently compared with those from theoretical predictions. Very good correlation was achieved as detailed in Chapter 6. Other relevant model test data, published in the literature, was also compared with the present theoretical predictions.

3.2 Conceptual Design and Structural Strength Estimations

This section deals with the structural strength formulation for cylindrical thin shell members based on the DnV Rules, subsequent computerisation of the strength formulation, structural weight optimisation and detailed discussions on the structural design considerations for the structural elements of an articulated tower. Clearly, it was necessary, in the process of dynamic response analysis, to estimate the structural weight based on strength calculations to obtain the mass inertia. The magnitude of the total structural weight can also be assessed. The effective structural arrangement can be recommended for major structural components of an articulated tower. The strength formulation is for large diameter thin shell cylinders, either unstiffened or ring/stringer-stiffened.

A structural weight optimisation program has been developed. The program utilises two different non-linear programming techniques: the simplex technique and flexible tolerance technique. The simplex

technique has been implemented using the NAG routines. The second technique has also been programmed and found to be very effective for the purpose of this study. This is detailed in Chapter 3.

3.3 Validation of the Fundamental Assumptions, Theoretically and Experimentally

In Chapter 7, the time domain simulation of angular dynamic response, which takes into account various sources of non-linear effects, was carried out to investigate the significance of these effects. This was intended to verify the first fundamental assumption made earlier, under regular wave excitation. Non-linearities may arise due to:-

a. free surface elevations,

b. large amplitude pitch motion affecting the phase angle of wave kinematics,

c. non-linear drag force in Morison's equation and,

d. Interaction of heaving force with pitch motion.

In addition, model tests were carried out to investigate the effects of non-linearity. The results, both from theoretical predictions and model testing, indicate that the linearisation of the non-linear drag force in Morison's equation is valid and the non-linear effects are insignificant as far as the steady state motion are concerned. However, allowance has to be made for the large motion magnitude in a transient state.

In Chapter 7, the possibility of dynamic instability is examined, both in theory and in model testing. The possibility is

demonstrated using a highly simplified mathematical model, which is basically due to the time varying restoring stiffness component associated with the interaction between the heaving force and pitch motion. The relationship between the wave frequency at which dynamic instability is likely to occur and the RBMV natural frequency of the structure is deducted. But with the inclusion of other non-linearities, it is concluded that the dynamic instability does not occur. This is also supported by model testing.

To ensure the validity of the third fundamental assumption made above, Chapter 4 studies the natural frequencies of FMV motion of a monolithic single articulated tower based on finite element procedure. The assumption of predominantly rigid body mode vibration motion of an articulated tower structure were justified if the natural frequencies of the first two low modes of the FMV motion could be placed well above the wave frequency range of high energy density, avoiding FMV resonance. In doing so, the maximum water depth beyond which FMV motion becomes significant was obtained.

In addition, the effect of various parameters on the natural frequencies of FMV of a monolithic articulated tower structures is examined. Similar studies on hybrid articulated tower structures are also presented in Chapter 9.

3.4 Parametric Studies and Geometry Optimisation

Under the three basic design specifications, namely, deck payload, water depth and environmental conditions, parametric studies based on monolithic articulated tower structures are carried out in Chapters 5 and 8. The parameters include those related to the

definition of environmental loadings and those related to the definition of the geometrical dimensions of the structures and material property.

Chapter 5 deals with the effect of those parameters defining the environmental conditions by varying these parameters over a wide range of practical interest, aimed at providing guidance on their selection. The effects of geometrical parameters are studied in Chapter 8. One can determine for the purpose of practical design, the optimum geometry of a monolithic articulated tower, using the computer programs and the results of this parametric study. Conclusions with regard to various design considerations are also drawn.

In addition, the shortcomings of monolithic single articulated tower structures are identified based on parametric studies. Structural modifications to a monolithic single articulated tower structure to overcome some of its shortcomings result in the hybrid articulated tower structure concepts such as double articulated towers, guyed towers and TLPs. Comparative studies between monolithic and hybrid articulated tower structures are carried out and various conclusions are also drawn.

Conclusions are given at the end of each chapter. However, in Chapter 10, some important conclusions are summarised with regard to various design aspects of the stand-alone single articulated tower. Finally, recommendations on future studies are briefly mentioned to end the present study. These include a detailed case study, functional and economic performances of the full scale measurement of articulated tower structures and comparative studies between single articulated tower structures and other compliant concepts.

LIST OF FIGURES

LIST OF TABLES

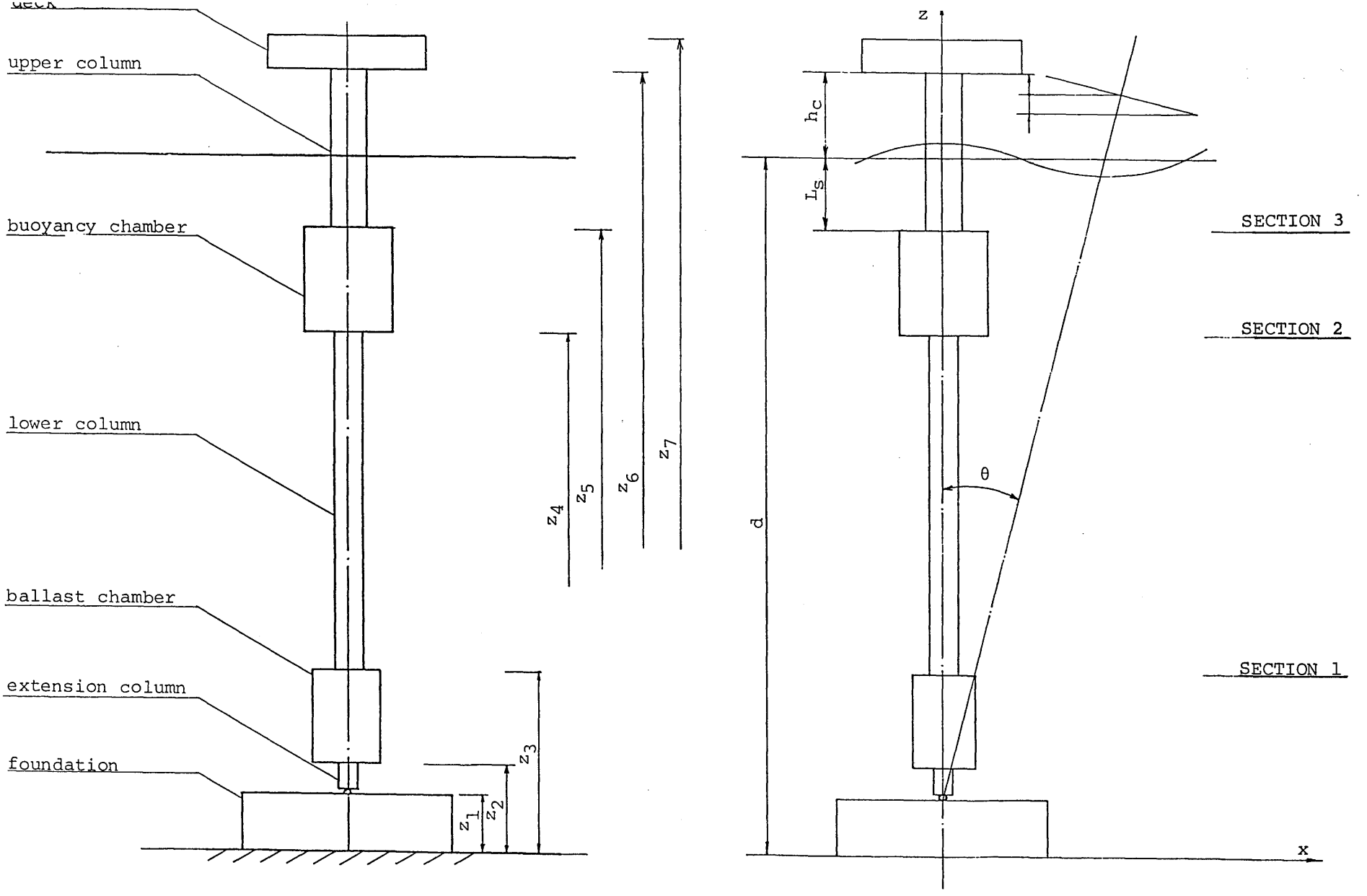

Fig. 1.1 sketch of a monolithic single articulated tower

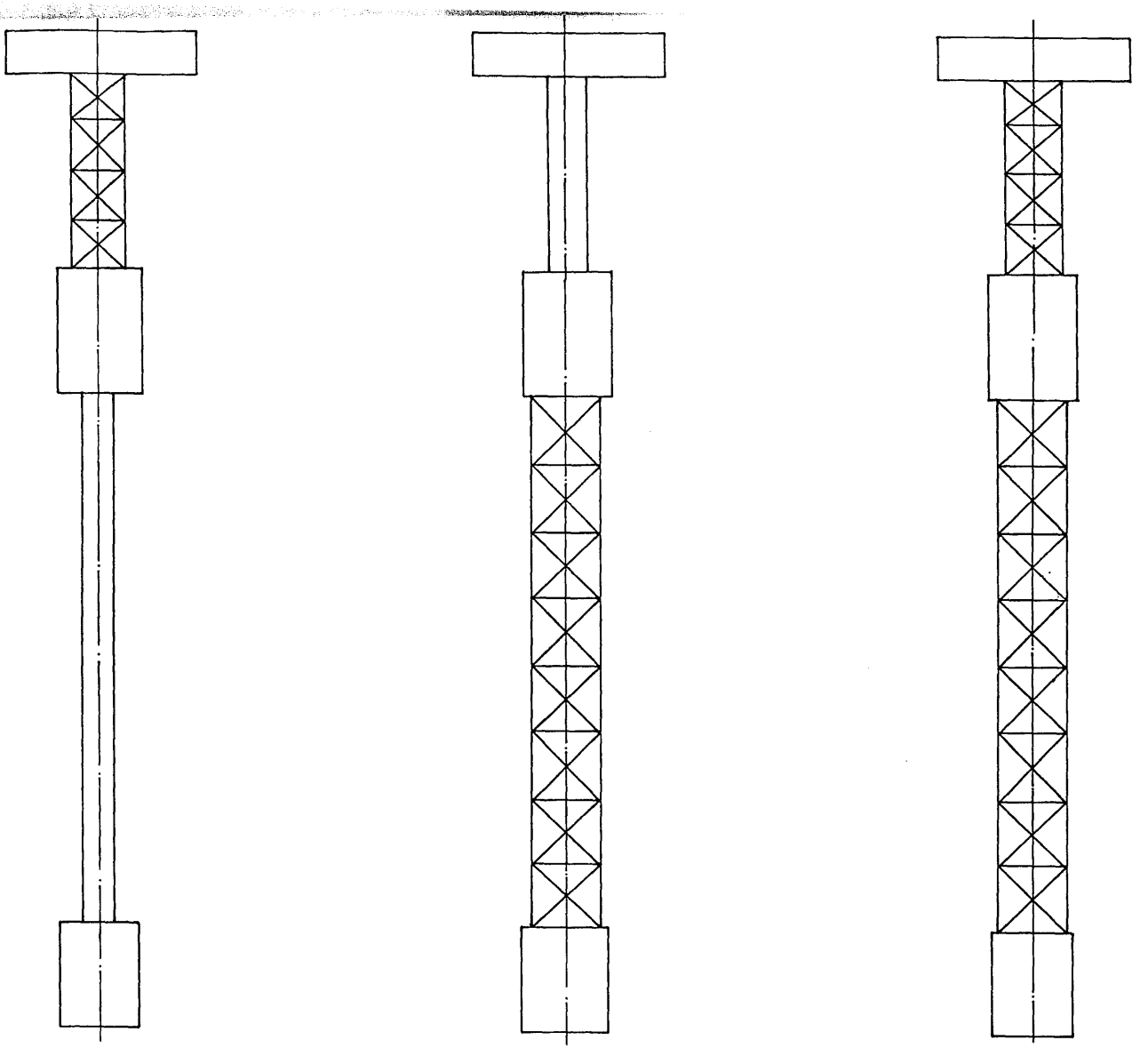

(a) type I (b) type II (c) type III

Fig. 1.2 sketch of hybrid single articulated tower (HAT)

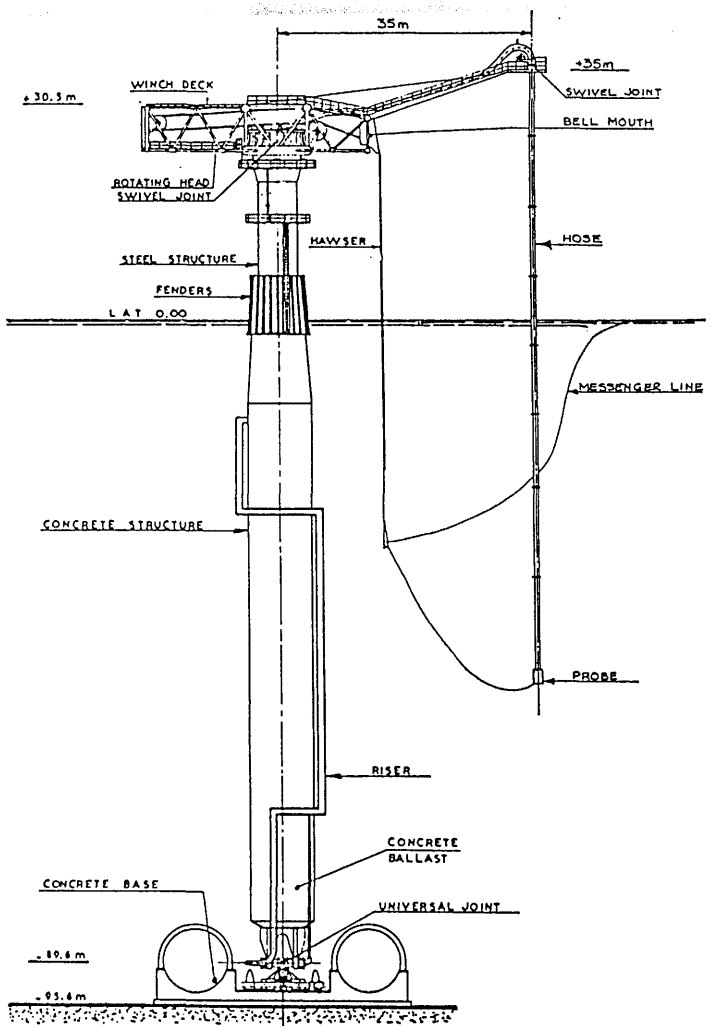

MAUREEN ALP [ref.]

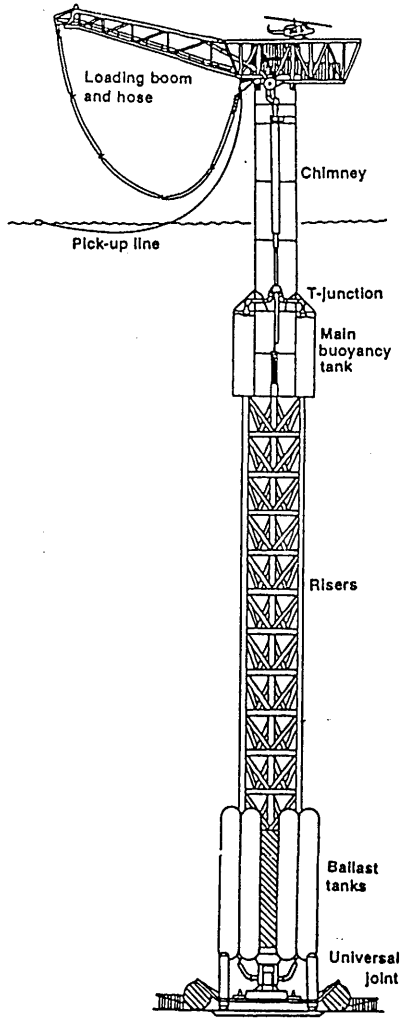

STATFJORD A ALP [ref.]

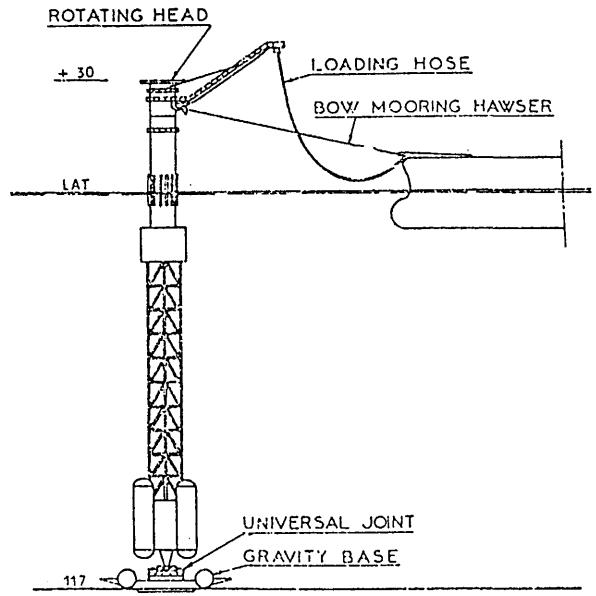

BERYL I ALP [ref.]

Fig. 1.3 some existing applications of articulated tower structures

Fig. 1.4 classification of articulated tower structures

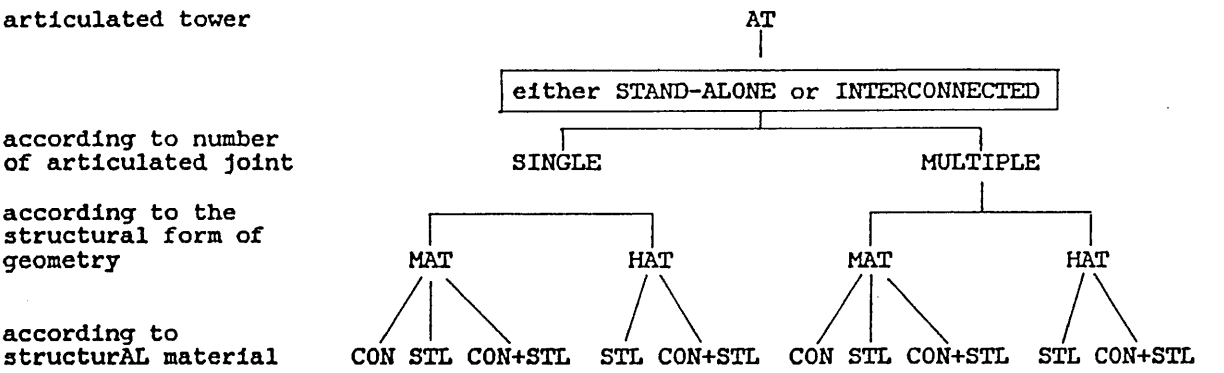

(CON for concrete and STL for steel)

Table 1.1 articulated tower systems installed so far

location	type	design and fabrication	year of installation	water depth	notes
U.K. North Sea (ref. 9)					
Frigg	flare		1975	106m	
Brent	flare		1975	136m	
Beryl I	ALP	EMH/CFEM	1976	395ft	abandoned Feb. 1985
Beryl II	ALP	EMH/CFEM	1981		
Maureen	ALP	EMH/CG,Doris Howard Doris	1983	145m	concrete ALP
Thistle	ALP	Exxon/SBM/DBV Mother Bridge	1976		2-joints ,abandoned 1984
Other North Sea Area (ref. 9)					
Gullfaks	ALP	EMH/Kvaerner (ACN)	1986		modified version of Beryl II
statfjord A	ALP	Kvaerner,Brown &Root	1978		Towed to Norway,1984 for repair
statfjord B	ALP	SBM/Thyssen	1980		
statfjord C	ALP	SBM/CFEM	1984	196m	
Installed with FPSO Systems					
Tapris Malaysia	SALS		1978	380ft	refs. 2,19
Castellon Spain	SALS	Shell Espana	1977		refs. 20,21,30
Hondo California	SALS			149m	ref. 2
Tazerka Tunisia	SALS			146m	ref. 2
Garoupa	Yoke+ ALP			400ft	ref. 31 two towers/vessels
Fulmar	Yoke				
North Sea				82m	ref. 2
Genoa Harbour	ALP	Tecnomare	1982	70m	ref. 9

Table 1.2 geometrical dimensions of an articulated tower

structural component	i	diameter	radius	length	position	shell thickness	equiv. shell thickness
deck	6	D_6	R_6	L_6	$z_6 - z_7$	t_6	
upper column	5	D_5	R_5	L_5	$z_5 - z_6$	t_5	$\bar{t}_5$
buoyancy chamber	4	D_4	R_4	L_4	$z_4 - z_5$	t_4	$\bar{t}_4$
lower column	3	D_3	R_3	L_3	$z_3 - z_4$	t_3	$\bar{t}_3$
ballast chamber	2	D_2	R_2	L_2	$z_3 - z_3$	t_2	$\bar{t}_2$
extension column	1	D_1	R_1	L_1	$z_1 - z_2$	t_1	$\bar{t}_1$
articulated joint					z_1		

the diameter/length ratio is : $\alpha_i = D_i / L_i$

CHAPTER 2

ESTIMATION OF THE ENVIRONMENTAL LOADING ON MEMBERS OF AN ARTICULATED TOWER

1. INTRODUCTION

This chapter summarises the methods used in modelling the environmental loading on members of an articulated tower.

An articulated tower structure is taken to be composed of a series of column members of different diameter and orientation. The load calculations are carried out on individual column elements. These are then summed up to give the total for the whole structure. The environmental loadings which are considered in this study arise from wind, waves and current. They are assumed to act on the structure independently but to coincide in direction as well as occurrence.

The estimation of the wave loading includes two aspects:

a. The first order forces which are linearly proportional to the wave height and have the same frequency as the waves.

b. The second order forces which are proportional to the square of the wave height and associated with wave grouping of very low frequency.

Morison's equation is thought to be appropriate and is subsequently used in modelling the structure-environment interaction and estimating the first order wave loading. The second order wave drift is estimated using the method outlined by Pinkster [28].

The velocity potential satisfies the Laplace equation and can be split into three parts in general in the surrounding flow field of a submerged body: the incident wave potential without the existence of the body, the diffracted wave potential when the body is fixed and the radiated wave potential resulting from the wave induced by the motions of the body.

On satisfying the linearised boundary conditions, the incident wave velocity potential, is obtained [33] from which the wave kinematic characteristics are derived as listed below.

Incident wave velocity potential
$$\Phi_I = \frac{H\omega}{2k}\frac{\cosh kz}{\sinh kd}\sin(kx - \omega t) \qquad (2.1)$$

Free surface elevation
$$\eta = \frac{H}{2}\cos(kx - \omega t) \qquad (2.2)$$

Horizontal wave particle velocity
$$U_x = \frac{H\omega}{2}\frac{\cosh kz}{\sinh kd}\cos(kx - \omega t) \qquad (2.3)$$

Vertical wave particle velocity
$$U_z = \frac{H\omega}{2}\frac{\sinh kz}{\sinh kd}\sin(kx - \omega t) \qquad (2.4)$$

Horizontal wave particle acceleration
$$\dot{U}_x = \frac{H\omega^2}{2}\frac{\cosh kz}{\sinh kd}\sin(kx - \omega t) \qquad (2.5)$$

Vertical wave particle acceleration
$$\dot{U}_z = -\frac{H\omega^2}{2}\frac{\sinh kz}{\sinh kd}\cos(kx - \omega t) \qquad (2.6)$$

Pressure
$$p(z,t) = \rho_w g(d - z) + P_w(z)\cos(kx - \omega t)$$
$$P_w(z) = \tfrac{1}{2}\rho_w gH\frac{\cosh kz}{\cosh kd} \qquad (2.7)$$

Dispersion relation
$$C^2 = \frac{\omega^2}{k^2} = \frac{g}{k}\tanh kd \qquad (2.8)$$

Breaking wave height $H_b = 0.14\lambda \tanh kd$ (2.9)

The above formulae are for waves in waters of finite water depths. If the ratio of d/λ is sufficiently large, i.e, the water depth is deep compared with the wave length, simplications can be made of the above formulae. In fact the complete range of water depths can be divided into shallow water, intermediate water and deep water ranges as follows:-

Shallow water waves $\frac{1}{20} > \frac{d}{\lambda}$ or $kd < \frac{\pi}{10}$

$\sinh kd = \tanh kd = kd$

$\cosh kd = 1$

Intermediate water waves $\frac{1}{20} < \frac{d}{\lambda} < \frac{3}{8}$ or $\frac{\pi}{10} < kd < \frac{3\pi}{4}$

Deep water waves $\frac{d}{\lambda} > \frac{3}{8}$ or $kd > \frac{3\pi}{4}$

$\sinh kd = \cosh kd = \frac{1}{2}e^{kd}$

$\tanh kd = 1.0$

The essential concern of the hydrodynamic problem is to calculate the total wave velocity potential from which the dynamic pressure can be calculated using Bernoulli's equation. The total force on the submerged body and its moment about a given point $P_o(x_o, y_o, z_o)$ can therefore be obtained by integrating the pressure around the submerged body surface.

2. ESTIMATION OF THE WAVE LOADING ON A SUBMERGED COLUMN

The wave loading is estimated in the drag-inertia regime or diffraction regime according to whether $D/\lambda < 0.2$, respectively [32]. In detail, the two regimes can be split into several regions according

to the relative importance of inertia to drag as follows:-

$D/\lambda > 1$ conditions approximate to pure reflection

$D/\lambda > 0.2$ diffraction increasingly important

$D/H_w > 0.2$ inertia increasingly predominant

$D/H_w < 0.6$ incipience of lift and drag and

$D/H_w < 0.2$ drag increasingly predominant and for $D/H_w < 0.125$ drag dominant

The above classification is shown in fig. 2.2.

In the drag-inertia regime the dimension of the column is small compared with the wave length so that the scattered waves due to the presence of the column is negligibly small. Therefore, the incident wave potential is undisturbed as if the column did not exist. The variation of the wave kinematic characteristics over the cross sections of the column dimension is neglected and their values are taken at the centre of the column cross section. The wave loading in this regime is estimated by a modified Morison's equation which takes into account the relative motion between the wave particles and the column. As the D/λ ratio becomes larger ($D/\lambda > 0.2$) the effect of scattered waves due to the presence of the column becomes more pronounced and the wave loading should be estimated in the diffraction regime. The scattered wave potential due to the presence of the large dimension column is added to the incident wave potential.

Regarding the two regimes, the following points should be made:-

a. The two regimes may be relevant for the estimation of the wave loading on the column over a wide range of wave frequency as D/λ ratio depends clearly on the variation of λ with frequency ω.

b. In a wave cycle there is one instant when the acceleration is zero and one instant when the velocity is zero, from which it is understood that the dominance of inertia/drag means that the amplitude of the wave loading due to inertia/drag is dominant compared with that due to drag/inertia.

c. In the case of an offshore structure composed of many members, the predominance of inertia/drag on one individual member does not imply that this is the case on the whole structure. The total wave loading may be drag dominant although it may be inertia dominant on a particular member. The wave loading tends to be over-estimated if the scattered potential is neglected [33].

d. The estimation of the wave loading is much more time-consuming in the diffraction regime than in the drag/inertia regime.

The above points have to be borne in mind in determining the relevance of the two regimes. In most cases the decision is centred around the trade-off between pragmatism and realism.

In the present case the column with the largest dimension is normally the buoyancy chamber which is submerged into the water and is from 10m to 30m in diameter. The major part of the wave loading on an

articulated tower structure is exerted on the upper support column and the buoyancy chamber, as is demonstrated in chapter 5. The wave frequency of concern regarding the nature of the wave structure interaction may vary from 0.4 rad/s(λ = 400m) up to 1.0 rad/s(λ = 50m). In this wave frequency range, Morison's equation is considered to give adequate accuracy, although at higher frequencies diffraction effects begin to be important. Morison's equation will over-estimate the forces in this region.

2.1. Wave Force on a Vertical Column of Small Dimensions

Referring to a submerged vertical column moving with a displacement X (z,t) or simply velocity $\dot{X}$ and acceleration $\ddot{X}$ in the direction of the incident stream, the horizontal wave force on it per unit length is given by [33]:

$$f_1(z,t) = \rho_w C_a A \dot{U}_x - \rho_w C_m A \ddot{X}$$

$$+ \tfrac{1}{2}\rho_w C_d D \left| U_x - \dot{X} \right| (U_x - \dot{X}) \qquad (2.10)$$

The first term is due to the pressure on the column (Froude-Krylov) and the second term is due to the relative acceleration and $C_a = C_m + 1$ is the added virtual mass coefficient.

It is noticed that in equation (2.10), the drag force is non-linearly related to the relative velocity. In some cases, the non-linear term needs to be linearised. The linearised form of equation (2.8) is then written as:-

$$f_1(z,t) = \rho_w C_a A \dot{U}_x - \rho_w C_m A \ddot{X}$$

$$+ \tfrac{1}{2}\rho_w C_d D \left[\frac{8}{3\pi}(\bar{U}_x - \bar{\dot{X}})\right](U_x - \dot{X}) \qquad (2.11)$$

in which the assumption is made that X is sinusoidal and the relationship:-

$$|\cos x|\cos x = \sum_{n=1}^{\infty} a_{2n-1}\cos[(2n-1)x]$$

$$a_n = \begin{cases} 0 & \text{for even } n \\ (-1)^{\frac{n+1}{2}} & \text{for odd } n \end{cases}$$

is used and approximated by the first term on the right-hand side only. $\bar{U}_x$ and $\dot{\bar{X}}$ are the amplitude of U_x and $\dot{X}$ respectively. Applying the above equations to the column segment, taken out of the ith column of an articulated tower shown in fig. 2.1, the total force on the column and its moment about y' axis, which is through point $z = z_o$ on the vertical axis of the column and parallel with y axis, can be readily obtained.

2.2. The Heaving Force on a Submerged Vertical Column of Small Diameter

The column in fig. 2.1 experiences a wave force on its top and/or bottom surface. This is due to the variation of wave kinematics with depth which in turn leads to the pressure variation. This force will exist as long as the column does not pierce the surface and extend down to the seabed. Excluding the buoyant force due to the hydrostatic pressure, the heaving force has three components:-

a. The component due to pressure change on the column surfaces, assuming that the presence of the column does not interfere with the wave flow.

b. The inertia force due to the pressure change on the

surfaces of the column interfering with the acceleration of the wave particles.

c. The drag force due to the pressure change on the surfaces of the column brought bout by the viscous effects arising from the column's interference with the wave particle velocity.

In general the pressure component will be the dominant part [34]. Omitting the drag force component, the heaving force on the top/bottom surface of the column of circular cross section exposed to waves at z = z above the seabed is given by:-

$$F_{1v}(z,t) = \frac{\pi D^2}{4}[Dp_v(z) \pm P_w(z)]\cos(kx - \omega t) = F_{1v}(z)\cos(kx - \omega t) \quad (2.12)$$

where $P_w(z)$ is given in equation (2.7) and $P_v(z)$ is obtained as:

$$p_v(z) = \frac{1}{6}\frac{\sinh kz}{\sinh kd}\rho_w g\ J\ C_{mv} kH \quad (2.13)$$

with C_{mv} using the added mass coefficients in vertical direction, $J = 2/\pi$.

2.3. Effect of the Column Orientation

If the column is arbitrarily orientated, equation (2.8) is no longer valid. The problem of wave loading in this case has been under extensive investigation but, by no means, has been fully understood. Nevertheless, there are four methods which are generally accepted by the industry and which are examined by Wade and Dwyer [35] for fixed offshore structures.

The first method assumes that the resultant drag pressure acts on an area projected on a plane normal to the total wave particle

acceleration. If the total wave particle velocity and acceleration vector were normal to the column axis this method would have been identical to that in equation (2.10).

The second method assumes that the resultant drag and inertial pressure may be resolved into normal and tangential components and the tangential component may be ignored. This method is not in conformity with the independence principle that the normal pressure forces are independent of the tangential velocity and acceleration components since the cosine of the angle rather than its square is multiplied with the square of the velocity.

The third method assumes that the resultant velocity and acceleration may be decomposed into normal and tangential components and the tangential kinematic pressure may be ignored as was originally proposed by Borgman [36] and improved by Chakrabarti [37]. This method is in conformity with the independence principle and the Morison's equation which can be seen as a special case, although it is one of the least conservative [35].

Finally, the fourth method assumes that the resultant velocity and acceleration act normal to the column. An area correction factor is applied to the pressure when the yaw angle is greater than 60 degrees. This method obviously relies heavily on experimental data.

In this study, the third method is used. The Morison's equation, equation (2.10) is modified, for a randomly inclined column, as:-

$$\vec{f}_{1n}(z,t) = \rho_w C_a A \dot{\vec{U}}_n - \rho_w A C_m \ddot{\vec{r}}_n + \tfrac{1}{2}\rho_w C_d D |\vec{U}_n - \dot{\vec{r}}_n| (\vec{U}_n - \dot{\vec{r}}_n) \tag{2.14}$$

giving the force vector per unit length of the inclined column normal to its axis. In calculating the normal velocity of the wave particles, $\vec{e}$ denotes the unit vector along the column axis as:

$$\vec{e} = e_x \vec{i} + e_y \vec{j} + e_x \vec{k} \tag{2.15}$$

and the wave particle velocity vector as:-

$$\vec{U} = U_x \vec{i} + U_z \vec{k} \tag{2.16}$$

then $\vec{U}_n$ is obtained as:-

$$\vec{U}_n = \vec{e} \times \vec{U} \times \vec{e}$$

$$= U_{nx} \vec{i} + U_{ny} \vec{j} + U_{nz} \vec{k} \tag{2.17}$$

The modulus of $\vec{U}_n$ is given by:-

$$|\vec{U}_n| = \vec{U}_n . \vec{U}_n \tag{2.18}$$

The normal wave particle acceleration is obtained in a similar manner. It is noted that total velocity and acceleration vectors are not co-linear. Also $\dot{\vec{r}}_n$ and $\ddot{\vec{r}}_n$ will have to be obtained by incorporating Morison's equation, equation (2.14), into the motion equation and subsequently solving the equation. The linearisation of the non-linear drag term would be carried out as in equation (2.11).

The wave force on the oblique column normal to its axis and its moments about point $P_o(x_o, y_o, z_o)$ can be obtained in vectoral form, in general, through integration.

2.4. Lift Force due to Vortex Shedding

The flow of fluid past the immersed column creates vortex

shedding which gives rise to a lift force on the column at right angles to the direction of fluid flow. However, in this study the lift force is neglected because it is small compared with the fluid force in the direction of fluid flow. The concern is mainly with the frequency of the vortex shedding which may be important, as in the case of hybrid articulated tower structures, the bracings of the lattice structure should be designed to avoid local resonance with the vortex shedding.

For steady flow of current with velocity V_c, the frequency of the vortex shedding f_ℓ is defined by the Strouhal number S:-

$$S = Df_\ell/V_c \tag{2.19}$$

In waves, the occurrence of vortex shedding is changed. The vortex shedding during wave motion is more complex because the flow is accelerating and reverses its direction regularly. In many cases the flow does not persist long enough in one direction for a vortex street or wake to develop. The disturbance of the fluid developed in one half cycle of the wave is swept back on the column in the following half-cycle, becoming superimposed on the approaching flow. Therefore, for vortex shedding to occur, the orbital velocity of the wave particle should stay sensibly constant for a certain time of the vortex shedding period. It is expected that the vortex shedding is only likely to occur in long waves past columns of small dimension. In addition, since the wave particle velocity decreases with depth below the surface; vortex shedding will only be likely to occur, if at all, near the free surface.

2.5. Interference Effects

When two or more columns are placed close in the flow field interference between them may occur, eg between the neighbouring bracings of a lattice. The interference effect depends on the spacing ratio L_o/D where L_o is the spacing and the angle of approach of the incident waves. Some experimental investigations have been conducted [38] but the mechanism is not fully understood. Experimental data related to the precise geometrical arrangement is needed if the interference effect is to be taken into account. In the present study, the interference effect is omitted.

3. WAVE DRIFT LOADING

Apart from the wave forces mentioned above on the column there exists wave drift forces of comparatively small magnitude. In regular waves the wave drift is steady. However, in irregular waves the wave drift has a slowly varying, as well as a steady, component referred to as the mean and the second order low frequency wave drift force, respectively. They can affect different structures in different ways. The importance of the effect of these force components on the motion of floating/compliant structures has been recognised [17,39,40].

An extensive survey of the literature, together with theoretical development and experimental results, is given by Pinkster [41] and Standing [42]. One of the common features of the methods in the mentioned literature is that the methods of predicting the second order wave drift forces require lengthy calculations and are not engineering-orientated. However, Pinkster [28] arrived at a

formula for the mean and the low frequency wave drift forces expressed in terms of the wave energy spectrum.

In this method which is used in this study, a general equation of the mean wave drift force in regular waves on the column which is either free floating or captive is given:-

$$F_{2s} = \tfrac{1}{2}\rho_w g\, D\, C_s(\omega)\, \zeta_a^2 \qquad (2.20)$$

This is proportional to the square of the wave amplitude. The drift coefficient, $C_s(\omega)$, for the column segment depends on the wave frequency, geometry, dimension and motion behaviour of the column and its immersed position with respect to the free surface. In certain cases it can be calculated and can be determined experimentally in other cases when the geometry is complex. In irregular waves the free surface elevation is taken as the sum of a large number of long-crested regular waves, ie:-

$$\eta(x,t) = \sum_{j=1}^{N} \zeta_j \cos(k_j x - \omega_j t - \varepsilon_j)$$

By assuming that the irregular sea is narrow banded and

$$C_s(\omega) = a + b\omega \qquad (2.21)$$

Equation (2.20) in irregular waves becomes:-

$$F_{2s} = \rho_w g D \int_0^\infty S_\eta(\omega)\, C_s(\omega)\, d\omega \qquad (2.22)$$

In addition, there exists a low frequency component of wave drift forces in irregular waves. The energy spectrum of the low frequency drift forces is given, in terms of the wave spectrum, as:-

$$S_{2f}(\omega) = 2(\rho_w g D)^2 \int_0^\infty S_\eta(\mu)\, S_\eta(\mu + \omega)\, C_s'(\mu + \frac{\omega}{2})\, d\mu \qquad (2.23)$$

where μ is a dummy frequency; $C_s'(\omega)$ is the drift coefficient in irregular waves. The corresponding moment is not explicitly available. The moment of the mean and low frequency wave drift force component about y' axis as shown in fig. 2.1, can be expressed as:-

$$M_{2S} = \rho_w g D \int_0^\infty S_\eta(\omega)\, L_c(\omega)\, C_s(\omega)\, d\omega \qquad (2.24)$$

and

$$S_{2m}(\omega) = 2\{\rho_w g D L_c(\omega)\}^2 \int_0^\infty S_\eta(\mu + \omega)\, C_s'(\mu + \frac{\omega}{2})\, d\mu \qquad (2.25)$$

where $L_c(\omega)$ is a characteristic length dimension representing the effective length of the lever arm of the wave drift forces to point $z = z_o$. It is noticed that $C_s'(\omega)$ and $C_s(\omega)$ are mean and low frequency wave drift coefficients for both surge and pitch mode, respectively. These coefficients are not always the same but are normally assumed to be equal [28]. This means that using $C_s(\omega)$ to calculate the low frequency wave drift forces only accounts for the contribution of the first order potential.

Theoretical calculation of $C_s(\omega)$ is tedious. For the column segment in fig. 2.1, $C_s(\omega)$ is difficult to find in the existing literature. However, if the column is a fixed surface piercing circular cylinder then $C_s(\omega)$ is available [42] and is approximated [43] for deep water condition as:-

$$C_s(\omega) = \begin{cases} 0.65(\omega^2 D/g) & \text{if } (\omega^2 D/g) < 1 \\ 0.65 & \text{otherwise} \end{cases} \qquad (2.26)$$

This can be compared with the numerical solution in fig. 2.3. By

assuming the rate of decay of the wave drift force to be $\left(\frac{\cosh kz}{\sinh kd}\right)^2$, the characteristic length $L_c(\omega)$ for the column segment in fig. 2.1 is given as:-

$$L_c(\omega) = 2k \frac{B(2k,z) + B(-2k,z) + (z - z_o)^2}{e^{2kd} - e^{-2kd} + 4kd} \Bigg|_{z = z_{1i}}^{z = z_{2i}} \qquad (2.27)$$

where $B(a,b) = \frac{e^{ab}}{a^2}\{a(z-z_o)-1\}$

The above calculations are based on the assumption of ideal fluid and potential flow. However, in real terms the diffraction effect of the column may well be negligible and the drag effect, on the other hand, may be dominant. Standing [42] classified the dominance of the drag effect on the mean wave drift on a fixed surface piercing vertical cylinder according to $H\lambda^2/D^3$ ratio.

a. Drag dominates when:-

$$\left(\frac{H}{D}\right)^3 > 60\left(\frac{H}{\lambda}\right)^2$$

Taking into account the wave steepness limit in deep waters given in equation (2.9), it can be seen that drag dominates the mean wave drift force if $H/D > 1$. That is to say, if the drag effect is significant for the first order wave forces, the same is generally true for the mean drift wave force.

b. The diffraction effect dominates when:-

$$\left(\frac{D}{\lambda}\right)^3 > \frac{H}{60\lambda}$$

With the same limit on the wave steepness, the diffraction effect dominates the mean wave drift force if $D/\lambda > 0.13$.

c. The situation is not clear when the first order wave forces are inertia dominated, with negligible drag and diffraction effects, which is obviously the case for an articulated tower structure.

The adoption of $C_s(\omega)$ for a fixed surface piercing cylinder for the present use neglects the motion effect of an articulated tower structure on $C_s(\omega)$. The real effect of the motion on $C_s(\omega)$ is not clear.

4. WIND LOADING ON THE COLUMN

The wind above the water surface generates waves and exerts wind loading on the above water part of offshore structures. It is commonly recognised that the occurrence of ocean waves and some form of currents is directly related to the occurrence of ocean winds. The interactions between them are discussed in Section 7 below.

In conventional fixed offshore structure design, the wind loading is often ignored. Also, even if it is accounted for, it can be estimated independently of the wave loading as the motion of the structure is negligible and the loading is quasi-static.

In the case of an articulated tower as a compliant offshore structure, the effect of the wind loading can be very significant as demonstrated in Chapter 5 as the mean wind loading is resisted by the restoring stiffness, for one thing, and the dynamic wind loading component is of a very low frequency nature, for another.

If articulated tower structures undergo a considerable motion, the wind and the wave loadings may not be exerted on the structure independently of each other. On the other hand, the effect will depend on the significance of the motion amplitude of the structure which is generally small so the wind loading may be estimated on the assumption that the structure is stationary.

The interaction between the wind and the wave loadings may also appear when they act on the articulated tower in different directions which is often the case in reality. The angle between the two directions also may be important with respect to the complexity of the motion trajectory. This can only be investigated by time simulation. Unfortunately, knowledge of this aspect of the behaviour of articulated tower structures is limited and the assumption has to be made that the wind and the waves are co-linear.

4.1 Description of the Wind

For practical purposes, the description of the wind is standardised by four parameters: Mean wind direction, mean wind velocity, its profile above sea level and the spectrum of the random differential wind velocity.

The mean wind direction is taken as coincidental with that of the waves here. The mean wind velocity is classified on the basis of the averaging time duration generally over 3 seconds, one minute or one hour, as gust wind velocity $\overline{V}_{w3sec}$, sustained wind velocity $\overline{V}_{ws}$ and one hour wind velocity $\overline{V}_{w1hr}$, respectively. The most probable velocity in a period of N yrs is referred to as the N yr wind velocity.

The calculation of the mean wind loading is generally based on the sustained velocity. The mean wind velocity is assumed to be steady. The instantaneous wind velocity at any special point can be expressed as the sum of a mean and a fluctuating differential wind velocity components, ie:-

$$V_w = \overline{V}_w + V'_w \tag{2.28}$$

They vary largely with the height above the water surface. The mean wind velocity profile above the water surface is recognised to follow an exponential function:-

$$\overline{V}_w = \alpha \overline{V}_{ws10} \left(\frac{z - d}{10} \right)^{\beta} \qquad (z \geqq d) \tag{2.29}$$

where z is in the co-ordinates system as in fig. 2.1. The datum sustained wind velocity $\overline{V}_{ws10}$ is measured at the height of 10m above the water surface. The gusty factor α takes into account the length of the averaging time interval. The fluctuating differential wind velocity is assumed to form a zero mean Gaussian process and, is usually presented in the form of velocity spectrum. This wind velocity component can be assumed to be constant up to the height of interest above the water surface with reasonable accuracy. In addition, it is very small compared with the mean wind velocity component and it is the low frequency nature of the wind gust that is important in this case.

4.2 Wind Loading on the Above Water Part of the Column

Because of the low density of the atmosphere, the wind loading is exerted in the form of drag which is recognised to be proportional to the square of the wind velocity. In fact, Morison's

equation can be applied to the wind loading per unit length, neglecting the inertia component, as:-

$$f(z) = 0.5\rho_a C_d D V_w^2 \tag{2.30}$$

The force should strictly take account of the motion of the column, as follows:-

$$f = \begin{cases} 0.5\rho_a C_{da} D|V_w - \dot{X}|(V_w - \dot{X}) & z > d \\ -\rho_w C_m A\ddot{X} - 0.5\rho_w C_d D|\dot{X}|\dot{X} & 0 \leq z \leq d \end{cases} \tag{2.31}$$

where the second equation is in effect the Morison's equation without the wave kinematics. It is dropped for the time being and only the first equation is developed. The second equation, which represents the motion effect of the column under the wind pressure, is taken into account in Chapter 5 when the response of an articulated tower under the wind pressure is calculated.

In the case of the column moving with a horizontal velocity X comparable in magnitude with V_w', the relative velocity should be used as in the first equation. For an articulated tower the motion velocity is expected to be small compared with the wind velocity and the relative velocity term in the first expression of equation (2.31) may well be safely approximated by V_w. Substituting equation (2.28) into (2.31) and neglecting the $V_w'^2$ term yield, the static and dynamic wind (loading per unit length) components.

$$f_{3S}(z) = 0.5\rho_a C_{da} D\bar{V}_w^2 \tag{2.32}$$

and $$f_3(z) = \rho_a C_{da} D\bar{V}_w V_w' \tag{2.33}$$

In order to calculate the surge force on the part of the column above the water surface in fig. 2.1 (ie, $z \geq d$) and its moments

about point $P_o(0,0,z_o)$ on the vertical axis, the wind loadings in equations (2.32) and (2.33) are integrated along the length of the column.

The dynamic component can be written in spectral form in terms of gusty wind velocity spectrum $S_w(\omega)$ as:-

$$S_{3f}(\omega) = H_{3f}^2(\omega)\ S_w(\omega) \tag{2.34}$$

for the surge force and

$$S_{3m}(\omega) = H_{3m}^2(\omega)\ S_w(\omega) \tag{2.35}$$

for the pitch moment.

where

$$H_{3m}(\omega) = \int_{\ell} \rho_a C_{da} D \overline{V}_w (z-z_o)\, dz$$

When the column is oblique in relation to the direction of the wind velocity the wind drag is affected. There are basically two recognised methods to calculate the wind drag pressure in this case. One is based on the projected length of the column in the direction normal to the wind velocity, with the force assumed to act horizontally and the other is based on the projected wind velocity in the direction normal to the axis of the column.

The second one is used which is coincident with the wave drag force in Morison's equation for arbitrarily orientated columns which are relevant to the bracings of the lattice structure on a hybrid articulated tower. The normal wind loading to the oblique column axis is calculated in a similar way to $\vec{f}_{1n}$ in equation (2.14).

5. CURRENT LOADING ON THE COLUMNS

Apart from waves, currents exert forces on the immersed column in fig. 2.1. In addition, the waves interact with the current. The effect is that the loading due to the combined effects of waves and current may be significantly different from the loadings due to waves and current separately when the current velocity is comparable with the wave particle velocity [44]. When the wave particle velocity is considerably greater than the current velocity, or vice versa, the waves and the current are expected to act largely independently. In the design conditions, the current is expected to have little effect on the waves as the wave particle velocity is much greater than the current velocity, eg wave particle velocity of 10m/s against a current velocity of 1.5m/s in the North Sea.

5.1. A General Description of the Currents

The current is described by its velocity, depth profile and direction of the current velocity. It includes wind induced, atmospheric pressure induced, tidal and residual components. The first two components are due to the wind blowing over the ocean surface and, therefore, related to the storm intensity and direction. This part of the current is concentrated immediately below the free surface and varies with the depth below the surface, in magnitude and direction. It does not coincide with the wind direction. The tidal and residual components are due to the celestial motion of the earth and interplanetary attractions and are, therefore, independent of ocean winds. The pattern of its direction is very much influenced by the geographical locations. Pure tidal current travels in the form of very long tidal waves and decays very slowly with depth. The presence of

the current, apart from interfering with the waves, also cause a fixed body to produce a standing wave pattern on the water surface and creates vortices. The current velocity, V_c, is considered to be steady and decomposed into tidal and wind driven components as:-

$$V_c = V_{ct} + V_{cw} \tag{2.36}$$

They are assumed to occur in the same direction as the waves with V_{ct} being constant over the water depth and V_{cw} varying along the depth below the surface.This is a very pessimistic assumption since the tidal current direction changes through 360^o during a tidal cycle.

5.2 Current Loading on the Column

First of all, the current loading on the vertically orientated column segment in fig. 2.1 of unit length is given as:-

$$f_{4S}(z) = 0.5\rho_w C_d D V_c^2 \tag{2.37}$$

The total surge force on the column segment and its pitch moment can be obtained by integrating $f_{4S}(z)$ over the column length.

If the column segment is arbitrarily orientated, the normal force to its axis is given, similarly to the wind loading calculation.

6. STATISTICAL DESCRIPTION OF THE ENVIRONMENT

The ocean environment, which is comprised of wind, waves, current and their combination, has a random nature. This section describes the statistical modelling of the short term occurrence of the wind, waves and the current individually. The description of their long term occurrence is given in section 8.

6.1 Gusty Wind Spectrum

There are two commonly used wind velocity spectra used in the ocean environment to describe the frequency content of the fluctuations differential wind velocity which is assumed to form a zero mean Gaussian process, namely, the Harris and Davenport wind velocity spectra [45,46] as listed in the table below.

Harris wind spectrum: $$S_w(f) = \frac{4\kappa \bar{V}_{ws10} \bar{f}}{f(2 + \bar{f}^2)^{5/6}} \tag{2.38}$$

Davenport wind spectrum: $$S_w(f) = \frac{4\kappa \bar{V}_{ws10} \bar{f}^2}{f(1 + \bar{f}^2)^{4/3}} \tag{2.39}$$

non-dimensional frequency: $$\bar{f} = \frac{fL}{\bar{V}_{ws10}}$$

The two spectra depend on three parameters κ,L, and $\bar{V}_{ws10}$; it is often preferable to work with a circular frequency ω instead of f. The transformation of $S_w(f)$ into $S_w(\omega)$ is given as:-

$$S_w(\omega) = \frac{1}{2\pi} S_w(f) \Big|_{f = \frac{\omega}{2\pi}}$$

Typical gusty wind velocity spectra are shown in fig. 2.4. The spectrum content increases with all three parameters.

6.2 Statistical Description of Short Term Waves

It is known that the ocean waves are generated by the wind acting on the water surface, causing surface irregularities. The

irregular sea surface varies from time to time and place to place, depending on the wind velocity, wind duration and the distance over which the wind flows (fetch) and the location of other storm areas from which the swell may travel.

The ocean waves during a storm are often assumed to be episodic and stationary random Gaussian process and are described in terms of their probabilistic distribution properties and spectral properties. The former concerns the probability distribution of wave height and period. The latter describes the frequency contents of the energy of the waves. It is known that if the free surface elevation has a Gaussian distribution, the wave height will possess a Rayleigh distribution. The wave spectrum is of the form:-

$$S_{\eta}(\omega) = (a/\omega^5) \exp(-b/\omega^4) \qquad (2.40)$$

where a and b are functions of significant wave height, H_s, and a characteristic wave period. They are normally functions of the wind velocity, duration and fetch, with either the fetch or the duration imposing a limit on H_s and T_z for a given wind speed. Some of the better known spectra are listed in the table below [47].

The Jonswap wave spectrum is one of the results of the Joint North Sea Wave Project (Jonswap) and applies to limited fetch areas and homogeneous wind fields. The shape of the spectrum is considerably different from those previously proposed. The ,major difference occurs in the vicinity of the spectral peak. A correction factor $A_c(\omega)$ is multiplied to parameter A of the ISSC spectrum accounting for the sharp peak and narrow band.

Bretschneider wave height spectrum

$$a = 262.5\ H_s^2\ T_{-1}^{-4}, \quad b = 1050\ T_{-1}^{-4} \tag{2.41}$$

International Ship Structure Congress (ISSC) wave height spectrum

$$a = 124.2\ H_s^2\ T_z^{-4}, \quad b = 496.0\ T_z^{-4} \tag{2.42}$$

Joint North Sea Wave Project (Jonswap) wave height spectrum

$$a = 124.2\ A_c(\omega)\ H_s^2\ T_z^{-4}, \quad b = 496.0\ T_z^{-4} \tag{2.43}$$

$$A_c(\omega) = \frac{1}{1.52}\gamma^{e^{-\nu(\omega)}}, \quad \nu(\omega) = \frac{\left(\frac{\omega}{\omega_o} - 1\right)^2}{2\sigma^2}, \quad \sigma = \begin{cases} 0.7 & \omega < \omega_o \\ 0.9 & \omega \geq \omega_o \end{cases}$$

ω_o is the peak frequency

γ is the peakedness ratio of mean value 3.3.

International Towing Tank Conference (ITTC) wave height spectrum

$$a = 177.7\ A_c(\omega)\ H_s^2\ T_z^{-4}, \quad b = 712.0\ T_z^{-4} \tag{2.44}$$

The ITTC spectrum is a limited fetch sea-spectral formulation recommended by the 15th International Towing Tank Conference (ITTC, 1984) to replace the older ITTC wave spectrum formulation. The wave spectra are shown in fig. 2.5.

6.3 Correlation Between Wind, Waves and Current

The correlation between wind, waves and current has a two-fold meaning: the correlation of their occurrence and direction. So far they have been described separately and the assumption is made that their occurrence and direction coincide. This is clearly not always true because although there exists a probability of such an occurrence, the probability is not so high for that particular correlation to become a certainty. Indeed, efforts are envisaged

towards an improved definition of offshore environmental loading for offshore design practices [48]. Nevertheless, their occurrence is expected to be highly correlated as the wind generates waves and currents. So far solid information is not available and this extreme of coincidence assumption is often made in the rules of offshore design practices recommended by classification societies.

6.4 Long Term Description of the Environment

An important step encountered often in design is the estimation of an extreme environment on the basis of a series of recorded short term environmental data over a fairly long period or on the basis of hindcasting. The extreme environmental conditions are expected to represent the most severe possible conditions which may be exceeded once in a long period of say 50 or 100 years. Those are characteristic conditions that might be expected with a small probability during the life time of the structure. In addition, less severe conditions which may happen, say r times in N years, typically 12 times a year, are regarded to be the more realistic conditions to define the worst operating conditions which is clearly directly related to the downtime of the structure operation.

The extreme wind velocity prediction in the design of buildings on land is done by multiplying a statistical factor 's' by the short term wind velocity profile given by equations (2.29) and (2.31). The statistical factor depends on the structure's anticipated exposure period and the probability of a given maximum velocity with a return period of 50 years. However, in the ocean environment, the above method is not applied due to lack of data. The DnV Rules [51] recommend the design wind velocity for survival conditions without specifying the probability of its

occurrence, orientated towards the North Sea, which is detailed in Section 8.

The extreme wave height is normally chosen according to the relevant wave height exceedance diagram, where available, with expected return period and probability of occurrence within this return period. The wave period associated with the chosen wave height is also needed. There are different ways of predicting the wave period. However, it is wise to specify a range of variation of the wave period and to use different values for the wave period to obtain the worst possible design wave condition in the design of compliant offshore structures.

The maximum current expected over the same return period as the waves can be obtained by extrapolation of the recorded current data over a long time or can be associated directly with the maximum wind in the case of lack of recorded current data.

7. DESIGN ENVIRONMENTAL CONDITIONS RECOMMENDED BY VARIOUS CLASSIFICATION SOCIETIES

The design conditions vary from site to site. For example, the environmental conditions in the North Sea is very different from those in the Gulf of Mexico or in the Mediterranian waters etc. They are recommended by different regulatory authorities applied to different sites such as API RP2A, DnV Rules and UK DOE guidance notes etc. The recommended design environmental conditions include those for waves, wind and current and are listed in Table 2.1. The extreme conditions are based on a return period of 100 years while the operational conditions are aimed at 12 times a year.

8. CONCLUSIONS

The main sources of environmental loading are recognised to be due to wind, waves and current and their combinations which interact with the structure. The structure environment interaction is modelled such that the above sources coincide in occurrence as well as direction but, nevertheless, interact with the structure independently of each other. A column of small diameter, which works in the drag and inertia regime, is taken as a typical structural component of an articulated tower and, consequently, the environmental loading on the column is estimated. Table 2.1 summarises the environmental conditions.

LIST OF FIGURES

LIST OF TABLES

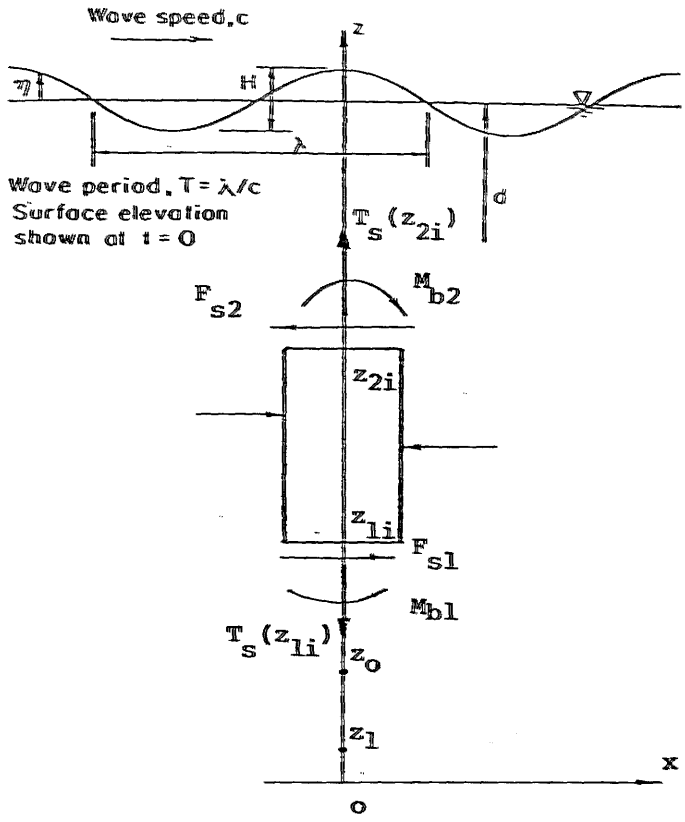

Fig. 2.1 a submerged column segment in waves

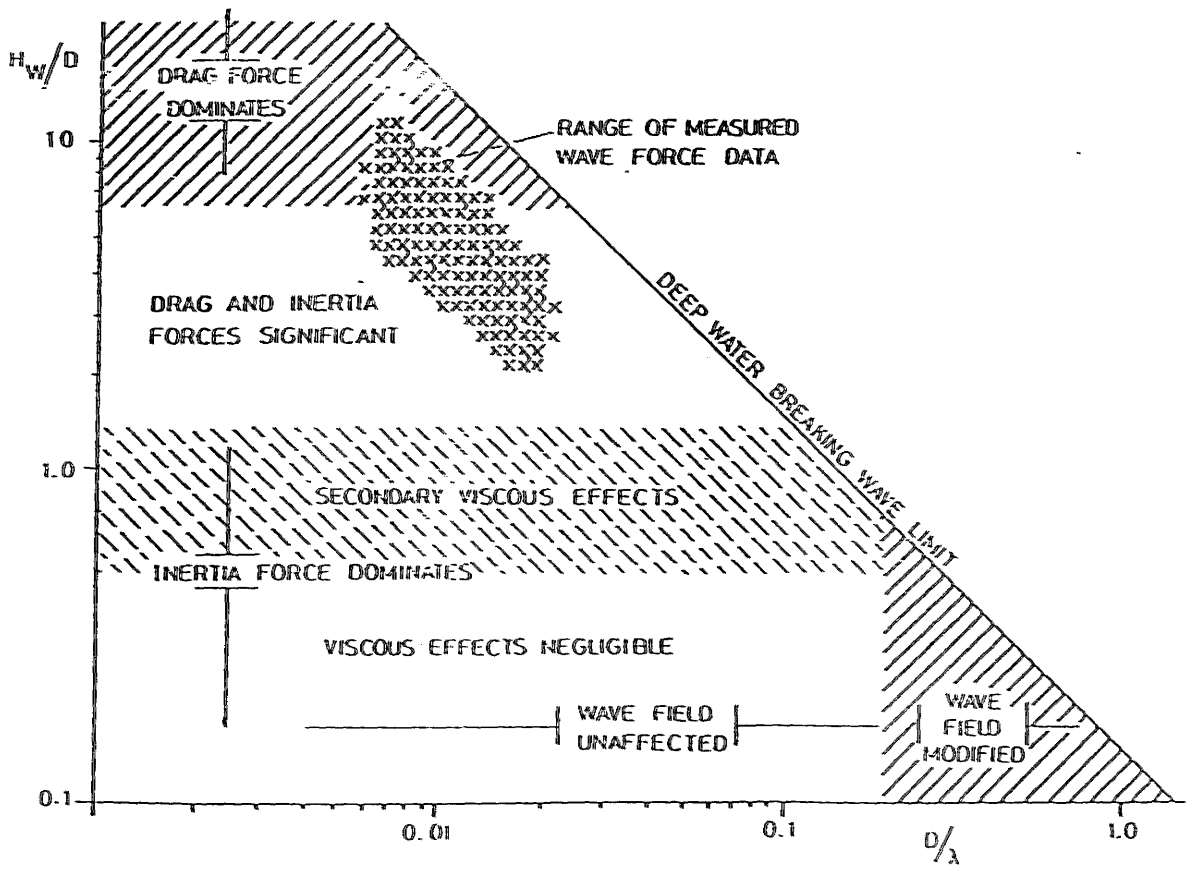

Fig. 2.2 wave force regimes [Hogben, 32

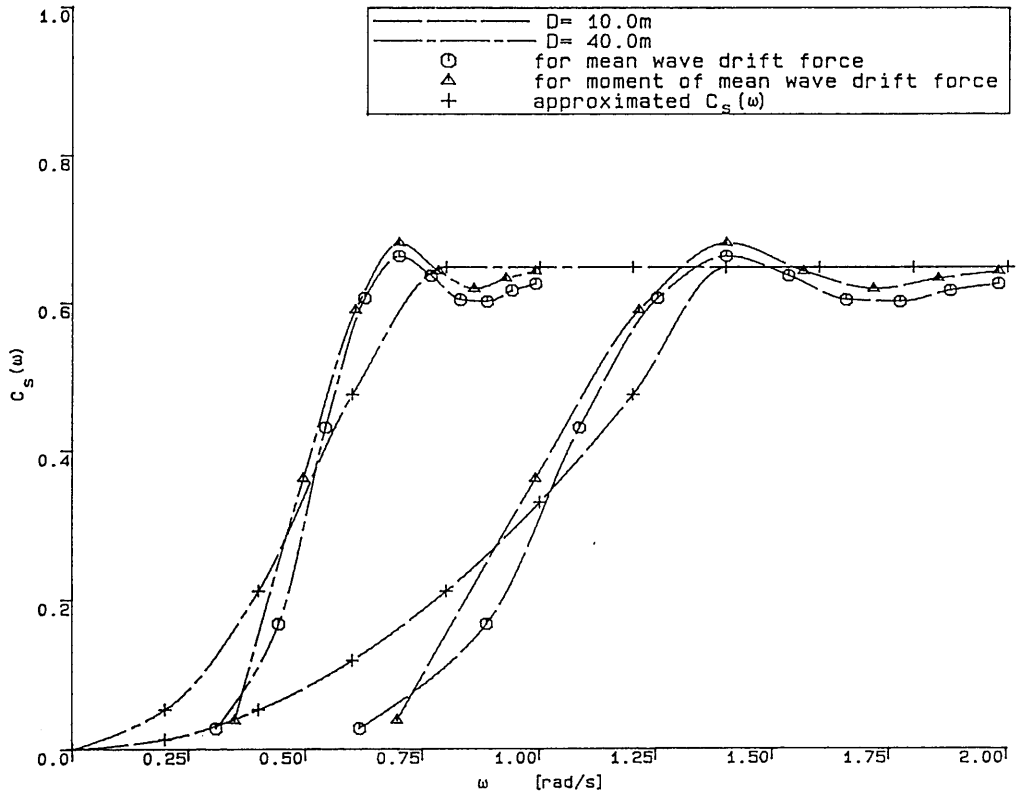

Fig. 2.3 drift coefficient for surface pericing cylinders[Kirk,14]

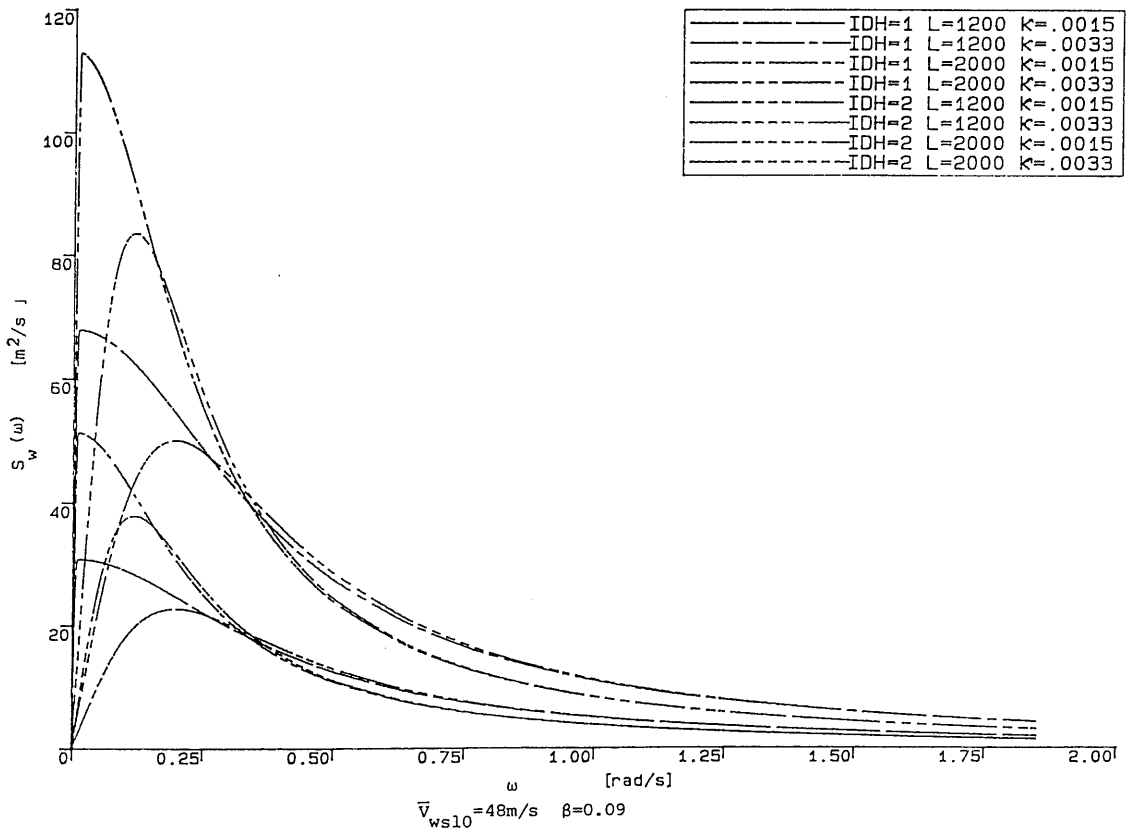

IDH=1 : Harris wind velocity spectrum; IDH=2 : Davenport wind velocity spectrum

Fig. 2.4 energy spectrum of gusty wind velocity[ref. 45,46]

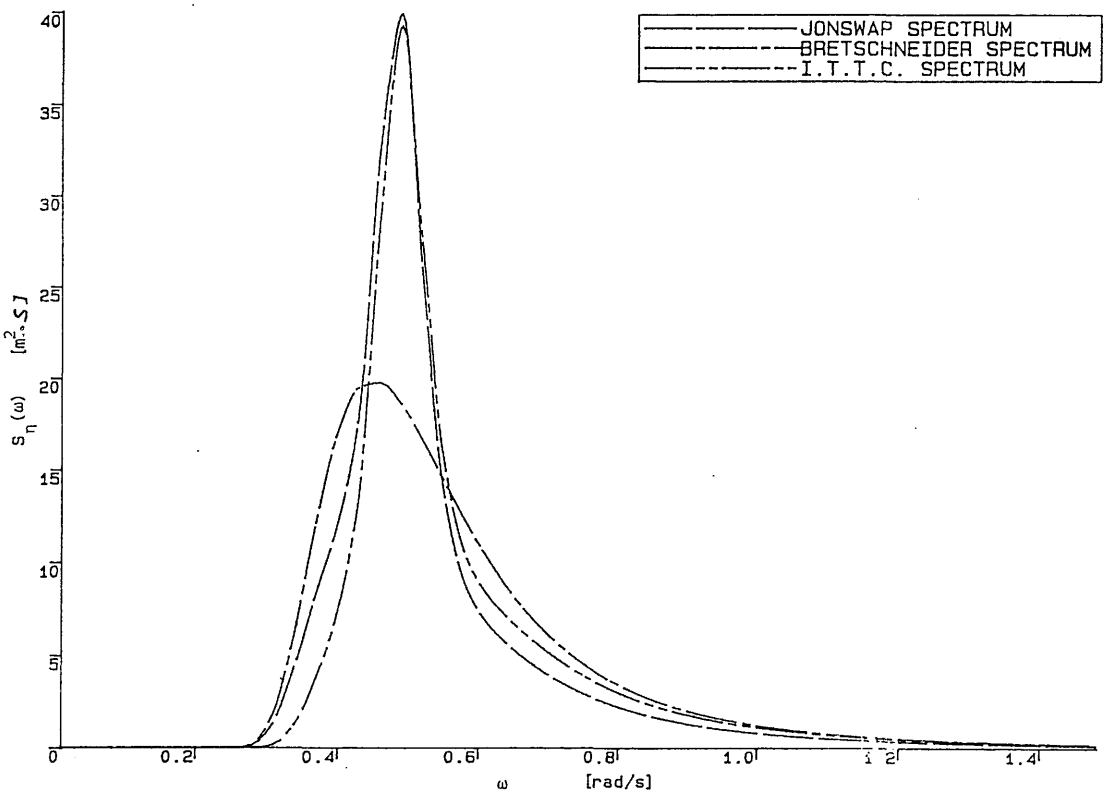

Fig. 2.5 wave height spectrum

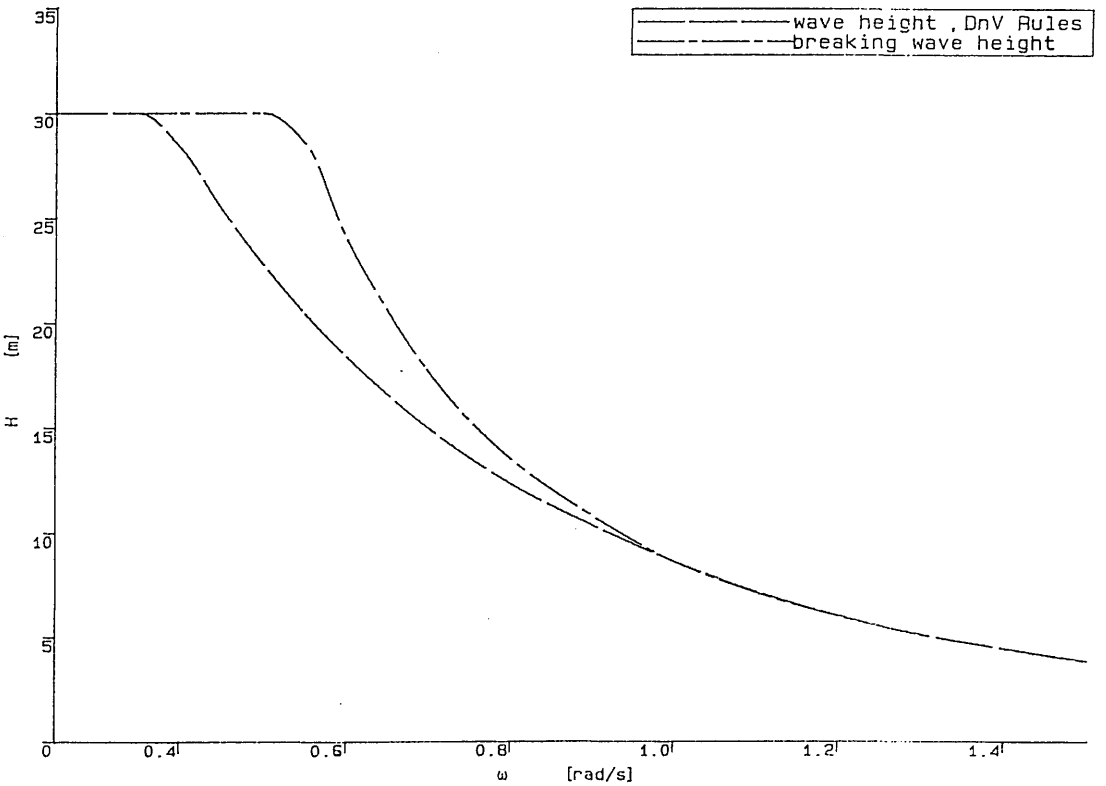

Fig. 2.6 variation of wave height with wave frequency

Table 2.1 recommendd environmental conditions by classification societies

		Extreme environmental conditions (1 in 100 yrs)	Normal operational condition (12 per yrs)
WATER DEPTH			
Water depth at LAL	(meters)		
Highest astronomical tide	(meters)		
Storm surge	(meters)		
RANDOM WAVES			
Significant wave height, H_s	(meters)	14.0-17.0	8.0-10.0
Zero up crossing period, T_z	(secs)	11.0-15.0	6.0-10.0
period of spectral peak, T_p	(secs)		
spectral type		Bretschneider I.T.T.C. I.S.S.C Jonswap	
DETERMINISTIC WAVES			
Wave height, H	(meters)	30.0	13.0-17.0
Wave period, T	(secs)	14.0-21.0	10.0-15.0
H-T relationship(DnV Rules)		$H=\begin{cases}\frac{0.22T^2}{T^2} & T\leq 6s\\ \frac{T^2}{4.5+0.02(T^2-36)} & T>6s\end{cases}$	($H\leq 30m$)
RANDOM WIND			
Spectral type		Davenport/ Harris	Davenport/ Harris
Reference length, L	(meters)	1200-2000	1200-2000
sea surface roughness ratio, κ		0.0018-0.0033	0.0018-0.0033
Hourly mean wind at 10m $\bar{V}_{wlhr10}$	(m/sec)	41.0	30.0
Profile exponent, β		0.0	0.0
MEAN WIND			
Sustained wind velocity at 10m, $\bar{V}_{ws10}$	(m/s)	48	35
Profile exponent , β (α is given in Table 2.2)		0.075 - 0.125	0.075 - 0.125
CURRENT			
Tide driven velocity, V_{ct}	(m/sec)	0.5	0.5
Wind driven velocity, V_{cw} (at surface)	(m/sec)	0.8	0.6
total velocity, V_c	(m/sec)	$V_c=V_{ct}+V_{cw}$	
profile		V_{ct}=constant, $V_{cw}=0.017\bar{V}_{ws10}\frac{50-d+z}{50}$ $d>z>d-50$	
Interaction coefficient For wave and current		$C_m=0.5-1.0$ $C_d=0.7-1.0$	
For wind		$C_{da}=0.6-0.9$ for support column $C_{da}=1.0-2.0$ for upper deck	

Table 2.2 factors for wind profile (ref.51)

factor	averaging time interval		
	1 hr	1 min (sustained)	3 s (gust)
α	.85	1.0	1.13
β	.126	.09	.076
$\bar{V}_{wlhr10}$		41 m/s	

CHAPTER 3

CONCEPTUAL DESIGN AND STRUCTURAL STRENGTH ESTIMATION OF ARTICULATED TOWER STRUCTURES

1. INTRODUCTION

This chapter deals with the structural strength of large diameter cylindrical columns. This is aimed at the structural design and strength estimations of articulated tower structures which are composed of large diameter columns.

Firstly, certain conceptual design considerations for the major components of an articulated tower are discussed. The effects of related parameters are argued qualititatively. Quantitative examination of their effects is carried out in Chapter 8. These factors are associated with the structural strength, overall design, construction and installation of articulated tower structures in general. Specific problems which are likely to be encountered in a particular design practice need specific treatment and are not covered here.

Secondly, on the structural strength of offshore structures, DnV Rules [58] are chosen for the present structural design purpose. The structural strength formulation has been computerised and used subsequently and a structural weight optimisation carried out. Two non-linear programming techniques are used: the simplex technique [59,60] and the flexible tolerance technique [61]. The objective function is the structural weight which is to be minimised. The flexible tolerance technique is programmed at present in a general

sense and is adopted for the purpose of structural weight optimisation.

2. CONCEPTUAL DESIGN CONSIDERATIONS

For the time being, a monolithic single articulated tower is considered to be composed of six major components ($N_e = 6$), as shown in fig. 1.1. The design of the whole structure can be divided into the design of the above water part and submerged part of the structure. However, it is logical to consider the structure, part by part.

2.1. Design of the Upper Deck

The upper deck is designed to accommodate the deck payload composed of necessary machinery, equipment, personnel and the short term supply, etc to fulfill the purpose for which the whole structure is designed.

The payload may vary over a wide range, depending on factors such as the application of the structure, the environmental conditions in situ and the characteristics of the oilfield. The deck payload may vary from virtually zero for the application of the structure as a flare tower to 3000-4000 tonnes for loading and production platforms. For other purposes, even larger payloads may be required.

Once the deck payload is known, the deck shape and internal space can be determined. The shape of the deck, conventionally, has been rectangular. However, there are incentives for a circular deck to be used in the present case, due to possibly less wind drag effect and advantageous weathervaning offered to offloading oil tankers.

However, a rotatable arm may also be mounted on a rectangular deck to provide the weathervaning ability without much difficulty. The advantage of a circular deck from the wind loading point of view may also be in doubt. First of all, a circular deck renders the use of the deck space inefficient compared with that of a rectangular deck. To obtain the same amount of effective deck space, the space of the circular deck may have to be enlarged. The enlarged deck attracts more wind loading, offsetting the reduced wind loading due to the use of the circular deck, partially or completely. What is more, the real deck structure, either circular or rectangular, has many level structures. The wind drag coefficient may not be very much different unless otherwise confirmed by the model test data. Therefore, a rectangular deck is used throughout the thesis.

In determining the deck space needed to accommodate the given payload, some data is available from the existing semi-submersibles [62] but very little is available from conventional fixed platform design or compliant platform design. For the present study, a ratio of α_{vw} = $5m^3/t$ and $10m^3/t$ between the deck space and the payload is assumed, with the maximum space being limited to $30,000m^3$. When the deck space is small a one-storey deck may be sufficient. Otherwise a multi-storey deck is necessary. Increase of deck height increases the windage area and therefore, the wind loading. The clearance of the deck, however, is likely to decrease with the deck height although the height of the centre of gravity of the deck payload is likely to increase. In practical terms, one-storey height cannot be less than 3m.

The deck clearance is given, from fig. 1.1, as:-

$$h_c = \frac{1}{1 - \frac{1}{2}\theta_\Sigma}\left(\frac{1}{2}H + g_a + \frac{1}{2}d\theta_\Sigma^2 + \frac{1}{2}\theta_\Sigma\sqrt{\frac{\alpha_{vw} W_o}{3n_d}}\right) \qquad (3.1)$$

H is taken to be 30m, the 100yr return design wave height.

2.2. Determination of the Upper Column Dimensions

The dimensions of the upper column are likely to be governed by the structural strength requirements. It should provide sufficient support to the deck, avoiding buckling of the column due to large axial compression and withstanding sectional shear and bending as well as wave slamming impact being avoided.

It is also to provide an adequately large dry access to the buoyancy chamber when the chamber is utilised to accommodate some of the machinery and equipment. Effective use of the space inside the buoyancy chamber has to be made, where technically feasible, to reduce the payload located on the deck and, therefore, the deck space. This not only has the advantage of possibly reducing the wind loading on the deck but also that of lowering the centre of gravity of the structure. A typical minimum diameter for dry access is taken to be 4m which, according to the DnV rules [29], leads to a minimum diameter of the upper column of 7m, (fig. 3.1).

The variation of both the upper column dimensions and the wall thickness affect its material weight and external loadings which, due to its high position above the articulated joint, have a significant impact on the structural response and the internal sectional forces. In this respect the minimum wall thickness, determined by the minimum structural strength requirements may not always be preferable, as demonstrated in Chapter 8.

2.3. Use of the Buoyancy Chamber

Fundamentally the buoyancy chamber is to provide the necessary buoyancy force to keep the tower close to its upright position in all conditions. Therefore, the chamber will not only have to be large enough but will have to be designed also against possible damage and loss of buoyancy.

For this purpose, an inner chamber is to be used together with vertical and horizontal bulkheads to divide the buoyancy chamber into small compartments, limiting the amount of flooding. The inner chamber can be safely designed to withstand the static pressure in the case of flooding of the outer chamber. From this point of view, a circular cylinder should be used as the inner chamber as a cylindrical shell can most effectively resist external pressure. Furthermore, the worst possible damage flooding, the flooding of four adjacent compartments, is thought to be representative as shown in fig. 3.1.

Those parameters defining the dimensions and position of the buoyancy chamber are very important owing to the significance of the buoyancy and structural weight of the chamber, especially in shallow waters. The effects of the variation of those parameters on the characteristics of the structure needs to be carefully examined.

Because of the pressure difference between the top and bottom surface of a shallowly submerged large buoyancy chamber, the heaving force is very considerable. This imposes severe cyclic loading on the articulated joint.

To reduce the heaving force the buoyancy chamber has either to be deeply submerged or to be streamlined in geometry. However, deep

submergence provokes penalties in terms of buoyancy efficiency and cannot substantially reduce the heaving force. To balance the pressure difference the exposed areas on the top and bottom of the chamber need to be reduced and enlarged, respectively. This leads to the use of a frustrum buoyancy chamber as indicated by the dashed lines in fig. 3.2. It is demonstrated in Chapter 9 that a frustrum chamber with a small taper angle can reduce the heaving force markedly without giving rise to any particular fabrication difficulties.

2.4. The Lower Column Dimensions

As the lower column is always under severe internal sectional loading, it must have sufficient structural strength. In addition, as the water depth increases, not only does the external hydrostatic pressure becomes increasingly great, but the lower column also becomes increasingly slender in terms of its diameter over length ratio. Therefore, the total structure becomes increasingly flexible.

Beyond a certain limit of water depth, the natural frequency of FMV motion will become unacceptably low. To prevent significant resonant FMV motion, either the diameter must be increased or the length of the lower column reduced.

However, the variation of its length depends primarily on the variations of the water depth. The only effective means is to increase its diameter. The limit of the water depth is reached when either the weight of the structure is increased so much by the increase in the lower column diameter that it is no longer technically or economically viable, or when the natural frequencies of FMV motion no longer increases with its diameter. This is examined in Chapter 4.

A potential dry access route into the base structure may also be provided by the lower column, facilitating the inspection and maintenance of the deeply submerged part of the structure which would otherwise be very difficult and/or costly to maintain. Alternatively, the lower column could be flooded or partially flooded, thus reducing the pressure on it and, consequently, the structural strength requirements. In doing so, the structural response is affected.

The flow and control lines can be located inside the column to the upper deck, alleviating the problems associated with riser design as the risers are protected by the column. This arrangement, together with a dry access, is expected to improve the inspection and maintenance economics over an oilfield's lifetime compared with 'wet' procedures. However, it calls for a very careful design to avoid potential damage to the risers inside and oil and gas leakage which will cause serious problems. Ventilation and other practical matters need to be carefully considered.

2.5. Use of the Ballast Chamber

The ballast chamber is located at the bottom of the lower column. This facilitates the addition of ballast if required. The following aspects may make the addition of the ballast chamber necessary:-

a. installation and relocation of the structure,

b. free floating stability considerations,

c. reduction of downtime, and

d. reduction of the tensile force on the articulated joint.

The procedures for installation, pullout and relocation of the structure involve controlled ballasting and/or deballasting. This may be done by pumping drilling mud or other ballasting materials in or out of the ballast chamber. Because of this, a steel ballast chamber would be preferable and is used throughout at present.

The free floating stability of the structure has proved to be a very important factor [9] and must be considered in design practice. The basic requirement is that the mass of the ballasting material inside the ballast chamber should render the structure hydrostatically stable in the case of joint failure and some secondary anchoring should be available.

In the intact condition, the structure is hydrostatically stable without ballasting, ie:-

$$K_{\ell} = V_{\Sigma} h_{cb} - W_{\Sigma} h_{cg} > 0 \qquad (3.2)$$

even if $h_{cb} < h_{cg}$ as $V_{\Sigma} > W_{\Sigma}$ in this case. By adding sufficient ballasting, the necessary free floating stable condition defined by $h_{cb} > h_{cg}$ can be obtained when the structure is freely floating. In doing so the axial tension on the articulated joint, $T_s(z_1) = V_{\Sigma} - W_{\Sigma}$ is reduced. However, $K_{\ell} > 0$ and $h_{cb} > h_{cg}$ in the intact condition does not always mean that the structure is stable in the free floating condition. The stability criteria are outlined in section 8.9 of Chapter 8.

THe position of the ballast chamber can vary slightly but must be close to the articulated joint. This affects the ballasting

efficiency and internal sectional forces in the main, as is demonstrated in Chapter 8.

2.6. The Design of the Articulated Joint

The articulated joint functions as a universal joint to allow the structure to undergo motions in any direction without transferring the bending to the seabed. It is also used as a permanent anchorage. Therefore, the transfer of the structural forces (shear and axial tension) and the crude oil/gas between the seabed and the structure has to be achieved. The transfer of hydrocarbons across the joint also calls for a flexible riser attachment and conductors designed to take on the bending stress.

The area around the joint can be very congested if many wells are required, limiting access for inspection. If the risers are led through, special care has to be taken to avoid leakages and procedures for replacement have to be worked out. Past experience has demonstrated, to a great extent, that the articulated joint is one of the most vulnerable parts of the structure. Therefore, the design has to ensure that the need for maintenance of the moving parts of the joint is kept low due to the difficulties and the cost involved in its inspection and maintenance. In addition, secondary mooring auxiliary to the articulated joint will have to be provided.

2.7. Local Reinforcement

Some parts of the structure need to be reinforced locally where geometrical discontinuity occurs and where the stress concentration factor is high. Those parts are typically near the

junctions between the different column sections as shown in fig. 1.1.

For an idealised physical model, the reinforcement is omitted together with its effect, such as the addition of material weight to the structure. In the response analysis, allowance can be made to take into account this material weight.

3. STRUCTURAL STRENGTH OF LARGE DIAMETER THIN SHELL CYLINDRICAL COLUMNS

Circular cylinders can be classified into two categories: large diameter internally stiffened cylinders to which the thin shell assumptions apply and small diameter cylinders, mainly for the trusses on an articulated tower structure.

At present the strength calculations are confined to internally stiffened cylinders with large diameters. There are certain design codes available for this purpose, such as BS5500 [63], which mainly deals with the strength of cylindrical pressure vessels, RCC rules [64] for the structural design of TLPs, and DnV rules [58] which are the most comprehensive. DnV rules are adopted and are computed in this section.

3.1. Characterisation of Cylinder Cross Sections

The characterisation of the cylinder cross section includes defining the dimensions of the cylinder cross section and of the stiffener cross sections, calculating the sectional forces (including moments) on the cross section and estimating the sectional stresses.

The cross section is characterised in the table below

Independent Parameters

$R, t, b, t_f, h, t_w, \ell, s, L$

Derived Parameters

Cross sectional area of stiffener: $A_{r,s} = h\, t_w + b\, t_f$

A_r is for ring frame and A_s is for stringer

total solid area of cylinder cross section

$$A = \begin{cases} 2\pi Rt + nA_s & \text{for SSCs and OSCs} \\ 2\pi Rt & \text{otherwise} \end{cases}$$

enclosed cross sectional area: $A_o = \pi R^2$

moment of inertia of A about principal axes of cross section

where

$$I_{x,y} = \begin{cases} \tfrac{1}{2}I_o + I_\Sigma & \text{for SSCs and OSCs} \\ \tfrac{1}{2}I_o & \text{otherwise} \end{cases}$$

where $I_o = \tfrac{1}{2}\pi[(R + \tfrac{1}{2}t)^4 - (R - \tfrac{1}{2}t)^4]$

$$I_\Sigma = \tfrac{1}{2}n(I_p + I_q) + \tfrac{1}{2}(I_p - I_q) \sum_{i=1}^{n} \cos \frac{4\pi i}{n} + A_s(R - \tfrac{1}{2}t - g_e)$$

$$\times \sum_{i=1}^{n} \sin^2 \frac{2\pi i}{n}$$

$$n = \begin{cases} \text{Integer } [\frac{2\pi R}{s}] & \text{for SSCs and OSCs} \\ \text{Integer } [\frac{L}{\ell}] + 1 & \text{otherwise} \end{cases} \qquad (3.3)$$

effective width of shell plating accounting for the effect of ring stiffener attachment to the shell

$$\ell_{ef} = 1.56\sqrt{Rt} \quad (\ell_{ef} \leq \ell)$$

Material property

Young's modulus : E (= 2×10^{11} - 2.1×10^{11} N/m^2 for steel)

Poisson's ratio : ν (typically = 0.3 for steel)

material resistance : f (yield stress)

A cylinder of a given length can be divided into several bays by transverse bulkheads. Within the length of a single bay, the cylinder can be stiffened by rings, stringers or both, denoted as RSC, SSC and OSC, respectively. The cylinder may even be unstiffened. It is assumed that it is stiffened by uniformly spaced stiffeners, although in reality, the stiffener spacings do not have to be the same, eg in the case of equal strength design. Furthermore, the characterisation is based on a single bay with the most severe sectional loading along the length of the cylinder. The stiffening pattern details of the stiffener cross section (T bar) are shown in fig. 3.3.

3.2 Representation of the Sectional Forces

The general loading condition governing the stresses in a closed cylinder is represented by the following quantities:-

the overall axial force, N,

the overall bending moment acting about the principal axis, x, M_x and about the principal axis, y, M_y,

the lateral pressure, P,

the overall torsional moment, T, and

the overall shear force acting normal to the principal axis x, V_x and the principal axis y, V_y.

At different sections along the length of the bay the above quantities may be different. They are assumed to be the maximum values at the section. However, it is stressed that the design values of the sectional forces do not always correspond to the design dynamic

loading condition at sections along the length of an articulated tower as is demonstrated in Chapter 5.

In addition, P may be a function of angular co-ordinate θ, measured from x axis anti-clockwise. It is always to be taken as the difference between internal and external absolute pressure. The sign for the sectional forces has to be defined. The axial force is defined such that the tensile force is positive. The moments are signed according to the right-hand principle. The lateral pressure is taken positive outwards. The shear force is signed according to its direction in relation,to the direction of the axes.

3.3. Stresses on the Cross Section

The direct stresses at an arbitrary point of the shell plating, due to any or all the above loadings, are completely defined by the following three stresses:-

a. The direct stress in the longitudinal direction, σ_z.

b. Direct stress in the circumferential direction, σ_θ and,

c. The direct shear stress, acting tangential to the shell surface (in sections intersected by planes z = constant and θ = constant) along z axis, $\tau_{z\theta}$.

σ_z is due to the axial force and/or bending moment. σ_θ is due to lateral pressure and $\tau_{z\theta}$ is due to the shear force and/or torsion.

They are calculated in the table below.

Design σ_z : $\sigma_{zd} = \sigma_{znd} + \sigma_{zmd}$ (3.4)

axial stress due to axial force

$$\sigma_{znd} = \frac{N}{A}$$

axial stress due to bending

$$\sigma_{zmd\theta} = \frac{M_x}{I_x} R\cos\theta + \frac{M_y}{I_y} R\sin\theta$$

$$\sigma_{zmd} = \max(\sigma_{zmd\theta}) = R\left[\left(\frac{M_x}{I_x}\right)^2 + \left(\frac{M_y}{I_y}\right)^2\right]^{\frac{1}{2}}$$

acting with direction angle $\theta_m = \tan^{-1}\left(\frac{M_x I_y}{M_y I_x}\right)$

Design σ_θ : $\sigma_{\theta d} = \frac{PR}{t}$ for SScs OSCs (3.5)

$$\sigma_{\theta d} = \left(\frac{PR}{t} - \upsilon\sigma_{znd}\right)\frac{1.56t\sqrt{Rt}}{A_r + 1.56t\sqrt{Rt}} + \upsilon\sigma_{znd} \quad \text{otherwise} \quad (3.6)^{[58]}$$

in the shell at the ring stiffener of RSCs and

$$\sigma_{\theta d} = \frac{P}{P_{c5}} f_y \quad (3.7)^{[64]}$$

$$P_{c5} = \frac{f_y t}{R(1-\gamma G)}, \quad \gamma = \frac{A_b(1-\upsilon)}{(A_b + t_w t)(1+B)}, \quad A_b = A_r\left[\frac{R}{R - t - g_e}\right]^2,$$

$$B = \frac{2t\,N_a}{\alpha(A_b + t\,t_w)}, \quad N_a = \frac{\cosh\alpha\ell - \cos\alpha\ell}{\sinh\alpha\ell - \sin\alpha\ell}, \quad \alpha\ell = \frac{1.285\ell}{\sqrt{Rt}}$$

$$G = 2\,\frac{\sinh\frac{\alpha\ell}{2}\cos\frac{\alpha\ell}{2} + \cosh\frac{\alpha\ell}{2}\sin\frac{\alpha\ell}{2}}{\sinh\alpha\ell + \sin\alpha\ell}$$

Design $\tau_{z\theta}$: $\tau_{z\theta d} = \tau_{ztd} + \tau_{zvd}$ (3.7)

shear stress due to shear force

$$\tau_{zvd\theta} = \frac{\beta_a}{2\pi Rt} (V_x \cos\theta + V_y \sin\theta), \quad \tau_{zvd} = \max(\tau_{zvd\theta})$$

(the shear coefficient of the cross section $\beta_a = 2$ for circular section)

shear stress due to torsional moment

$$\tau_{ztd} = \frac{T}{2A_o t}$$

In calculating the circumferential stress, P is assumed to be constant (gas pressure) or a sine or cosine function of θ (liquid pressure). In addition, the presence of stringers is ignored in calculating the stress due to shear force and simple beam theory is used to obtain direct design shear stress.

3.4 Strength of Cylindrical Shells

The strength calculation in the DnV Rules covers beam frames and plane unstiffened and stiffened plates as well as stiffened and

unstiffened cylindrical shells. Characteristic strengths and interaction formulae are provided to give guidance for proportioning member sizes where instability is the governing structural constraint.

Not all potential cylindrical shell buckling modes are explicitly considered. Only those relating to curved panels, ring-stiffened, unstiffened cylinders and cylindrical beam columns are dealt with. They are assumed to be subjected to generalised sectional loading. An orthogonally stiffened cylinder is also covered in the DnV Rules and can easily be adopted but it is excluded at the present.

4. GENERAL NON-LINEAR PROGRAMMING PROBLEMS

A brief statement of the general non-linear programming problem is made in this section, followed by the introduction of the two algorithms to be employed for the present study, namely, the simplex technique and the flexible tolerence technique.

The problem can be stated mathematically as:-

$$\begin{cases} \min f(\vec{X}) \\ \vec{X} \in \Omega \\ \Omega = \{\vec{X} \mid g_j(\vec{X}),\ j = 1,2\ldots\ldots,\ p\} \in U^n \end{cases} \tag{3.10}$$

meaning that the objective function $f(\vec{X})$ is to be minimised in terms of variable vector $\vec{X}$ in the feasible region Ω defined by constraints $g_i(\vec{X})$. $g_i(\vec{X})$ are non-linear functions of $\vec{X}$ and the problem is called a constrained non-linear programming problem. Without these constraints, it is called unconstrained non-linear programming. $\vec{X}$ is defined in n-D Euclidean space U^n.

The constrained problem is normally transformed into an equivalent unconstrained problem so that it can be treated after transformation in the same way as unconstrained problems.

In addition, it is assumed that there is at least one solution to the problem. It is so required because, in fact in most practical cases, $f(\vec{X})$ may have several 'local' minima, one of the common problems with non-linear programming. The flexible tolerence technique to be introduced is claimed [61] to be more effective in avoiding sticking at 'local' minima to reach the 'global' minimum.

Three types of constraints are encountered in general. They are equality constraints, inequality constraints and range constraints expressed, respectively, as:-

$$h_j(\vec{X}) = 0 \qquad j = 1,2....,p_1$$

$$g_j(\vec{X}) > 0 \qquad j = p_1 + 1.....,p_2$$

$$\text{and } a < g_j(\vec{X}) < b \qquad j = p_2 + 1....,p_3 \tag{3.10}$$

The equality and range constraints can be transformed into inequality constraints. For example, an equality constraint $h_j(\vec{X}) = 0$ can be expressed as two inequality constraints, $h_i(\vec{X}) \leqq 0$ and $-h_i(\vec{X}) \geqq 0$. Nevertheless,the effects of the three types of constraints may not always be the same. The equality constraints are the most rigorous and difficult to satisfy. The range constraints are next and the inequality constraints are the easiest to satisfy in general. Some of the non-linear programming techniques may not be applicable to problems with a large number of equality constraints.

First of all, algorithms applicable to unconstrained non-linear programming problems are roughly classified into two categories - one where the information from the derivatives of the $f(\vec{X})$ is needed and, the other where only the information about the $f(\vec{X})$ itself is needed. The former is omitted here due to its rigorous requirement on the objective function.

The overall strategy in the second category is very much the same although the tactics may vary from one algorithm to another, ie based on direct search by varying the variables, smaller values of the objective function keep on replacing the present value till the minimum is reached. The difference in tactics lies in the way in which the variables are varied, varying one variable at a time till the optimum of $f(\vec{X})$ in this direction is reached, or varying all the necessary variables, with the direction changing systematically.

The two algorithms, based on direct search are subsequently used in the flexible tolerence technique. The first one is termed as the Golden section technique [67] which is a uni-dimensional direct search technique. The other is termed the simplex technique [59].

The constrained problem becomes an unconstrained problem after transformation, expressed as:-

$$F(\vec{X}) = f(\vec{X}) + \mu T(\vec{X}) \tag{3.11}$$

where $F(\vec{X})$ is called the penalty function which is the objective function added with a penalty term $T(\vec{X})$, μ is a constant, $T(\vec{X})$ is a function of the constraints defined such that $T(\vec{X}) = 0$ when all the constraints are satisfied and $T(\vec{X}) > 0$ otherwise. The expression for $T(\vec{X})$ often varies deliberately for a particular algorithm. In flexible

tolerence technique, $T(\vec{X})$ is defined as:-

$$T(\vec{X}) = +\left(\sum_{i=1}^{p_1} h_i^2(\vec{X}) + \sum_{i=p_1+1}^{p} \mu_i g_i^2(\vec{X}) \right)^{\frac{1}{2}} \qquad (3.12)$$

μ_i is the Heaviside operator defined as $\mu_i = 0$ if $g_i(\vec{X}) > 0$ and $\mu_i = 1$ otherwise. It is seen that $T(\vec{X})$ is the root mean square value of all the violated constraints. $T(\vec{X}) = 0$ when all the constraints are satisfied and $T(\vec{X}) > 0$ otherwise. The equivalence of the transformed unconstrained problem to the original constrained problem is ensured by the fact that $F(\vec{X})$ and $f(\vec{X})$ have the same optimum on satisfying the constraints.

The constrained optimisation problem after transformation into an unconstrained problem, represented by equation (3.11), can be solved by using the simplex technique. In the flexible tolerance technique, however, the penalty on violating the constraints is not added to the objective function. The search for the optimum is carried out directly, according to the values of the objective function. The conditions with regard to the satisfaction of the constraints under which the search is carried out is slack at the beginning and is tightened gradually in the search process. As a result, less computation time is spent at the beginning on satisfying rather rigorous feasibility requirements.

Finally, scaling of the problem is necessary in most cases, to advance the search process towards its solution efficiently. The scaling of the constrained problem is threefold: scaling between x_i of vector $\vec{X}$, between constraints and between $f(\vec{X})$ and $T(\vec{X})$ so that, after scaling, x's vary in about the same order relative to each other, constraints vary in about the same order to each other as does $f(\vec{X})$ to $T(\vec{X})$.

5. STRUCTURAL WEIGHT OPTIMISATION

Using the non-linear programming technique, outlined in the previous section, the minimum structural weight of a stiffened/unstiffened cylinder was calculated in the case of the cylinder subjected to general sectional loading. Again, the cylinder can be unstiffened, ring-stiffened or stringer-stiffened.

5.1. Identification of the Design Variables

The independent parameters are listed previously in section 3. Apart from the cylinder radius being specified all the other parameters can be regarded as free design variables.

The bulkhead spacing, L, is to be specified according to the damage control requirements and only a discrete number of possible ring/stringer spacings may be used. Therefore, there is only one variable for an unstiffened cylinder, its shell thickness t. For a stiffened cylinder, the number of the variable can be 2, ie t and ℓ or s, if the dimensions of the stiffeners are specified according to the relevant design codes, or 6 at most.The values of the geometrical parameters defining the cross sectional dimensions of the stiffeners, obtained on finishing the structural weight optimisation, are to be rounded up to the nearest values of the stiffener dimension in the relevant design codes.

5.2. Composition of the Objective Function - The Structural Weight

The structural weight is clearly a function of the above

variables and is taken to be the objective function in the non-linear programming to be minimised. It is calculated for a single bay between bulkheads. It is given in the table below:-

Weight of shell plating between bulkheads:

$$W_1 = 2\pi\rho_s g\ R\ t\ L \tag{3.13}$$

Weight of web of the stiffeners:

$$W_2 = n\pi\rho_s g\ \ t_w \left[(R - \tfrac{1}{2}t)^2 - (R - \tfrac{1}{2}t-h)^2\right] \tag{3.14}$$

n is given in equation (3.3)

Weight of flange of the stiffeners:

$$W_3 = \begin{cases} 2n\pi\rho_s g\, b\, t_f (R - \tfrac{1}{2}t_f - \tfrac{1}{2}t - h) & \text{for RSCs} \\ n\rho_s g\, L\, b\, t_f & \text{for SSCs} \end{cases} \tag{3.15}$$

Total weight:

$$W_{\Sigma s} = \begin{cases} \sum_{i=1}^{3} W_1 & \text{for a stiffened cylinder} \\ W_1 & \text{for an unstiffened cylinder} \end{cases} \tag{3.16}$$

In the program, the structural weight is scaled to $W_{\Sigma s}$ as:-

$$W = \frac{W_{\Sigma s}}{2\pi R t_o L \rho_s g} \tag{3.17}$$

t_o is the initial value of t so that W is about 1.0. In addition, the variables are scaled, divided by their initial values which are input to the program.

Once the minimum structural weight of an unstiffened cylinder is obtained, its corresponding equivalent shell thickness to an

unstiffened cylinder is calculated by:-

$$\bar{t} = \frac{W_{\Sigma s}}{2\pi RL\rho_s g} \tag{3.18}$$

where $W_{\Sigma s}$ is to be the minimum structural weight calculated, obviously, for an unstiffened cylinder, $\bar{t} = t$.

5.3. Constraints

The constraints are due to structural length limitations, scope of the design code and other considerations. The type and number of constraints vary.

When the dimensions of the stiffeners are specified there are only two variables: the shell thickness t and the stiffener spacing ℓ/s. The total number of constraints is four for an unstiffened cylinder, eight and nine for ring and stringer stiffened cylinders, respectively. Otherwise, there are six variables with h, t_w, b and t_f kept freely varying, apart from the above two variables. The number of constraints is sixteen for ring stiffened cylinders and thirteen for stringer stiffened cylinders.

5.4. Verification of the Program

Two programmes were written - STRUCLIB.SUBSET6 with six variables and STRUCLIB.SUBSET2 with two variables. To check the present program the same input data of forces, moments and main dimensions of the cylinder as used by Das [65] is used. The data is listed in Table 3.1. The present results are compared with the results given by Das as is shown in Table 3.2. Good agreement is achieved.

However, minute differences exist which are considered to be due to the following reasons:-

a. The radius of the cylinder is taken to be 8.86m as the mean radius for the present input data rather than 8.85m as the inner radius of the cylinder.

b. The modulus of the elasticity E is taken as $2.07 \times 10^{11} N/m^2$ against $2.05 \times 10^{11} N/m^2$.

c. The number of stiffeners between bulkheads is taken as $n = \text{Integer} \left[\frac{L}{\ell}\right] + 1$ as given by equation (3.3) against $n = L/\ell$, which is obviously unreasonable as there can only be integer number of stiffeners between bulkheads.

The last one is expected to make the most of the difference. It is noted that in obtaining the results, only the stiffener spacing ℓ or s and the shell thickness, t, are kept as free variables.

At present, the results corresponding to six free variables are obtained both for ring-stiffened and for stringer-stiffened cylinders under the given loading conditions in Table 3.1.

The minimum structural weight is 182.4 tonnes for the ring-stiffened cylinder and 181.2 tonnes for the stringer-stiffened cylinder. It is noticed that the minimum structural weight for the ring-stiffened cylinder, in this case with six free variables, is higher than that given in Table 3.2, with two free variables. This is because the values specified for h, t_f, b and t_w as given in Table 3.1, do not satisfy all the constraints which are related to the stiffener dimensions.

In addition, the structural weight optimisation with six free variables is much more time consuming to perform. In reality, the optimisation can be performed by specifying several options of the stiffener dimensions, keeping the shell thickness and the stiffener spacing freely variable. The solution is the particular one which has the minimum structural weight.

6. DISCUSSION OF THE RESULTS

Structural weight optimisation of circular cylinders is performed with two free variables, t and ℓ/s. The dimensions of the stiffeners are, h = 0.5m, t_f = 0.025m, b = 25m and t_w = 0.03m. It is also assumed that T = V =0. The external pressure throughout is expressed in terms of water depth. For example, P = 20m means that the pressure is P = 20 x 9806.4 N/m . The following conclusions are drawn from figs 3.4a and 3.4b:-

a. Stringer-stiffened cylinders have greater bending strength in general. This is represented in fig. 3.4 by the smaller structural weight of stringer-stiffened cylinders than that of ring-stiffened cylinders of the same diameters under the sectional bending. This is also represented by the slow increase of the structural weight of the stringer-stiffened cylinder compared with the ring-stiffened cylinder. When the sectional bending is very small, the strength reserve of the stringer-stiffened cylinder is greater, due to the constant stiffener dimension which should be reduced in this case.

b. In the process of structural weight optimisation of the ring-stiffened cylinder in fig. 3.4, the most difficult constraint to satisfy is imposed by the general stability requirement in equation (C3-10) of ref [58]. However, when $R = 12.5m$ and $M \geqq 20 \times 10^8$ N.m, the constraint imposed by equation (C3-14) of ref [58] becomes the dominant one. For stringer-stiffened cylinders, on the other hand, the dominant constraint is imposed by the structural strength requirement to avoid local shell buckling as defined in equation (C2-3) when M is small and by equations (C2-4) and (C2-21) of ref [58] defining the strength requirement of the lateral buckling of stringers.

c. The shell thickness obtained is between 0.02m and 0.032m. Normally, the equivalent shell thickness from the point of view of structural mass varies between 0.04m and 0.08m.

d. Under the same loading conditions, use of small diameter cylinders does not always result in smaller minimum structural weight. When the sectional loading condition is mild, the smaller the diameter is, the smaller is the structural weight provided that the cylinder diameter is not too small. When the sectional loading condition is severe, the structural weight of smaller diameter cylinders increases more rapidly until it is not possible to satisfy the constraints in which case the loading capacity limit of the cylinders is reached.

The minimum structural weight variation of stiffened cylinders with external pressure is shown in fig. 3.5. The pattern can be described as set out below:-

a. When the pressure is small, stringer-stiffened cylinders have less structural weight but when the pressure is small and the diameter of the cylinder is small, the gradient of the increase of the structural weight of a stringer-stiffened cylinder is steeper. When the pressure increases above a certain limit, the stringer-stiffened cylinder will have greater structural weight.

b. As the cylinder diameters increase, the gradient of the structural weight variation with pressure increases. This means that larger diameter cylinders are less effective to resist pressure loading.

c. The resistance capacity of ring-stiffened cylinders is higher than stringer-stiffened cylinders. The difference between the pressure resistance capacities of the ring and stringer stiffened cylinder is especially marked when the cylinder diameter is small but, as the diameter increases, the difference is reduced and the structural weight of the stringer-stiffened cylinder increases less rapidly than that of the ring-stiffened cylinder.

d. For stringer-stiffened cylinders, the dominant constraints in low and high pressure (in relation to the cylinder diameter) range are imposed by equations (C2-3) and (C2-23) of ref [58], respectively. These define the strength requirement to avoid local shell buckling and buckling of stiffeners, respectively. However, for the ring-stiffened cylinders, the dominant one is defined by the general stability requirement.

The variation of the minimum structural weight of stiffened

cylinders with the axial loading is shown in fig. 3.6. The structural weight of the ring-stiffened cylinder tends to increase linearly with N while the structural weight of the stringer-stiffened cylinder also tends to increase linearly but more slowly with N. The structural weight of the ring-stiffened cylinder is greater. The difference can be as much as 50%, as seen in figs. 3.6a and 3.6b. When the axial loading and associated external pressure is small, the strength of the stringer-stiffened cylinder is excessive. Consequently, the structural weight of the stringer-stiffened cylinder hardly changes with N in this case.

It is noticed that in the above figures, some of the curves are not ideally smooth. This is understood to be due to the fact that the non-linear programming problems are initial value dependent in general. That is to say, to obtain a particular solution for a given constrained non-linear programming problem, different initial values are tried in order to avoid sticking in a local optimum. In most cases, there are several local optimums. This problem is clearly encountered in the process of the present structural weight optimisation. There is no non-linear programming technique available yet which can always avoid thee local optima completely. Some of the existing ones are only comparatively better.

Another problem often encountered in the optimisation process is that the problem is ill-conditioned. This is normally meant in the sense that the objective function itself is mathematically defined without rigour, in which case a special non-linear programming technique is to be used to avoid the shortcomings of the objective functions. This ill-conditioning may also occur to the penalty function in the case of constrained non-linear programming problems.

Another form of ill-conditioning which can occur is that, in the case of a constrained problem, the problem may be under or over-constrained, which often occurs in the early stage of the optimisation process, because unlike purely mathematical problems, the conditions for an engineering problem may not be clearly defined. Clearly, if the problem is over-constrained, it is not possible to satisfy all the constraints. Consequently, no solution is obtained. However, if it is under-constrained, the solution is not unique. In these cases, particular attention is needed.

7. CONCLUDING REMARKS

A monolithic single articulated tower is composed of several large diameter thin shell columns which are normally circular cylinders, apart from the upper deck structure. The conceptual design of each part involves different considerations which are summarised below:-

1. The deck design includes the determination of the deck space to accommodate the given deck payload and the subsequent selection of the deck shape and deck height. Variation of the deck dimensions affects the wind loading on the deck, the deck clearance and the centre of gravity of the deck payload. The deck payload may vary from virtually zero up to 3,000-4,000 tonnes or more, depending on the type of application. The deck space should be kept as small as is possibly allowed to reduce the wind loading. However, there is no empirical relationship available between the deck payload and the deck space. In the present study, a ratio of deck space/deck payload of $5m^3/t$ to $10m^3/t$ was used, respectively, with the maximum deck space being limited to under $30,000m^3$.

2. The upper column dimensions are principally governed by the structural strength requirements. Also, in the case of utilising the space inside the buoyancy chamber to accommodate part of the deck payload, a dry access is to be provided inside the upper column. The minimum diameter in this case is thought to be 7.0m. In addition, the structural mass variation of the upper column will have considerable impact on the structural motion response and internal sectional forces.

3. The parameters defining the location and the dimensions of the buoyancy chamber are expected to be the most influential parameters owing to its functional importance. They deserve very careful examination. In addition, the buoyancy chamber is sub-divided into small compartments by an inner chamber together with vertical and transverse bulkheads, limiting the amount of maximum flooding in case of any damage to the outer chamber. A cylindrical inner chamber is appropriate for resisting external pressure. The worst flooding damage is assumed such that four adjacent compartments between the two chambers are flooded with water. Also, frustrum geometry can be utilised to reduce the heaving force.

4. The lower column, in providing a stiff anchorage, is designed to avoid possible structural failures due to inadequate structural strength and flexible vibration motion. In shallow waters the structural strength requirements are likely to be critical. However, in deep waters the structural bending stiffness is likely to be the dominant factor.

5. Use of a ballast chamber is made necessary not only by the installation and relocation of the structure but also by the stability

considerations, the reduction of the axial loading on the articulated joint and the requirement of possible built-in oil storage. To meet the stability requirements, a low position of the ballast chamber provides more efficient ballasting. However, the effect of the ballast chamber on the sectional forces is yet to be investigated.

6. The articulated joint is expected to be the most vulnerable part. Due to its deep submergence, inspection and maintenance will be very difficult. Also, the hydrocarbon transfer can be inside the articulated joint. Any structural failure, malfunction or oil leakage will cause serious problems. These factors have to be considered in the design. Secondary anchoring auxiliary to the articulated joint should be available.

7. Because of the geometrical discontinuities, on the sections between columns of different diameters along the structure, local reinforcement is necessary to avoid high stress concentration on those sections.

Based on the DnV Rules, structural weight minimisation of ring-stiffened and stringer-stiffened cylinders has been performed using non-linear programming techniques. The major conclusions are drawn from these results below.

8. Stringer-stiffened cylinders usually have less structural weight than ring-stiffened cylinders under sectional bending. Their strength is also greater in that not only do they weigh less but their structural weight increases with bending more slowly. Therefore, the bending resistance capacity of ring-stiffened cylinders is lower than stringer-stiffened cylinders of the same diameters.

9. The dominant constraint is imposed on the local shell buckling strength when the bending moment is low and is the lateral buckling strength of the stringers when the bending moment is high. For ring-stiffened cylinders under bending, the dominant constraint is the general stability requirement when the bending is low and is the minimum effective second moment of inertia requirement of the stiffener cross section associated with the effective shell thickness.

10. When the cylinder diameter is small, the minimum structural weight of the stringer-stiffened cylinder is lower than that of the ring-stiffened cylinder when the lateral pressure is fairly low. However, it tends to increase more rapidly with the lateral pressure than that of the ring-stiffened cylinder. Therefore, when the lateral pressure is high, the opposite happens. The minimum structural weight of the ring-stiffened cylinder is also greater under axial compression. In addition, it increases more rapidly with axial compression. The weight saving is also significant, especially when the axial compression is great. The variation of the minimum weight of both ring-stiffened and stringer-stiffened cylinders tends to increase linearly with axial compression.

11. The strength formulations of the DnV Rules, provides a simple and useful means to assess the structural strength and weight needed in the dynamic response analysis of articulated tower structures as well as in their practical design. But the formulations are mainly of a deterministic nature. Some are based on very conservative assumptions. Also, the tensile axial force cannot always be incorporated.

12. The two non-linear programming techniques can be complimentary in the case of the structural weight optimisation. Using the two techniques simultaneously with different initial values, the local optima are more likely to be avoided.

13. Finally, minimum structural weight is desirable from the point of view of reducing the material cost but using cylinders on an articulated tower with minimum structural weight may not always be desirable from the point of view of the motion response characteristics of the structure, in which case a compromise would have to be achieved.

There are other practical and economic considerations, apart from the above purely technical considerations. These considerations impose constraints and could be added to the non-linear programming to achieve a compromised solution.

LIST OF FIGURES

LIST OF TABLES

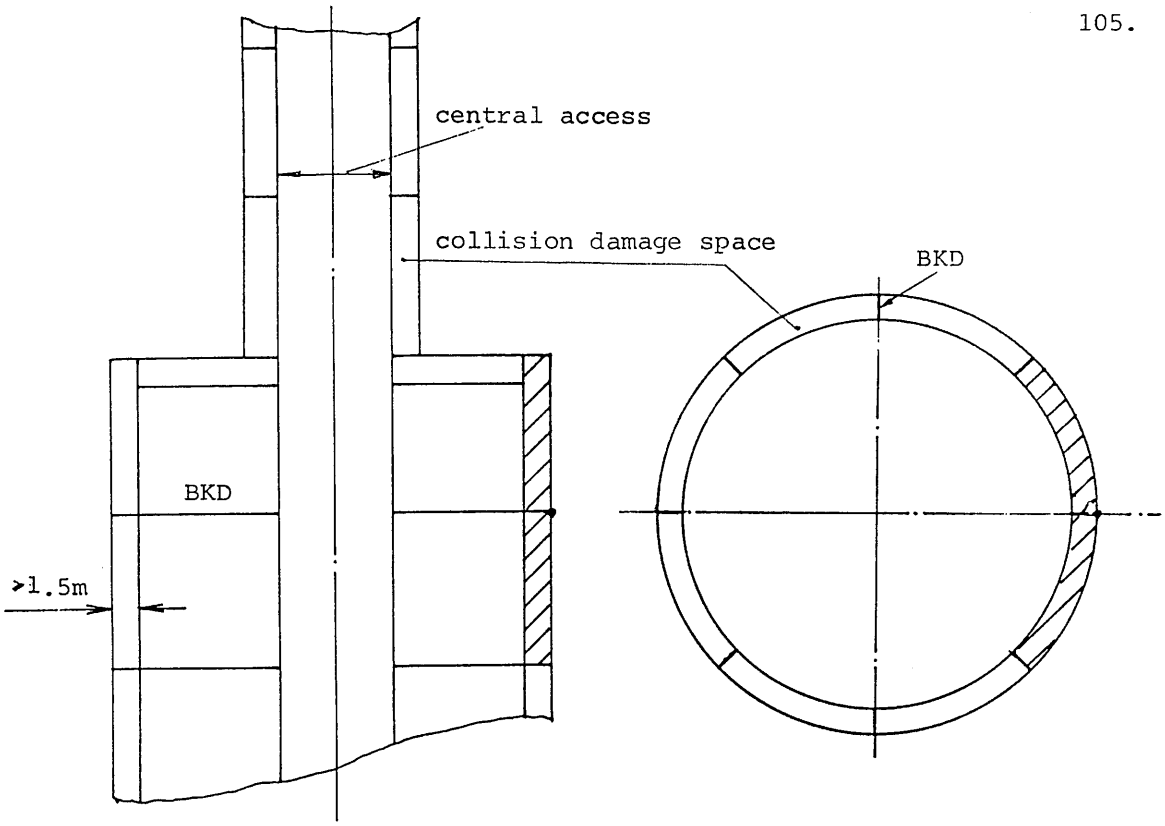

ig. 3.1 inner structural arrangement of the buoyancy chamber

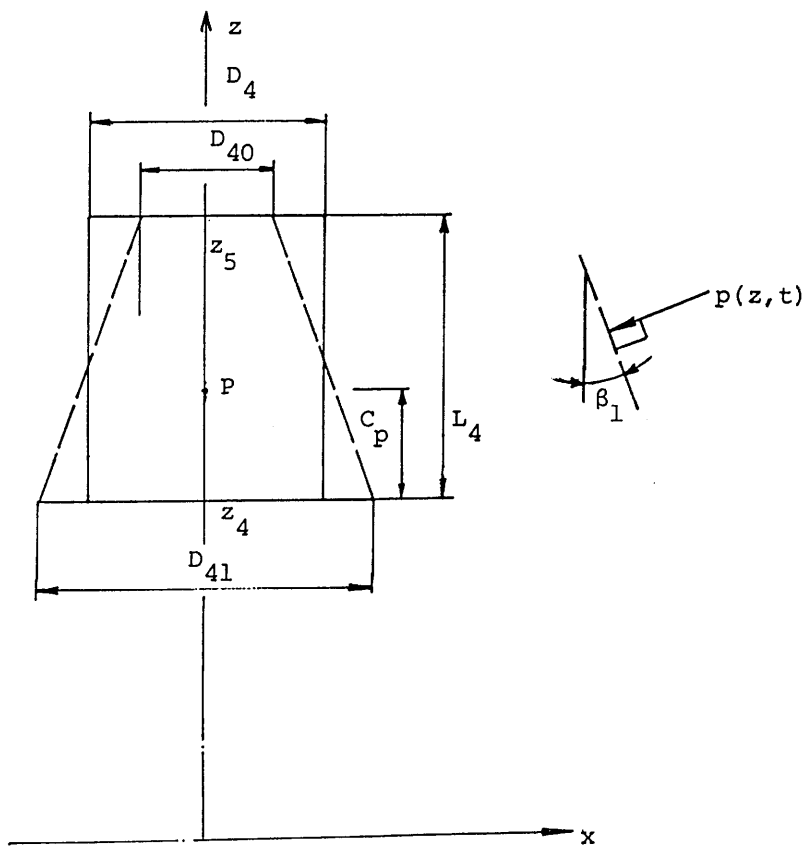

Fig. 3.2 sketch of a frustrum buoyancy chamber

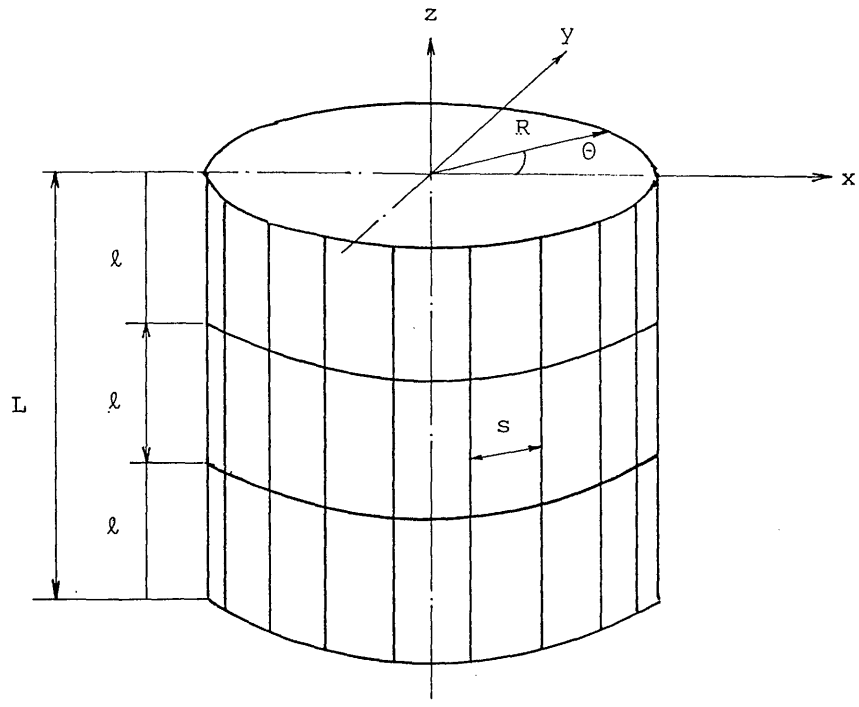

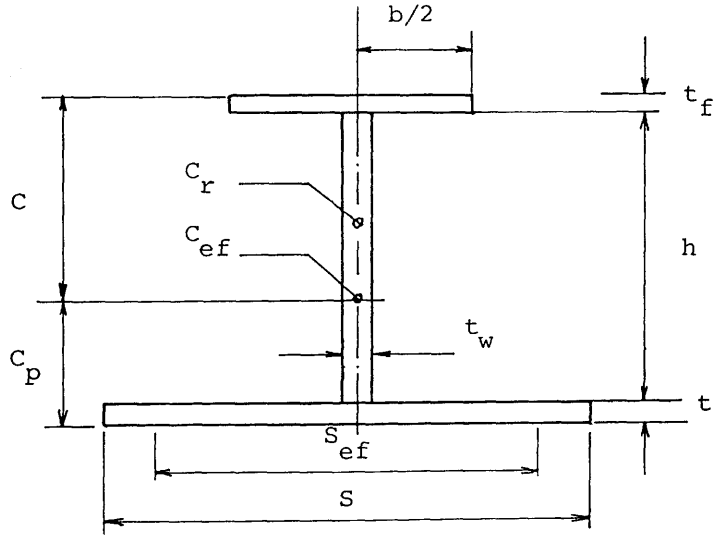

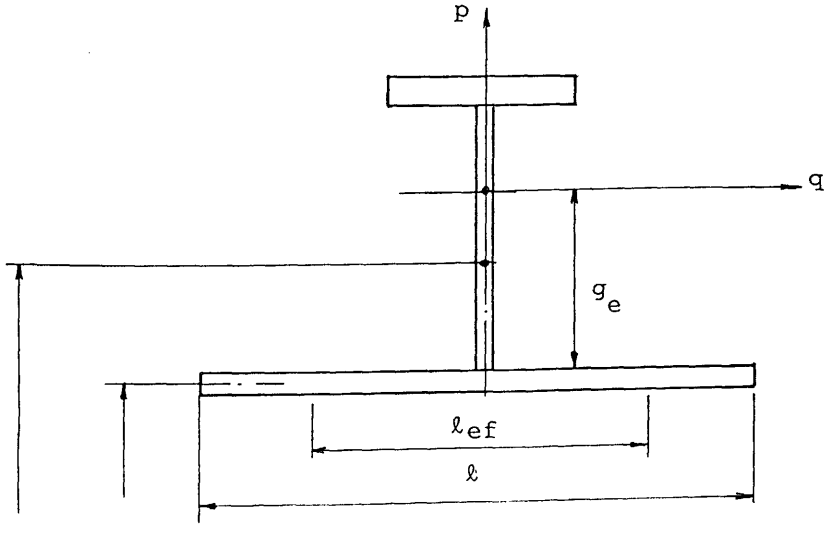

Fig. 3.3 geometrical details of stiffened cylinders

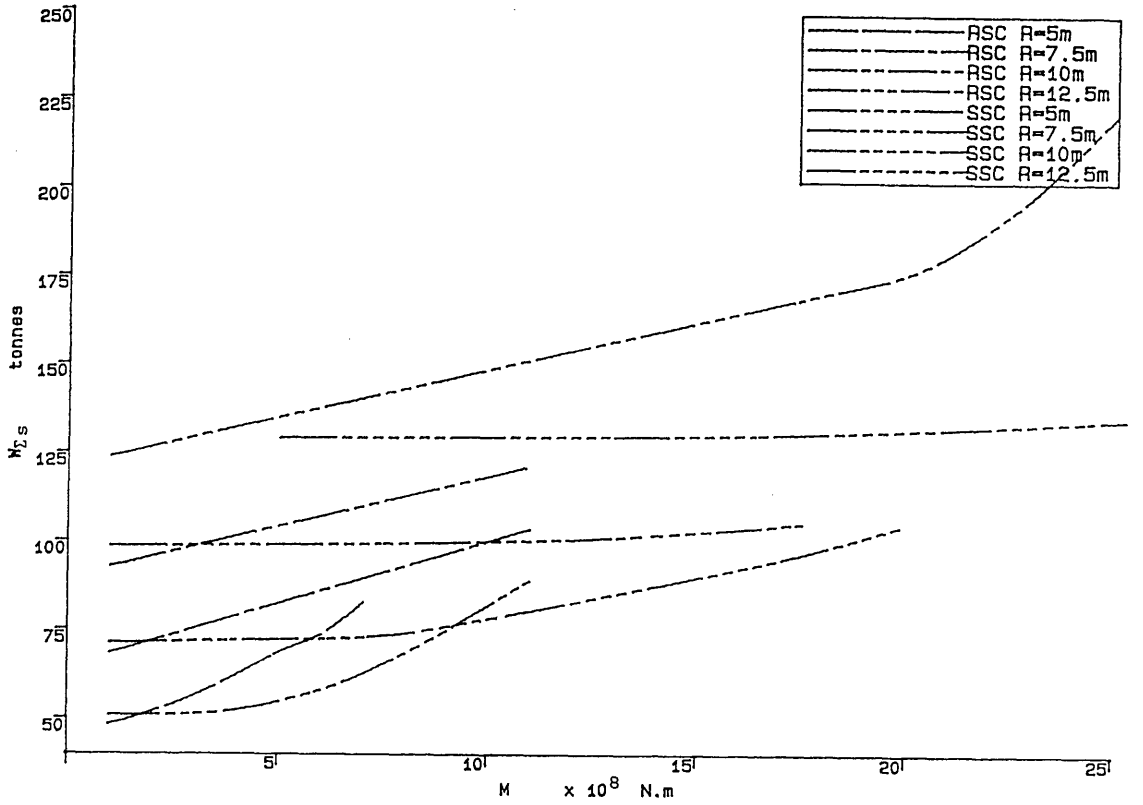

(a) associated loading:

N=4.9 x10^7 (N) P=20 (m)

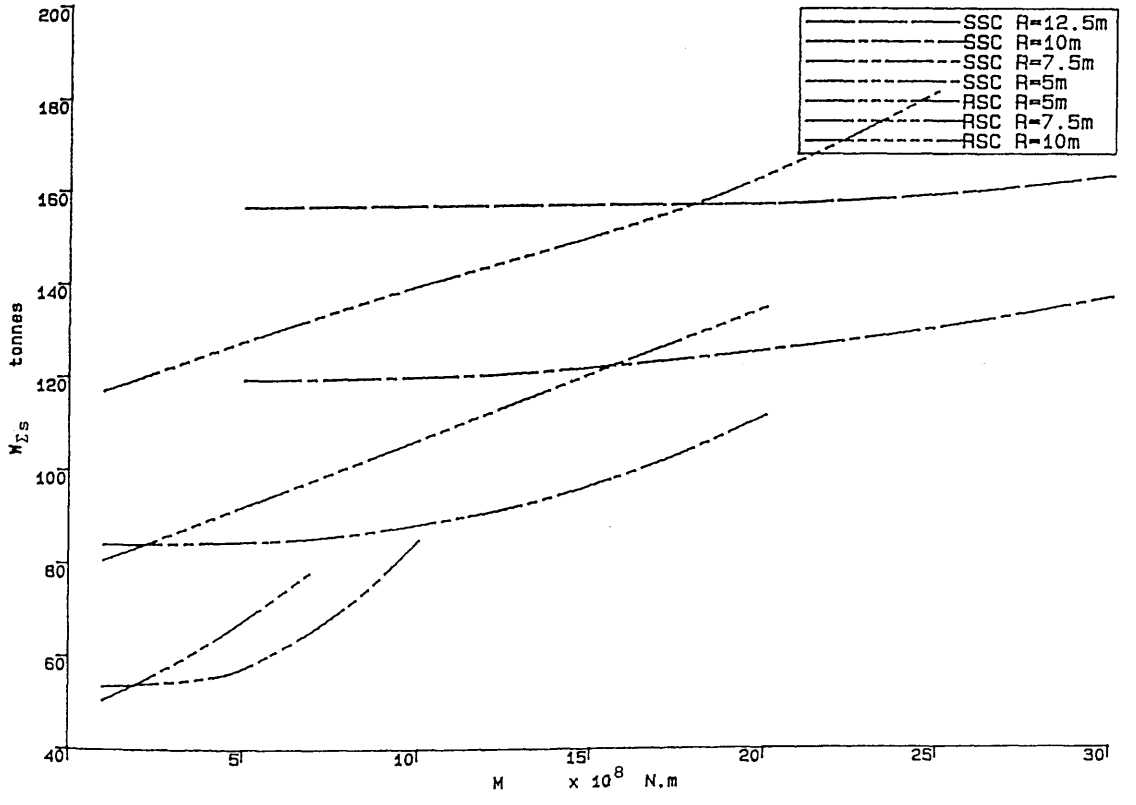

(b) associated loading:

N=4.9 x10^7 (N) P=50 (m)

Fig. 3.4 minimum structural weight of stiffened cylinders under varying sectional bending moment

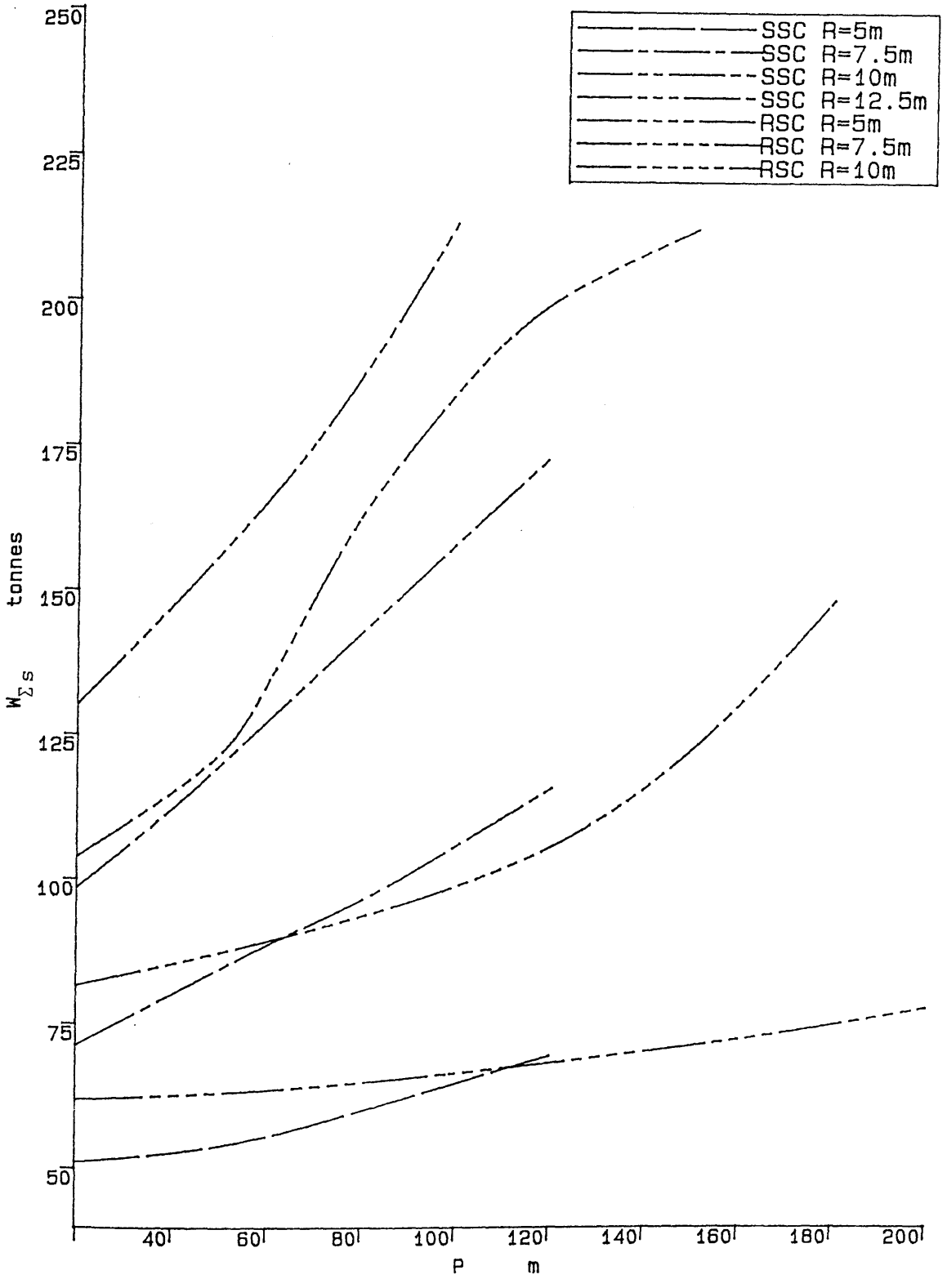

associated loading:

M=3.0 $\times 10^8$ (N.m) N=4.9 $\times 10^7$ (N)

Fig. 3.5 minimum structural weight of stiffened cylinders under varying external pressure

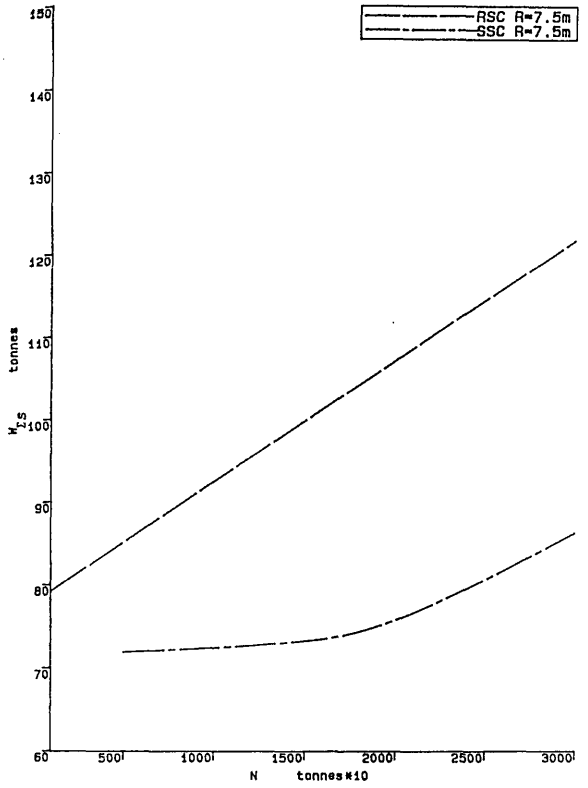

(a) associated loading:
M=4.0 x10^8 (N.m) P=20 (m)

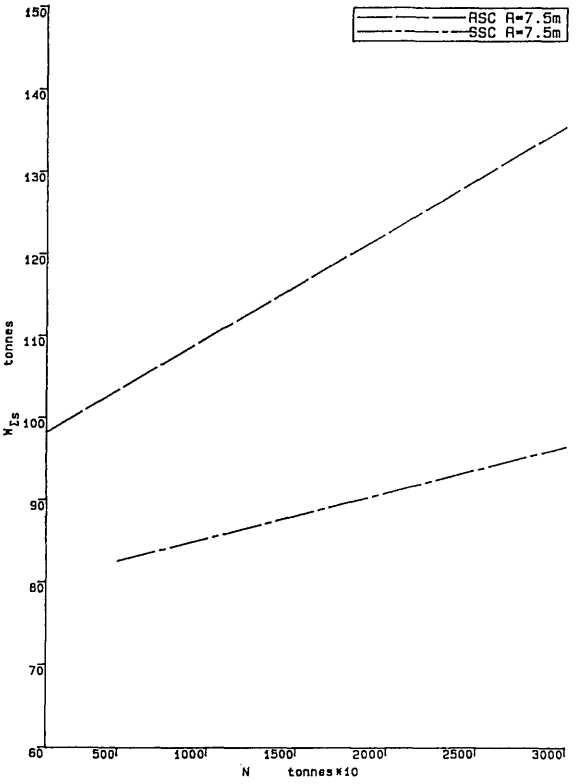

(b) associated loading:
M=8.0 x10^8 (N.m) P=40 (m)

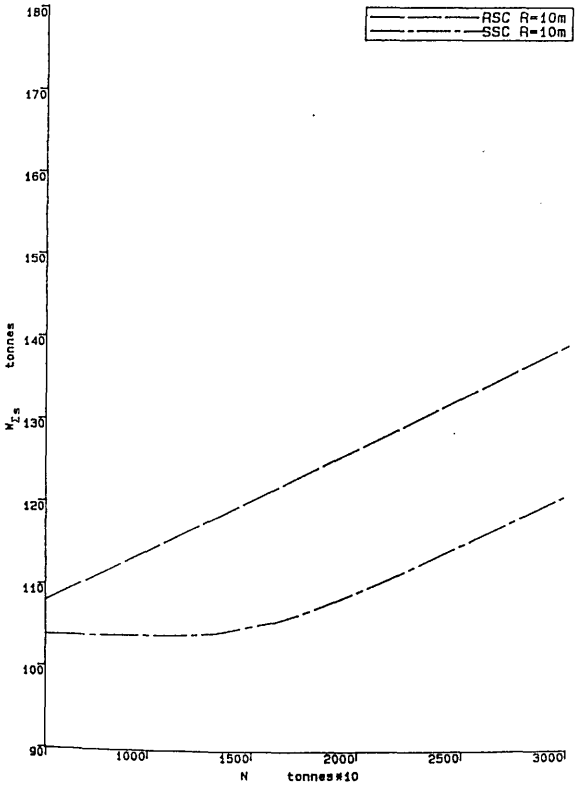

(c) associated loading:
M=5.0 x10^8 (N.m) P=30 (m)

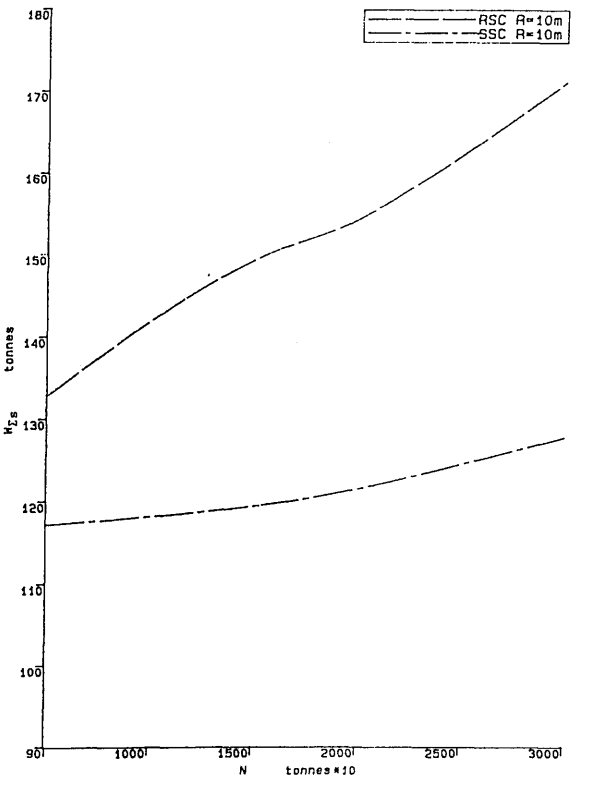

(d) associated loading:
M=5.0 x10^8 (N.m) P=60 (m)

Fig. 3.6 minimum structural weight of stiffened cylinders under varying axial loading

Table 3.1 list of the data used to verify the present computer program (ref. 65)

axial force	$N=12.22 \times 10^4$ kN
torsion	$T=180.3$ kN.m
maximum bending moment	$M=7.21 \times 10^5$ kN.m
maximum shear force	$V=2.161 \times 10^4$ kN
external pressure	$P=0.371 \times 10^3$ kN/m^2
column radius (inner)	$=8.85$m
bulkhead spacing	$L=7.5$m
shell thickness	$t=0.037$m
ring frame spacing	$\ell=1.0$m
ring frame dimensions	$h=0.525$m $t_w=0.025$m $b=0.25$m $t_f=0.030$m
yield stress	$f_y=345 \times 10^3$ kN/m^2
Young's modulus	$E=2.05 \times 10^{11}$ N/m^2
Poisson's ratio	$\nu=0.3$
material density	$\rho_s=7800$kg/m^3

Table 3.2 structural weight optimisation results for the ring stiffened cylinder in Table 3.1

method	initial t (m)	initial ℓ (m)	optimum t (m)	optimum ℓ (m)	minimum W_{rs} (ton)	No. of evaluations
(a) results from ref. 65						
Neldor& Mead	0.037	1.0	0.03674	1.11189	177.619	367
	0.04	1.0	0.03674	1.11190	177.617	339
Hooke& Jeeves	0.04	1.0	0.03672	1.10825	177.746	133
(b) results from present calculations						
Neldor& Mead (NAGF)	0.037	1.0	0.0396	1.250	176.890	214
FTT	0.037	1.0	0.0396	1.250	176.890	147

CHAPTER 4

ESTIMATION OF THE WATER DEPTH CAPACITY OF A MONOLITHIC ARTICULATED TOWER

1. INTRODUCTION

Using the finite element method and dividing an articulated tower structure into beam elements the natural frequencies of the FMV motion of the structure can be obtained by solving the eigenvalue problem.

The division of the structure into beam elements is carried out such that each major column component is divided into several beam elements. The number of elements depends on the length/diameter ratio of the column component so that at sections where geometrical discontinuity occurs, nodes of the relevant beam elements are taken.

The parameters which affect the natural frequency include the water depth d, the payload W_o and those associated with the geometrical dimensions and the weight distribution of the structure. The significance of their effect on the natural frequency is examined in the following, systematically. For this purpose, the program MONO.FLEXURE was written based on the above outlined procedure. NAGF routine FO2AEF [68] was used to solve the eigenvalue problem.

The program MONO.FLEXURE is checked using a simple beam. The theoretical solution of the natural frequencies of the beam under different boundary conditions are compared with the results from the computer program both in vacuo and in fluid. It is finally concluded

that under the condition that $\omega_1 > 1.0$ and $W_{\Sigma_s} \leqq 15{,}000t$, monolithic single articulated tower structures can be installed up to 300m to 350m without experiencing significant FMV motion.

2. FORMULATION OF THE ELEMENTAL MATRICES

2.1 Elemental Matrices in Local Coordinates System

Figure 4.1 shows a flexible plane beam of a uniform cross section together with annotations and local and global co-ordinate systems. The beam undergoes axial, transverse and angular displacements at each end (node).

In the finite element analysis, the displacement patterns along the beam element are assumed and expressed in terms of shape functions and nodal displacements. By applying the virtual displacement principal to stress calculation, the elemental bending stiffness matrix $[K^e]$is found [74]

The explicit form of $[K^e]$ for a beam element is given by:-

$$[K^e] = \begin{bmatrix} -EA/\ell & & & & & \\ 0 & 12EI/\ell^3 & \text{Symmetric} & & & \\ 0 & 6EI/\ell^2 & 4EI/\ell & & & \\ -EA/\ell & 0 & 0 & EA/\ell & & \\ 0 & -12EI/\ell^3 & -6EI/\ell^2 & 0 & 12EI/\ell^3 & \\ 0 & 6EI/\ell^2 & 2EI/\ell & 0 & -6EI/\ell^2 & 4EI/\ell \end{bmatrix} \quad (4.1)$$

In the vibration analysis, the axial displacement is often neglected and only the transverse and angular displacements are considered. In this case, the stiffness matrix for a beam element are given by

$$[K^e] = \begin{bmatrix} 12EI/\ell^3 & & & \\ 6EI/\ell^2 & 4EI/\ell & \text{Symmetric} & \\ -12EI/\ell^3 & -6EI/\ell^2 & 12EI/\ell^3 & \\ 6EI/\ell^2 & 2EI/\ell & -6EI/\ell^2 & 4EI/\ell \end{bmatrix} \tag{4.2}$$

Applying D'Alembert's principle to a dynamic element, taking into account the inertia force, to calculate the distributed load over the element and following a similar procedure, the elemental mass matrix can be obtained which, for a beam element, can be written explicitly as:-

$$[M^e] = \frac{M}{420}\begin{bmatrix} 156 & 22\ell & 54 & -13\ell \\ 22\ell & 4\ell^2 & 13\ell & -3\ell^2 \\ 54 & 13\ell & 15 & -22\ell \\ -13\ell & -3\ell^2 & -22\ell & 4\ell^2 \end{bmatrix} \tag{4.3}$$

The elemental mass matrix so obtained is called a consistent mass matrix. In addition, the lumped mass matrix is also very often used which is the mass matrix obtained by assuming that the entire mass is concentrated at the nodal points of the element. It is given simply by:-

$$[M^e] = M \begin{bmatrix} 1/2 & & & \\ & 1/2 & & 0 \\ & & 1/2 & \\ 0 & & & 1/2 \end{bmatrix} \tag{4.4}$$

In the finite element analysis, the effect of the axial force interacting with the transverse deformation of the beam element is

accounted for by means of the geometrical stiffness matrix, also called initial stress stiffness matrix, which is often used in the stability analysis as well as in analysis of geometrical non-linear structures. It is given for a beam element as:-

$$[K_\sigma^e] = \frac{N}{30\ell} \begin{bmatrix} 36 & 3\ell & -36 & 3\ell \\ 3\ell & 4\ell^2 & -3\ell & -\ell^2 \\ -36 & -3\ell & 36 & -3\ell \\ 3\ell & -\ell^2 & -3\ell & 4\ell^2 \end{bmatrix} \qquad (4.5)$$

This elemental geometrical stiffness matrix is added directly to the elemental bending stiffness in equation (4.2) to form the elemental stiffness matrix.

2.2. Formation of the Global Matrices

This involves the transformation of the element matrices from local into global co-ordinates and assembly of the transformed element matrices to form the global matrices. The transformation is done by means of a transformation matrix $[T^e]$, taking $[K^e]$ as an example, so that:-

$$[K^e] = [T^e]\,[K^e]\,[T^e]^{-1} \qquad (4.6)$$

From the local co-ordinates oxy, to the global co-ordinates OXY, as shown in fig. 4.1, the transformation matrix is, therefore, obtained as:-

$$[T^e] = \begin{bmatrix} t & 0 \\ 0 & t \end{bmatrix} \qquad (4.7)$$

$$\text{with} \qquad [t] = \begin{bmatrix} \cos\alpha & -\sin\alpha & 0 \\ \sin\alpha & \cos\alpha & 0 \\ 0 & 0 & 1 \end{bmatrix} \tag{4.8}$$

when the axial displacement is included as well. For an articulated tower structure $\alpha = 0$, therefore, the global and local co-ordinates are coincident.

Before assembling the element matrices to form the global matrices, the nodes have to be numbered. The assembly is carried out thereafter by first expanding the transformed element matrices into the global matrices and adding the expanded elemental matrices together to form the global matrices [74]

3. EIGENVALUE PROBLEM

3.1 Derivation of the Eigenvalue Problem

On obtaining the total global matrices [M] and [K], the equation of the free vibration motion is written as:-

$$[M]\{\ddot{\delta}\} + [K]\{\delta\} = 0 \tag{4.9}$$

Substitution of a harmonic solution $\{\delta\} = \{\delta_o\}.\sin\omega t$ into equation (4.9) yields the necessary condition for a non-zero solution as:-

$$\det([K] - \omega^2[M]) = 0 \tag{4.10}$$

Equation (4.10) is called the Eigenvalue problem. Solving equation (4.10), a solution vector $[\Omega] = [\omega_i, \ldots, \omega_j]^T$ is obtained with $\omega_i < \omega_{i+1}$ $(1 \leq i < j + 1)$. For each ω_i, i = 1,...., j, a nodal displacement vector $\{\delta_{oi}\}$ is obtained which is normally non-dimensionalised, referred to as the ith mode shape of vibration. ω_i is the corresponding natural frequency of the ith FMV motion.

3.2. Imposition of Boundary Conditions

The mass matrix [M] is singular without modification by imposition of the boundary condition.

Basically, there are two types of boundary conditions - displacement (or essential) boundary conditions and force (or natural) boundary conditions. Using the displacement-based finite element method the force boundary conditions are taken into account in the evaluation of externally applied nodal force vector with external forces being transformed into the equivalent nodal forces. The selection of the nodes positions, in principle, is such that the nodes coincide with those points at which:-

a. externally applied concentrated forces act, or

b. base support is applied, or

c. discontinuity of geometry or material property occurs, or

d. externally applied distributed force ends.

There are two ways in which the boundary conditions are normally imposed [74] The first one is to partition the matrices of

the equilibrium equation in terms of known and unknown displacement sets, respectively, that is:-

$$[M]\{\ddot{X}\} + [K]\{X\} = \{F\}$$

and can be partitioned as:-

$$\begin{bmatrix} M_{aa} & M_{ab} \\ M_{ba} & M_{bb} \end{bmatrix} \begin{Bmatrix} \ddot{X}_a \\ \ddot{X}_b \end{Bmatrix} + \begin{bmatrix} K_{aa} & K_{ab} \\ K_{ba} & K_{bb} \end{bmatrix} \begin{Bmatrix} X_a \\ X_b \end{Bmatrix} = \begin{Bmatrix} F_a \\ F_b \end{Bmatrix}$$

such that X_b contains all the known displacements and X_a contains the unknown displacements. From the partitioned form we obtain:-

$$[M_{aa}]\{\ddot{X}_a\} + [K_{aa}]\{X_a\} = \{F_a\} - [M_{ab}]\{\ddot{X}_b\} - [K_{ab}]\{X_b\}$$

and $$[M_{ba}]\{X_a\} + [M_{bb}]\{X_b\} + [K_{ba}]\{X_a\} + [K_{bb}]\{X_b\} = \{F_b\}$$

It is seen that all the quantities on the right-hand side of the first equation are known. Therefore, $\{X_a\}$ can be solved from the first equation. Subsequent substitution of $\{X_a\}$ into the second equation yields the force vector $\{F_b\}$.

Another way of imposing the displacement boundary is to modify the whole stiffness and mass matrix simultaneously without partition. That is, to set to zero all the elements except the diagonal one in those rows and columns corresponding to the known displacements and set to one the diagonal element. The Eigenvalues for the whole matrices can be solved. The Eigenvalues corresponding to the known displacements will be unity and the others will be those corresponding to the unknown displacements. The latter are of interest so that the eigenvectors corresponding to the known displacements are obtained only. The obvious advantage of the latter approach is purely

computational as the storage of the stiffness and mass matrices need not be changed.

4. VERIFICATION OF THE COMPUTER PROGRAM MONO.FLEXURE

A computer program named MONO.FLEXURE was written to calculate the natural frequencies of FMV motion of a monolithic single articulated tower. First of all, it was used to calculate the natural frequencies of FMV motion of a uniform beam, which are compared with the theoretical solutions to verify the program in this section.

4.1. Theoretical Solution of the Flexural Vibration of a Uniform Beam

A uniform beam is shown in fig. 4.2 under the action of transversely distributed force p(x,t) and constant axial force N (positive tension). The equation of motion is given [69] by:-

$$\frac{\delta^2}{\delta x^2}\left(EI\frac{\delta^2 v}{\delta x^2}\right) - N\frac{\delta^2 v}{\delta x^2} + m\frac{\delta^2 v}{\delta t^2} = p(x,t) \qquad (4.11)$$

where m is the mass per unit length. The motion equation (4.11) is simplified as:-

$$EI\frac{\delta^4 v}{\delta x^4} - N\frac{\delta^2 v}{\delta x^2} + m\frac{\delta^2 v}{\delta t^2} = p(x,t)$$

as the beam is uniform. By assuming the solution of the free vibration motion to be of the form:-

$$v(x,e) = \phi(x) \sin(\omega t - \psi) \qquad (4.12)$$

it is obtained that $\phi(x)$ satisfies:-

$$EI\phi^{(4)} - N\phi'' - m\omega^2\phi = 0 \qquad (4.13)$$

If the beam is simply supported, ϕ is assumed to be:-

$$\phi_1(x) = \sin \frac{i\pi x}{\ell} \quad (i = 1,2.....) \tag{4.14}$$

Substitution of equation (4.14) into equation (4.13) yields:-

$$\omega_i = \frac{i^2\pi^2 a}{\ell^2}\sqrt{1 + \frac{N\ell^2}{i^2EI\pi^2}} \tag{4.15}$$

where a is the frequency parameter:-

$$a = \sqrt{EI/m} \propto R \tag{4.16}$$

From equation (4.15), the following conclusions are drawn:-

a. The natural frequencies are proportional to R/ℓ^2 without N but are independent of the shell thickness in the case of the beam being a thin shell cylinder.

b. The effect of the axial force is such that tensile axial force increases the natural frequencies and compressive axial force reduces the natural frequencies.

c. The presence of a small axial force only affects the natural frequencies of low flexural modes.

It is noted that equation (4.11) is the motion equation of a uniform beam in vacuum. However, if the beam is immersed in fluid, say in sea water, p(x,t) should also include the added mass effect due to the relative motion. Following the same procedure, the 'wet' mode natural frequencies, taking into account the added hydrodynamic mass effect, are given also by equation (4.15) given as:-

$$a = \sqrt{EI/(m + m_a)} \tag{4.17}$$

where m_a is the sectional added mass of the beam given as:-

$$m_a = \rho_w C_m A$$

The 'wet' mode natural frequencies are reduced compared with the 'dry' mode ones in equations (4.15).

In addition, the approximation solution of the first three natural frequencies of FMV motion of a cantilever beam, free from axial force, are obtained [69] as:-

$$\omega_1 = 1.875^2 \frac{a}{\ell^2}, \omega_2 = 4.644^2 \frac{a}{\ell^2}, \omega_3 = 7.855^2 \frac{a}{\ell^2}$$

4.2. Verification of the Computer Program

An example is taken here of a uniform cylinder. The geometrical parameters are: the diameter D = 1.5m, length L = 50m and shell thickness t = 0.1m. Two cases are examined: a simply supported beam and a cantilever beam, each with an axial force of N = -500t, 0.0t and 500t. With n = 26, the accuracy of the numerical solution is within 1% of the theoretical one, as listed in Table 4.1. In addition, when N is changed from -500t to 500t, the variation of ω_1 and ω_2 is under 5% and 15%, respectively.

5. PARAMETRIC STUDIES ON THE NATURAL FREQUENCIES OF FMV MOTION OF A MONOLITHIC SINGLE ARTICULATED TOWER

The parameters affecting the natural frequencies of FMV motion of a monolithic single articulated tower are identified to include its payload and parameters defining the geometrical dimensions of the structure apart from the water depth. In the following, the ballast chamber is assumed to be at the bottom of the lower column and its size is determined such that the static tension on the joint is

zero. Its dimension is such that the diameter/length ratio is unity. In addition, the diameter/length ratio of the buoyancy chamber, is also unity.

In modelling the sectional bending stiffness of the structure, the equivalent shell thickness of the stiffened columns, as defined in equation (3.18) of Chapter 3, is used to calculate the second moment of inertia of the solid sectional area. The same equivalent shell thickness is used to calculate the structural mass. This is expected to over-estimate the natural frequencies as the inner stiffeners of the columns contribute much structural mass but little bending stiffness. Therefore, it might be more realistic to use the real shell thickness to calculate the sectional bending stiffness but use the equivalent shell thickness which is given as $\bar{t} = (1+\beta_w)t > t$ to calculate the structural mass. The difficulty lies in the selection of the appropriate β_w.

The modelling of the deck structure is done in the same way as in calculating the angular dynamic response of the structure in Chapter 5, ie it is regarded as a solid column with the payload uniformly distributed over the deck space. The total number of elements into which the structure is divided is from 7 up to 10.

Column	No of element divided	Comment
E.C	0	$L_1 = 0$
Ba.C	1	it is very stiff as $\alpha_2 = 1.0$
L.C	2.5	depends on the water depth $[L_3 \doteq 2.5D_3]$
B.C	1	$\alpha_4 = 1.0$
U.C	2	it is divided into two elements at the MWL
Deck	1	$\alpha_6 < 1.0$

The axial force varies along the length of the structure as is shown in Table 5.3 in Chapter 5. In the program only the axial force, due to the hydrostatic pressure, is accounted for with the axial force along each element calculated at its central cross section and taken to be constant along the element length.

The added hydrodynamic mass is accounted for with $C_m = 1.0$ for simplicity. Therefore, the following natural frequencies are the wet mode natural frequencies. The natural frequency of FMV motion corresponding to a rigid body motion is zero and, therefore, is excluded. Only the first flexural mode vibration natural frequencies are listed which are the lowest and are of concern.

5.1. Effects of the Axial Force

It is found that the effect of the axial force is always insignificant, except in the case of a large deck payload supported by a very slender upper column. In this case, the stiffness of the upper column determines the overall stiffness to a great extent. Quantitative effect is very difficult to define as it depends on many other parameters but for the upper column the dimension of which is determined from the structural strength calculation, its stiffness should not affect the overall stiffness very much. In addition, the significance of the effect of the deck dimensions becomes noticeable in shallow waters. A slender deck gives rise to low natural frequencies of FMV motion but the effect of the deck dimensions on the natural frequencies in such water depths is not of any concern, in fact, as the natural frequencies are very high.

The buoyancy chamber and the ballast chambers are also very

rigid compared with the lower and upper columns. Therefore, practical variations of their size do not alter their rigidity relative to that of the lower or upper column but it does affect the length of the upper and/or lower column. The relative alteration of the length of the upper/lower column essentially depends on water depths. In shallow waters it will be great, especially when W_o is great due to the fact that the length of the lower column is small itself and the variation of the size of the chambers can be large.

Therefore, in shallow waters the size variation will have a significant effect on the natural frequencies. On the other hand, in deep waters the size of the ballast chamber is not important as far as the natural frequencies of FMV motion are concerned. The size of the buoyancy chamber is small and the lower column, in particular, is very long. Therefore, the relative alteration of the water column length by the variation of the buoyancy chamber is small, although it affects the axial force along the lower column, the effect of which is not significant. In all, the effect of the size of the buoyancy and ballast chambers is not important from the point of view of the natural frequencies in deep waters, though important in shallow waters.

As for the effect of the shell thickness of the columns; from a very comprehensive investigation it is found that an increase of shell thickness does not always result in the increase of the frequencies and, in fact, decreases in certain cases. Variation of the natural frequencies is marginal.

The natural frequencies are virtually unaffected by the axial force. For all practical purposes the effect of the axial force can be

safely omitted. Nevertheless, it is interesting to mention the pattern of variation of the natural frequencies. In very shallow waters, inclusion of the axial force has little effect when W_o is small and causes the natural frequency to decrease very slightly when W_o is large up to $W_o \leq 5{,}000$t. However, in deep waters the inclusion of the axial force is to increase the natural frequency very slightly.

5.2. Effects of the Geometrical Parameters

The major geometrical parameters include those defining the dimensions of the deck, the size of the buoyancy chamber and the ballast chamber and the lengths and diameters of the upper and lower columns. In addition, the shell thicknesses of the columns have certain effects on the natural frequencies although these are not very significant. This is due to the interaction between the columns.

The deck structure is normally highly rigid to resist bending and can be regarded as a rigid body compared with the stiffness of the columns. The change of deck dimensions will not change the stiffness of the structure of the deck structure from this point of view. However, it does affect the mass distribution along the structure.

Therefore, the effect of the deck dimension is expected to be small when the deck payload is small. For structures with large payloads, say $W_o = 5{,}000$t, it is found that when $d > 150$m, the effect of the variation of the deck dimension is under 7% for all the cases examined, with $\alpha_{vw} = 5.0$ to 10.0 m^2/t. When $d > 250$m, the natural frequencies are hardly affected.

The most influential parameters are the diameters of the

upper and lower columns. The lengths of the columns are largely unchanged once the water depth is specified. The overall bending stiffness of the structure depends on the stiffnesses of those two columns, principally. It is seen from Table 4.2 that:-

a. When the stiffness of the upper column is considerably smaller than that of the lower column, the frequencies depend on the stiffness of the upper column.

b. When the stiffness of the lower column is considerably smaller, which is often the case, the frequencies depend on the stiffness of the lower column.

c. When the stiffnesses of both columns are comparable, the frequencies depend on both.

d. The stiffness of the columns is directly related to their diameters.

In shallow waters, the stiffnesses of both columns are comparable so that the increase of diameter in either column is effective to increase the natural frequency. However, in deep waters, the lower column is much softer. As a result, the natural frequency is largely independent of the upper column diameter and is only affected by the lower column diameter.

Table 4.3 lists the natural frequencies of the first flexural mode vibration motion of monolithic single articulated towers and their corresponding total structural weight. If the water depth capacity of those structures is estimated under the condition that $\omega_{1min} > 1.0$ rad/s and $W_{\Sigma s} > 15{,}000$t, the water depth capacity is then between 300m and 350m.

It is mentioned that $t = 0.075$ for the effective bending shell thickness of the columns is a gross over-estimation of the sectional bending stiffness of the columns. Therefore, 300m to 350m of water depth estimated above is most likely to be the upper limit of the maximum water depth in which a monolithic single articulated tower can be used without flexural vibration problems. Furthermore, taking into account all the structural weight of the internal structures and stiffeners of the columns, the equivalent shell thickness $\bar{t}$, from a structural mass point of view, is more likely to exceed 0.075m plus the fact that at d = 300m to 350m, even the increase of D_3 becomes unsatisfactorily ineffective to increase ω_1. The practical water depth capacity of monolithic single articulated towers can be set between 300m and 350m.

6. CONCLUSIONS

1. A comparison between theoretical calculations and the finite element program MONO.FLEXURE, written for this project, has shown that the program gives an accurate estimate of the vibration frequencies for a uniform beam under different boundary conditions.

2. It is observed that in shallow waters, geometrical parameters such as deck dimensions and payload, the size of the buoyancy chamber and its submergence depth are also important in determining natural frequencies. In deep waters, (d > 200m), those parameters tend to have a very insignificant effect. The overall structural bending rigidity and the natural frequencies of FMV motion depend mainly on the relative rigidity of the upper and lower columns. Normally the lower column has lower stiffness and determines the frequencies. When the rigidity of the two columns is very similar, both their stiffnesses

are important. When d > 250m the stiffness of the lower column is normally dominant. Under the specification of ω_{1min} = 1.0 rad/s and $W_{\Sigma s}$ = 15,000t, the estimated water depth capacity of monolithic single articulated towers is between 300m and 350m which is largely the same for all $W_o \leqq$ 5,000t.

3. It is most likely that the water depth capacity quoted above is an over-estimation as β_w = 0.0 is assumed so that $t = \overline{t}$ which renders t unreasonably high.

LIST OF FIGURES

LIST OF TABLES

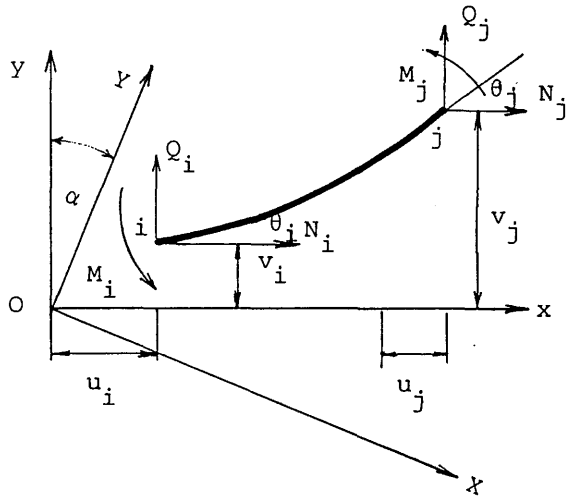

Fig. 4.1 coordinate system for beam element

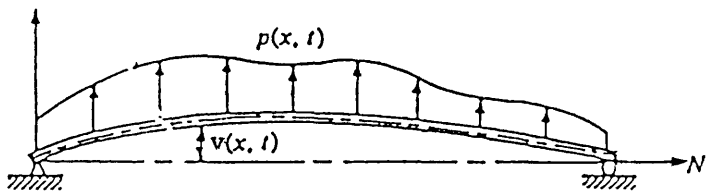

Fig. 4.2 deflected beam with static force and dynamic lateral load

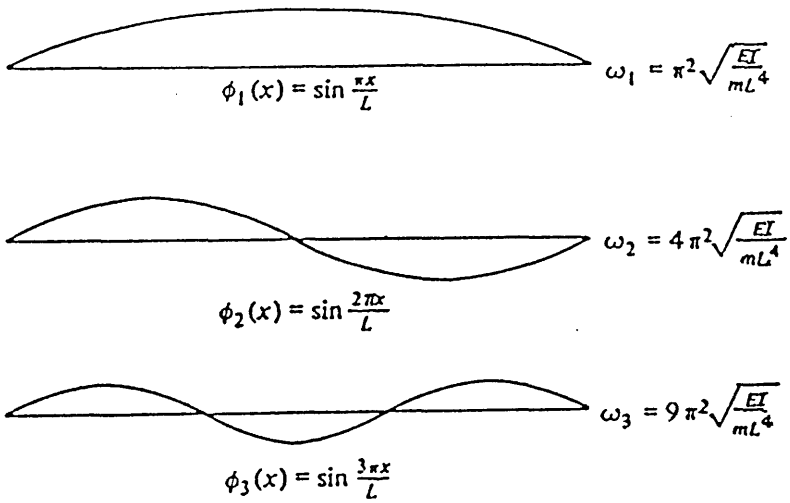

Fig. 4.3 first three vibration modes of a simply supported beam

Table 4.1 comparison between theoratical solution and numerical solution of the natural frequencies of FMV motion for a uniform beam (unit in rad/s)

		simply supported beam			cantilever beam		
N		-500t	0.0t	500t	-500t	0.0t	500t
		theoratical solution from Eq.(4.15)					
ω_1	W	8.627	8.825	9.022		3.143	
	D	10.539	10.786	11.027		3.843	
ω_2	W	35.099	35.299	35.498		19.701	
	D	42.897	43.142	43.385		24.079	
		numerical solution from MONO.FLEXURE					
ω_1	W	8.606	8.807	9.005	2.859	3.139	3.389
	D	10.519	10.764	11.005	3.494	3.836	4.143
ω_2	W	34.825	35.024	35.220	19.232	19.526	19.805
	D	42.563	42.806	43.047	23.505	23.865	24.218

beam dimensions: L=50m , D=1.5m , t=0.1m (n=25)

other related conditions: $E=2.07\times10^{11}N/m^2$, $C_m=1.0$, $\rho_s=7800kg/m^3$

D: dry mode ; W: wet mode

Table 4.2 ω_1 of FMV motion for articulated tower structures (unit in rad/s)

W_o		1000t				3000t				5000t			
d	D_5 \ D_3	7m	8m	9m	10m	7m	8m	9m	10m	7m	8m	9m	10m
100m	7m	4.561	4.796	4.919	4.990	2.995	3.225	3.376	3.479	2.381	2.816	2.982	3.100
	8m	5.040	5.385	5.604	5.900	3.271	3.606	3.847	4.012	2.809	3.130	3.376	3.564
	9m	5.422	5.891	6.205	6.395	3.493	3.912	4.243	4.483	2.973	3.376	3.700	3.962
	10m	5.718	6.309	6.723	7.000	3.647	4.159	4.572	4.889	3.092	3.564	3.962	4.290
150m	7m	2.775	2.798	2.800	2.803	1.944	2.000	2.032	2.050	1.640	1.703	1.738	1.758
	8m	3.121	3.159	3.162	3.165	2.195	2.283	2.330	2.358	1.875	1.949	2.005	2.037
	9m	3.435	3.493	3.407	3.507	2.425	2.542	2.613	2.653	2.047	2.175	2.256	2.307
	10m	3.728	3.808	3.834	3.847	2.613	2.777	2.876	2.934	2.209	2.379	2.488	2.560
200m	7m	1.817	1.841	1.805	1.795	1.407	1.425	1.432	1.435	1.212	1.237	1.249	1.253
	8m	2.017	2.015	2.005	1.995	1.578	1.600	1.613	1.616	1.367	1.400	1.418	1.425
	9m	2.209	2.205	2.195	2.182	1.735	1.766	1.780	1.789	1.510	1.552	1.578	1.591
	10m	2.390	2.367	2.377	2.362	1.884	1.924	1.944	1.952	1.643	1.700	1.732	1.749
250m	7m	1.269	1.265	1.261	1.253	1.068	1.702	1.077	1.077	0.950	0.960	0.965	0.968
	8m	1.393	1.386	1.378	1.371	1.175	1.183	1.183	1.182	1.054	1.063	1.072	1.072
	9m	1.510	1.503	1.493	1.487	1.277	1.285	1.285	1.284	1.149	1.162	1.170	1.175
	10m	1.625	1.616	1.606	1.597	1.395	1.382	1.386	1.386	1.241	1.257	1.269	1.273
300m	7m	0.946	0.942	0.940	0.935	0.844	0.846	0.847	0.847	0.772	0.777	0.780	0.782
	8m	1.025	1.420	1.015	1.010	0.909	0.912	0.912	0.910	0.837	0.843	0.845	0.846
	9m	1.105	1.100	1.091	1.086	0.974	0.976	0.976	0.972	0.900	0.906	0.908	0.909
	10m	1.179	1.174	1.166	1.162	1.039	1.039	1.039	1.039	0.961	0.967	0.970	0.970

Table 4.3 ω_1 and $W_{\Sigma s}$ of monolithic single articulated tower structures

			$W_{\Sigma s}$ (tonnes)				ω_1 (rad/s)			
L_s	W_o	D_5 \ D_3	10m	12m	14m	16m	10m	12m	14m	16m
40m	5,000t	10m	8248	8527	8813	9109	.783	.784	.783	.782
		12m	9397	9668	9945	10230	.884	.880	.875	.868
		14m	10482	10747	11016	11290	.978	.970	.963	.952
		16m	11490	11747	12009	12274	1.068	1.063	1.049	1.034
20m	5,000t	10m	8248	8432	8620	8812	.778	.779	.775	.774
		12m	9487	9668	9851	10038	.873	.869	.865	.860
		14m	10659	10826	11016	11199	.962	.957	.950	.943
		16m	11747	11920	12096	12274	1.049	1.039	1.034	1.025
40m	3,000t	10m	8315	8593	8880	9176	.840	.834	.827	.820
		12m	9451	9727	10000	10284	.939	.928	.916	.903
		14m	10525	10788	11058	11333	1.034	1.02	1.005	.988
		16m	11521	11778	12040	12305	1.131	1.114	1.095	1.077
20m	3,000t	10m	8315	8520	8686	8879	.825	.821	.817	.812
		12m	9541	9722	9905	10092	.917	.910	.903	.895
		14m	10702	10878	11058	11240	1.005	.997	.987	.977
		16m	11778	11951	12127	12305	1.091	1.082	1.072	1.058

CHAPTER 5

RESPONSE OF A MONOLITHIC SINGLE ARTICULATED TOWER TO THE ENVIRONMENTAL EXCITATION

1. INTRODUCTION

This chapter outlines the motion response of an articulated tower under the environmental loading as discussed in Chapter 2. The motion response of an articulated tower may be either static or dynamic depending on the nature of the loading. The dynamic motion response is induced by the first order wave loading, the second order slowly varying wave loading and the wind loading due to fluctuating differential wind velocity component. The static motion response is caused by the steady component of second order wave loading, the wind loading due to mean wind velocity component and the current loading. In calculating the dynamic response the effect of inclination angle under the static loading was neglected.

The equation of motion of a generalised single degree-of-freedom system (GSDF) was applied to the rigid body mode vibration (RBMV) motion of an articulated tower.

Under the regular wave excitation, the internal sectional force; along the length of the structure was calculated. The effect of variation of the relevant design parameters on the motion or the internal sectional forces of the structure was examined.

A sample structure of a monolithic single articulated tower was used to carry out the linear dynamic response analysis. The

recommended design wave height in DnV Rules [45] was used. Constant viscous damping in terms of wave frequencies was assumed and estimated by assuming an angular response amplitude of $\overline{\theta} = 2.5^{o}$ at wave frequency $\omega = 0.4$ rad/s.

2. EQUATION OF MOTION OF AN ARTICULATED TOWER AS A GSDF SYSTEM

The equation of RBMV motion of an articulated tower can be derived by regarding it as a GSDF system [69].

Referring to the articulated tower illustrated in fig. 1.1, undergoing RBMV motion, the shape function can be expressed exactly as:-

$$\psi(z) = \frac{z - z_1}{d - z_1} \tag{5.1}$$

with the generalised co-ordinate $X_o(t)$ chosen to be the horizontal displacement of the structure at the mean water level $z = d$. The horizontal displacement along the vertical axis of the structure is then given by:-

$$X(z,t) = \frac{z - z_1}{d - z_1} X_o(t) \tag{5.2}$$

It is clearly seen from fig. 1.1 that:-

$$X(z,t) = (z-z_1)\tan[\theta(t)] \tag{5.3}$$

where $\theta(t)$ is the angular displacement. Initially, $\theta(t)$ is assumed to be small, so that $\tan[\theta(t)] = \theta(t)$ holds. According to equation (5.3), this leads to:-

$$X(z,t) = (z-z_1)\,\theta\,(t) \tag{5.4}$$

In deriving the linear motion equation, further assumptions are made as follows:

a. Small amplitude wave theory is valid so that the effect of the free surface elevation is neglected.

b. $X(z,t) = (z-z_1)\,\theta(t)$ is also regarded to be small so that $-[k\,X(z,t) - \omega t] = \omega t$ is applied to the wave kinematics.

c. The dynamic component is neglected in deducing the linear motion equation upon dividing the axial force into static and dynamic components as:

$$T(z,t) = T_s(z) + T_d(z,t) \tag{5.5}$$

where $T_d(z,t)$ is the dynamic component due to wave and,

$$T_s(z) = T_b(z) - T_w(z) \tag{5.6}$$

is the static component due to static buoyancy and the weight of structural material.

Substitution of equation (5.4) into the motion equation of the GSDF system [69], after certain manipulation, yields:-

$$I_\ell \ddot{\theta} + C_\ell \dot{\theta} + K_\ell \theta = M_\ell(t) \tag{5.7}$$

in which the linearised Morison's equation, as given by equation (2.11), is used.

I_ℓ, C_ℓ, K_ℓ and $M_\ell(t)$ are the mass moment of inertia, damping, restoring stiffness and pitch moment of the surge wave force, respectively, given as:-

$$I_\ell = I_s + I_{\ell a} \tag{5.8}$$

$$C_{\ell} = C_s + C_{\ell d} \tag{5.9}$$

$$M_{\ell}(t) = M_{\ell i}(t) + M_{\ell d}(t) \tag{5.10}$$

I_s is due to the structural mass and the mass of the ballasting material. $I_{\ell a}$ is due to the added hydrodynamic mass. They are calculated as:-

$$I_s = \left[\int_{z_1}^{z_{N_e+1}} m_s(z)(z - z_1)(z - z_o)dz + \sum_{n=1}^{N_q} M_{qn}(z_{qn} - z_1)(z_{qn} - z_o) + \int_{z_1}^{z_{N_e+1}} I_m(z)dz \right]_{z_o=z_1} \tag{5.11}$$

$$I_{\ell a} = \int_{z_1}^{z_{N_e+1}} m_a(z)(z - z_1)(z - z_o)dz \Bigg|_{z_o=z_1} \tag{5.12}$$

C_s is due to the structural damping and is neglected in the present study. $C_{\ell d}$ is due to viscous effects induced by the structural motion, given as:-

$$C_{\ell d} = \int_{z_1}^{z_{N_e+1}} m_c(z)(z - z_1)(z - z_o)dz \Bigg|_{z_o=z_1} \tag{5.13}$$

K_{ℓ} is reduced to the geometrical stiffness in the motion equation of GSDF system and is given as:-

$$K_{\ell} = \int_{z_1}^{z_{N_e+1}} T_s(z)dz \tag{5.14}$$

In addition, $M_{\ell}(t)$ is given as:-

$$M_{\ell} = [M_{\ell i}^2 + M_{\ell d}^2]^{1/2}$$

$$M_{\ell i} = -\int_{z_1}^{z_{N_e+1}} (z - z_o)E_I(z)\cosh kz\, dz\, \sin\omega t \Bigg|_{z_o=z_1}$$

$$= M_{\ell i}\sin\omega t \qquad (5.15)$$

$$M_{\ell d} = \int_{z_1}^{z_{N_e+1}} (z - z_o)E_D(z)\cosh kz\, dz\, \cos\omega t \Bigg|_{z_o=z_1}$$

$$= M_{\ell d}\sin\omega t \qquad (5.16)$$

The above formulation is obtained with respect to y' axis, as shown in fig. 2.1. Such terms as $m_s(z), m_a(z), m_c(z), E_I(z)$ and $E_D(z)$ etc, in the above equations, are given in Table 5.1.

The calculation of the above quantities can be obtained for the whole structure according to the formulae but, in order to carry out the formation of equation (5.7), in a general sense at present, the column segment cut out of the structure in fig. 1.1 is considered in the following, as shown in fig. 2.1. Once the relevant quantities for the column segment are obtained the quantities for the whole structure can easily be obtained by adding the corresponding quantities for all the individual column segments of the structure.

Referring to the vertical column segment taken out of the ith column of an articulated tower in fig. 2.1, it is described in the table shown below.

In modelling the deck structure it is assumed that the deck is a solid body with the payload uniformly distributed over the deck. In such deck modelling, the deck can be regarded as a solid column. The relevant quantities for the column segment are calculated in Table 5.1.

Details of the column segment in fig. 2.1

Shape in cross section : N_i = 1 solid rectangular section

= 2 solid circular section

= 3 thin shell cylindrical section

= 4 thin wall rectangular section

Column shell thickness : t_i

t_i = 0.0 for a column of solid cross section

Equivalent column shell thickness : $\bar{t}_i$

Column material density : ρ_{si}

Column length : from z_{1i} to z_{2i}

Submerged length : from z_{1i} to z_{5i}, $z_{5i} = \begin{cases} z_{2i} & \text{if } z_{2i} \leqq d \\ d & \text{if } z_{1i} < d < z_{2i} \\ z_{1i} & \text{if } z_{1i} \geqq d \end{cases}$

Flooded length : from z_{3i} to z_{4i} $z_{1i} \leqq z_{3i} \leqq z_{4i} \leqq z_{2i}$

Flooding material density : ρ_i

ρ_i = 0.0, if is is not flooded and is taken to be the structural material density if the column section is solid with $z_{3i} = z_{1i}, z_{4i} = z_{5i}$.

In general, let $Y^{(i)}$ be any of these terms: $I_s^{(i)}$, $I_{\ell a}^{(i)}$, $C_{\ell d}^{(i)}$, $K_\ell^{(i)}$ and $M_\ell^{(i)}(t)$. The total of $Y^{(i)}$ on the part of the structure between z and z_{N_e+1}, denoted as:-

$$Y = \text{Sum}Y^{(i)}\Big|_{z=z} \tag{5.17}$$

can be obtained as

$$\mathrm{SumY}^{(i)}\Big|_{z=z} = \begin{cases} Y^{(i)}\Big|_{z_{1i}=z}^{z_{2i}=z_{N_e+1}} & , j_z = N_e \\ Y^{(i)}\Big|_{z_{1i}=z}^{z_{zi}=z_{j_z}} + \sum_{i=1+j_z}^{N_e} Y^{(i)}\Big|_{z_{1i}=z_i}^{z_{zi}=z_{i+1}} & , j_z < N_e \end{cases} \tag{5.18}$$

where $z_{j_z-1} < z \leqq z_{j_z}$. By now the formation of the linear motion equation, equation (5.7) can be carried out according to the above equation. For example, the total restoring stiffness K_ℓ is given from the above equation as:-

$$K_\ell = \mathrm{SumK}_\ell^{(i)}\Big|_{z=z_1, z_o=z_1}$$

Equation (5.18) is also used in formulating the internal sectional bending moment distribution along the structure in Appendix 1.

It has been suggested in the formulation of the linear motion equation, that to calculate the wave force and its moment the integrations should be carried up to (d + H/2) instead of to d, the mean water level. This is expected to give rise to conservative results of motion response. In this case the formulae of the wave kinematics have to be 'stretched' above z = d [70]. The most conservative way is to assume that the wave kinematics above z = d is the same as they are at z = d.

The dynamic and static angular responses of an articulated tower to regular waves, random waves, slowly varying wave drift and gusty wind are formulated and listed in Table 5.2.

When an articulated tower is subjected to wave loading only, the internal sectional forces are calculated, as listed in Table 5.3. The deduction of the internal sectional shear force and bending moment is demonstrated in Appendix 1.

3. LINEAR DYNAMIC RESPONSE OF AN ARTICULATED TOWER

Based on the above formulation computer programs were generated and named MONO.DYNAMIC, to calculate the static and dynamic responses of a sample articulated tower, as given in Table 5.4. The characteristics of the sample are listed in Table 5.5. The effect of various parameters associated with the environmental conditions on the structural motion responses are examined in the following. (Articulated towers of different structural geometry are compared in Chapter 8).

As is shown in fig. 5.1a, the resonance arises in the vicinity of the natural frequency which is 0.1487 rad/s, from Table 5.5. Above the natural frequency, the RAO of the angular response decreases monotonically with frequency. For the angular acceleration, however, its RAO does not always decrease monotonically with frequency although the resonance effect also exists around the natural frequency, as is seen from fig. 5.1b. For a regular wave of H/T = 30m/16-21s in extreme conditions and H/T = 17m/12-15s in operational conditions, the angular displacement varies from 3.5^{o} to 7^{o} and 2^{o} to 3^{o}, respectively.

The resonance effect also exists in the RAOs of the internal sectional forces, ie the shear force and the bending moment. Typically, the shear force on the articulated joint is shown in fig. 5.1c. Also their RAOs are multi-peaked as above the natural frequency and sectional forces on the structure and do not always decrease monotonically with frequency. Therefore, the design sectional forces to be used in the structural strength calculation has to be obtained by selecting the maximum values of shear forces and bending moments over the wave frequency range of practical concern.

The shear force amplitude does not vary smoothly though continuously along the structure (fig. 5.2), due to the geometrical discontinuities. In the case of any lumped mass being present along the structure, the shear force will be discontinuous at the section where the lumped mass is located. The sectional bending moment varies smoothly where there are no lumped masses. The magnitude of the sectional forces depends on the water depth, the deck payload and the geometrical dimensions of the structure apart from the frequency.

The bending moment distribution along the structures is normally double-peaked. As the frequencies increase,, the upper peak tends to disappear.

The pitch moment of the surge wave force and mass inertia force are the two major components of the external excitations. It is seen from fig. 5.3 that, at any frequency, the moment of the external forces at the ballast chamber is negligible. The moment of the wave force along the other three columns are equally important at wave frequencies below 1.0 rad/s. At higher frequencies, however, the wave forces are mainly exerted on the upper column.

The moment of the mass inertia force has a similar variation pattern with frequency to that of the angular acceleration. It is greater than that of the total wave force. The wave excitation on the structure is mainly counteracted by the inertia of the structure. The transfer of those external forces into the structure depends upon their relative balance in terms of magnitude of motion and phase angle which, in turn depends largely upon the damping effect. This is due to the dynamic nature of the structural response.

In spectral analysis, the angular response spectrum to random waves is single-peaked. The peak frequencies at which the wave and response spectra, figs 2.5 and 5.4. are at their maximum, respectively, are well above the natural frequency and depend largely on T_z. However, the response spectra of angular acceleration and internal sectional forces are normally multi-peaked. Furthermore, the ISSC (2 parameter) (or identically Bretschneider) wave spectrum has more low frequency content than the ITTC or Jonswap spectra and thus the response spectrum using ISSC spectrum absorbs more low frequency content of the RAOs of dynamic response.

The angular response spectra to slowly varying wave drift and gusty wind are much more narrowly concentrated in the vicinity of the natural frequency, indicating the low frequency nature of the response, as is seen from figs. 5.6 and 5.8. It is mentioned, however, the gusty wind velocity spectrum, depending on three such parameters as κ, L, and $\overline{V}_{ws10}$, spreads over a much wider frequency range with the Harris spectrum yielding higher energy content than the Davenport spectrum, especially at low frequencies.

Quantitatively, the random dynamic responses are to be represented by the rms of the relevant response spectra.

The rms angular displacement, due to random waves, by all the four wave spectra, is linearly related to H_s and increases with T_z, as seen from Table 5.6. However, the rms horizontal acceleration at the middle deck level of the sample structure and the rms sectional shear force and bending moment do not vary with T_z, though monotonically they increase with H_s. This is due to the double-peaked nature of their RAO curves. Taking H_s/T_z = 10m/10s and 16m/16s for the operational and the extreme conditions, the rms angular displacement and the horizontal acceleration at the middle deck, ie about 0.24° and 2.4^2m/s and 2°, 0.36^2m/s , respectively, varying slightly with the use of different wave spectra.

In addition, the rms angular displacements of the sample structure due to fluctuating wind and low frequency wave drift are given in Tables 5.8a and 5.7a, respectively. The rms angular displacement in Table 5.8a increases with κ, L, β and $\bar{V}_{ws10}$ especially $\bar{V}_{ws10}$ but decreases with ζ. When κ is changed from 0.0015 to 0.0033, the rms angular displacement obtained by both wind spectra were increased by as much as 48%. When $\bar{V}_{ws10}$ was changed from 35m/s to 48m/s the rms angular displacement was increased by about 71% and 81%, using Harris wind spectrum and by 62.5% and 79% using Davenport wind spectrum in the case of C_a = 1.5, corresponding to L = 1200m and 2000m, respectively. The effects become slightly less pronounced as C_a increases.

On the other hand, the rms angular displacement was decreased by about 30% when ζ was increased from 10% to 20%. As for the rms

angular displacement; due to the low frequency wave drift, it is seen from Table 5.7a that it increases with H_s but decreases with T_z. This is in contrast with the rms angular displacement due to the random waves as in Table 5.6.

4. PARAMETER SPECIFICATIONS

Except when the values of those parameters of concern are specific, it is important to be aware of the effect of varying those parameters over certain ranges on the relevant design aspects. This section examines the effect of certain parameters on the relevant aspects of the dynamic response analysis, which may be of importance in conceptual design.

4.1 Selection of the Interactive Force Coefficients

These coefficients are used in modelling the structural environment interactions and estimating the environmental loadings on the structure, namely, C_a,C_d,$C_s(\omega)$ and C_{da}. Greater values of these coefficients always results in greater loadings on the structure. However, this may not always be true of the structural responses of articulated towers, due to the dynamic nature of the structural responses, as demonstrated in this section.

4.1.1 Effect of C_a

It is understood that the effect of increasing C_a is to increase $M_\ell(t)$ as well as $I_{\ell a}$. Consequently, the natural frequency of the RBMV motion of the articulated tower, ω_n, is reduced and the motion response and the transfer of the external loading into the structure are affected.

The effect of increasing C_a from 1.5 to 2.0 on the angular displacement and acceleration is to cause the resonance to move towards lower frequencies. The response amplitude below the resonance frequency is increased but the response is reduced at higher frequencies. Nevertheless, the RAO of the angular displacement remains single-peaked and that of the horizontal displacement, double-peaked, as is seen in fig. 5.1.

In addition, it was found that the moment of the wave force increases with C_a in all the frequencies as is expected. The moment of the mass inertia force also increases despite the decrease of the angular response amplitude, which is over-compensated by the increase of the second moment of the added hydrodynamic mass.

As for the shear force on the articulated joint, the resonance effect is amplified by an increase in C_a, as seen in fig. 5.1c. In the high frequencies immediately above the resonance frequency, the sectional shear force does not increase with C_a in all frequencies as it does in the case of conventional fixed offshore structures. The effect of C_a on the internal sectional forces on other sections is found to depend, similarly, on the position of the sections and the wave frequency. Therefore, use of larger C_a does not necessarily always yield greater internal sectional forces.

Spectrally, the effect of C_a, varying from 1.5 to 2.0 is to reduce the rms angular displacement and, similarly but less significantly, the rms angular acceleration. The effect, depending on use of different wave spectrum, increases with T_z, from 14.5% when T_z = 8s, to 51.3% when T_z = 16s. This is to be expected from the variation of the RAOs with C_a.

Returning to the RAOs of the internal sectional shear force and bending moments, their spectral response pattern can easily be explained. Like the rms angular displacement, the ratios of the rms sectional forces with C_a = 2.0 over those with C_a = 1.5 decrease with T_z although the rms sectional forces themselves do not. Unlike the rms values of the angular displacement and the horizontal acceleration where the ratios are always under 1.0, the effect of increasing C_a from 1.5 to 2.0 on rms values of the sectional shear force and bending moment has no monotonic trend. There is a definite T_z value under and above which, the effect of increasing C_a is to increase and reduce the rms values, respectively.

Quantitatively, the rms shear force and the bending moment values are increased by as much as 90% in some cases and decreased by more than 60% in other cases, when C_a changes from 1.5 to 2.0.

Decrease of the natural frequency with C_a also affects the low frequency sensitivity of the structure in its dynamic response to low frequency wave drift and wind velocity fluctuation.

It was found that the use of C_a = 2.0 gives rise to slightly reduced results compared with those when C_a = 1.5. The reduction is from 8% to about 11%. This is less than the reduction of the rms angular displacement due to random waves. In addition, the effect of C_a is largely independent of the damping ratio although the rms values are reduced by the use of greater damping ratio.

The rms angular displacement due to gusty wind, on the other hand, is reduced by 3% to 13% when C_a is changed from 1.5 to 2.0. The

ratio of the rms angular displacement with C_a = 2.0 over that with C_a = 1.5 is largely independent of β, ζ, κ and C_{da}.

4.1.2 Effect of C_d

Variation of C_d affects the linearised wave exciting force, the viscous damping and the drag force of the current. The effect of C_d on the wave exciting force depends on wave frequency. It is known that the importance of the linearised drag force term compared with the inertia term decreases with wave frequency and is very small even at low frequencies. For the sample structure, this is confirmed in Table 5.9.

The effect of C_d on the angular dynamic response to regular waves, represented by the damping ratio, is only pronounced in the vicinity of natural frequency. Consequently, the rms values are only affected markedly when T_z is greater (Table 5.6). The effect of varying C_d on the internal sectional shear force and bending moment depends again on the position of the section and frequency. A similar effect is found on their rms values, as shown in Table 5.6.

The moment of the drag force of the current on the model structure about the articulated joint is also affected by C_d. For the sample structure with C_d = 0.7 in design current condition as specified in Table 2.1, the moment was obtained, as listed in Table 5.9. As is demonstrated in section 4.4 below, the current loading is not important with respect to the static angular displacement it causes. Therefore, the variation of C_d is not important with respect to the effect of the current loading.

4.1.3 Effect of the Wind Drag Coefficient

Increase of the wind drag coefficient for the deck or the upper column increases the wind loading of the mean and fluctuating components to increase and, consequently, the structural response also increases. The wind loading on the deck normally comprises the major part of the total loading. The wind loading on the upper column and on the deck and the structural response were calculated. Assuming C_{da} = 0.7 and 0.9 for the upper column and C_{da} = 1.0, 1.5 and 2.0 for the upper deck, respectively. The dynamic response of the structure in the case of C_{da} = 0.7 for the column and C_{da} = 1.0 for the deck was calculated as previously shown in Tables 5.8a and 5.8b. The dynamic response, especially that for the upper deck, was found to increase with C_{da}.

The mean wind loading and the corresponding structural response are linearly related to the wind drag coefficients of the column and the deck and increase with the coefficients.

4.2. Selection of the Wave Spectrum

Selection of the wave spectrum depends on the environmental conditions, first of all. As far as articulated tower structures are concerned, ISSC or Bretschneider spectrum has more low frequency contents than either ITTC or Jonswap spectrum and, therefore, leads to greater angular dynamic response. These two spectra are also more sensitive to C_a and C_d than the other two. As for internal sectional forces and angular acceleration, there is no steady pattern for any of these spectra to yield greater results. This is confirmed in Table 5.6.

4.3. Selection of the Wind Velocity Spectrum

In general, the use of the Harris wind velocity spectrum yields the greater response, as is seen from Table 5.8b. In this case, the difference between the rms values from the Harris spectrum and that from the Davenport spectrum is about 5.8%, 8% and 12% with the damping ratios of 5%, 10% and 20%, respectively. This difference is not notedly affected by parameters such as L, κ and C_{da} and increases as $\overline{V}_{ws10}$ increases.

The exponent of the mean wind profile, β, has a certain effect on the rms angular response. The response is increased by about 3.5% when β changes from 0.075 to 0.125, independently of other parameters. This may be practically negligible. The other parameters have very significant effects in general.

4.4 Relative Importance of the Environmental Loadings

The relative importance of the environmental loadings from different sources can be compared in terms of their magnitude and, more representatively, in terms of the response of the structure induced by the environmental loadings.

The dynamic loading, due to the second order wave drift of the slowly varying component and fluctuating wind velocity component is expressed in the spectral form and, therefore, cannot be compared with those in Table 5.9.

As expected, the current loading and the mean wind loading in

the extreme operational conditions are small compared with the first order wave loading being well under 10% of it, as seen in Table 5.9.

As for the static response of the sample structure, the steady current loading and the mean wave drift loading induce a static tilt of the same order. The mean wind loading induces a greater static tilt. In fact, in Chapter 8 it is shown that the steady current loading is of the same order as that due to the lateral offset of the deck payload from the vertical axis of the structure. All the above shows that the relative importance of the structural response to various loadings may be very different from the relative magnitude of the loadings. This is due to the different nature of the interaction between those loadings and the structure.

4.5. Effect of the Free Surface Elevation

For simplicity, the wave kinematics were stretched above the mean water level such that they are the same as at the mean water level.

Using breaking wave height H as given in equation (2.9) to integrate the moment of the surge wave force from 0.0 up to d + H/2, the maximum effect of the free surface elevation was obtained. As the wave height and frequency decrease, the contribution of the surface elevation to the angular response decreases. This is easily understood as in high frequencies the wave force is mainly concentrated on the part of the structure immediately below the free surface and the wave force above the mean water level becomes significant compared with that below the mean water level. In this case, an increase up to 34% is achieved using the breaking wave height at frequency ω = 1.0 rad/s,

as is seen from Table 5.11.

In addition, it should be mentioned that the wave force above the mean water level is non-linearly related to the wave height. Hence, a spectral analysis cannot be performed.

4.6. Importance of Damping

The damping effect on the dynamic response of the structure to harmonic waves is not very significant, except in extreme conditions in which the resonance effect of the RAO curves of concern is partially accounted for. In this case, the linearised viscous damping is thought to be dominant.

Under the excitation of low frequency wave drift and fluctuating wind, more damping is likely to be present in the motion of the structure but estimation of the damping in this case is difficult. However, it is expected that the variation of the damping ratio is between 5% and 20% which is previously used in Tables 5.7 to 5.8. As the motion is largely centred around the resonance frequency, the effect of damping is very important, as is shown in those tables. For instance, about 50% reduction was achieved on the rms angular response of the sample structure to the fluctuating wind when the damping ratio was increased from 5% to 20%. In the case of the rms angular response to the low frequency wave drift, the damping effect is of much the same significance, as is shown in Table 5.12.

5. AXIAL FORCES ON THE ARTICULATED JOINT

The static tension on the articulated joint is -1018.4 tonnes

for the sample structure, to be varied by changing the dimension of the ballast chamber effectively.

The presence of the waves gives rise to a dynamic component, the heaving force, due to the discontinuous geometry of the structure. On the articulated joint, the heaving force, due to dynamic pressure, in terms of the wave frequency can be obtained from Table 5.3.

The magnitude of the heaving force varies significantly with frequency and at maximum is significant compared with the static tension and the shear force on the joint. It is always desirable to minimise the dynamic heaving force. Various parameters affecting the heaving force are examined in Chapter 8. Effective reduction in heaving force was shown to be achieved in Section 10 of Chapter 9 by using a frustrum buoyancy chamber.

6. CONCLUSIONS

The following conclusions are drawn.

1. The RAO of the angular displacement is single-peaked, due to the resonance effect at the natural frequency and decreases with frequency monotonically above the resonance frequency. But the RAOs of the angular acceleration and internal sectional forces (shear force and bending moment), typically at the articulated joint, do not always decrease with frequency. Therefore, the design sectional forces which are to be the maximum possible over the wave frequency range of practical interest may have to be obtained using a series of waves of varying periods.

2. The rms of the spectral response is linearly related to H and is essentially a function of T_z. The rms angular response increases with T_z which is due to the single peak pattern of the RAO of angular displacement. The rms values of the horizontal acceleration or angular acceleration, as well as the sectional shear force and bending moment, do not always increase with T_z, due to the double peak pattern of their RAOs.

3. Angular dynamic responses to the fluctuating wind and the slowly varying wave drift was found to be centred around the resonance frequency. The significance of the structural response so induced is readily recognised when it is compared with that induced by random waves. UnlikE the random response of the structure to random waves, the response of the structure to low frequency wave drift decreases with T_z and is directly proportional to the square of H_s.

4. The two parameter wave spectra contains more low frequency content than the Jonswap type spectra. Consequently, they give rise to greater rms angular response to random waves and to slowly varying wave drift. These two spectra are also more sensitive to the variation of C_a and C_d. However, this pattern is not always the case in the calculation of the acceleration and sectional force and bending moment.

5. In this study, a variation of β is found to have little effect on the rms angular response due to the fluctuating wind. An increase in any of the other three parameters L,κ and $\bar{V}_{ws10}$ leads to an increase of the rms angular response significantly when they are varied in the range examined.

6. The relative magnitude of the rms angular displacement by Harris and Davenport wind spectra depends on C_a, $\overline{V}_{ws10}$ and L but the difference is under 10% for all the cases examined.

7. The effect of C_a, typically varying from 1.5 to 2.0, is to reduce natural frequency but also to increase the moment of surge wave force. This leads to reduced angular response in the wave frequency range of practical importance, as well as the rms response to random waves, slowly varying wave drift and gusty wind. The reduction is pronounced in severe conditions. The effect of varying C_a on the angular acceleration and internal sectional forces is not monotonic and is frequency dependent.

8. Variation of C_d affects the linearised viscous damping and the drag force. It has significant effect on the RAOs of angular displacement and acceleration only in the vicinity of the resonance frequency. Consequently, their rms values are only affected when T_z is sufficiently great. The effect of C_d on the linearised drag force is of little concern.

9. The effect of C_d on the sectional shear force and bending moment depends on the position of the section and frequency.

10. The effect of damping is significant in the low frequency motion of the structure in response to the low frequency excitation of the wave drift and wind fluctuation. Reduction of the structural response to the wind fluctuation by about 50% was achieved when the damping ratio was increased from 5% to 20% but estimation of the damping in the low frequency range of the structural motion is difficult. No attempt was made to estimate the damping theoretically.

11. The wind loading and the corresponding response increases with C_{da} for the upper deck, in particular, as it may vary over a wider range in practice and is much greater than it is for the support column.

12. By stretching the wave kinematics above the mean water level, the integration of the moment of the wave force on the structure up to d + H/2 and taking into account the free surface elevation, gives a greater angular response. This increases with wave steepness and wave frequency. Using the breaking wave height, increase in the angular response of as much as 34% was detected. The wave force above the mean water level is non-linearly related to the wave height and cannot be accounted for in spectral analysis.

13. The first order wave loading is far greater than the other sources of loading. The wind loading and the current loading are under 10% of the wave loading yet due to the low frequency nature of the random wind and the slowly varying wave drift induces a structural response of the same order as the wave loading. Also the mean wind loading and the mean wave drift loading induce a static tilt which is important compared with the angular displacement of the structure due to regular waves. However, the steady current induced static tilt is comparatively small.

14. The static tension on the articulated joint of the sample structure is -1018.4 tonnes. The magnitude of the heaving force at its maximum is comparable with the horizontal shear force on the joint.

LIST OF FIGURES

LIST OF TABLES

Table 5.12 The ratios of the rms angular displacement of the model structure due to the low frequency wave drift with ζ = 20% over that with ζ = 10%, showing the effect of the damping ratio, ζ.

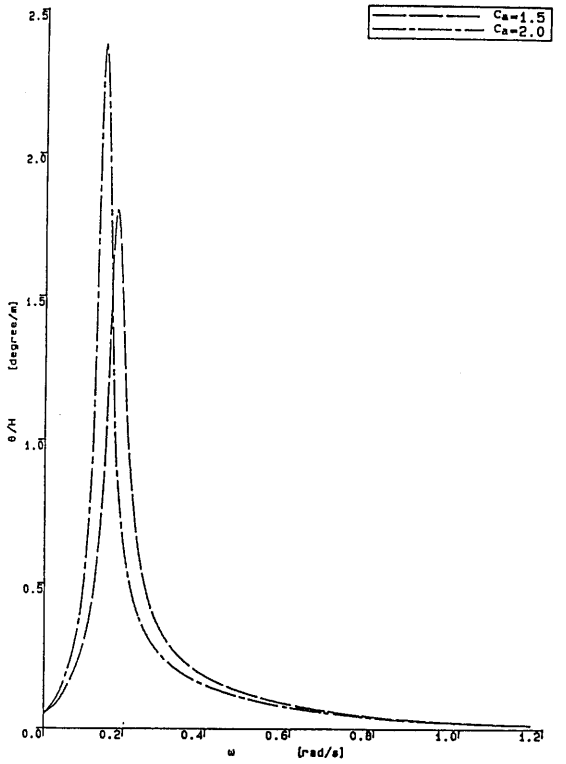

(a) RAO of angular displacement

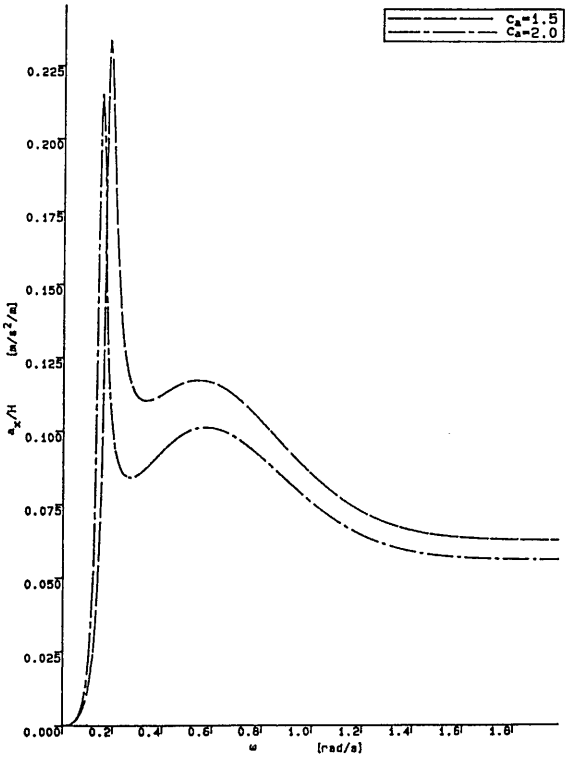

(b) RAO of horizontal acceleration at the middle deck level

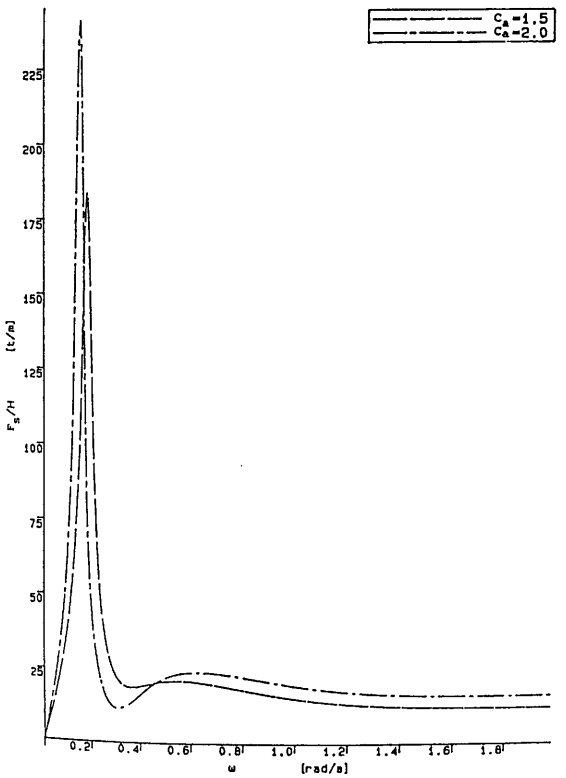

(c) RAO of horizontal shear force on the articulated joint

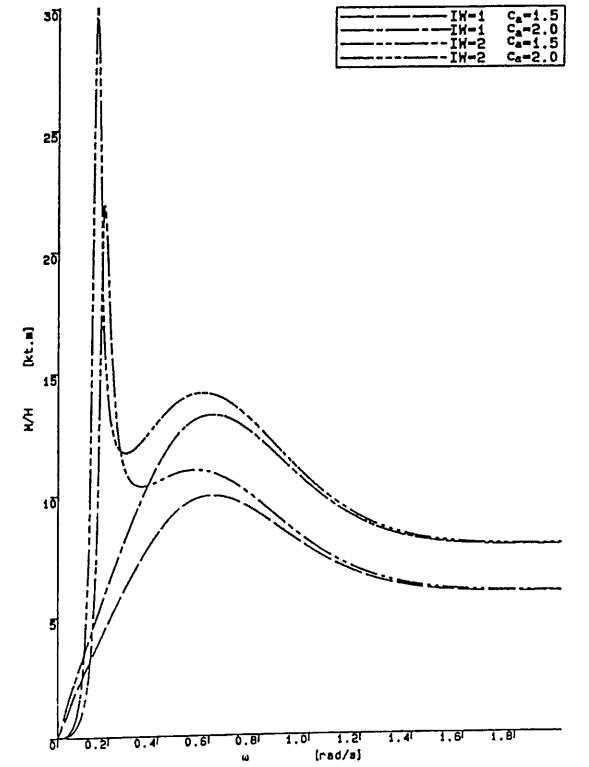

(d) pitch moment (amplitude) of surge wave force and mass inertia force of about the joint

Fig. 5.1 external loadings and dynamic response of articulated tower in regular waves

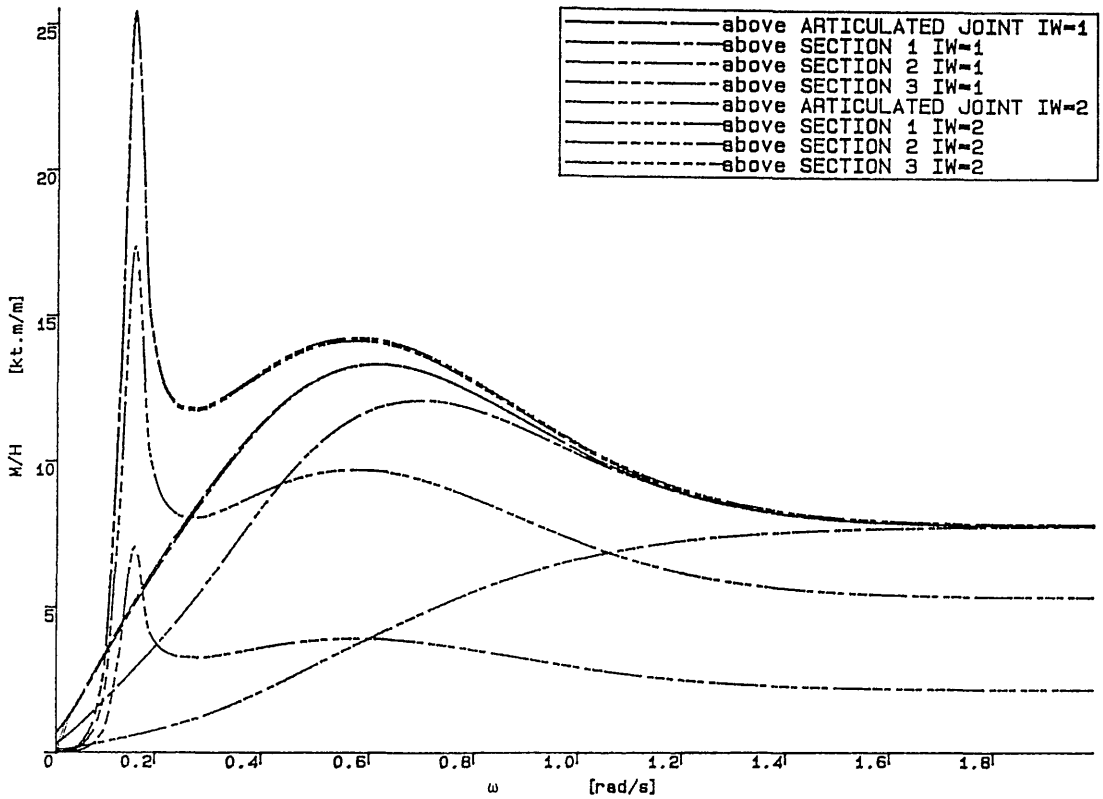

Fig. 5.3 distribution of the pitch moment of the wave (IW=1) and mass inertia (IW=2) forces along the articulated tower

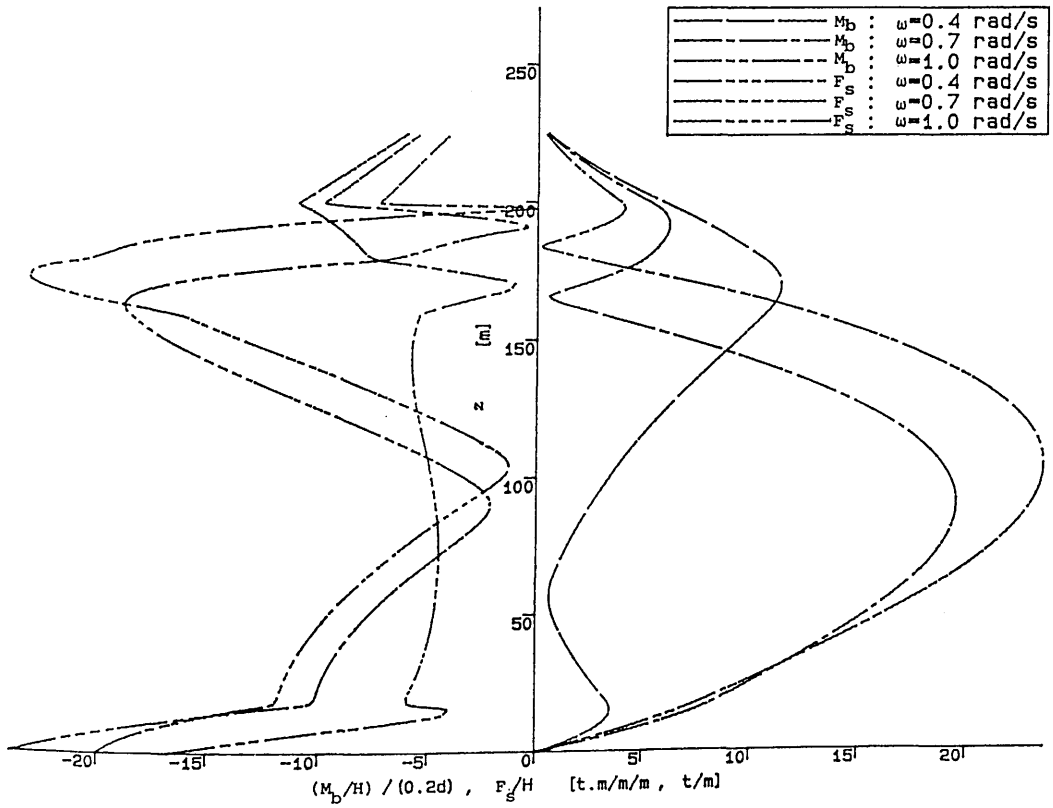

Fig. 5.2 distribution of the internal sectional shear force and bending moment along the articulated tower in regular waves

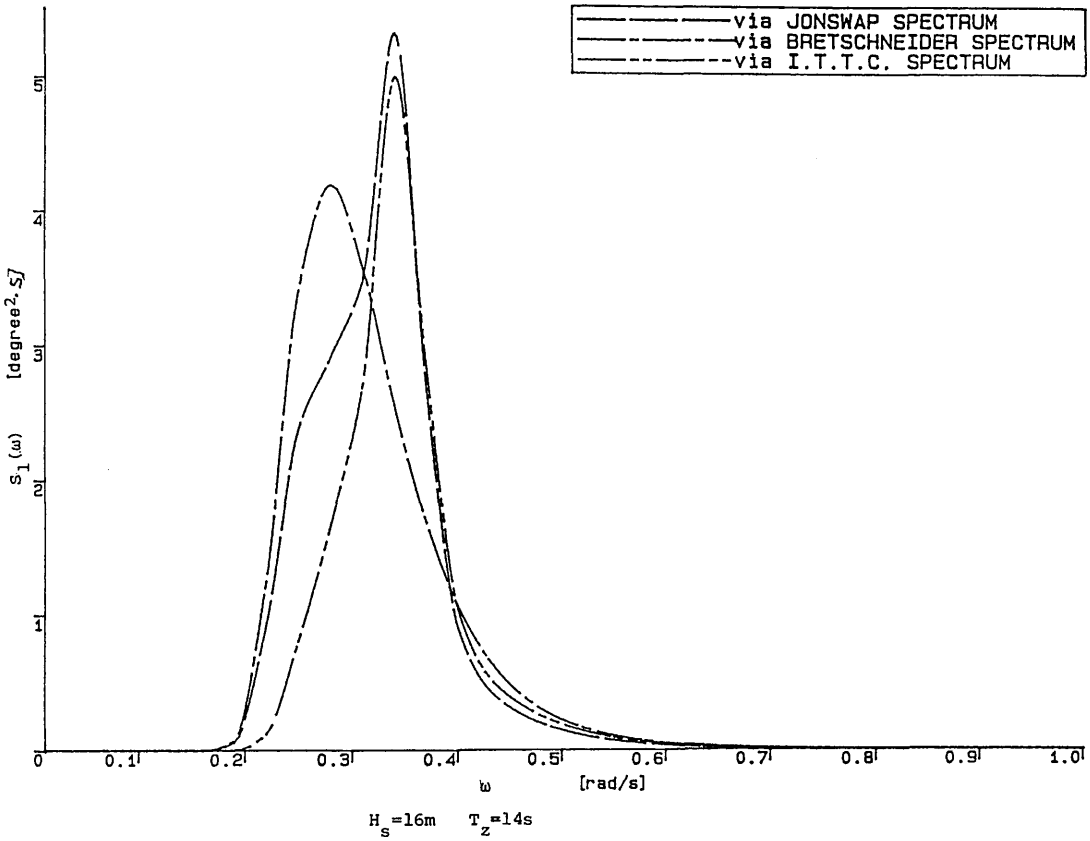

Fig. 5.4 angular displacement spectrum

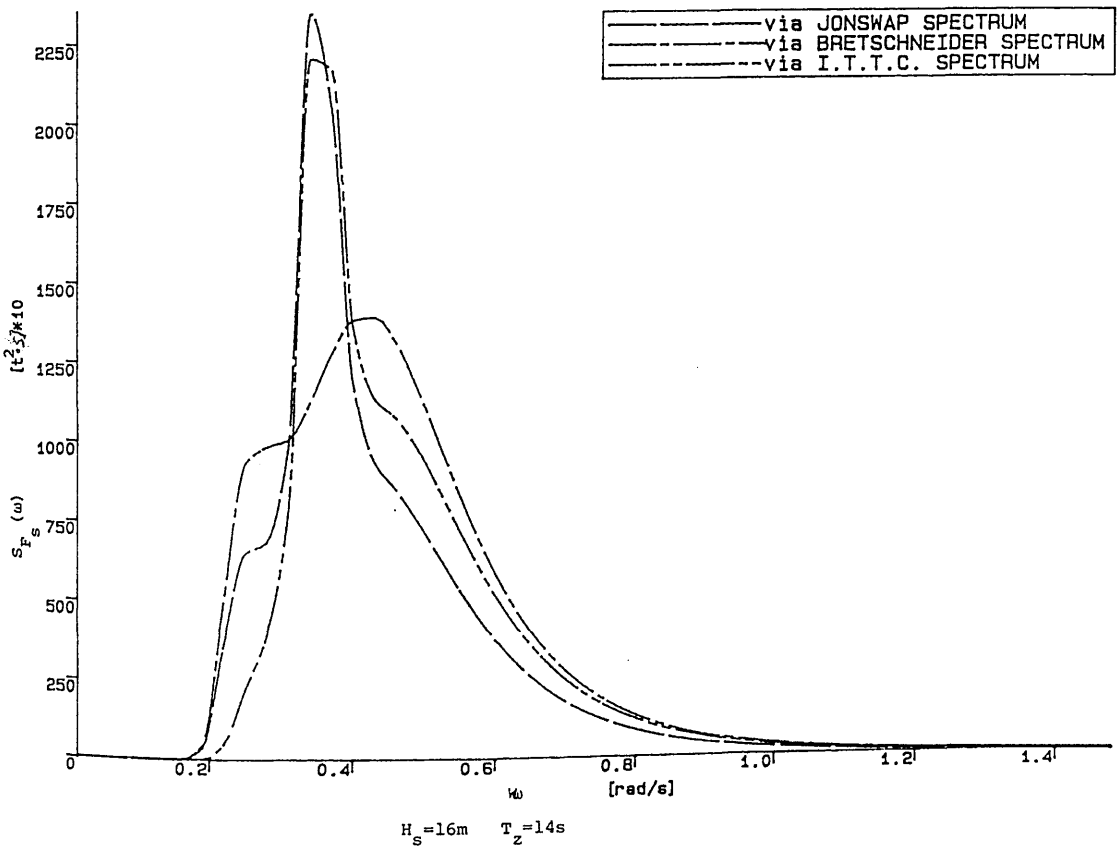

Fig. 5.5 spectrum of the shear force on the articulated joint

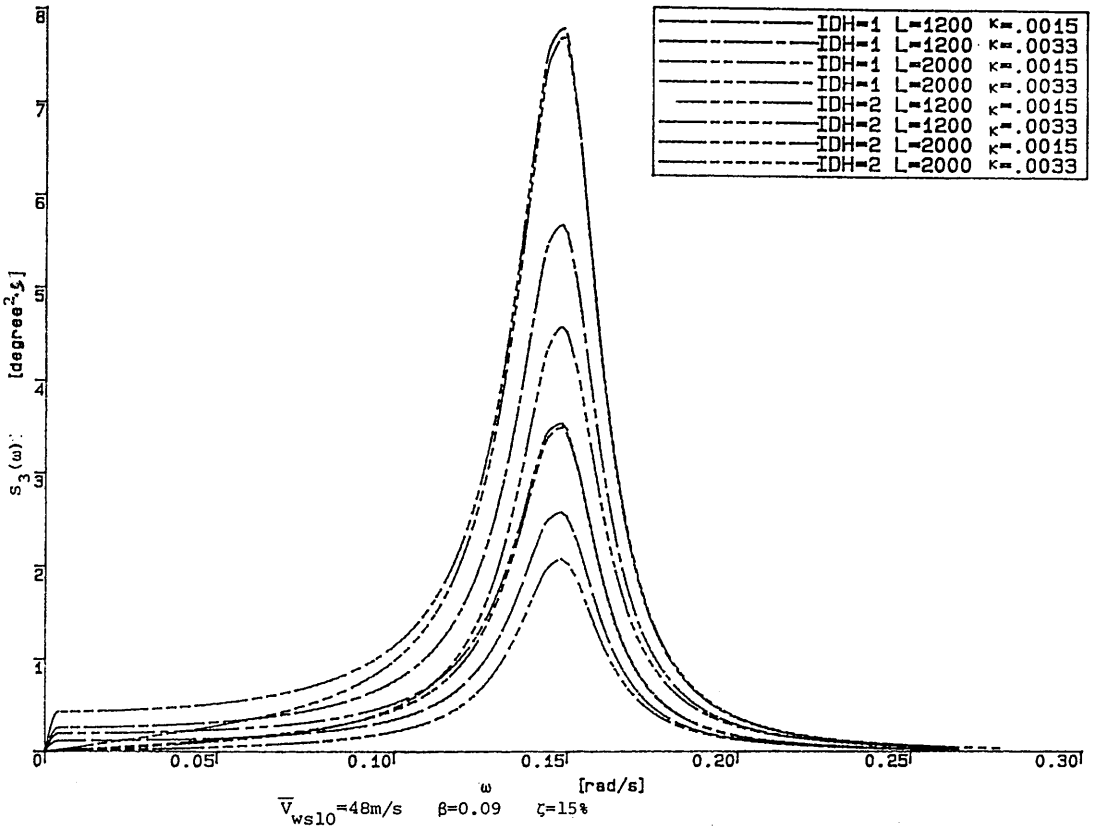

IDH=1: Harris wind velocity spectrum; IDH=2: Davenport wind velocity spectrum

Fig. 5.6 angular response spectrum to gusty wind drag force

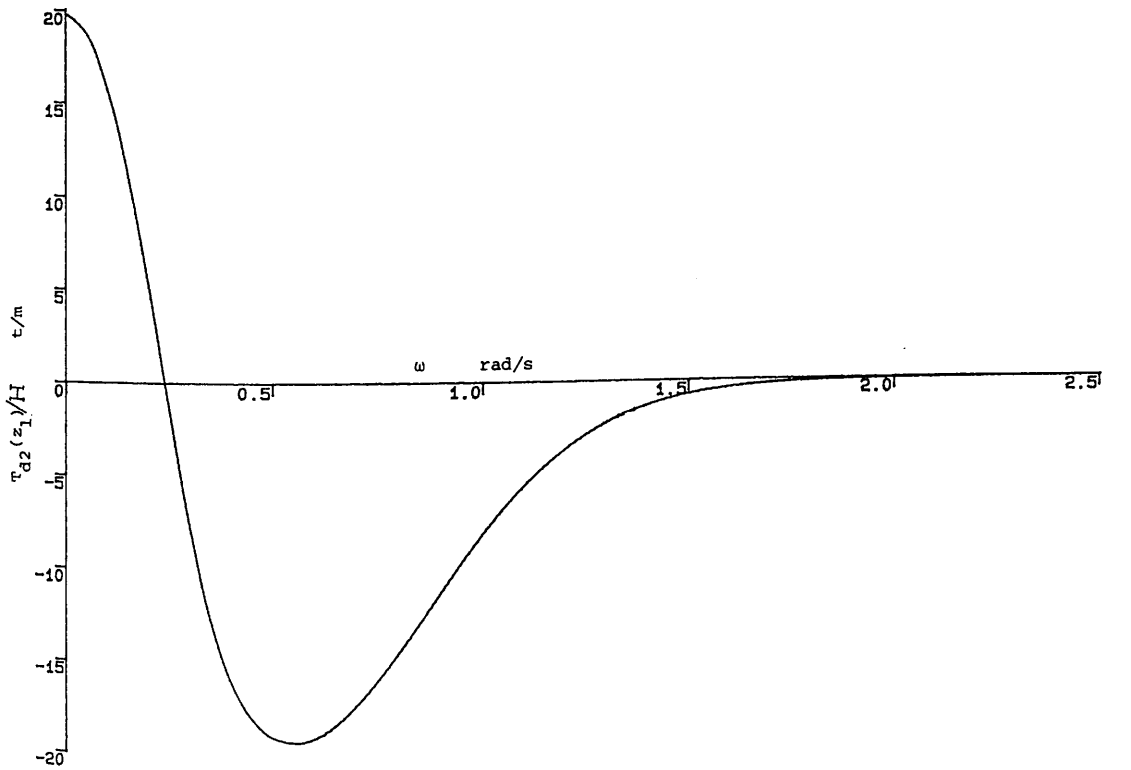

Fig. 5.7 heaving force on the articulated joint due to dynamic pressure

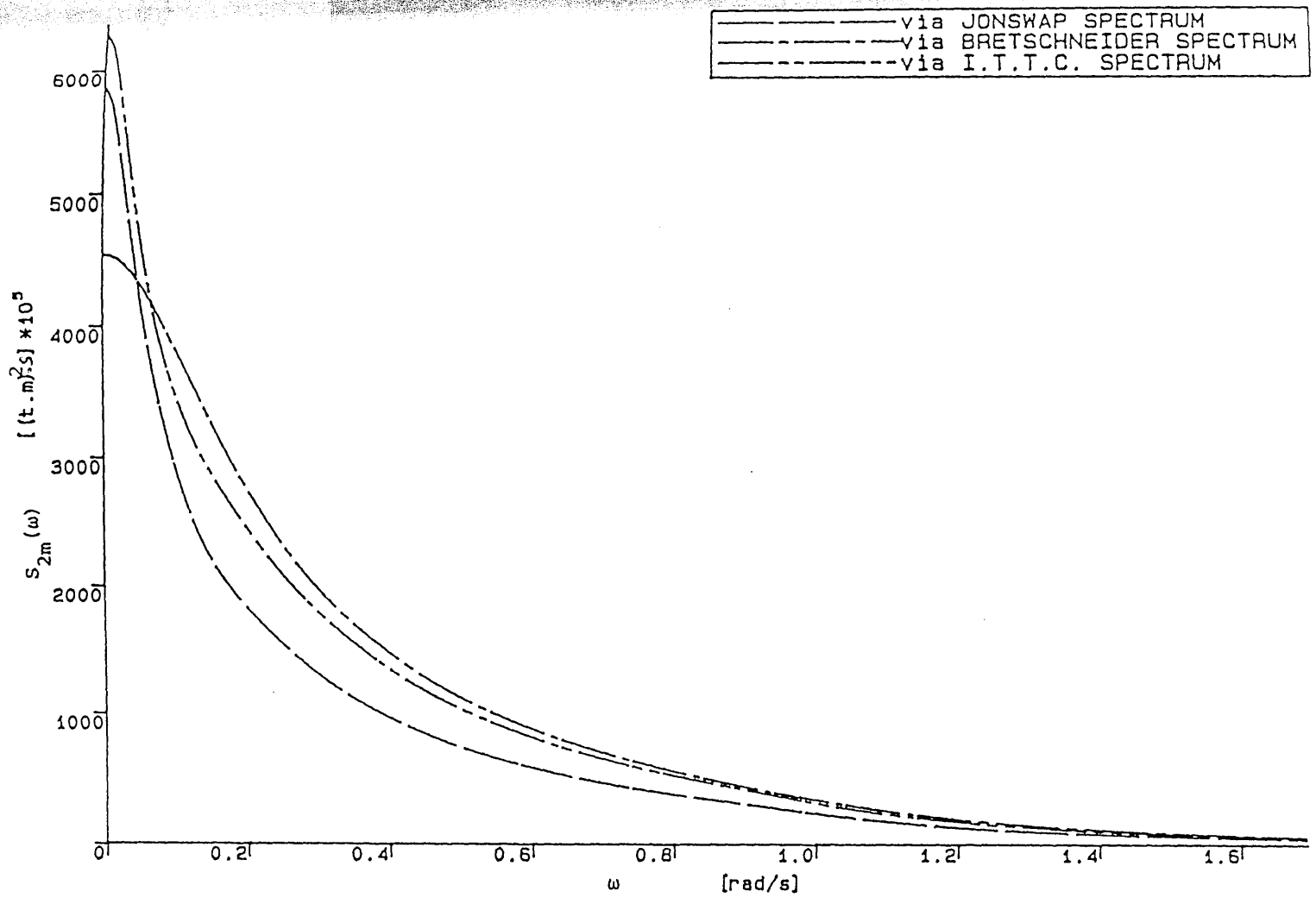

(a) moment spectrum of the slowly varying wave drift force about the articulated joint

H_s=16m T_z=14s

Fig. 5.8 dynamic response to slowly varying wave drift

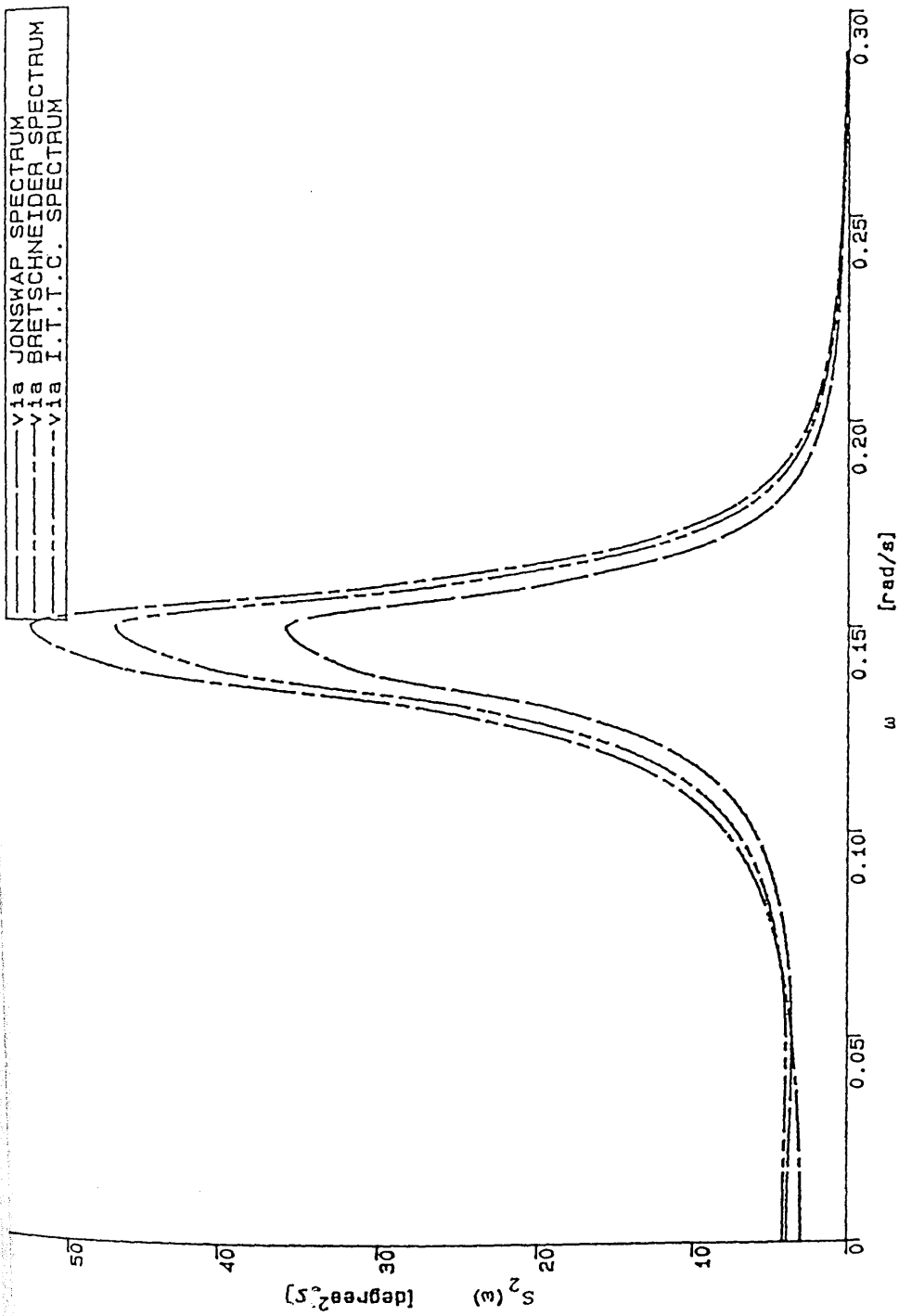

(b) angular response spectrum to slowly varying wave drift force

H_s=16m T_z=14s ζ=15%

Fig. 5.8 dynamic response to slowly varying wave drift

Table 5.1 Characterisation of the Column Segment in Figure 2.1

second moment of inertia of structural + ballasting mass

$$I_s^{(i)} = m_s(z)[E_m(z_{2i}) - E_m(z_{1i}) + Q_s(N_i)(z_{2i} - z_{1i})D_{1i}^2]$$

$$+ m_{sf}(z)[E_m(z_{4i}) - E_m(z_{3i}) + Q_f(N_i)(z_{4i} - z_{3i})D_i^2]$$

$$+ \sum_{n=J_1}^{J_2} M_{qn}(z_{qn} - z_o)(z_{qn} - z_1)$$

second moment of inertia of added hydrodynamic mass

$$I_{\ell a}^{(i)} = m_a(z)[E_m(z_{5i}) - E_m(z_{1i}) + Q_f(N_i)(z_{5i} - z_{1i})D_i^2]$$

linearised viscous damping

$$C_{\ell d}^{(i)} = m_c(z)[E_c(z_{5i}) - E_c(z_{1i})]$$

restoring stiffness

$$K_\ell^{(i)} = g\left[\sum_{n=J_1}^{J_2} M_{qn}(z_{qn} - z_o) + \frac{m_a(z)}{C_{mi}}(z_{5i} - z_{1i})\left[\frac{z_{5i} + z_{1i}}{2} - z_o\right]\right.$$

$$\left. - m_s(z)(z_{2i} - z_{1i})\left[\frac{z_{2i}+z_{1i}}{2} - z_o\right] - m_{sf}(z_{4i}-z_{3i})\left[\frac{z_{4i}+z_{3i}}{2} - z_o\right]\right]$$

pitch moment of surge wave force of inertia component

$$M_{\ell i}^{(i)} = - E_I(z)[E_{mm}(z_{5i}) - E_{mm}(z_{1i})]\sin\omega t$$

pitch moment of surge wave force of drag component

$$M_{\ell i}^{(i)} = E_D(z)[E_{mn}(z_{5i}) - E_{mn}(z_{1i})]\cos\omega t$$

$$A_i = Q_{sf}(N_i)D_i^2,\quad E_c(z) = \frac{1}{12}(z - z_1)^3[4(z - z_o) - (z - z_1)],$$

$$E_e(x) = \frac{1}{2k}\,[e^{2kx} - e^{-2kx}] + 2x$$

$$E_f(x,y) = \frac{1}{k}[\sinh kx - \sinh ky],\quad E_m(z) = \frac{1}{2}(z - z_o)^2[(z - z_1) - \frac{1}{3}(z - z_o)]$$

$$E_D(z) = \frac{\rho_w C_{di} D_i H^2 \omega^2}{3\pi \sinh^2 kd},\quad E_I(z) = \frac{\rho_w A_i C_{ai} H\omega^2}{2\sinh kd},\quad E(z) = \frac{1}{k}[(z - z_o)\sinh kd - \frac{1}{k}\cosh kd]$$

$$E_{mn}(z) = \frac{e^{-2kz}}{4k^2}\,\{[2k(z-z_o)-1]e^{4kz} - [2k(z-z_o) + 1]\} + (z-z_o)^2,\quad m_a(z) = \rho_w A_i C_{mi}$$

$$m_c(z) = \frac{4}{3\pi}\,\rho_w C_{di} H\omega\theta,\quad m_s(z) = Q_{ss}(N_i)D_i t_i \rho_{si},\quad m_{sf}(z) = Q_{sf}(N_i)D_i^2\rho_i$$

N_i =	1	2	3	4
$Q_s(N_i)$ =	0	0	1/8	1/6
$Q_f(N_i)$ =	1/12	$\pi/64$	$\pi/64$	1/12
$Q_{sf}(N_i)$ =	1	$\pi/4$	$\pi/4$	1
$Q_{ss}(N_i)$ =	4	π	π	4

Table 5.1 (Contd)

first moment of inertia of structural + ballasting mass	$I_s^{(i)} = m_s(z)[(z_{2i} - z_1)^2 - (z_{1i} - z_1)^2] + m_{sf}(z)[(z_{4i} - z_1)^2 - (z_{3i} - z_1)^2] + \sum_{n=J_1}^{J_2} M_{qn}(z_{qn} - z_1)$
first moment of inertia at added hydrodynamic mass	$I_{\ell a}^{(i)} = m_a(z)[(z_{5i} - z_1)^2 - (z_{1i} - z_1)^2]$
first moment of linearised viscous damping	$C_{\ell a}^{(i)} = \frac{1}{3} m_c(z)[(z_{5i} - z_1)^3 - (z_{1i} - z_1)^3]$
first moment of gravitational and buoyant force	$K_{\ell}^{(i)} = g\left[\frac{m_a(z)}{C_{mi}}(z_{5i}-z_{1i}) - m_s(z)(z_{2i}-z_{1i}) - m_{sf}(z)(z_{4i}-z_{3i}) - \sum_{n=J}^{J_2} M_{qn}\right]$
surge wave force of inertia component	$F_{\ell i}^{(i)} = - E_I(z)E_f(z_{5i}, z_{1i})\sin\omega t$
surge wave force of drag component	$F_{\ell d}^{(i)} = E_D[E_e(z_{5i}) - E_e(z_{1i})]\cos\omega t$

Table 5.1 (Contd)

Table 5.2 Dynamic and Static Angular Response of an Articulated Tower

(a) Dynamic Response	
pitch moment	$M_\ell(t) = M_\ell \sin(\omega t+\Phi_{id})$
angular response to regular waves	$\theta(t) = \theta\sin(\omega t+\Phi)$
response amplitude	$\theta = \frac{M_\ell}{K_\ell}\, amf(r,\zeta)$
phase angle	$\Phi = -\Phi_o + \Phi_{id},\ \Phi_o = \tan^{-1}\frac{2\zeta r}{1-r^2}$
natural frequency	$\omega_n = \sqrt{K_\ell/(I_s + I_{\ell a})}$
frequency ratio	$r = \frac{\omega}{\omega_n}$
damping ratio	$\zeta = \frac{C_\ell}{2\omega_n(I_s + I_{\ell a})}$
dynamic amplification factor	$amf(r,\zeta) = [(1 - r^2)^2 + (2\zeta r)^2]$
response amplitude operator (gain)	$G_o(\omega) = \frac{\theta}{H}$
system transfer function	$T_f(\omega) = \frac{amf(r,\zeta)}{K_\ell}$
angular response to random wave pitch moment spectrum	$S_{1m}(\omega) = \left[\frac{M_\ell}{H}\right]^2 S_\eta(\omega)$
angular response spectrum	$S_1(\omega) = [G_o(\omega)]^2 S_\eta(\omega)$

angular response to slowly varying wave drift pitch moment spectrum according to equation (2.25)

$$S_{2m}(\omega) = \int_o^{\infty} \left[S_\eta(\mu) S_\eta(\mu+\omega) \left[\sum_{i=1}^{N_e} (2\rho_w g D_i L_{ci}(\omega) C_s(\mu+\omega/2)) \right]^2 \Bigg|_{z_{1i}=z_i}^{z_{2i}=z_{i+1}} \right] d\mu \Bigg|_{z_o=z_1}$$

angular response spectrum

$$S_2(\omega) = [T_f(\omega)]^2 S_{2m}(\omega)$$

angular response to gusty wind pitch moment spectrum

$S_{3m}(\omega)$ from equation (2.35)

angular response spectrum

$$S_3(\omega) = [T_f(\omega)]^2 S_{3m}(\omega)$$

rms angular displacement

$$\sigma_j = \int_o^{\infty} S_j(\omega) d\omega$$

j=1,2,3 correspond to rms angular displacement due to random waves, slowly varying wave drift and gusty wind, respectively

(b) Static Response

static tilt under mean wave drift loading pitch moment) according to equation (2.24)

$$M_{2s} = \sum_{i=1}^{N_e} \rho_w g D_i \int_o^{\infty} S_\eta(\omega) L_{ci}(\omega) C_s(\omega) \Bigg|_{z_{1i}=z_i}^{z_{2i}=z_{i+1}} d\omega$$

static tilt under mean wind wind loading. Pitch moment according to equation (2.32)

$$M_{3s} = \sum_{i=1}^{N_e} \left[\int_{z_{1i}=z_i}^{z_{2i}=z_{i+1}} f_{3s}(z)(z-z_o) dz \right]_{z_o=z_1}$$

static tilt under steady current loading. Pitch moment according to equation (2.37)

$$M_{4s} = \sum_{i=1}^{N_e} \left[\int_{z_{1i}=z_i}^{z_{2i}\ z_{i+1}} f_{4s}(z)(z-z_o) dz \right]_{z_o=z_1}$$

static tilt

$$\theta_j = \frac{180 M_{js}}{\pi K_\varrho} \quad \text{(degree)}$$

j = 2,3,4 correspond to the static tilt due to mean wave drift, mean wind and steady current loadings, respectively

Table 5.2 (Contd)

Table 5.3 Distribution of the Internal Sectional Forces Along an Articulated Tower in Regular Waves

static tension : $T_s(z) = \text{Sum } \bar{K}_{\ell}^{(i)} \Big|_{z=z}$, ($K_{\ell}^{(i)}$ is from Table 5.1)

dynamic tension : $T_d(z,t) = T_{d1}(z,t) + T_{d2}(z,t)$

$$T_{d1}(z,t) = \begin{cases} 0 & \text{otherwise} \\ Q_{sf}(N_{j_\eta}) D_{j_\eta}^2 \rho_w g, & z < d+\eta,\ z_{j_\eta} < z < z_{j_\eta+1} \end{cases}$$

$$T_{d2}(z,t) = \sum_{i=j_z+1}^{N_e} F_{1v}(z_i,t)$$

$$F_{1v}(z_i,t) = \begin{cases} \rho_w g H \left[0.5(A_i - A_{i-1}) \dfrac{\cosh kz_i}{\sinh kd} - \dfrac{\pi}{3} Jk(C_{mvi} R_i^3 - C_{mvi-1} R_{i-1}^3) \dfrac{\sinh kz_i}{\sinh kd} \right] \cos(kx - \omega t), & z_i < d+\eta \\ 0, & z_i > d+\eta \end{cases}$$

shear force : $F_s(z,t) = F_s \sin(\omega t + \theta_s)$ (See Appendix 1)

bending moment : $M_b(z,t) = M_b \sin(\omega t + \theta_b)$ (See Appendix 1)

Table 5.4 data of the sample monolithic single articulated tower used in Chapter 5

structural element	length	diameter	equivalent shell thickness
DECK	6m	30m	W_o=500t
U.C.	45m (h_c=25m)	7.0m	0.1m
B.C.	20m	15m	0.1m
L.C.	141.6472m	8.0m	0.1m
Ba.C.	18.3528m	18.3528m	0.1m
E.C.	0.0	0.0	
water depth	200m (z_1=0.0)		
drilling mud density	2.5t/m^3 (filling the ballast chamber)		
force coefficients	C_a=2.0 C_d=0.7 (except where stated otherwise)		

Table 5.5 characteristics of the sample structure in Table 5.4

	DECK	U. C.	B. C.	L. C.	Ba. C.	TOTAL
I_s (t.m x10^7)	2.603	3.179	2.129	2.679	0.150	10.74
$I_{\ell a}$ (t.m x10^7)	0.000	2.856	10.50	7.040	0.060	20.46
$C_{\ell a}$ (t.m.s x10^7)	0.000	0.154	0.265	0.333	0.001	0.753
K_ℓ (kN.m x10^7)	-0.112	-0.006	0.483	0.397	-0.072	0.690
V_i (t)	0.000	790.5	3630.	7312.2	4986.2	16719
W_{si} (t)	0.000	771.9	735.1	2776.8	825.37	4609
W_{bi} (t)	0.000	0.000	0.000	0.0000	12138	12138
h_{cb} (m)	87.63					
h_{cg} (m)	42.93					

Table 5.6 r.m.s. spectral response characteristics of the sample structure in Table 5.4 in random waves

NT		1				2				3			
C_a		1.5		2.0		1.5		2.0		1.5		2.0	
C_d		0.0	0.7	0.0	0.7	0.0	0.7	0.0	0.7	0.0	0.7	0.0	0.7
NI	Tz (=Hs)												
1	8	0.208	0.207	0.178	0.177	0.206	0.206	0.177	0.177	0.181	0.181	0.157	0.156
	10	0.322	0.320	0.267	0.267	0.321	0.320	0.268	0.268	0.284	0.283	0.240	0.240
	12	0.465	0.460	0.367	0.366	0.459	0.455	0.367	0.367	0.402	0.400	0.329	0.329
	14	0.691	0.657	0.486	0.484	0.661	0.636	0.482	0.480	0.551	0.544	0.428	0.427
	16	1.333	0.977	0.649	0.638	1.178	0.916	0.632	0.624	0.801	0.746	0.547	0.544
2	8	0.270	0.270	0.234	0.234	0.279	0.278	0.242	0.242	0.272	0.271	0.237	0.236
	10	0.280	0.279	0.238	0.238	0.286	0.285	0.243	0.243	0.282	0.282	0.242	0.241
	12	0.282	0.281	0.234	0.234	0.285	0.283	0.236	0.236	0.282	0.281	0.236	0.236
	14	0.289	0.285	0.229	0.228	0.287	0.283	0.228	0.227	0.282	0.280	0.229	0.228
	16	0.329	0.298	0.226	0.224	0.316	0.293	0.223	0.222	0.290	0.284	0.223	0.222
3	8	48.524	48.901	55.871	56.258	50.132	50.530	57.775	58.176	48.942	49.325	57.323	57.690
	10	49.792	50.125	52.405	52.920	50.905	51.283	53.308	53.854	50.395	50.798	54.359	54.863
	12	51.390	51.308	46.879	47.470	50.835	50.876	45.663	46.323	49.706	49.945	47.484	48.115
	14	62.944	59.378	43.424	43.883	58.829	56.243	40.271	40.863	52.062	51.591	41.293	41.961
	16	125.879	84.986	47.665	46.916	107.935	76.875	42.711	42.327	68.640	62.071	39.464	39.868
4	8	12.095	14.198	21.221	22.372	10.740	13.188	20.503	21.762	11.380	13.462	21.872	22.927
	10	14.818	17.275	17.512	19.409	12.774	15.714	14.728	17.069	11.002	14.030	15.489	17.540
	12	23.305	25.299	19.997	22.056	22.152	24.374	17.673	20.094	18.588	21.013	15.948	18.408
	14	35.566	36.254	26.685	28.498	34.346	35.461	25.779	27.737	28.641	30.471	22.535	24.615
	16	63.229	51.536	35.385	36.773	57.386	49.569	34.997	36.517	41.730	41.655	30.540	32.273

a) NI= 1,2,3,4 correspond to r.m.s. angular displacement (in degree),horizontal acceleration at the middle deck level (in m/s^2),shear force on the articulated joint (in tonnes),and internal sectional shear force on SECTION 1 (in tonnes) respectively.

b) T_s is in seconds and H_s is in meters.

Table 5.7a r.m.s. angular response (in degree) of the sample structure due to low frequency wave drift

NT	H_s/T_z \ C_a, ζ	1.5		2.0	
		10%	20%	10%	20%
1	8.0m/8.0s	0.1852	0.1303	0.1640	0.1156
	10.0m/10.0s	0.2109	0.1488	0.1883	0.1330
	12.0m/12.0s	0.2263	0.1601	0.2037	0.1442
	14.0m/14.0s	0.2366	0.1680	0.2146	0.1523
	16.0m/16.0s	0.2439	0.1737	0.2229	0.1586
2	8.0m/ 8.0s	0.1726	0.1241	0.1586	0.1139
	10.0m/10.0s	0.1851	0.1336	0.1704	0.1230
	12.0m/12.0s	0.1933	0.1400	0.1780	0.1290
	14.0m/14.0s	0.1996	0.1447	0.1838	0.1334
	16.0m/16.0s	0.2044	0.1484	0.1881	0.1374
3	8.0m/ 8.0s	0.1832	0.1311	0.1660	0.1190
	10.0m/10.0s	0.2039	0.1461	0.1844	0.1324
	12.0m/12.0s	0.2176	0.1559	0.1969	0.1416
	14.0m/14.0s	0.2274	0.1631	0.2065	0.1487
	16.0m/16.0s	0.2346	0.1685	0.2142	0.1542

Results corresponding to NT=1,2,3 are obtained using the Bretschneider,Jonswap,and ITTC wave spectrum respectively.

Table 5.7b ratios of the r.m.s. angular displacement of the sample structure due to low frequency wave drift with C_a=2.0 over that with C_a=1.5 showing the effect of C_a

T_z \ NT, ζ	10%			20%		
	1	2	3	1	2	3
8.	0.8855	0.9189	0.9061	0.8872	0.9178	0.9077
10.	0.8928	0.9206	0.9044	0.8938	0.9207	0.9062
12.	0.9001	0.9208	0.9049	0.9007	0.9214	0.9083
14.	0.9070	0.9208	0.9081	0.9065	0.9219	0.9117
16.	0.9139	0.9203	0.9130	0.9131	0.9259	0.9151

Table 5.8a r.m.s. angular displacement of the sample structure in Table 5.4 due to fluctuating wind (unit in degree)

IHD				1				2			
C_a	$\bar{V}_{ws10}$	β	L	1200		2000		1200		2000	
			ζ \ κ	.0015	.0033	.0015	.0033	.0015	.0033	.0015	.0033
1.5	35.	.075	.05	.175	.259	.189	.280	.170	.252	.190	.282
			.10	.124	.185	.136	.202	.119	.176	.135	.200
			.20	.089	.132	.100	.148	.082	.122	.096	.143
		.125	.05	.180	.268	.195	.290	.176	.261	.196	.291
			.10	.129	.191	.141	.209	.123	.182	.140	.207
			.20	.092	.137	.103	.153	.085	.126	.099	.147
	48.	.075	.05	.299	.444	.342	.507	.276	.410	.340	.504
			.10	.212	.315	.245	.363	.192	.285	.239	.354
			.20	.151	.224	.176	.262	.132	.195	.167	.247
		.125	.05	.309	.459	.354	.525	.286	.424	.351	.521
			.10	.220	.326	.253	.376	.199	.295	.247	.366
			.20	.156	.232	.182	.271	.136	.202	.172	.255
2.0	35.	.075	.05	.165	.245	.185	.275	.156	.232	.185	.274
			.10	.117	.174	.133	.197	.109	.161	.131	.194
			.20	.084	.124	.096	.143	.075	.111	.092	.136
		.125	.05	.171	.253	.191	.284	.161	.239	.191	.284
			.10	.121	.180	.137	.204	.113	.167	.135	.200
			.20	.087	.128	.100	.148	.077	.115	.095	.141
	48.	.075	.05	.278	.413	.328	.486	.245	.363	.319	.473
			.10	.197	.293	.234	.347	.170	.252	.223	.331
			.20	.140	.208	.167	.248	.116	.172	.154	.229
		.125	.05	.288	.427	.339	.503	.253	.375	.330	.490
			.10	.204	.303	.242	.359	.176	.261	.231	.343
			.20	.145	.215	.173	.257	.120	.178	.160	.237

Results corresponding to IHD=1 and 2 are obtained using the Harrris and Davenport wind spectrum respectively.

Table 5.8b ratio of the r.m.s.angular displacement of the sample structure in Table 5.4 to fluctuating wind with Ca=2.0 over that with Ca=1.5 showing the effect of Ca

	IHD=1		IHD=2	
$\bar{V}_{ws10}$ \ L	1200	2000	1200.	2000.
35.	0.9457	0.9800	0.9179	0.9746
48.	0.9300	0.9579	0.8853	0.9400

Table 5.9 environmental loading on the sample structure, the moment of various forces on the structure about the joint

	design conditions		operational conditions			
H/T	30m/16s	30m/21s	13m/11s	13m/15s	17m/11s	17m/15s
$M_{\ell d}$ (kt.m)	15.36	16.54	5.438	6.494	7.112	8.492
$M_{\ell i}$ (kt.m)	-333.15	-280.6	-171.68	-150.8	-224.5	-197.2
	$\bar{V}_{wsl0}$=48m/s β=0.09 C_{da2}=0.7 C_{da1}=2.0		$\bar{V}_{wsl0}$=35m/s β=.09 C_{da2}=0.7 C_{da1}=2.0			
M_{3s} (kt.m)	18.33		9.749			
	C_d=0.7					
M_{4s} (kt.m)	3.62		2.957			

Table 5.10 angular response of the sample structure to the environmental loading (in degree)

(a) dynamic response

		design conditions		operational conditions			
regular waves	H/T	30m/16s	30m/21s	13m/11s	13m/15s	17m/11s	17m/15s
		4.534	7.161	1.016	1.769	1.329	2.315
random waves	NT / H_s/T_z	16m/14s	16m/16s	8m/8s	8m/10s	10m/8s	10m/10s
	1	0.774	1.022	0.142	0.213	0.177	0.267
	2	0.768	0.998	0.142	0.214	0.177	0.268
	3	0.683	0.870	0.125	0.192	0.156	0.240
slowly varying wave drift	ζ=10% NT / H_s/T_z	16m/14s	16m/16s	8m/8s			10m/10s
	1	0.2803	0.2229	0.1640			0.1883
	2	0.2479	0.1881	0.1586			0.1704
	3	0.2697	0.2142	0.1660			0.1844
random wind	$\bar{V}_{wsl0}/\beta$	48m/s / 0.09		35m/s / 0.09			
	L/κ	2000m / 0.0033		2000m / 0.0033			
	IHD	1	2	1	2		
		.352	.337	.200	.197		

(b) static response

mean wave drift	NT / H_s/T_z	16m/14s	16m/16s	8m/8s			10m/10s
	1	0.1501	0.1172	0.0961			0.1060
	2	0.1335	0.1035	0.0899			0.0964
	3	0.1501	0.1169	0.0976			0.1066
mean wind	$\bar{V}_{wsl0}/\beta$	48m/s / 0.09		35m/s /0.09			
		1.49		.795			
steady current	V_{ct}/V_{cw}	0.5m/s / 0.8m/s		0.5m/s / 0.8m/s			
		.295		.241			

related parameters: C_a=2.0 and C_d=0.7 C_{da2}=0.7 C_{da1}=1.5 ζ=10%

Table 5.11 the significance of the surface elevation contribution to the linear angular response amplitude

ω (rad/s)	0.3	0.4	0.5	0.6	0.7	0.8	0.9	1.0
$M_{\ell d}$ (kt.m) Int=(0,d)	18.21	16.80	15.13	10.61	6.75	4.46	3.05	2.16
$M_{\ell i}$ (kt.m) Int=(0,d)	-296.9	-371.6	-420.7	-350.1	-252.2	-181.9	-132.4	-98.1
$M_{\ell d}$ (kt.m) Int=(d,d+H/2)	3.05	4.07	5.09	3.86	2.42	1.61	1.12	0.819
$M_{\ell i}$ (kt.m) Int=(d,d+H/2)	-33.87	-60.10	-94.08	-85.80	-62.55	-47.65	-37.52	-30.30
θ (degree) Int=(0,d)	7.126	4.401	3.017	1.694	0.881	0.481	0.275	0.164
θ (degree) Int=(0.,d+H/2)	8.022	5.187	3.761	2.151	1.122	0.620	0.361	0.220

H is taken to be the breaking wave height given in Eq.(2-9), and $\mathrm{Int}(x,y)=\int_x^y dz$

Table 5.12 ratios of the r.m.s. angular displacement of the sample structure due to low frequency wave drift with ζ=20% over that with ζ=10% showing the effect of dp

	C	1.5			2.0	
Tz	NT 1	2	3	1	2	3
8	0.712	0.732	0.728	0.710	0.727	0.725
10	0.714	0.735	0.728	0.712	0.731	0.726
12	0.717	0.738	0.729	0.714	0.735	0.727
14	0.720	0.740	0.730	0.716	0.737	0.728
16	0.723	0.742	0.732	0.719	0.739	0.729

Results of the r.m.s. angular displacement of the model structure due to the low frequency wave drift with ζ=10% and 20% are listed in Table 5.8

CHAPTER 6

DYNAMIC RESPONSE OF A MONOLITHIC SINGLE ARTICULATED TOWER - MODEL TESTING

1. INTRODUCTION

This chapter details the model testing of a monolithic single articulated tower in regular waves and makes comparisons between measured results of its forces and motion and computed predictions. The model test is described first and then the data of measured forces and motions are analysed. Finally, conclusions are drawn on the correlation between the model test results and the theoretical predictions.

2. DESCRIPTION OF THE MODEL STRUCTURE

The model structure of the monolithic single articulated tower is shown in fig. 6.1, together with the relevant geometrical dimensions. An aluminium bar and the articulated joint were the only alloy components of the model. The remainder of the structure was built of PVC tubes of density $\rho_s = 1.400 t/m^3$.

There were six major cylinders of different diameter which, with the top plate, were divided into 7 column components ($N_e = 7$) as indicated in fig. 6.1 and Table 6.2. There was no ballasting of the model structure.

The alloy bar was used to measure the shear forces on the articulated joint in the direction of the wave propagation and

perpendicular to it and the tension on the joint, owing to the difficulties of strain-gauging PVC. The tension in the articulated joint can be directly measured by measuring the strain on the bar section. The shear forces on the joint were obtained by measuring the bending strains on the section of the bar caused by the shear forces on the joint. The bar was made of aluminium to obtain a sensitive reading from the strain-gauges which were stuck to its surface. To increase the sensitivity of the strain-gauges to axial tension/compression, a circular hole was drilled along its vertical axis. The details are also shown in fig. 6.1. The bar surface was designed to give an adequate area for the strain-gauges to be mounted on it and to avoid reducing the sensitivity of the strain-gauges to tension. The bar was of sufficient length to minimise the effect of possible position variation of the pin which acts as the hinge of the joint due to its possible loose fit into the hole, perpendicular to the notch on the bar. The hole through which the pin was fitted, was made very close to the top of the bar to avoid possible interference with the motion of the structure.

3. OUTPUT AND SET-UP OF THE MODEL TEST

The motion in the direction of waves and in the direction normal to waves, shear forces on the articulated joint in both directions and the heaving force on the articulated joint were recorded.

Apart from using strain-gauges to measure the forces on the articulated joint, the motion was recorded using the Selspot equipment to measure the horizontal displacements on the deck plate at its centre point. The effect of the vertical displacement was negligible

because of the long distance between the centre point and the articulated joint coupled with the small angular displacement of the structure.

The wave profile was measured using wave probes in three different positions across the width of the tank.

Figures 6.2 and 6.3 show the instrumentation and set-up of the model testing, ie the way in which Selspot was used to pick up the motion, wave probes to record the wave profiles and strain-gauges connected into Wheatstone Bridges to measure the forces on the articulated joint.

Calibration of the instruments used in the model test did not involve any particular difficulty. Two pulleys were mounted on the bottom plate along each direction to apply horizontal forces to the bar in both directions on the articulated joint. Wires were led through each pulley horizontally so that loads were applied through the wires above the water.

In the present study, the results were recorded on the computer only in the steady state while the chart recording was used for the responses in both the steady and transient states. The computer digitisation of the output recording follows a linear relationship between the output voltages and the computer digits as:

Output voltage	-5.12V	0.0V	5.12V
Computer digit	0	2047	4095

4. PRESENTATION OF THE MEASUREMENTS

The number of complete cycles recorded is obtained as follows:-

$$NC = \frac{T_t}{T} \tag{6.1}$$

where T_t and T are the total recording time and wave period, respectively. By picking up the maximum and the minimum values in the recordings of each complete cycle NC maximum and minimum numbers are obtained, denoted as X_{mci} and X_{mti}, $i = 1,2,\ldots,NC$. Meanwhile, from the zero recording, the zero position is obtained, denoted as X_{mz}. The zero-to-crest mean and the zero-to-trough mean are obtained then as:-

$$X_c = \frac{1}{NC} \sum_{i=1}^{NC} (X_{mci} - X_{mz})$$

and

$$X_t = \frac{1}{NC} \sum_{i=1}^{NC} (X_{mz} - X_{mti}) \tag{6.2}$$

The output values corresponding to X_c and X_t were obtained by substituting them into the appropriate calibration function. The mean value between the trough and the crest was obtained as $X_d = X_c - (X_c + X_t)/2.0$ which represents the drift. The mean response amplitude is then $X_m = (X_c + X_t)/2.0$.

The model test results are presented in Table 6.1. Where appropriate, they are divided by the corresponding wave height which is also presented in the table.

The original recordings of the motion in both x and y directions were translational. The angular motions can easily be obtained from the translational motions. The wave height from each

wave probe was obtained as $H_i = X_c + X_t$ where X_c and X_t are defined as before. The wave heights from the three wave probes were then averaged to obtain the mean wave height H, as listed in the table.

There were three groups of wave heights for different frequencies generated by three different input voltages to the wavemaker, ie 4V, 8V and 12V, respectively. The higher input voltages are meant to generate steeper waves aimed at measuring non-linearity in the motion responses. Model tests were also carried out with two specific wave frequencies to test the dynamic instability discussed in Chapter 7. The two frequencies correspond to $f = \frac{2}{i} f_n \sqrt{1 - \zeta^2}$ with $i = 1,2$ where f and f_n are the wave frequency and natural frequency (in Hz) of the rigid body mode motion of the model, $f_n = 0.2857$Hz as is listed in Table 6.1. The input voltage to the wavemaker is 16V.

The results for steady state motion, in Table 6.1 are explained below.

The scale factor was chosen as 100 so that the model scale frequencies were in the region between 0.16 rad/s and 1.0 rad/s at full scale. The wave height generated varied from 1.5m up to 9m at full scale.

The drift of the angular response is very small, in general. At high frequencies, the negative drift shown in the table is thought to be attributable to the longlasting unsteady response recorded as there is little damping. The unsteady response is discussed in Chapter 7.

The motion in the y direction is about 10%-33% of the motion amplitude in the x direction at frequencies below 0.4Hz, but becomes greater at higher frequencies. The ratio between the shear force on the articulated joint in the y and x directions seems to decrease with frequency.

The axial force recorded is very significant in comparison with the shear force, due to the shallow submergence of the large diameter buoyancy chamber.

5. COMPARISON BETWEEN THE MODEL TEST MEASUREMENTS AND THEORETICAL PREDICTIONS

Two theoretical models were used. The first one divides the model structure into five column sections ($N_e = 5$). The other divides it into seven column sections ($N_e = 7$) which is more accurate. The details are listed in Table 6.2. Where two or more columns of different diameters are concentric, they are modelled as one column which has the same sectional weight as that of all the columns and which has the same diameter as the outer column. This is done by using an equivalent shell thickness. Results from the model tests and from theoretical calculations are compared in Table 6.1.

The natural frequencies of the two theoretical models were calculated with $C_a = 1.7$ and match the measured natural frequency. C_a should theoretically have been about 2.0 in most cases for the present model test. Therefore, there may be certain discrepancies in selecting the present $C_a = 1.7$. Nevertheless, it is still between 1.5 and 2.0 as is used in Chapter 5.

The measured damping ratio varies from 6.51% to 12.5%. The

average of the measured damping ratios is 9.16%. This is listed in Table 6.1.

In selecting C_d for the calculation of viscous damping, the scale factor should be taken into account. In model scale, Re, the Reynolds Number is likely to be in the subcritical region. Therefore, C_d is expected to vary between 1.0 and 1.2. When $C_d = 1.0$ was used in the theoretical calculations, a good agreement between the measured damping ratio an the calculated was obtained. In the full scale, on the other hand, Re is likely to be in the supercritical region and C_d is about 0.6 to 0.7. Using $C_d = 0.7$, the damping ratio is much lower than the model scale calculation and is about 5.5% in full scale compared with 9.16% measured in the model test. The measured damping is thought to justify the theoretically predicted value.

Using $C_a = 1.7$ and $C_d = 1.0$, theoretical calculations of angular dynamic response and shear force on the articulated joint were carried out. The results obtained from the present computer program MONO.DYNAMIC are also listed in Table 6.1. In addition, comparisons in graphical form are shown in figs. 6.4 and 6.5.

The angular dynamic responses obtained using the two theoretical models were nearly the same. Therefore, the angular dynamic response, using the second model only is plotted in fig. 6.4. It is seen, that apart from the resonance region where the theoretical predictions give a grossly higher response than the model test results, the agreement is very good.

In fig. 6.5, results from theoretical prediction of the shear force on the articulated joint of the two physical models are compared

with the model test data. Good agreement is also achieved.

In addition, model test results of a concrete model structure from Snowdon [24] as shown in figs. 6.8 to 6.10 are further compared with the results from the MONO.DYNAMIC program. The agreement between the model test and theoretical calculations on the angular dynamic response and shear force on an articulated joint, is excellent. The concrete model is shown in fig. 6.7.

In calculating the heaving force on the articulated joint, $C_{mv} = 1.0$ was taken for all the column sections in figs. 6.6 and 6.10. The agreement between the present model test and theoretical prediction in fig. 6.6 was found to be good at wave frequencies above f = 0.4Hz. In the low frequency region, the difference is marked, however. This is thought to be attributed to the fact that at low frequencies the wave height generated in the tank was small and that the calibration of axial tension/compression was very insensitive. In addition, this may be partially attributed to the fact that the drag force terms were discounted in the theoretical calculations. The theoretical prediction agrees very well, however, with the concrete model test in the low frequency region. At high frequencies, the theoretical prediction tends to over-estimate axial tension/compression as shown in fig. 6.10.

In addition, the angular dynamic response from the concrete model test in Ref. [24] to slowly varying wave drift is taken and compared with results from the present computer program calculation, as listed in Table 6.3 in the form of surge at the top of the model. The amount of damping used may vary from 5% to 15% which is expected in low frequency motion. The predicted result agrees satisfactorily

with the model test result. The damping ratio seems to be around 10%.

It should be noted that the P-M type spectrum should be the same as the Bretschneider spectrum as it would also be of the form as defined in equation (2.40) if H_s and T_z were used.

In addition, the model test results also confirms the conclusion drawn in Chapter 5, that use of smaller T_z gives rise to greater angular response for the same H_s, to the slowly varying wave drift force.

6. CONCLUDING REMARKS

Good agreement was achieved in the tension on the articulated joint between the model test and the theoretical prediction, except at very low frequencies. The difference at low frequencies is thought to be attributed to the insensitive measurement of the axial tension and the omission of the viscous effect. The agreement on shear force on the articulated joint was found to be very satisfactory.

The theoretical models have been shown to model the physical behaviour of the angular motion accurately, providing appropriate values of C_a and C_d are selected. The only area of pure agreement exists around resonance where the angular response to regular waves was overestimated.

LIST OF FIGURES

LIST OF TABLES

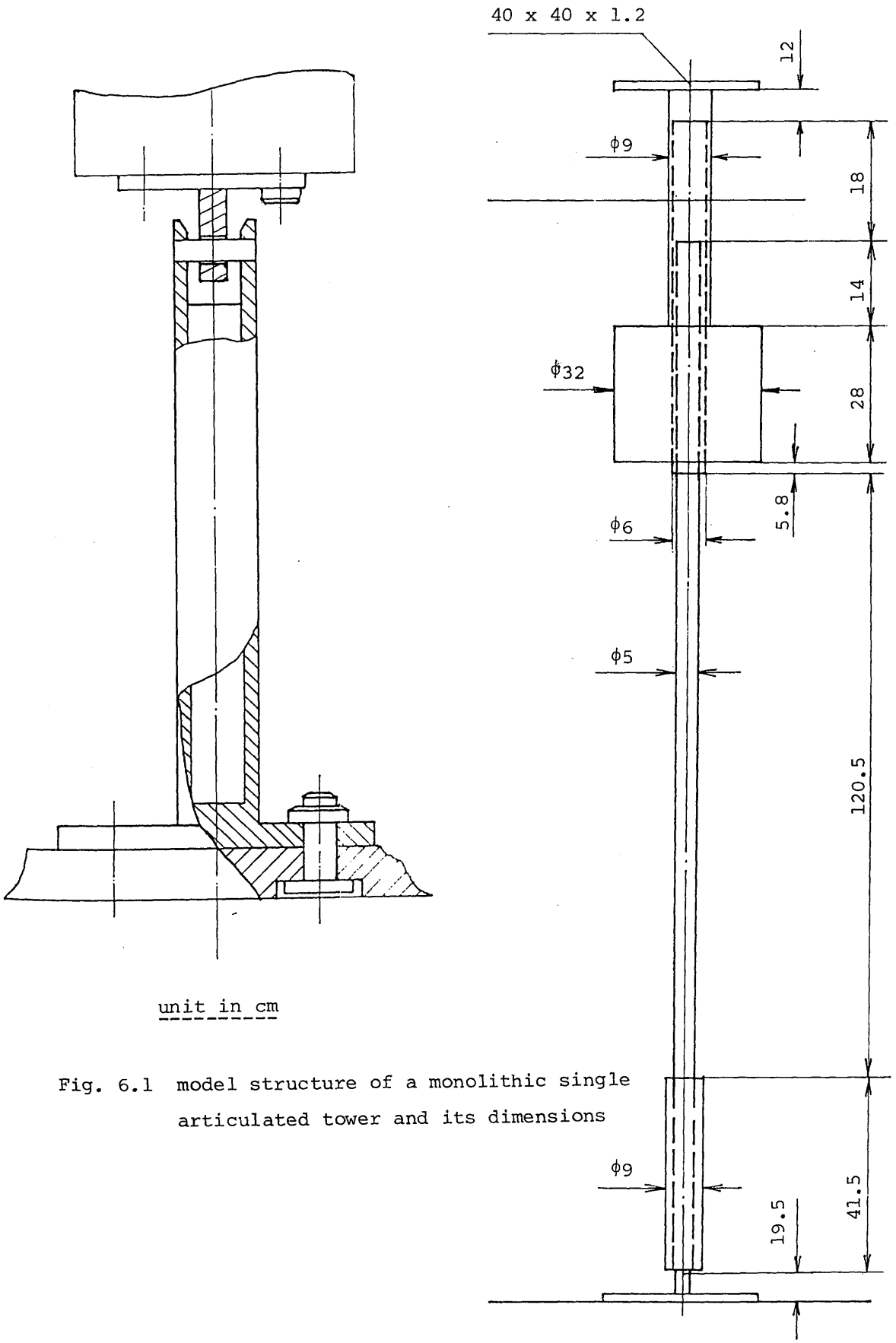

unit in cm

Fig. 6.1 model structure of a monolithic single articulated tower and its dimensions

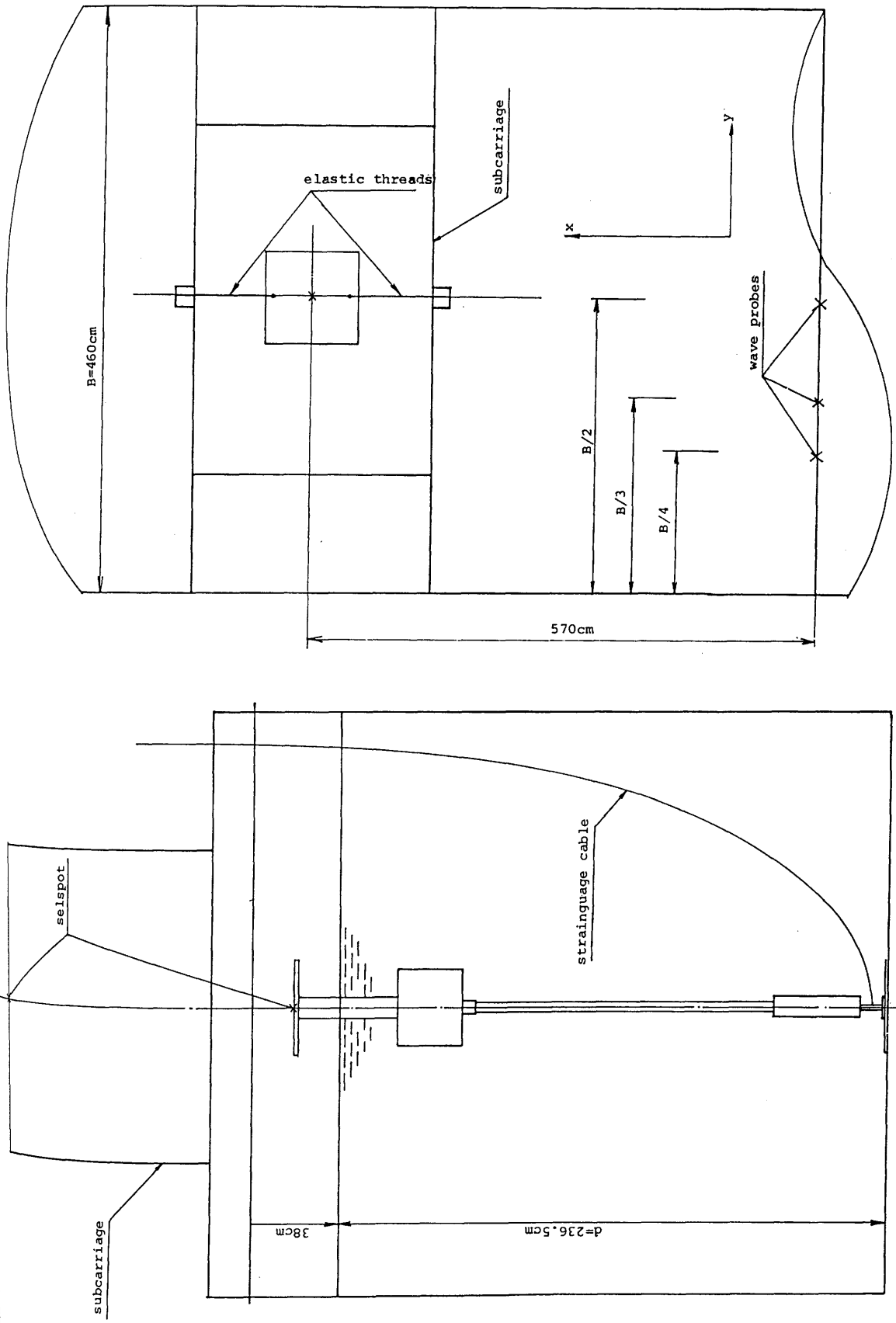

Fig. 6.2 set-up of model test

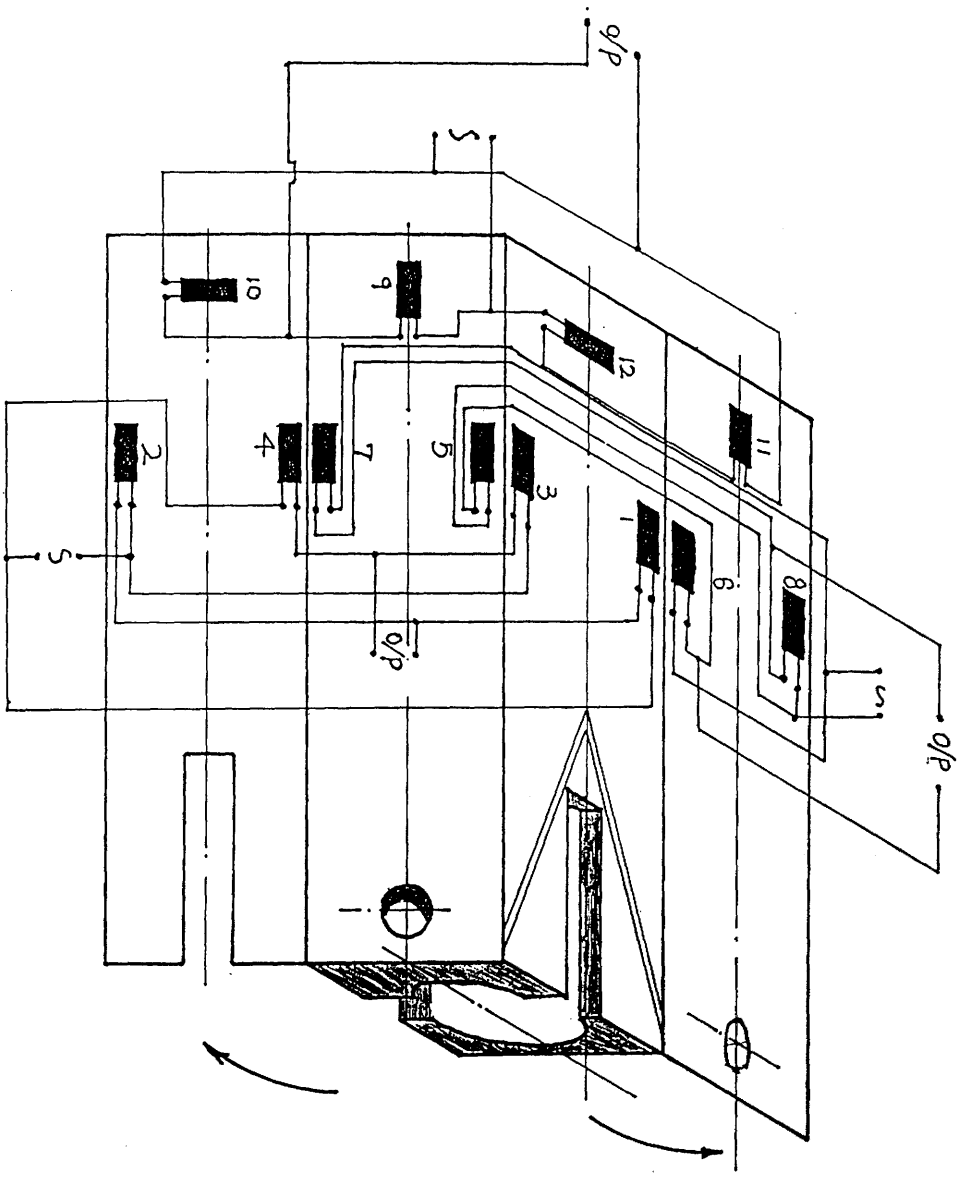

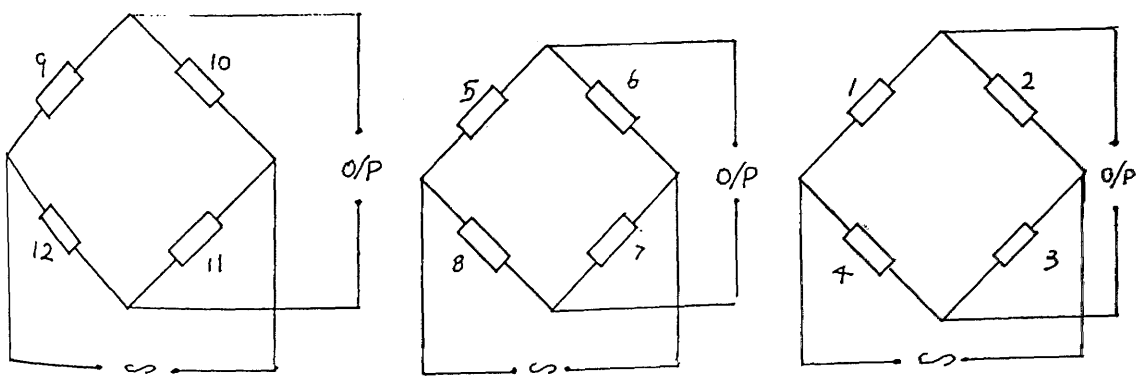

tension shear - y shear - x

Fig. 6.3 connection of the strainguages for the measurement of tension and shear force on the articulated joint

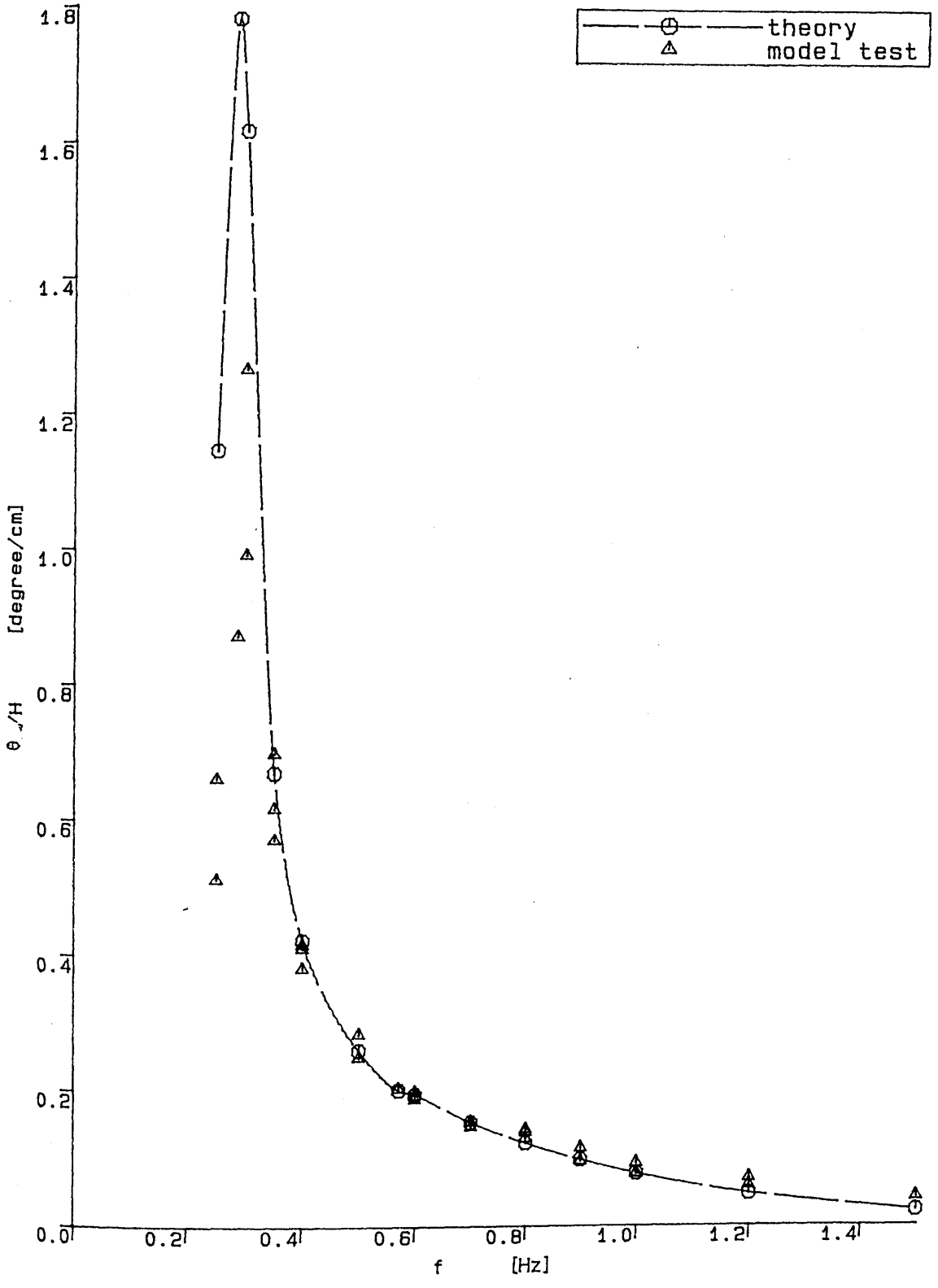

Fig. 6.4 angular dynamic response

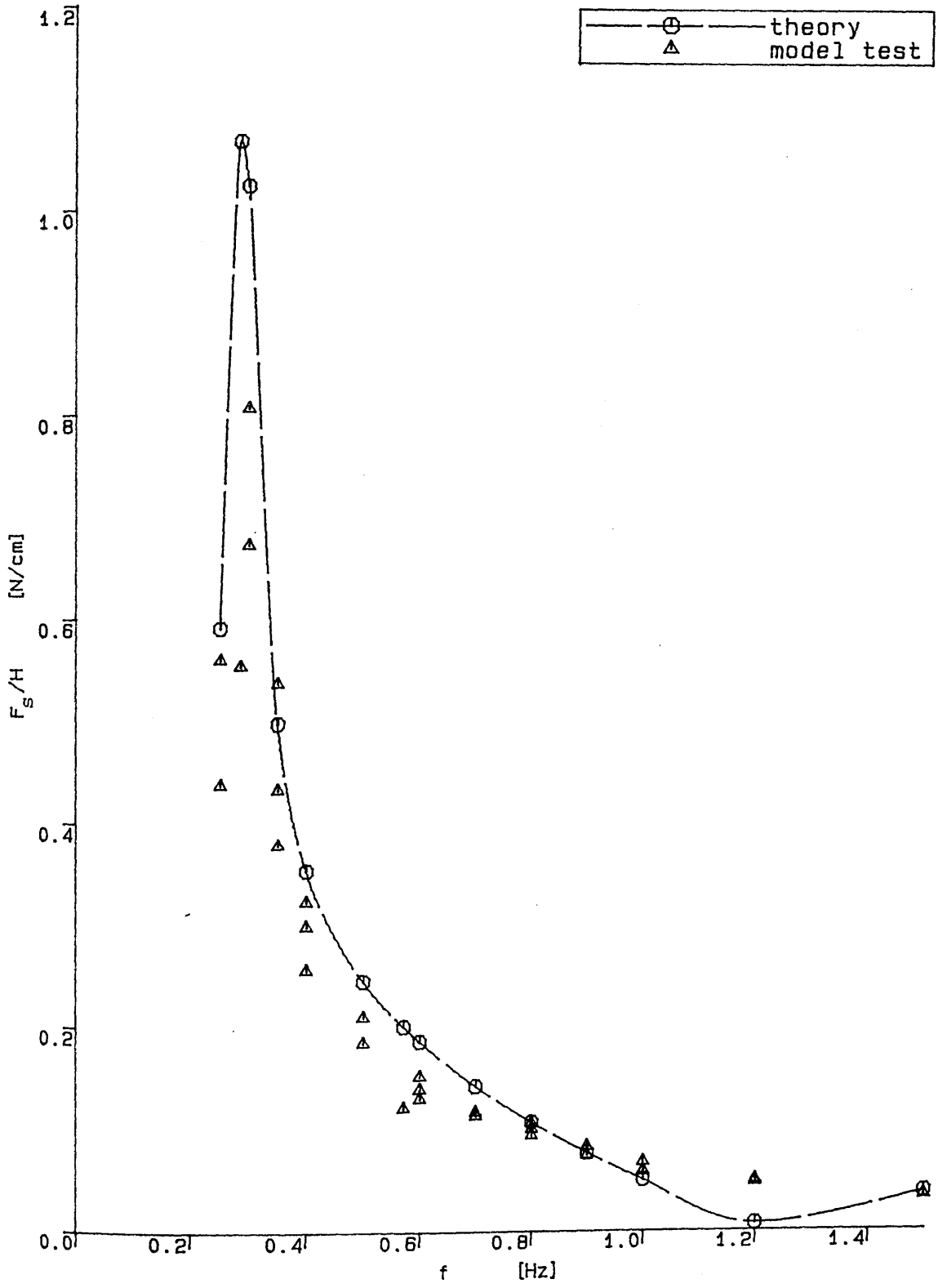

Fig. 6.5 shear force on the articulated joint

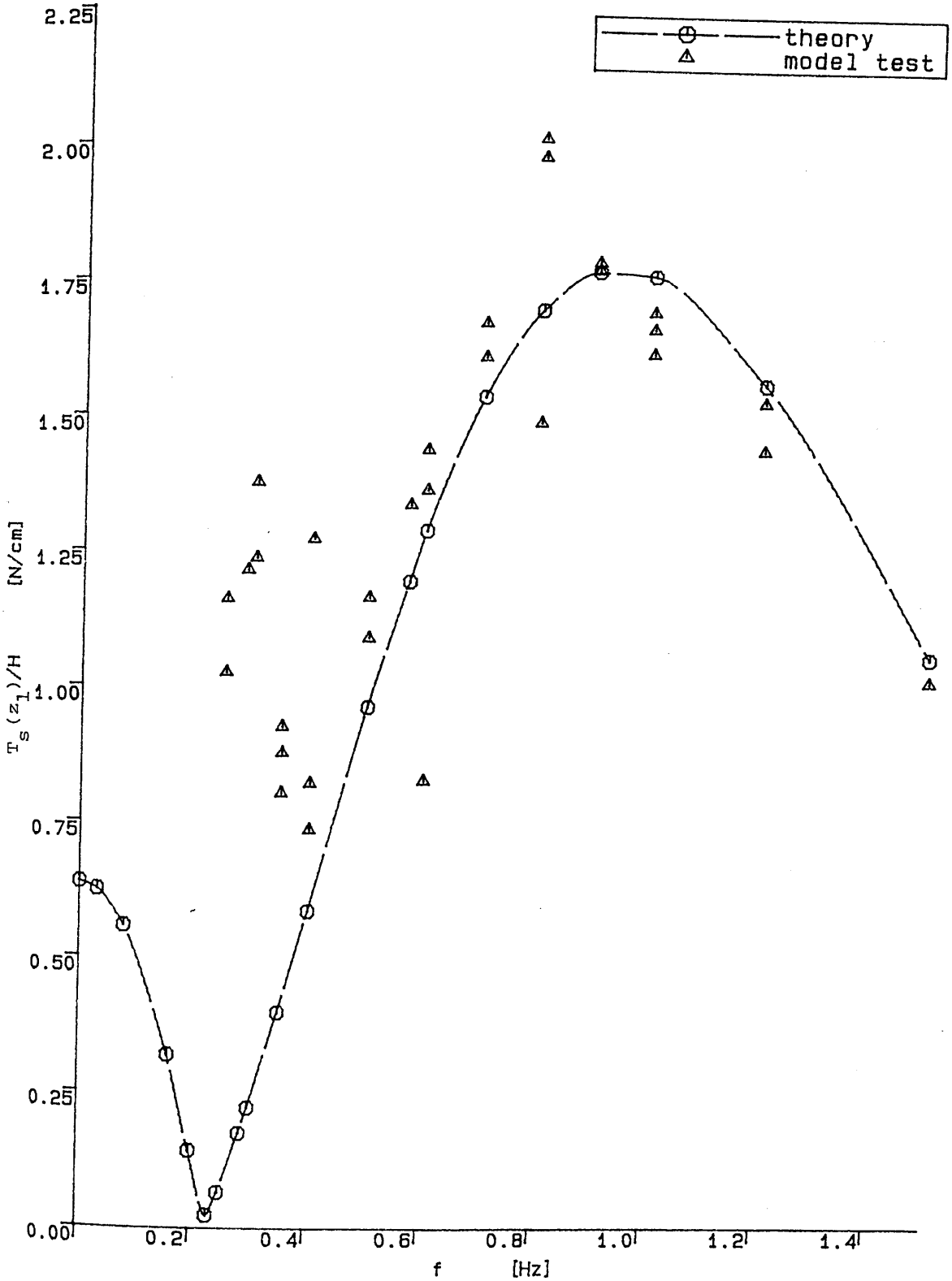

Fig. 6.6 heaving force amplitude on the articulated joint

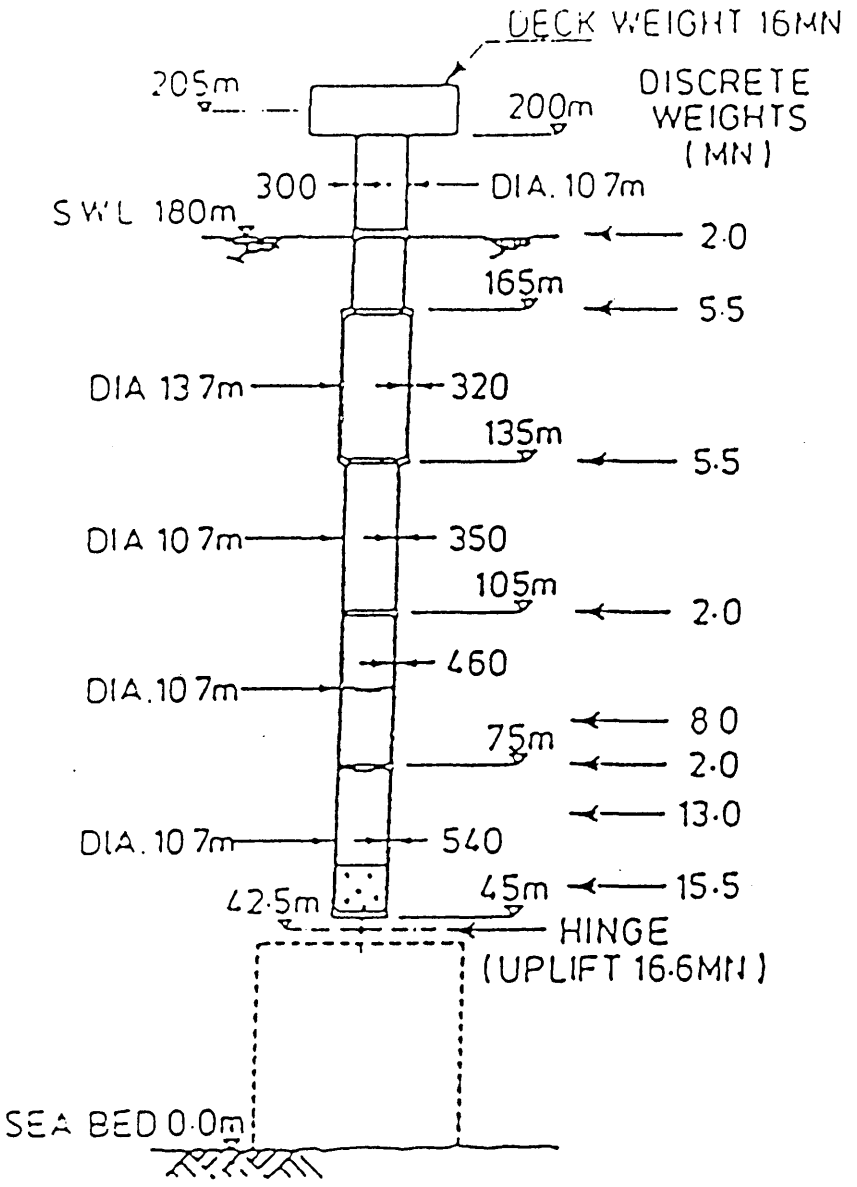

Fig. 6.7 model test structure (ref. 24)

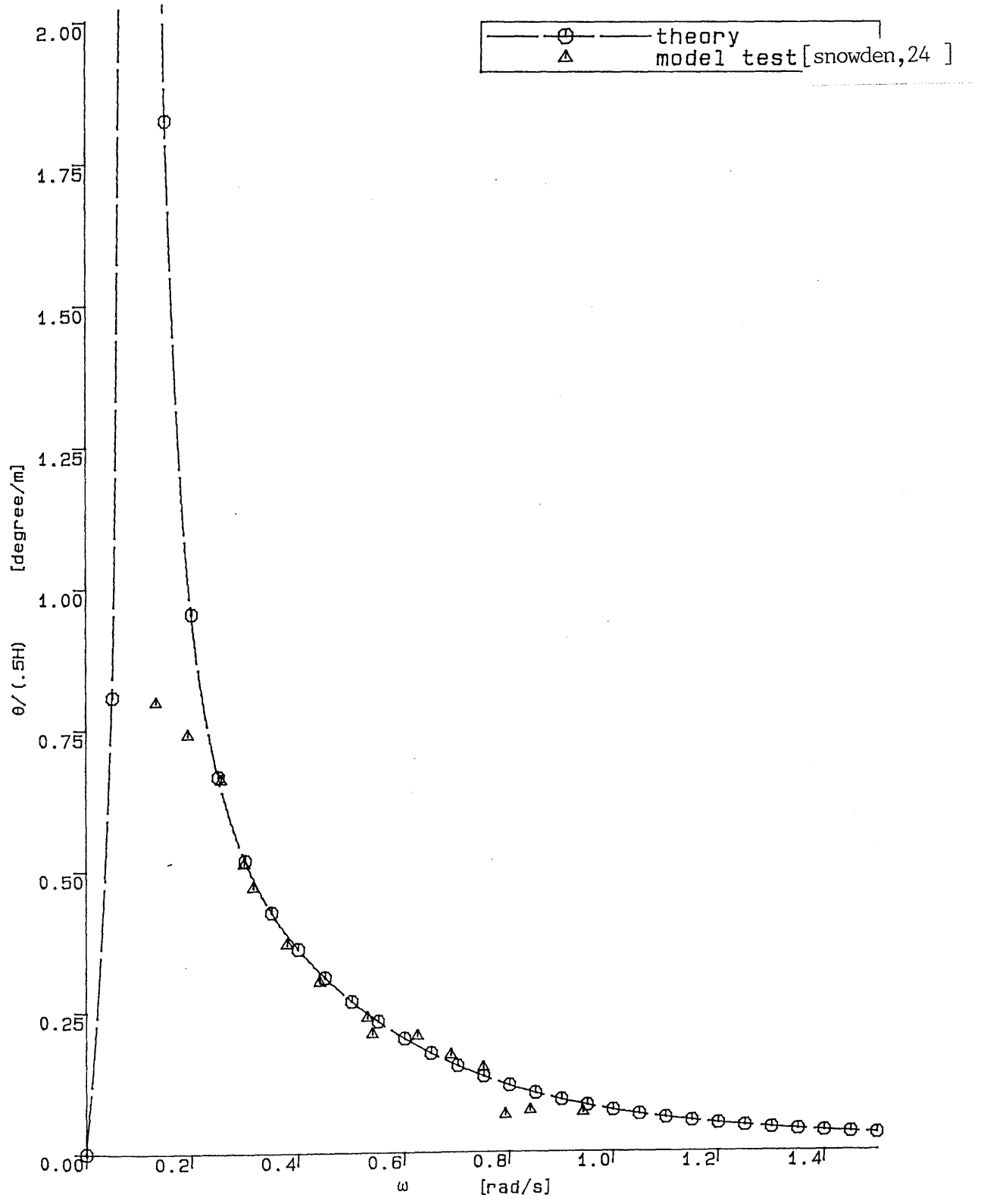

Fig. 6.8 comparison of angular dynamic response between theoretical prediction and model test

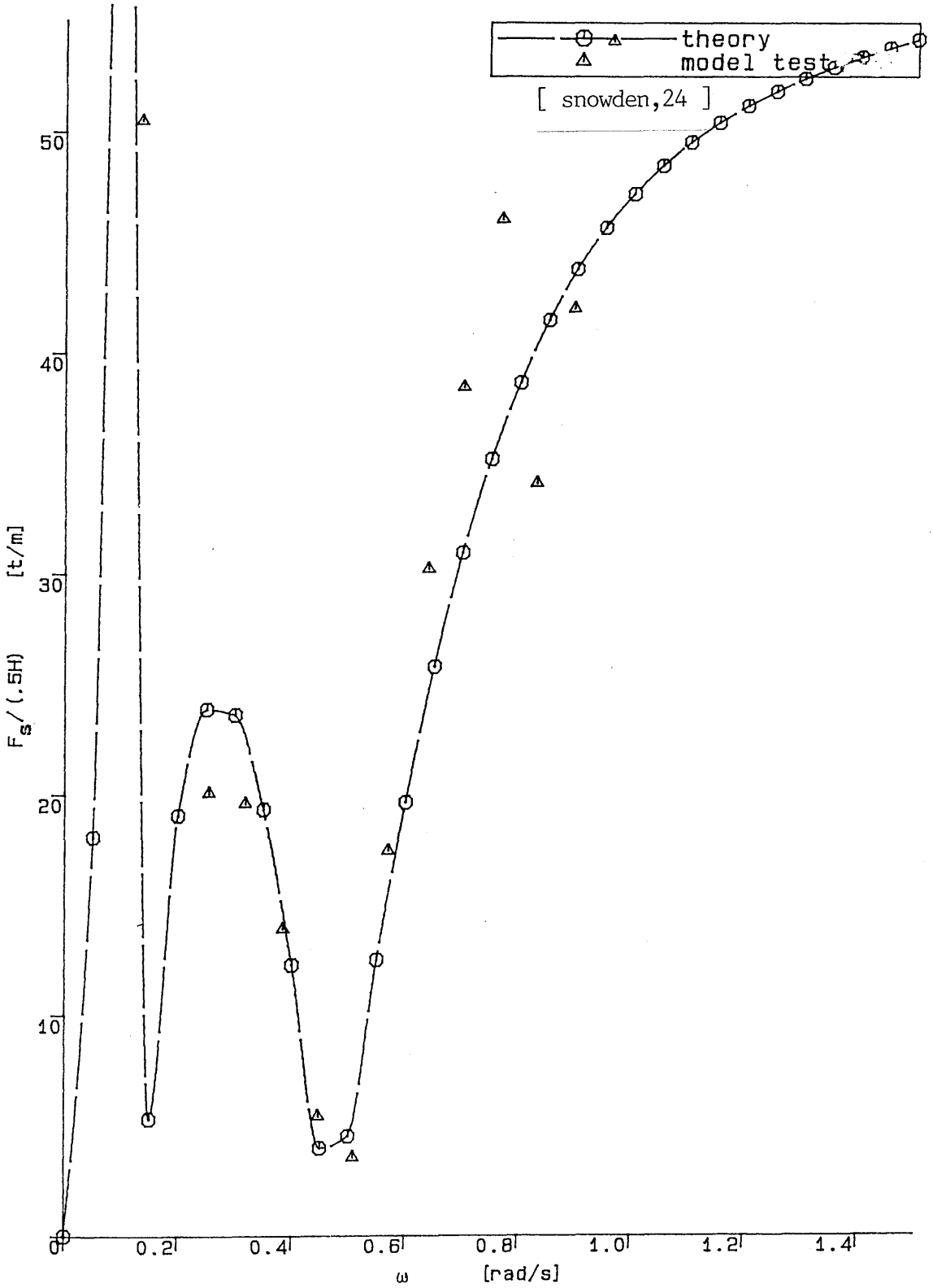

Fig. 6.9 comparison of shear force on articulated joint between theoretical prediction and model test

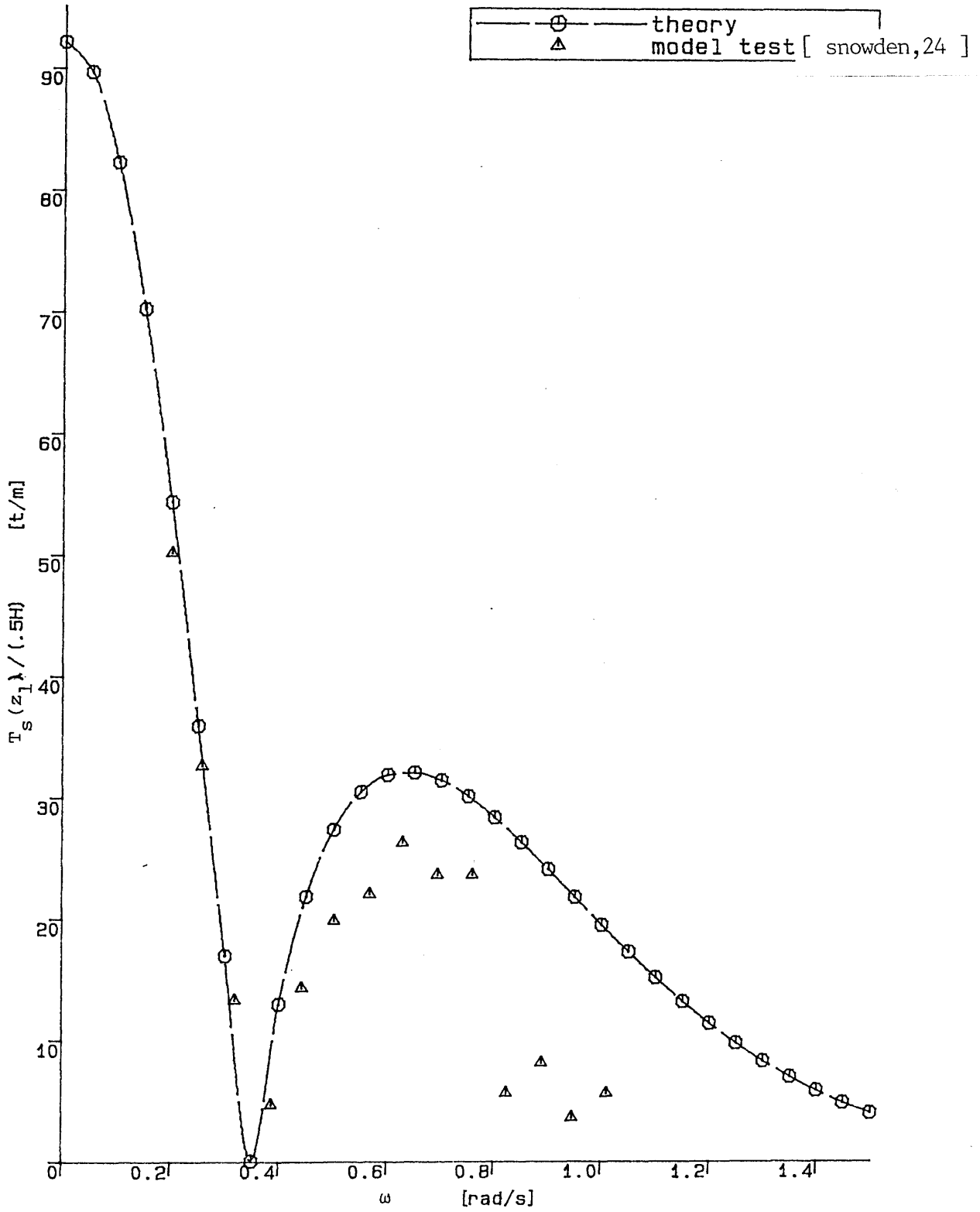

Fig. 6.10 comparison of heaving force between theoretical prediction and model test

Table 6.1 model test results and comparison with theoretical predictions

(a) chacteristics of the model

	W_Σ (kg)	V_Σ (kg)	K_ℓ (N.m)	ω_n (rad/s)	ζ (%)	$T_s(z_1)$ (N)
theory (C_e=1.7 , C_d=1.0)	9.399	28.83	291.4	1.774	8.06	190.5
model test	9.4	28.83	285.1	1.796	9.16	190.5

(b) wave height unit: cm

f	.25	.3	.35	.4	.5	.6	.7	.8	.9	1.	1.2	1.5
4V	1.418	1.5946	1.8253	2.2412	2.7619	3.5554	3.8522	3.3143	3.7035	3.7652	3.4150	3.9504
8V	2.5009	2.6629	3.1671	3.6579	4.8624	5.8941	6.3225	5.8814	6.3257	6.4666	5.7668	
12V			4.5932	5.3089		8.1512		8.3988		8.9805		

(c) motion in the direction of wave propagation: degree/cm

4V	X_c	.6931	1.2914	.7008	.4330	.2872	.1948	.1368	.1438	.1203	.09395	.06428	.01799
	X_t	.62618	1.2361	.6919	.3977	.2794	.20236	.15673	.1416	.1090	.09082	.07573	.06458
8V	X_c	.52158	1.03267	.6350	.3887	.2513	.18776	.15964	.1383	.09223	.07635	.05389	
	X_t	.50113	.94674	.59565	.4305	.24686	.187	.1481	.1399	.09832	.07667	.06398	
12V	X_c			.60307	.39433		.17898		.12669		.07245		
	X_t			.53693	.3655		.20577		.13183		.0819		
theory (N_e=8)		1.1440	1.6150	.6676	.4214	.2594	.1531	.1223	.0974	.0771	.0471	.0216	
(N_e=6)		1.153	1.603	.6644	.4201	.2588	.1528	.1221	.09724	.07694	.04699	.02159	

(d) motion in transverse direction to wave propagation unit: degree/cm

4V	X_c	.10886	.20954	.18324	.11154	.09805	.06040	.05391	.05598	.04589	.04081	.03498	.01736
	X_t	.24981	.21722	.14404	.1011	.05954	.05803	.04438	.04765	.03053	.03131	.02328	
8V	X_c	.10832	.19686	.14288	.09723	.06344	.04661	.03646	.04232	.03430	.02899	.02268	
	X_t	.16705	.21968	.08875	.08579	.04378	.03895	.03536	.03605	.0309	.023	.02397	
12V	X_c			.11983	.0718		.03676		.0345		.02148		
	X_t			.10843	.07287		.03738		.03032		.01908		

(e) shear force in the direction of wave propagation unit: N/cm

4V	X_c	.5729	.8196	.5306	.3352	.2133	.1565	.1202	.1062	.08280	.06905	.03705	.01985
	X_t	.5473	.10	.5902	.3102	.2084	.1481	.1140	.1063	.08324	.06577	.06151	.04702
8V	X_c	.4273	.5826	.3855	.2918	.1887	.1428	.1155	.1017	.07778	.05726	.03623	
	X_t	.4478	.7628	.4791	.3052	.1808	.1357	.1114	.09932	.07115	.05867	.05790	
12V	X_c			.3187	.2314		.1273		.09746		.06287		
	X_t			.4386	.2804		.1332		.09088		.05425		
theory (N_e=8)		.5912	1.024	.4971	.3531	.2450	.1423	.1069	.07678	.05015	.006747	.03785	
(N_e=6)		.6052	1.032	.5022	.3572	.2483	.1447	.1091	.07878	.05197	.008	.3687	

(f) shear force in transverse direction to wave propagation unit: N/cm

4V	X_c	.6231	1.193	.5792	.3604	.2935	.1945	.1753	.1114	.0976	.08537	.02871	.03472
	X_t	.5655	.9259	.4931	.3460	.2184	.1941	.1429	.08976	.08853	.09626	.07648	.05623
8V	X_c	.5224	.7430	.4486	.2898	.2345	.1718	.1468	.10920	.07310	.06767	.04084	
	X_t	.3304	.5496	.3964	.2617	.1722	.1610	.1360	.08476	.07873	.07660	.06488	
12V	X_c			.3734	.2760		.1453		.08982		.05706		
	X_t			.3418	.2273		.1434		.09621		.09582		

(g) tension unit: N/cm

4V	1.161	1.3765	.8019	.7347	1.166	1.441	1.615	1.9875	1.7782	1.701	1.4466	1.019
8V	1.0242	1.2366	.9244	.8201	1.0913	1.366	1.678	2.0221	1.793	1.624	1.5355	
12V			.8763	1.273		.8271		1.495		1.6705		
theory (N_e=8)	.06568	.2222	.3976	.5852	.9627	1.541	1.703	1.776	1.769	1.569	1.063	
(N_e=6)	.06581	.2224	.3979	.5855	.9629	1.541	1.703	1.776	1.769	1.569	1.063	

Table 6.2 details of the two theoretical models

i=	D_i(m)	t_i(m)	L_i(m)	notes
		model one : N_e=5		
1	9cm	.467cm	41.3cm	z from 21cm to 62.3cm
2	5cm	.32cm	126.3cm	z from 62.3cm to 188.6cm
3	32cm	.754cm	28cm	z from 188.6cm to 216.6cm
4	9cm	.5cm	44cm	z from 216.6cm to 260.6cm
5	40cm			rectangular deck solid body of 1.2cm thick
model height 240.8cm lumped weight M_{q1}=0.6259kg ,position z_{q1}=188.6cm lumped weight M_{q2}=0.6259kg ,position z_{q2}=216.6cm				
		model two : N_e=7		
1	9cm	.47cm	41.3cm	z from 21.cm to 62.3cm
2	5cm	.32cm	126.3cm	z from 62.3cm to 188.6cm
3	32cm	.754cm	28cm	z from 188.6 to 216.6cm
4	9cm	.67cm	14cm	z from 216.6 to 230.6cm
5	9cm	.5cm	18cm	z from 230.6 to 248.6cm
6	9cm	.3cm	12cm	z from 248cm to 260.6cm
7	40cm			rectangular deck solid body of 1.2cm thick
model height 240.8cm lumped weight M_{q1}=0.6259kg ,position z_{q1}=188.6cm lumped weight M_{q2}=0.6259kg ,position z_{q2}=216.6cm				

Table 6.3 comparison of surge response to slowly varying wave drift in random seas between theoretical prediction(I.T.T.C. spectrum) and model test(P-M spectrum)

wave spectrum:H_s/T_z		10m/12s	14.5m/13.5s	15m/15s
surge measured[6-3]		1.09m	2.08m	1.89m
surge predicted	ζ=10%	1.525m	2.662m	2.402m
(C_m=1.0)	ζ=15%	1.245m	2.175m	1.964m
	ζ=20%	1.078m	1.884m	1.702m

CHAPTER 7

TIME DOMAIN NON-LINEAR DYNAMIC RESPONSE OF MONOLITHIC SINGLE ARTICULATED TOWER STRUCTURES - THEORY AND MODEL TEST

1. INTRODUCTION

The dynamic response analysis of monolithic single articulated tower structures presented in Chapter 5 is based on a fundamental assumption that the structural system and structure-environment interactions are linear. This leads to a linear motion equation of the structure, which is solved in the frequency domain. The implication of this is that the non-linear effects are negligibly small. However, the validity of the above assumption needs to be demonstrated. This chapter examines the significance of various sources of non-linearities and their combinations in terms of the motion response of monolithic single articulated tower structures. The assumption of linearity was also investigated experimentally.

The non-linear equation of motion was solved, subsequently in the time domain by direct integration using the Wilson-θ [74] and Runge-Kutta methods [75].

In seeking a time domain solution, transient response phenomena and the effect and importance of the non-linearities on the steady state response were investigated. In the end, simplifications were made to the non-linear motion equation to arrive at a motion equation which enables the phenomenon of dynamic instability in the motion of articulated tower structures to be examined.

The model which was used in the experiments was a stand-alone monolithic single articulated tower, as detailed in Chapter 6 and it was tested in regular waves.

2. NON-LINEAR MOTION EQUATION

2.1. Formulation of the Non-Linear Motion Equation

If no assumption that $\theta(t)$ is small, is made and if the integrations are carried out up to the free surface $(d + \eta)$ in deducing equation (5.7), the equation of non-linear motion is obtained. It is, in general, written in a similar form to equation (5.7) as:-

$$I_n\ddot{\theta}(t) + C_n\dot{\theta}(t) + K_n\theta(t) = M_n(t) \tag{7.1}$$

where I_n, C_n, K_n and $M_n(t)$ are the corresponding quantities which are functions of $(\theta, \dot{\theta}, \ddot{\theta})$ in general and are given in relation with the linear quantities in equation (5.7), as:-

$$I_n = I_s + [I_{\ell a} + I_{\eta a}]\ (1 + \tan\theta)\cos^2\theta \tag{7.2}$$

where $I_{\eta a}$ is the amount of fluctuation of the second moment of added hydrodynamic mass due to free surface elevation and is given, from Table 5.1, as:-

$$I_{\eta a} = I_{\ell a}^{(i)} \Bigg|_{\substack{z_{2i} = d + \eta \\ z_{1i} = d,\ z_o = z_1}}$$

$$C_n = C_s + 2\, I_s\, \dot{\theta}\, \tan(\theta) \tag{7.3}$$

$$K_n = [K_\ell + K_t]\ \sin(2\theta)/(2\theta) \tag{7.4}$$

with $$K_t = K_{t1} + K_{t2} \tag{7.5}$$

$$K_{t1} = T_{d1}(z,t)\ (d + \eta - z_1) \tag{7.6}$$

and $$K_{t2} = \sum_{i=1}^{N_e+1} F_{1v}(z_i,t)(z_i - z_1) \tag{7.7}$$

according to Table 5.3. In addition:-

$$M_n(t) = \int_{z_1}^{d+\eta} \{f_{nx}(z,t) + f_{nz}(z,t)\tan\theta\}(z-z_o)dz \Big|_{z_o=z_1} \cos^2\theta \tag{7.8}$$

where $f_n(z,t)$ is given according to equation (2.14), as:-

$$f_n = \frac{\pi D^2}{4}\rho_w C_a \dot{\vec{U}}_n + \tfrac{1}{2}\rho_w C_d D \,|\, \vec{U}_n - \dot{\vec{r}}_n \,|\, (\vec{U}_n - \dot{\vec{r}}_n)$$

with $$\dot{r}_{nx} = (z - z_1)\dot{\theta}, \dot{r}_{nz} = (z - z_1)\dot{\theta}\tan\theta$$

and $$\vec{e} = \sin\theta\vec{i} + \cos\theta\vec{k}$$

in equation (2.15)

The wave kinematics are calculated with phase angle:-

$$\Omega = [k(z - z_1)\tan\theta - \omega t]$$

From the above formulation, it becomes clear that the non-linearities are due to one of the following aspects or their combination:-

a. interaction of the time varying axial force with the pitch motion of the structure,

b. non-linear drag term in Morison's equation,

c. the free surface elevation, and

d. large amplitude motions of the structure.

2.2. Modification of the Wave Kinematics

It is noted that the wave kinematics in equations (2.1) to (2.6) are only valid up to the still water level. The integration above the mean water level, ie from d to d + η, will be incorrect, using wave kinematics derived based on small amplitude wave theory. It was suggested that the wave kinematics in the region of free surface elevation be modified 'stretching' the wave kinematics above the mean water level [70]. In finite water depth, the 'stretched' water particle kinematics are obtained by assuming the same values at the wave trough and the wave crest. For example, the wave particle velocity in horizontal direction is given in equation (2.3) becomes, in its stretched form:-

$$U_x = \frac{H\omega}{2} \frac{\cosh\{kxd/(d+\eta)\}}{\sinh kd} \cos\Omega \tag{7.11}$$

The conservative form of the horizontal velocity after stretch may be such that:-

$$U_x = \begin{cases} \frac{H\omega}{2} \tanh kd \cos\Omega & d \leq z \leq d + \eta \\ \frac{H\omega}{2} \frac{\cosh kz}{\sinh kd} \cos\Omega & 0 \leq z < d \end{cases} \tag{7.12}$$

The stretched form of wave kinematics as in equation (7.11) was used in this study.

3. DISCUSSION OF THE RESULTS

Computer program MONO.TIME was written to calculate the

motion response in the time domain. The wave frequency used was varied from 1.5 rad/s up to 10 rad/s in model scale. The Wilson-θ method and the Runge-Kutta method were found to give very much the same results. The non-linear dynamic response calculation were centred around three aspects:-

a. transient state response in theory and model test,

b. steady state response in theory and model test, and

c. significance of the non-linear effect in theory and model test.

3.1 Transient State Motion Response

The transient state response was obtained in theory and in model test. Figure 7.1 shows some of the model test records on the horizontal motion response of the model structure in the direction of waves. Figure 7.2 shows the simulated motion response of the model structure at certain frequencies. From the two figures, the following conclusions are drawn.

The oscillation frequency is the wave frequency. The duration of the transient state becomes increasingly long as the wave frequency increases. This is because of the decreasing viscous damping effect associated with decreasing motion response of the model structure with frequency.

Dynamic response to slowly varying wave drift was observed only at high wave frequencies, increasing with wave height. This wave drift effect is clearly associated with the significant effect of wave scattering from both sides of the tank walls and from the motion of

the model and a poor wave profile generated at high frequencies, and also some transverse wave systems in the tank.

It was difficult to simulate the transient state response as it is very sensitive to the initial conditions. In addition, the wave profile recorded during the model test is by no means strictly sinusoidal as it is in theory.

3.2. Steady State Motion Response

The steady state response can be obtained using a sufficiently small time step to avoid amplitude decay and the period elongation [74], especially at high frequencies.

a. The steady state angular response amplitude, either zero-to-crest or zero-to-trough, can be over 50% less than the maximum angular displacement encountered in transient state response at high frequencies. This is associated with the low viscous damping and significant wave scattering effect.

b. There was very little mean wave drift effect on the non-linear angular displacement.

3.3 Significance of the Non-Linear Effect

The non-linear motion response was compared with the linear response obtained from the frequency domain calculation in order to examine the effect of non-linearities. The shape of the response curve obtained from the non-linear analysis seems to be sinusoidal. More importantly, the zero-to-crest amplitude and zero-to-trough amplitude

of the non-linear response are not very different from the linear response amplitude. The maximum difference was found to be about 1.0% of the mean amplitude. Figure 7.4 shows the results from model testing, frequency domain linear response analysis and the present time domain non-linear dynamic response analysis. It shows very good agreement. This means that the frequency domain linear dynamic response analysis is valid, in general, in steady state.

However, allowances have to be made in the frequency domain calculation to account for the maximum response which is likely to occur in the transient state, especially at high frequencies.

4. BRIEF DISCUSSION OF THE DYNAMIC INSTABILITY

In the non-linear motion equation, equation (7.1), if all the non-linearities are omitted except that associated with the heaving force, then it can be re-written, after normalisation, in the following general form(assuming ω_n=1.0 rad/s):-

$$\ddot{y} + 2c\dot{y} + [1 + b\cos(\omega t + \psi)]y = f_0(t) \qquad (7.14)$$

In ref [76] it is suggested that the equation could have a solution which becomes unstable for sufficiently small c. The nature of this solution is inherently associated with the basic homogeneous equation:-

$$\ddot{y} + 2c\dot{y} + [1 + b\cos(\omega t)]\, y = 0 \qquad (7.15)$$

where ψ is dropped from the phase without losing its generality. This equation can be transformed into Mathieu's equation through two consecutive transformations. Firstly, substitution of $y = x \exp(-ct)$ and, secondly, of $2z = \omega t$ into equation (7.15) yields

$$\ddot{p} + [a - 2q\cos(2z)]p = 0, \tag{7.16}$$

where $$a = \frac{4(1 - c^2)}{\omega^2}, \quad q = -\frac{2b}{\omega^2} \tag{7.17}$$

Equation (7.16) has a solution of the following form [77]:-

$$P = \exp(i\varepsilon z)\, P(z) \tag{7.18}$$

where $P(z)$ is a periodical function of the same period as that of the coefficient of Mathieu's equation and ε is the characteristic exponent depending on b and c. It is clear that in order for p to be stable, ε has to be real. Essentially the solution would be unstable at $\sqrt{a} = j$ $(j = 1,2,...)$ depending on the $-q/a$ ratio [77]. From the original motion equation, equation (7.14), $\sqrt{a} = j$ means:-

$$\omega = \frac{2}{j}\omega_n \sqrt{1 - \zeta^2} \tag{7.19}$$

In the vicinity of those ω's, the solution could also be unstable if $-q/a$ is sufficiently large.

The damping plays an important role in limiting the instability [76] and, when it is sufficiently large, it could suppress the instability. Rainey [76] calculated this minimum damping ratio for various modulation depths. In this study the lowest wave frequency possible from equation (7.19) will correspond to $j = 2$ and $j = 1$. In both cases the wave frequency will be very low.

Equation (7.14) is highly simplified from equation (7.1). If the non-linearities in the motion response are to be taken into account, the response will not become unstable even when ω follows the relationship given by equation (7.19). Theoretically, this is

confirmed in Fig. 7.2 where the time simulation was carried out employing equation (7.1) with $\omega = \omega_n$. The conclusion to be drawn from the simulation is that the time varying heaving force contributes to non-linearity and gives rise to possible dynamic instability but other non-linear effects eliminate the dynamic instability completely. In addition, the following two points should be borne in mind

a. The wave frequency $\omega = 2\omega_n$ would normally safely represent the lower limit of the frequency of real waves.

b. Even if the waves with those critical wave frequencies occur, they would have to last a sufficiently long time to excite the structure to dynamically unstable motion. It is unlikely, therefore, that the dynamically unstable motion response will occur in reality.

To test the dynamic instability, experiments were carried out with frequencies, corresponding to $j = 1$ ($\omega_n = 1.795$ rad/s) and $j = 2$ ($\omega = 3.59$ rad/s) in equation (7.18). During the tests, very high waves were selected to supply high energy flux. (No dynamic instability was observed during the tests). Records from model tests are shown in Fig. 7.5.

In addition, it is not expected that dynamic instability would occur in random waves. Although it is more likely to encounter subharmonic waves associated with wave groups, which should theoretically, have enough energy, it is not likely that those waves would last long.

5. CONCLUSIONS

The following conclusions can be drawn with respect to the transient state motion response.

1. The time period of the transient state motion increases with frequency. Also, the maximum response likely to occur in the transient state motion can be twice as much as that in the steady state motion, especially at high frequencies.

The non-linear effects are found to be small and the frequency domain linear dynamic response is valid in the steady state although due attention has to be paid to the transient state response.

With regard to the dynamic instability, there is a possibility, on the basis of a highly simplified theoretical model, that the non-linear behaviour of the articulated tower could be unstable under certain conditions. However, dynamic instability is very unlikely due to the following three reasons:-

a. the existance of the non-linear damping,

b. the unlikely occurrence of sufficiently low frequency regular waves, and

c. the persistance of a sufficiently long time interval of the regular wave excitation is improbable.

LIST OF FIGURES

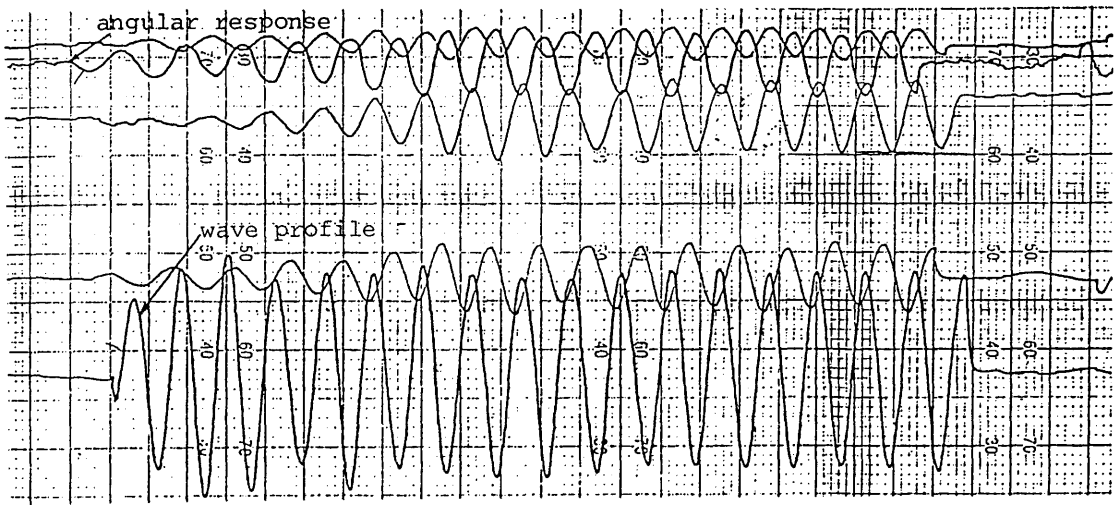

f=0.8Hz v=4V

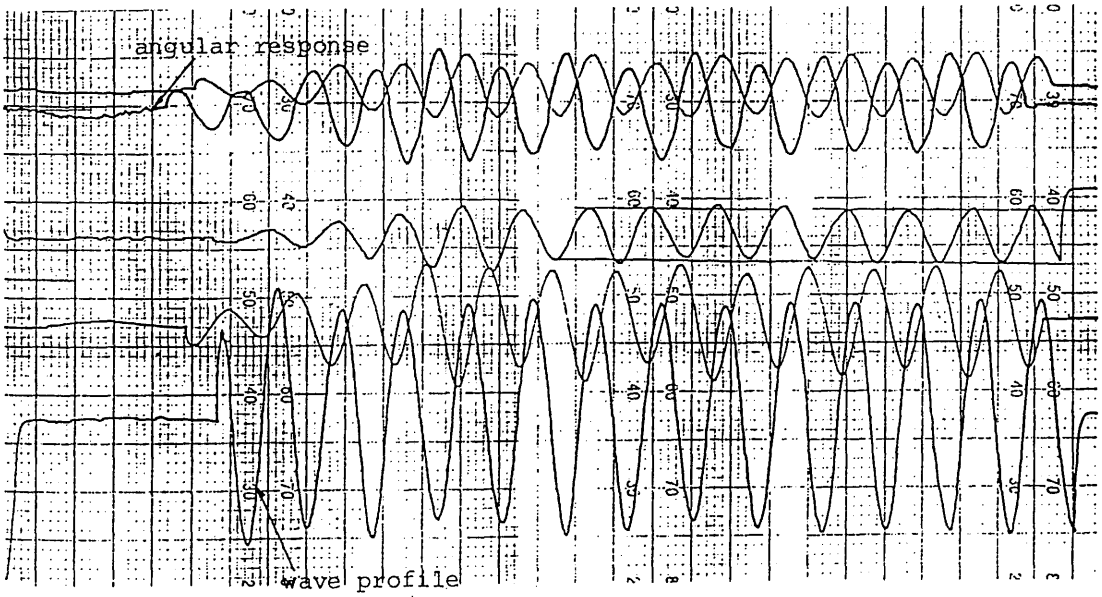

f=0.6Hz v=4V

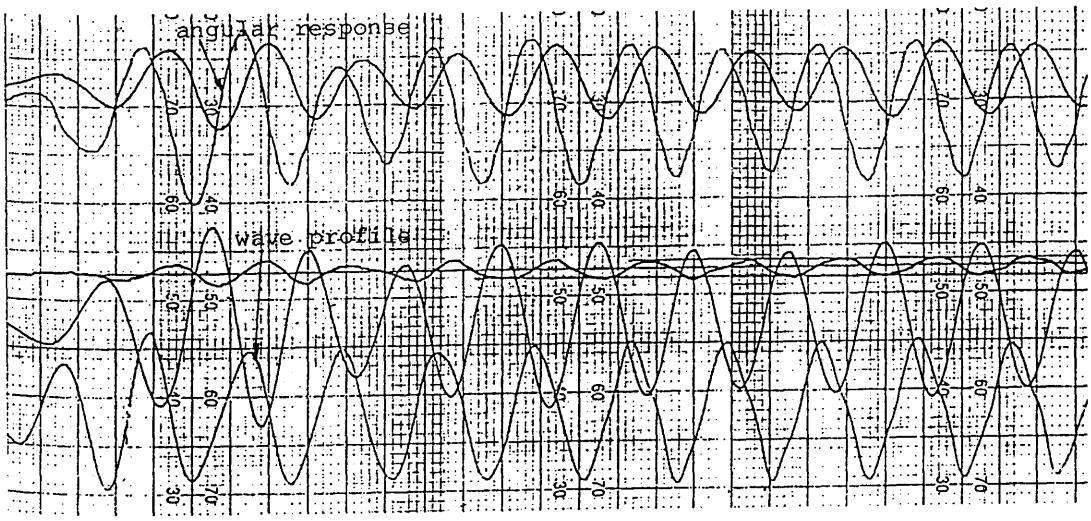

f=0.4Hz v=4V

Fig. 7.1 recorded angular dynamic response

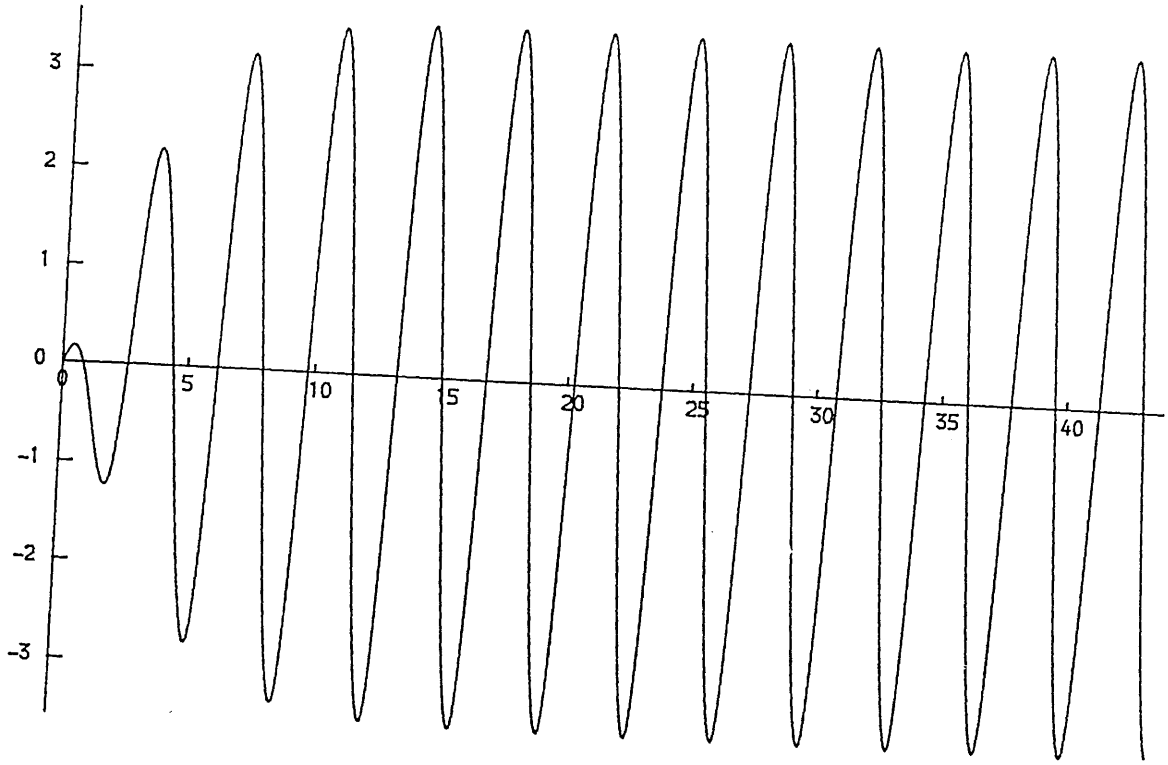

$\omega=\omega_n$

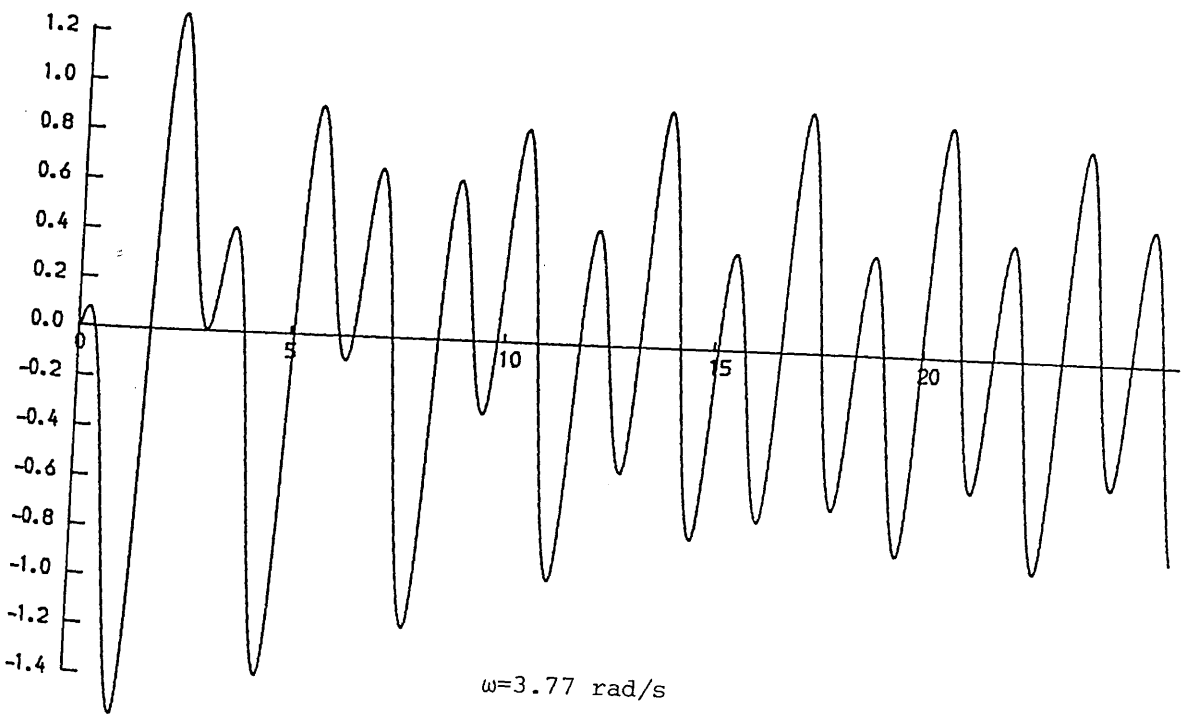

$\omega=3.77$ rad/s

x : t seconds ; y : θ degree

Fig. 7.2 calculated angular dynamic response of the model structure in Fig. 6.1

Fig. 7.3 recorded response at high frequencies

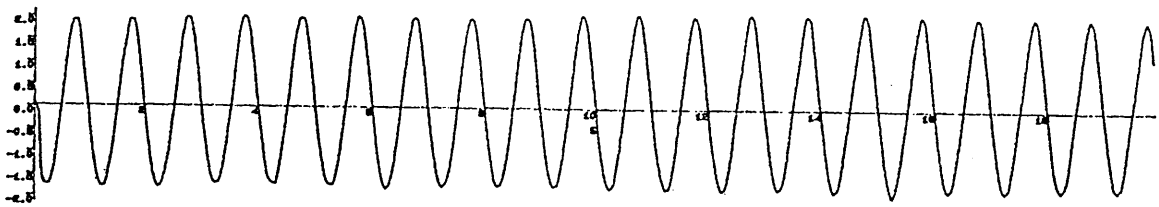

f=1.0Hz v=4V (wave profile)

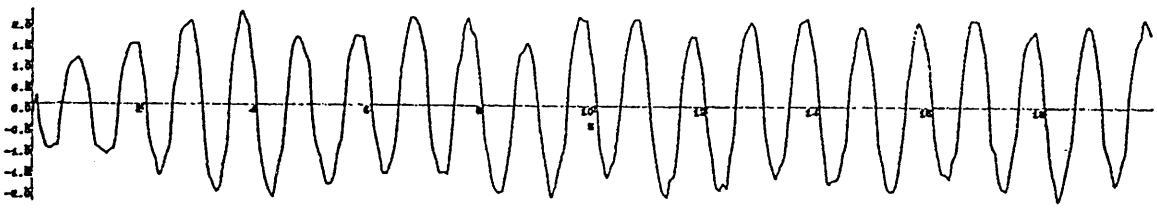

f=1.0Hz v=8V

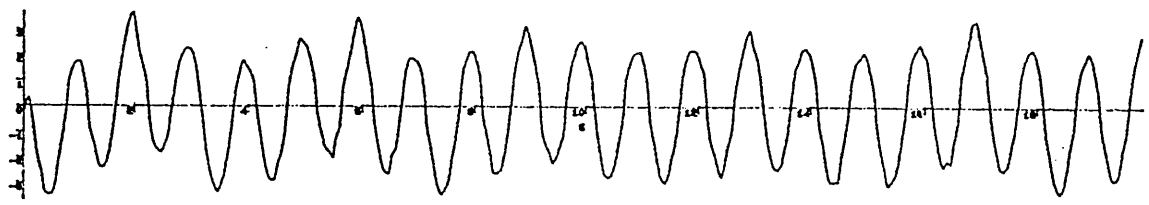

f=1.0Hz v=12V

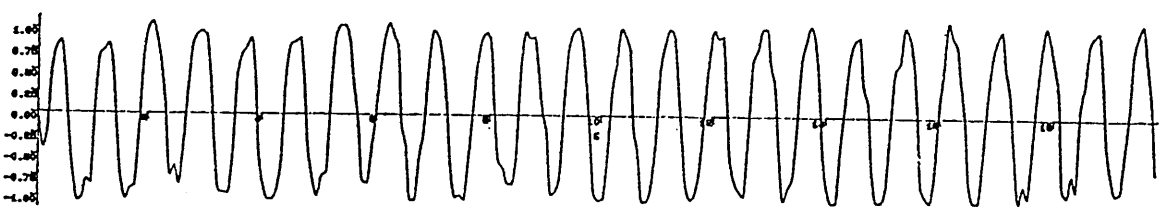

f=1.2Hz v=4V

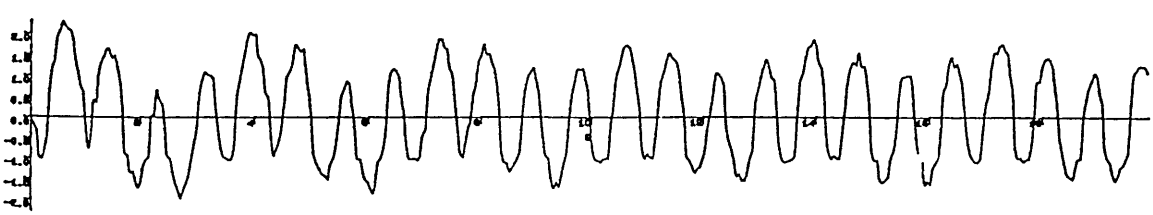

f=1.2Hz v=8V

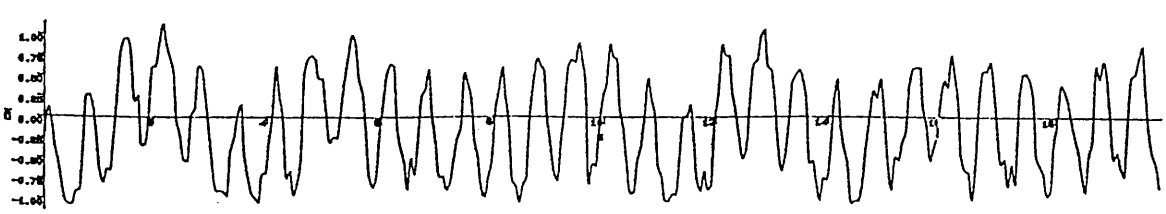

f=1.5Hz v=4V

y : horizontal displacement at the top of the model structure (in cm)

x : time (in second)

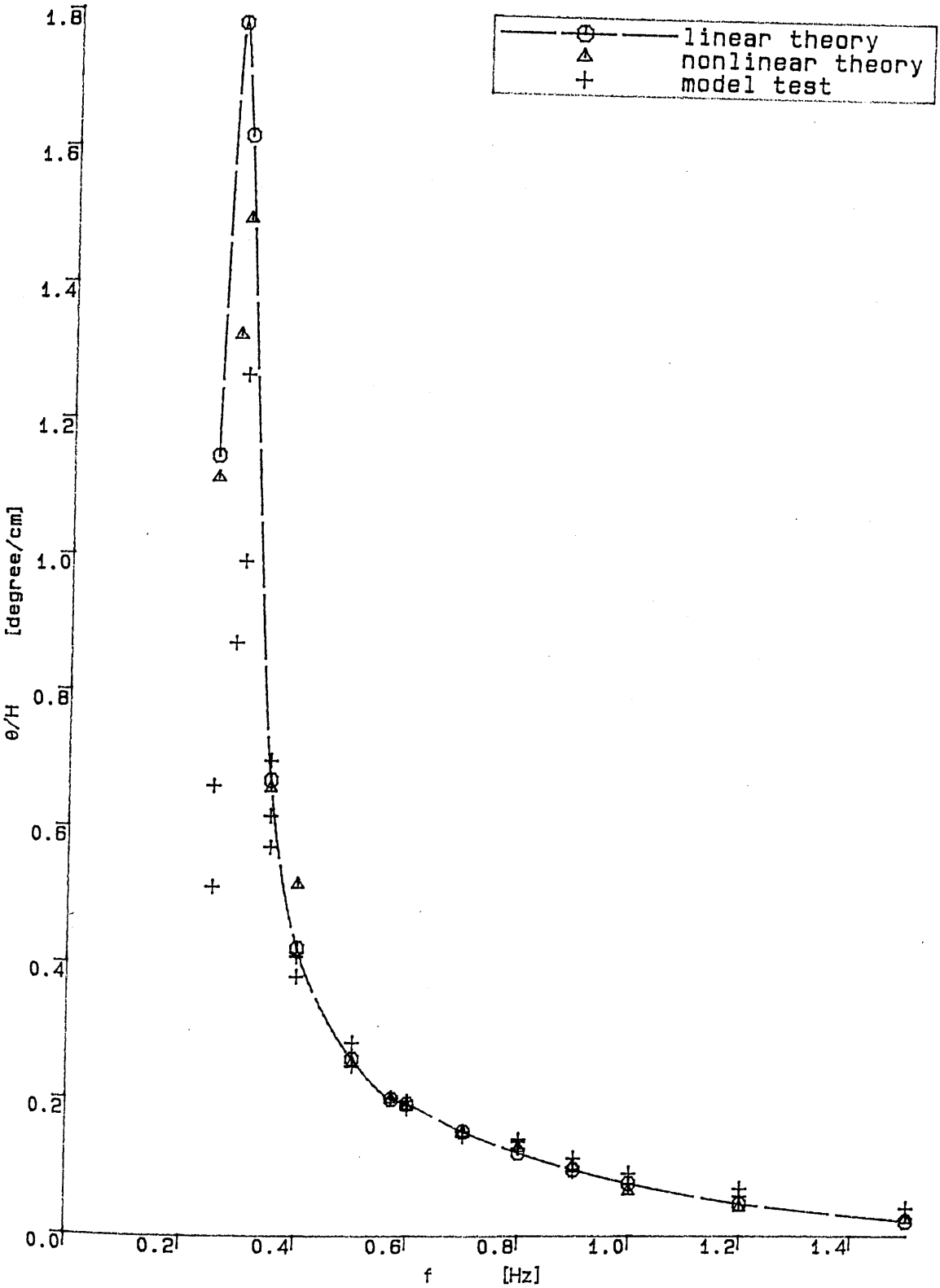

Fig. 7.4 angular response from model test and from time domain computer calculations

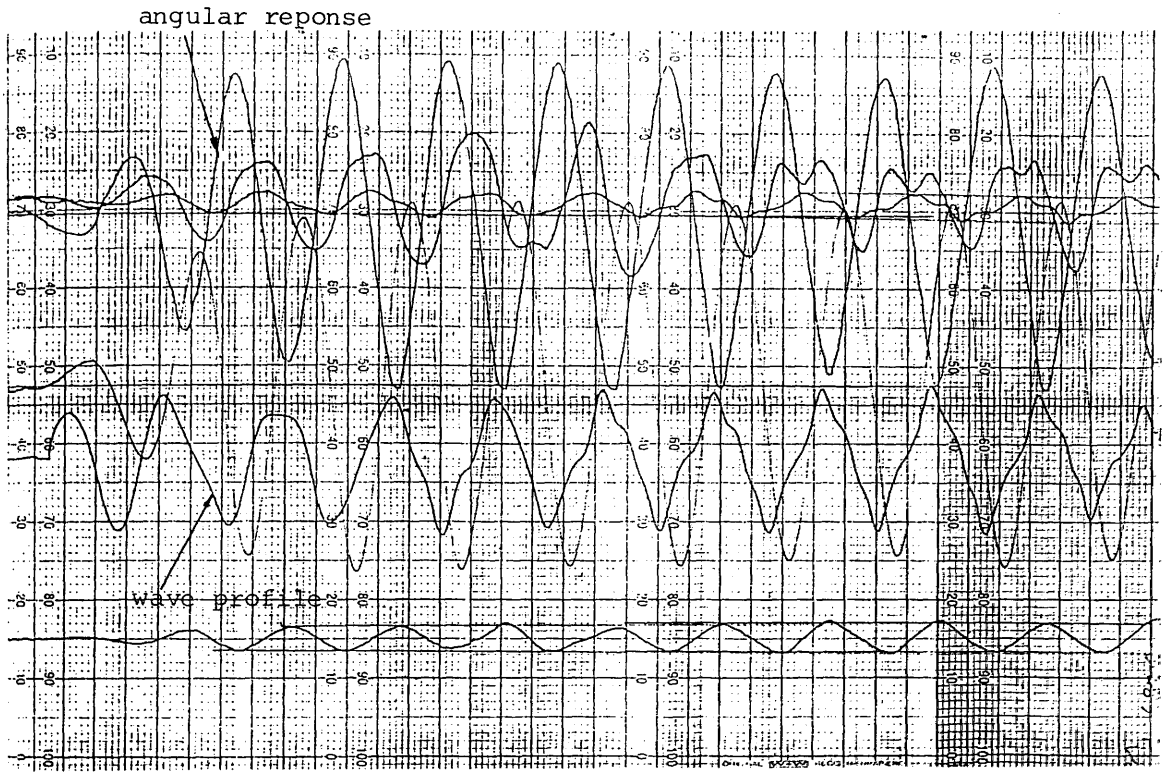

f=0.2857Hz

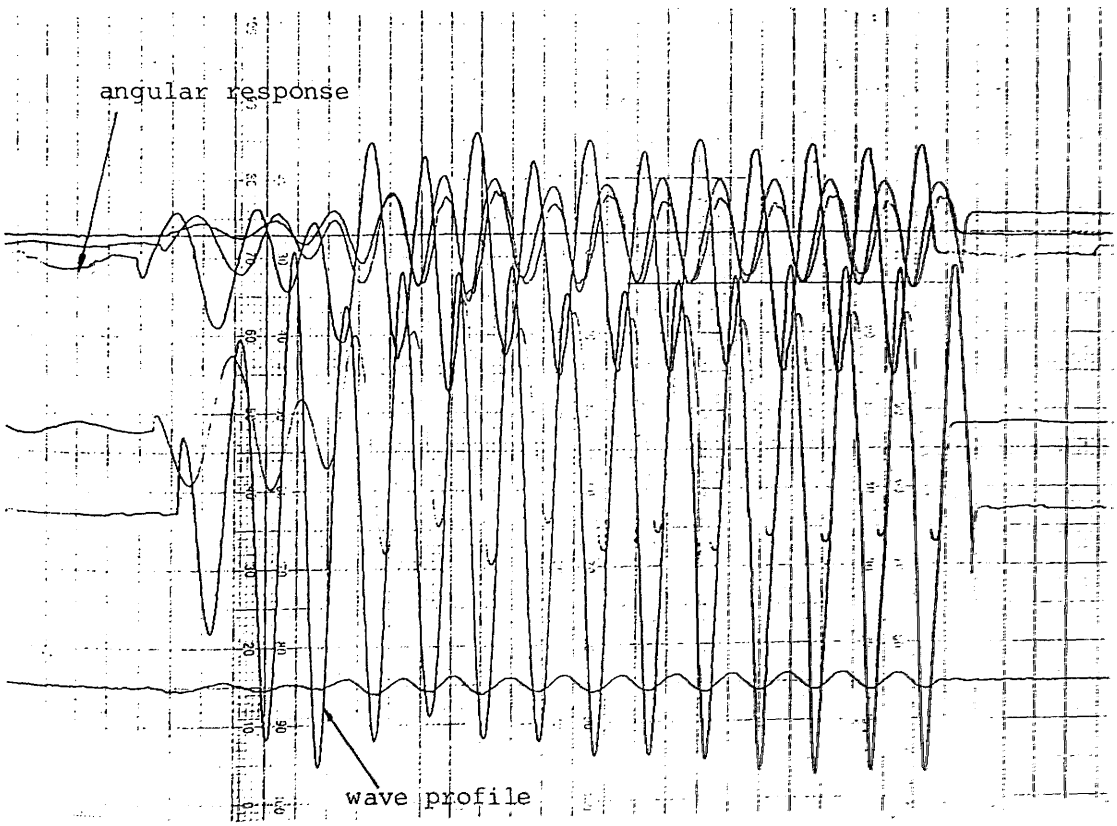

f=0.5714Hz

Fig. 7.5 recorded angular dynamic response

CHAPTER 8

DESIGN DATA ON A MONOLITHIC SINGLE ARTICULATED TOWER - BASED ON PARAMETRIC STUDIES

1. INTRODUCTION

Certain conceptual design considerations for the major components of an articulated tower were discussed in Chapter 3. The parameters related to the environmental conditions were studied in Chapter 5 for a representative structure as given in Table 5.4. In this chapter, parametric studies of those parameters defining the geometrical dimensions of an articulated tower are presented.

These parameters are influenced primarily by three basic design specifications: the water depth, deck payload and the environmental conditions. By varying these parameters in the range of practical interest, their effects are shown quantitatively so that the optimum geometry of an articulated tower, for a particular design, can be determined on the grounds of objective judgements.

The major design aspects of the articulated tower structure examined in the present chapter include: static and dynamic response, water depth capacity, deck payload capacity, stability requirements, amount of total structural material consumption and the relocatability of the structure, etc.

The general requirement for the structure is, as always, to have viable technical performance, favourable economic application and a reasonable safety margin. The safety margin is taken to be ensured

by satisfying the standard design codes in the structural strength calculation, first of all, and satisfying the stability requirements. The technical performance is evaluated by the response characteristics of the structure under the specified environmental conditions with due regard to its construction and installation. The economic aspects of the structure, however, are discussed only on the basis of material consumption here because of the lack of other related information.

Four sample structures were used to represent structures with small and large payloads in shallow waters and in deep waters, respectively. The details of the sample structures together with other relevant parameters, are given in Table 8.1.

There are several options in selecting the geometry of a monolithic single articulated tower as is shown in fig. 8.1. The following parametrical studies lead to the conclusion that the geometry in fig. 8.1d is the optimum one.

2. OPTIMISATION OF THE DECK DIMENSIONS

For those structures with little or very small deck payloads, there is obviously no need of optimisation of the deck dimensions but for the structures with large deck payloads, the deck dimensions may have to be designed carefully.

As mentioned earlier in Chapter 3, the variation of the deck dimensions mainly affects the wind loading and the centre of gravity of the deck payload above the water surface, h_{dg} and the deck clearance, h_c.

It is difficult to estimate the variation of the total of the extreme angular displacement, θ_Σ and therefore h_c with d as it is also associated with other parameters. A crude relationship between d and θ_Σ was found to be:-

$$\theta_\Sigma = \begin{cases} -\frac{1}{2}(-7 \times 10^{-4}d^2 + 42 \times 10^{-2}d - 75) & 100 \leqq d \leqq 300\text{m} \\ 6 - \frac{d - 300}{100} & 300 < d \leqq 400\text{m} \end{cases} \qquad (8.1)$$

The deck clearance, h_c, as illustrated in fig. 8.17 is calculated according to equation (3.1) and is listed in Table 8.4.

It is easily seen that h_c is between 20m and 35m. h_c decreases with d. This trend should be indicative as the static stability improves rapidly with d. In addition, the angular dynamic response also decreases rapidly with d.

Next, when the deck space/deck payload ratio $\alpha_{vw} = 5 - 10\text{m}^3/\text{t}$ is used to obtain the maximum possible range of variation of the deck dimensions, the static tension on the articulated joint is kept zero, ie $T_s(z_1) = 0$. The results obtained from program MONO.DYNAMIC show that even for structures with a payload as high as 5000 tonnes in a water depth of 100m, the maximum variation of h_{cg} and restoring stiffness K_ℓ is under 1% with the possible maximum variation of deck height. This means that the effect of variation of the deck dimensions on the dynamic response of the articulated tower structures to waves is negligible.

The dimensions of a rectangular deck are optimised by minimising the wind loading on the deck. It can be shown from the total mean wind loading calculation that, for a given deck space, the

total mean wind loading on the deck, modelled as a solid box, increases as the deck height increases. Therefore, a flat deck structure should be used when possible.

The total wind loading varies with the wind drag coefficients. As the major part of the total wind loading, in the case of the large deck payloads, is exerted on the deck structures, the variation of the wind drag coefficient of the deck C_{dal}, is especially important. In reality C_{dal} is not likely to be less than 1.0 because of the ragged surface of the deck. Owing to the importance of the wind loading on the deck structure, model testing can be justified in real design practices.

3. DIMENSIONS AND POSITION OF THE BALLAST CHAMBER

The impact of the use of the ballast chamber on the free floating stability and the reduction of the tensile loading on the articulated joint of an articulated tower structure is demonstrated in Section 9. This section investigates the possible impact of the use of the ballast chamber on the distribution of the internal sectional shear force and bending moment values along the structure, and in particular the lower section. This includes the impact of ballasting the structure, the extent of ballasting, the position of the ballasting and the section of ballast material. Figure 8.16 shows the parameters defining the dimensions and position of the ballast chamber.

3.1 Impact of the Use of the Ballast Chamber

The ballast chamber is assumed to be immediately above the

articulated joint in order to have maximum effect on lowering the CG and minimising its inertia about the joint. In this case, the size of the ballast chamber is such that $T_s(z_1) = 0.0$ when it is filled with the ballasting material of density $2.5t/m^3$. The internal forces are calculated in two situations: when the ballast chamber is filled with ballasting material and when the ballast chamber is empty. Four different sample structures are used with different payloads and water depths as listed in Table 8.3.

The shear force on the articulated joint of these four sample structures when ballasted is compared with that when they are unballasted in fig. 8.2. As expected, the ballasting effect depends on wave frequency, water depth and deck payload and is roughly summarised below.

a. In a water depth of 150m, the ballasting effect is to decrease the maximum shear force on the joint in design wave conditions and, most likely, to increase the shear force on the joint in operational wave conditions.

b. In a water depth of 300m, the ballasting effect is to increase the shear force on the joint in all wave conditions.

Reduction in shear force by as much as 95% in some cases, and increase by as much as 300% in other cases are achieved. In addition, it is found that the internal sectional bending moment on SECTION 1 is affected equally significantly. The frequency pattern of the ballast effects is very much the same as for the shear force but the internal sectional forces on other sections are only slightly affected.

The explanation of the ballasting effect on the distribution of the internal sectional forces along the bottom.part of the sample structures lies in the variation and the magnitude of the mass inertia along this part of the structures relative to the mass inertia over the upper part of the structures. When the structures are ballasted, the mass inertia of the ballast chamber is increased so that SECTION 1 acts as a clamped support to the lower end of the lower column at certain frequencies. In addition, the ballasting effect on the restoring stiffness and angular dynamic response is also attributed to the variation of the sectional forces.

3.2 Selection of the Dimensions of the Ballast Chamber

This includes the selection of the size and diameter/length ratio of the ballast chamber. First of all, the size of the ballast chamber can be determined in two different ways:-

a. According to the specification of a minimum $\delta = h_{cb} - h_{cg} > 0$ from the free floating stability consideration or

b. According to the specification of $T_s(z_1) = 0$, ie zero static tension (compression) on the articulated joint.

It is shown earlier in Section 2 of Chapter 3 that the size of the ballast chamber, determined according to $T_s(z_1) = 0.0$, always ensures that $\delta > 0$. The effect of the ballast chamber size is examined by varying the size but keeping $L_1 = 0.0$ and $\alpha_2 = 1.0$ (fig 8.16). The results for the sample structures are shown in fig. 8.3. $\overline{V}_s$ is the volume of the ballast chamber of the structures, determined so that $T_s(z_1) = 0.0$ when $\alpha_2 = 1.0$, $L_1 = 0.0$ and $\rho_2 = 2.5 t/m^3$ (fig.8.16).

The shear force on the articulated joint of all the sample structures, except the one in case 3, increases with the size of the ballast chamber $\overline{V}_2$ for all the wave frequencies of practical interest. The sectional bending moment values on SECTION 1 of those three structures are similarly affected to an even greater degree. For the structure in case 3, the shear force on the articulated joint is actually reduced in the low frequency range from 0.3 rad/s to 0.5 or 0.6 rad/s when heavily ballasted. The minimum shear force is achieved with the ballast chamber size $\overline{V}_2 = \overline{V}_s$. Greater reduction of sectional bending moment on SECTION 1 is achieved, on the other hand, by heavier ballasting. Practically, one is not likely to use a ballast chamber of a greater volume than $\overline{V}_s$. From the above analysis, it is clear that in deep waters (above 150m), the structures should be as lightly ballasted as possible to reduce the shear force on the articulated joint and the bending moment on SECTION 1. For those structures in shallower waters, light ballasting is also desirable if the payloads are great. Otherwise, appropriately heavy ballasting may be desirable to reduce the significant shear force on the articulated joint.

The effect of diameter/length ratio α_2 varying from 0.5 up to 2.0 with $T_s(z_1) = 0.0$, on the shear force on the articulated joint of the four sample structures is shown in fig. 8.4. This figure clearly indicates that a wider ballast chamber gives rise to less shear force on the articulated joint. The comparison of the bending moment on SECTION 1 of those structures with a different α_2 ratio is barred by the difference in the position of SECTION 1 which varies with α_2.

3.3 Position of the Ballast Chamber

The size of the ballast chamber increases with L_1 when

$T_s(z_1) = 0.0$. As L_1 increases, the shear force on the articulated joint increases at all wave frequencies of practical concern as is shown in fig 8.5. The increase is appreciable in all conditions and can be over 100%.

Variation of the shear force and the bending moment on SECTIONS 1 or 2 cannot be directly compared due to the fact that they vary with the position of the ballast chamber. Nevertheless, the results show that the sectional forces along the bottom part of the structure will be increased in general as the ballast chamber is elevated to a high position above the articulated joint.

In addition, if the size of the ballast chamber, which is determined so that $T_s(z_1) = 0.0$ when $L_1 = 0.0$, is then kept unchanged as L_1 varies, the shear force on the articulated joint of all the sample structures, except the one in fig. 8.6c, is increased when L_1 increases. In fig. 8.6c the shear force is reduced when L_1 is increased from 0.0 to 0.1d but it is again increased when L_1 is further increased from 0.1d to 0.2d.

3.4 Selection of Ballasting Material

From the point of view of static stability, higher density material gives more efficient ballasting and reduces the size of the ballast chamber needed. In order to achieve the reduction of axial tension on the articulated joint, the ballasting material density must be greater than the density of the sea water. To examine the effect of the ballasting material density on the internal sectional forces along the lower part of an articulated tower, the results obtained for the four sample structures in Table 8.3 show that:-

a. Only the shear force on the articulated joint and the bending moment on SECTION 1 are affected.

b. Using higher density ballasting material, lower shear force on the articulated joint and bending moment on SECTION 1 are obtained (fig. 8.7). The reduction rate in fig. 8.7 is particularly great when the material density varies from 1.5 t/m^3 to 2.5 t/m^3. The reduction achieved when the material density is changed from 2.5 t/m^3 to 3.5 t/m^3 is much less significant. Normally the ballast material density is under 2.5 t/m^3.

The advantages of using high density ballast material are pronounced in all water depths and deck payloads over the complete wave frequency range of practical concern.

4. EFFECT OF THE LOWER COLUMN DIMENSIONS

Both the length and diameter of the lower column can be varied. The length of the lower column depends on the geometry and the submergence depth, L_s, of the buoyancy chamber as shown in fig. 8.17. Thus the effect of the lower column dimensions is examined by varying its diameter only.

The effect of the lower column dimensions on the flexural mode vibration motion of articulated tower structures has been discussed in Chapter 4. Attention is concentrated here on the characteristics of articulated tower structures, variation of the external loadings, mainly due to waves and mass inertia, static and

dynamic response characteristics and, variation of the internal sectional forces.

The effects of the lower column dimensions on these features of an articulated tower structure are affected by other parameters such as water depth, deck payload, dimensions of other column components. The conditions specified include the diameter/length ratio of the buoyancy chamber $\alpha_4 = 1.0$ and the equivalent shell thicknesses of the columns, $\bar{t}_i = 0.1$ $(i = 1,2,...5)$. In addition, the viscous damping is estimated according to an estimated angular response amplitude $\bar{\theta}$ to harmonic waves, as given by:

$$\bar{\theta} = \begin{cases} 0.3 & d \geq 400\text{m} \\ \dfrac{\bar{\theta}_1 - \bar{\theta}_2}{d_1 - d_2}(d - d_1) + \bar{\theta}_1 & 100\text{m} \leq d_1 \leq d < d_2 \leq 400\text{m} \end{cases} \tag{8.2}$$

where d and θ_i are given as

i =	1	2	3	4	5	6	7
d_i =	100	150	200	250	300	350	400
$\bar{\theta}_i$ =	5	3.5	2.5	1.5	0.7	0.5	0.3

The practical range of the lower column diameter D_3 is between 4 and 20m. The minimum restoring stiffness, $K_{\ell min}$, is found by setting $D_4 = \min(D_3, D_5)$.

In examining the effect of D_3, for a given structure, the same static tilt due to mean wind loading, θ_3, is specified and denoted as θ_{mwo}. The restoring stiffness $K_{\ell o}$, corresponding to θ_{mwo} is then obtained as $K_{\ell o} = M_{3S}/\theta_{mwo}$ where M_{3S} is given in Table 5.2.

Having determined $K_{\ell min}$ and $K_{\ell o}$, the dimensions of the buoyancy chamber are adjusted, keeping $\alpha_4 = 1.0$ (see fig. 8.17), so that K_ℓ varies with D_3, as illustrated in fig. 8.8. That is, for a given D_3, K_ℓ is determined so that $K_\ell = K_{\ell o}$ if $K_{\ell min} < K_\ell$ and $K_\ell = K_{\ell min}$ if $K_{\ell min} > K_{\ell o}$. In calculating K_ℓ and $K_{\ell min}$, the minimum total buoyancy is used.

4.1 Variation of the Characteristics with the Lower Column Dimensions

In Table 8.4, typical results are presented corresponding to W_o = 500t and 5000t in water depths of 150m and 300m, respectively. The lower column diameter D_3 ranges from 4m to 20m. The minimum restoring stiffness increases quickly with D_3. The increase of $K_{\ell min}$ is so great for large D_3 that $K_{\ell min}$ can be several times greater than any meaningful specification of $K_{\ell o}$. (See fig. 8.8). The minimum total buoyancy and total structural weight both increase, indicating that the effectiveness of the buoyancy decreases with increasing D_3. Material consumption also increases with D_3. This is also shown by the reduction of h_{cb} and h_{cg} with D_3. The impact is especially important in deep waters. The total buoyancy needed to obtain the same restoring stiffness is increased by 250% in a water depth of 300m when D_3 varies from 4m to 20m. The total material consumption is then doubled in this case. When D_3 is fairly small and $K_{\ell o} > K_{\ell min}$ is satisfied so that K_ℓ can be kept constant when D_3 varies, the variation of D_3 does not significantly affect the second moment of inertia of either the structural mass or the added hydrodynamic mass. But when D_3 becomes large, $K_{\ell min}$ becomes greater than $K_{\ell o}$ and the moment of inertia and K_ℓ are then increased.

As $K_{\ell min}$ increases with D_3, the range of variation of K_ℓ is narrowed and the freedom of varying K_ℓ by varying the buoyancy dimensions is very limited. In extreme cases, $K_{\ell min}$ becomes excessively high.

4.2 Variation of the External Loading

The wave and mass inertia forces on an articulated tower structure and their pitch moment vary with D_3. The results obtained show that the pitch moments of the wave and mass inertia force do not vary monotonically with D_3 but depends on the wave frequency and K_ℓ. In most cases, the wave and mass inertia forces and their pitch moments decrease with increasing D_3.

4.3 Static and Dynamic Response

The static tilts of an articulated tower to the mean wave drift, mean wind and steady current can be summed on the assumption of independence. The total of the extreme static and dynamic response is estimated by:

$$\theta_{\Sigma s} = 4\theta_2 + \theta_3 + \theta_4 \tag{8.3}$$

and

$$\theta_{\Sigma d} = 4\sqrt{\sigma_1^2 + \sigma_2^2 + \sigma_3^2} \tag{8.4}$$

respectively, where subscripts 2,3 and 4 in equation (8.13) indicate those due to mean wave drift, mean wind and steady current, respectively. A factor of 4 is suggested [71] by which to multiply the rms angular displacement to obtain the total of the extreme. Subscripts 1,2 and 3 in equation (8.4) indicate the rms angular displacement due to random waves, slowly varying wave drift, and gusty wind, respectively.

On satisfying $K_{\ell} = K_{\ell o}$ (ie to keep a constant θ_3), θ_2 and θ_4 are likely to increase slightly with D_3 but this can be safely neglected. Their total is therefore roughly constant. In the case of very large D_3, so that $K_{\ell o} < K_{\ell min}$, the static response decreases with increasing D_3.

The rms angular displacement, σ_1 due to harmonic waves tends to increase with D_3 when the deck payload is 500t in which case the minimum restoring stiffness is very high. When the deck payload is 5000t, σ_1 decreases steadily with increasing D_3 in a water depth of 300m and increases with D_3 in water depth of 150m as long as $K_{\ell} = K_{\ell o}$ is satisfied. The difference can be by as much as 15% and 9% in water depth of 300m and 150m, respectively, when D_3 is increased from 4m to 16m. In addition, in no more severe than operational conditions, it is most likely that σ_1 decreases with D_3. In any case, σ_1 increases very rapidly when $K_{\ell o} < K_{\ell min}$.

Results corresponding to extreme values of D_3 may be outside the practical range but serve to indicate the possible improvements which can be made. If D_3 is very large so that $K_{\ell min}$ is very large, the angular dynamic response to harmonic waves will be extremely high owing to high ω_n. The rms angular displacement is consequently impractical as is shown in Table 8.4. In very deep waters, large D_3 is necessary to avoid any significant flexural mode vibration motion of articulated tower structures. Large diameter lower columns may be accommodated due to the insensitivity of the angular response to the lower column diameter. The buoyancy and the added mass effect, however, will be excessive. The direct consequences are that the internal sectional forces, with the shear force on the articulated

joint in particular, are greatly increased. This effect is not confined to deep waters. If a small diameter lower column is used, the magnitude of the total dynamic response (as well as the static response) can be adjusted over a wide range with considerable freedom as the dimensions of the buoyancy chamber can be enlarged or reduced while the internal sectional forces can be kept low.

4.4 Distribution of the Internal Sectional Forces

With regard to the effect of the lower column diameter D_3 on the overall distribution of the internal sectional shear force and bending moment, the following conclusions can be drawn.

The shear force on the articulated joint is increased dramatically as D_3 increases. The increase of the shear force becomes more significant in deeper waters (fig. 8.9). In a water depth of 300m, the shear force on the articulated joint is increased for a design wave of $H = 30m/\omega = 0.4$ rad/s, from 3900 tonnes to 5400 tonnes when D_3 is changed from 4m to 20m, an increase of nearly 40%.

The internal sectional forces along the structures are difficult to compare in terms of D_3 as the variation of D_3 has a significant impact on the dimensions of other column components as well.The shear forces on the sections along the structure above the joint, especially along the lower part of the lower column and the upper column, are increased. The increase of the sectional shear force along the lower part of the lower column in the vicinity of SECTION 1 is particularly pronounced in shallow waters. In a water depth of 300m, the sectional bending moment along the lower column sections are increased very significantly.

From the above discussions, it is clear that the bottle shaped and uniformed sectioned articulated tower structures in figs. 8.1a and 8.1b are bad designs from the point of view of buoyancy efficiency, material consumption, as well as internal sectional loadings. In general, designs of articulated tower structures with large diameter lower columns are to be avoided.

5. POSITION AND DIMENSIONS OF THE BUOYANCY CHAMBER

The position and dimensions of the buoyancy chamber can be defined by:

$$L_s,\ \alpha_4 \text{ and } \beta_o = \frac{\theta_{mwo}}{\theta_\Sigma}$$

where θ_2 is given in equation (8.1) and the geometrical parameters are illustrated in fig. 8.17.

The conditions specified in obtaining Table 8.4 are observed and the effects of varying the above parameters are listed in Table 8.5.

5.1 Effect of the Submergence Depth of the Buoyancy Chamber (L_s)

The minimum submergence depth of the buoyancy chamber is taken to be 15m primarily for two reasons:-

a. to avoid the exposure of the buoyancy chamber above the free surface in a 30m high regular gesign wave and,

b. to minimise the damage to the buoyancy chamber caused by possible collision of the structure with ships.

The buoyancy efficiency decreases with L_s. The significance of the effect increases with W_o but decreases with α_4 and d. The total structural material consumption follows the same trend but less steeply.

The natural frequency of RBMV motion increases with L_s due to the reduced second moment of inertia of structural as well as added hydrodynamic mass. This effect increases with W_o but decreases with d but the variation is always under 7% and may be ignored.

Only the total static response decreases as L_s increases due to the reduction in the steady current loading and the mean wave drift loading with L_s, but the effect can be safely discounted.

The rms angular dynamic response, σ_1, in the extreme conditions of harmonic waves tends to increase with increasing L_s in shallow waters but to decrease with L_s in deep waters. In no more severe than operational sea states σ_1 always decreases with increasing L_s. In deeper water the angular dynamic response is not sensitive to the variation of L_s. In relatively shallow waters the response becomes sensitive to L_s. Increasing L_s will lead, in most cases, to a significant reduction of dynamic response to harmonic waves except in extreme conditions.

The dynamic response to random wind σ_3, is hardly affected. Variation of the rms angular displacement due to wave drift σ_2 with L_s follows the same pattern as σ_1 but the changes are very much reduced.

The total of the extreme angular dynamic response, $\theta_{\Sigma d}$,

obtained according to equation (8.4) is increased in water depths of 150m and is reduced in 300m when L_s varies from 10%d to 30%d.

The heaving force decreases with L_s depending on ω, α_4 and β_o. At ω = 0.4 rad/s, the heaving force is calculated and listed in Table 8.5.

The effect of L_s on internal shear force and bending moment along the structure length depends on the position of the section concerned and the wave frequency as well as the deck payload and water depth. It is case related and is, therefore, very difficult to generalise but the most important aspect of the effect of varying L_s is that the shear force on the articulated joint changes significantly. This is shown in fig. 8.10.

Concentrating on low frequencies, the shear force on an articulated joint decreases as L_s increases in nearly all the cases examined except when W_o = 5000t and d = 150m in which it increases with L_s. The significance increases with payloads and water depths. In fig. 8.10, when W_o = 5000t and d = 300m, the shear force in the design wave condition could be reduced by as much as 810t (27%) when L_s changes from 30m to 90m.

In the case of structures with large payloads in shallow waters, because of the large dimensions of the buoyancy chamber, the effectiveness of buoyancy decreases rapidly with increasing L_s. According to Table 8.5 and fig. 8.10, the shear force on the articulated joint increases very quickly with L_s under these circumstances.

The effect of L_s is significant only when L_s varies between 10% and 20% of the water depth. Excessively deep or shallow submergence of the buoyancy chamber is neither practical nor necessary.

5.2 Effect of the Diameter to Length Ratio of the Buoyancy Chamber (α_4)

As α_4 increases, the buoyancy chamber becomes concentrated closer to the surface. To keep the same restoring stiffness, the total buoyancy needed is reduced as the buoyancy becomes efficient. The centre of buoyancy CB is elevated but the significance of the effect is pronounced only in shallow waters when the deck payload is large. In addition, the effect is more significant when α_4 varies from 0.5 to 1.0 than that from 1.0 to 1.5 as expected. Nevertheless, the effect of α_4 is much less significant than that of L_s, in general. The only exception, is the effect on the heaving force.

Again, the greatest influence of all of the variations of α is on the internal sectional shear force and bending moment distributions, especially when the payload is large. This is typically seen in fig. 8.10. The shear force on the articulated joint decreases with α_4 in shallow water but increases with α_4 in deep waters. When the α_4 ratio varies from 0.5 to 1.5 and W_o = 5000t, the shear force on the articulated joint is increased by 14% in a water depth of 300m and decreased by about 48% in a water depth of 150m.

5.3 The Effect of the Size of the Buoyancy Chamber

Keeping α_4 and L_s unchanged and varying the specification of θ_{mwo} for a given structure, changes $K_{\ell o}$ and hence the size of the buoyancy chamber. Results so obtained are listed in Table 8.6. The

shear force on the articulated joint is plotted in fig. 8.11, in terms of wave frequency. Conclusions are drawn from Table 8.6.

The second mass moment of inertia as well as the restoring stiffness increase with the size of the buoyancy chamber. The natural frequency expectedly increases as well. As the buoyancy chamber size increases, the angular static responses all decrease so that the total angular static response also decreases. The angular dynamic response to both regular harmonic waves and random waves increases dramatically both in operational and in extreme conditions. The angular dynamic response to subharmonic waves, however, decreases but only slowly. The angular dynamic response to random winds, which is more restoring stiffness dependent decreases rapidly.

In estimating the total of the extreme angular dynamic response, $\theta_{\Sigma d}$, by equation (8.4), it is found that $\theta_{\Sigma d}$ increases with the buoyancy chamber size when W_o = 500t. But $\theta_{\Sigma d}$ does not change monotonically and has a minimum when W_o = 5000t. In addition, $\theta_\Sigma = \theta_{\Sigma s} + \theta_{\Sigma d}$ also has a minimum in all the cases examined in Table 8.6. Let the size of the buoyancy chamber at which the minimum total of the extreme angular response is reached be $\bar{V}_m$. The total of the extreme angular dynamic responses does not change very much when the size of the chamber varies below $\bar{V}_m$. When the size of the chamber varies well above $\bar{V}_m$, on the other hand, the total of the extreme angular dynamic responses increases very rapidly with the size of the chamber. The total of the extreme angular static response is always very sensitive to the change of the buoyancy chamber size.

The use of a large volume buoyancy chamber generally results in a large shear force on the articulated joint. The size of the

increase is accelerated when the size of the chamber further increases above $\overline{V}_m$. The exception, however, is for structures with large deck payloads in shallow waters at low frequencies.

In Table 8.6, the buoyancy chamber is shallowly submerged below the free surface and the heaving force which is very important, further increases with the chamber size. The magnitude of the heaving force can be extremely great for those structures with large deck payloads.

6. OPTIMUM GEOMETRY OF A MONOLITHIC SINGLE ARTICULATED TOWER

Among the possible options for the geometry of an articulated tower as shown in fig. 8.1, those in figs. 8.1a to 8.1d are basically derived from the structure in fig. 8.1e by varying the diameters of the column components and setting $z_1 = 0.0$. The following conclusions can be drawn from the above studies.

Both the bottle-shaped and single column tower structures may be built more economically in relation to the process of fabrication but they have greater material content. Therefore, the overall net economical advantage may be in doubt. On the other hand, it has very restricted stability during tow-out due to the unbalanced buoyancy/weight distribution. In addition, the high shear gorce on the articulated joint, particularly in deep waters, is also disadvantageous.

The extended telescopic type tower structure in fig. 8.1c tends to offer advantages with regard to the installation of the deck structures and payloads. The disadvantages are related to the fact

that during the worst storm, the total buoyancy which is mainly produced on the immersed part of the upper column will be reduced greatly when the wave trough passes through the upper column. Take an upper column of 20m in diameter, as an example, for a design wave of 30m in height. The loss of buoyancy when the wave trough passes through the upper column is about 4700t. Such an amount of buoyancy in so critically high, a position is bound to have a significant impact on the motion characteristics as well as the sectional shear force/bending moment along the whole structure. To compensate for such a great loss of buoyancy, the immersed length of the upper column even in the worst conditions has to be long enough to avoid reducing the restoring stiffness to an unacceptable low level (or even becoming negative). This effectively means an extra 15m of the immersed length of the upper column. This has immediate disadvantages.

First of all, the structure will be excessively stiff in all conditions, except in some extreme cases. This may worsen the dynamic motion response to a great extent.

Secondly, the sectional shear force and the sectional bending moments will be considerably increased., particularly on the articulated joint and around SECTION 2 and SECTION 3. The heaving force amplitude and both the short and long term damages to the articulated joint might be intolerably high.

In an attempt to avoid all the shortcomings of the three structures, the position and the dimensions of the buoyancy chamber of the structure in fig. 8.1d can be adjusted with considerable freedom to achieve a good compromise or even to provide the best solution in

terms of construction, installation and structural performance of structure-environment interaction.

The upper column diameter is likely to be governed by structural strength considerations. The lower column diameter is also likely to be governed by structural strength considerations in a water depth range from 200m to 250m. In deeper waters, the lower column diameter is probably governed by flexural vibration motion considerations. In order to reduce the sectional forces along the structure and on the articulated joint slender columns should be used when possible.

The structure in fig. 8.1e is built on top of a concrete base which may sometimes be used for oil storage. It is not expected that the top of the concrete base will be very high in relation to the water depth.

7. STRENGTHENING PATTERN OF ARTICULATED TOWER STRUCTURES

The stiffening pattern of the column components of an articulated tower structure is related to the distribution of the internal sectional forces along its length, and concerned with material saving. It is important to see the effect of the structural weight distribution. This is done by varying the equivalent shell thicknesses, $\bar{t}_i$, of the columns.

Keeping the equivalent thickness, $\bar{t}_2 = 0.1$m of the ballast chamber unchanged and, changing the $\bar{t}_i$, $i = 3,4,5$, collectively or individually from 0.05m, 0.1m to 0.2m, the results are listed in Table 8.7.

Keeping the same restoring stiffness, an increase of the equivalent shell thickness results in an increase of structural mass distribution along the structure. As a result, the total buoyancy as well as the total structural weight must be increased. The total structural weight is much more sensitive to the variation of the shell thicknesses than the total buoyancy. Also the sensitivity of the total structural mass to the variation of the shell thicknesses is largely independent of water depth, while that of the total buoyancy depends on the water depth.

Both the CB and CG increase as the shell thicknesses increase. This is clearly due to a higher mass distribution and larger dimensions of a buoyancy chamber with thicker shell columns.

The second mass moment of inertia is increased. Consequently, the natural frequency of RBMV motion is reduced considerably. This leads to the reduction of the rms angular dynamic response to harmonic waves, especially in severe conditions, although the wave loading is increased as the result of enlarging the buoyancy chamber dimensions. On the other hand, the rms angular response to slowly varying wave drift is increased. The rms angular response to gusty wind is largely unchanged as expected. Nonetheless, the total of the extreme angular response from equation (8.4) is reduced as the result of the increased mass distribution. The quantitative amount is 70% and 60% in the case of d = 150m and 300m, respectively, when W_o = 500t and by 26.7% and 29.8% when W_o = 5000t for the two water depths.

The total of the extreme angular static response is also increased by about 30% in the extreme case as the result of increased

buoyancy chamber size.

Individually, $\bar{t}_3$, for the lower column has an insignificant impact on V_Σ, the total buoyancy but it has the greatest impact on $W_{\Sigma s}$, the total structural weight, particularly in deep waters. $\bar{t}_4$ has an apperciable effect on both V_Σ and $W_{\Sigma s}$ except for those structures with small payloads in deep waters, while $\bar{t}_5$ also has a significant impact on both V_Σ and $W_{\Sigma s}$ except for those structures with large payloads in deep waters. The effect of $\bar{t}_4$ and $\bar{t}_5$ decreases with water depth.

The shear force on an articulated joint, showing the effect of all the three column shell thicknesses, is plotted in fig. 8.12. It normally decreases with the shell thicknesses. The effect is considerable, especially when the payload is small but the shear force on an articulated joint may be increased in a very low frequency region when the deck payload is large and the water depth is shallow.

The effect of individual column shell thicknesses on the shear force on the articulated joint is shown in fig. 8.13. Increasing the lower column shell thickness causes the shear force to increase but increasing the shell thicknesses of the upper column and buoyancy chamber causes it to decrease. The effect is more pronounced for structures with less payloads. Variation of the shell thickness of the buoyancy chamber has much less effect on the shear force on an articulated joint than either that of the lower column or the upper column. In deep waters, the lower column shell thickness has a greater effect than the upper column shell thickness while in shallow waters the opposite is true for structures with small payloads.

From the above discussion, it is concluded that to keep the same shell thicknesses, the use of lower density material results in greater dynamic response and shear force on an articulated joint. In practice, the net effect of using different materials on the angular dynamic response and shear force on the articulated joint is difficult to predict as both the diameters and shell thickness of the columns would change with the material property due to structural strength requirements.

In addition, with regard to the selection of the individual column shell thicknesses, it can be concluded that the use of the minimum shell thickness (equivalent) for the upper column is not desirable from the point of view of reducing the angular dynamic response and shear force on an articulated joint. However, it is preferable to use the minimum shell thickness for the lower column.

8. WATER DEPTH LIMITS

8.1 Deep Water Limit

The determination of the maximum water depth was previously carried out in Chapter 4, on the ground of limiling the flexural mode vibration motion of articulated tower structures. It was shown that the limit is between 300m and 350m beyond which the application of articulated tower structures will encounter problems associated with their flexural mode vibration motion.

In fact, another serious problem associated with the deep water application of articulated tower structures is the critical structural strength of the articulated joint. This is because the rapid increase of the lower column diameter with water depth above

200m to 250m to eliminate the FMV motion problem leads to a rapid increase of structural weight and added hydrodynamic mass.

However, if the lower column diameter could be reduced (while maintaining the overall bending stiffness in deep water applications of articulated tower structures) the shear force on the articulated joint would be significantly reduced. The angular dynamic response which is of little concern in deep water may be worsened to a certain extent. Therefore, it is conceived that a lattice structure might offer a better option in place of large diameter lower columns in deep water applications of articulated tower structures. It can be easily demonstrated that in water depths over 300m, the shear force on the articulated joint could be increased by over three times at certain low frequencies when the lower column diameter changes from 7.0m to 17.0m. (The use of lattices on articulated tower structures is examined in Chapter 9).

8.2 Shallow Water Limit

There are, basically, two problems with the applications of articulated tower structures in very shallow water, say $d \leqq 100m$, namely bad static and dynamic responses. The shallow water depth limit also depends on the deck payload specified.

Articulated tower structures are likely to be preferred for those tasks which do not demand low levels of motions, such as for auxiliary purposes. This is because they involve lower material consumption than the conventional fixed platforms in such shallow waters. In addition, articulated tower structures are expected to be much more easily relocatable.

The range of variation of the submergence of the buoyancy chamber is limited as the L_s/d and h_c/d ratios are very high in shallow water and buoyancy efficiency is essential.

The effect of random motion on human response has to be taken into account in relevant cases of applications. In fact, according to certain regulations as shown in fig. 8.14, the effect of the random motion on human response is likely to be the major concern, when personnel are required to spend a long period of time on board the deck in shallow waters. In any case, excessively high motion response will result in more down-time. However, if the articulated tower structure is in a relatively mild ocean environment, the down-time due to excessively severe structural motion can still be low.

The magnitude of the internal sectional shear force and bending moment can be very high in the case of a large deck payload. The shear force on the articulated joint is then of particular concern. This is mainly because of the high natural frequency, large dimensions of the buoyancy chamber and very shallow submergence of the chamber in shallow waters. When the deck payload is very large, the natural frequency and the dynamic response may be reduced but the shear force on the articulated joint will increase.

8.3 Effective Water Depth Range of Application

The water depth range in which stand-alone articulated tower structures could be effectively used may be regarded to vary from about 100m to 300m with deck payloads varying from 500t up to 5000t. In such water depths, the structural response, internal sectional

forces and the material consumption are moderate. With the deck payload varying in a wide range, even up to 10000t or more, there is considerable freedom for adjustment to those aspects of concern in articulated tower structures. When an articulated tower is used as single point mooring for oil tankers etc, however, the effective water depth range of application may be different.

The dimensions and the position of the buoyancy chamber are the most effective parameters of all. As the water depth increases, there is more freedom of choice over the position of the buoyancy chamber to reduce the shear force on articulated joint but the magnitude tends to increase with water depth.

The use of large diameter lower/upper columns reduces the effectiveness of the buoyancy chamber. Together with other disadvantages associated with the use of large diameter lower columns, it is indicated that a slender cylinder should be used where possible. It is expected that the upper column diameter will be determined by structural strength considerations, while the lower column diameter will also be determined by structural strength considerations in a water depth below 200m and by FMV motion in deeper waters.

The effects of fluctuating wind loading and wave drift loading is important in all water depths in relation to the effect of harmonic wave loading on the motion of articulated tower structures. This is seen from Table 8.7 that the rms angular response to random waves σ_1, depends on ω_n more than those to wave drift and gusty wind σ_2 and σ_3, while σ_2 and σ_3 are more sensitive to K_ℓ. It is seen from Table 8.6 that when K_ℓ is reduced to a certain extent, σ_3 tends to override σ_1.

The static angular response to mean wind loading is the predominant part of the total static response. The static angular response to steady current loading is about 10% to 40% of that due to mean wind loading, and becomes increasingly important as W_o decreases and d increases. The static angular response to mean wave drift is greater than that to the current in extreme conditions.

The total static and dynamic angular response decrease rapidly with d. At a certain depth, the dynamic response also tends to decrease with W_o while the total static response is kept constant.

8.4 Relocatability of Articulated Tower Structures

The economic background of articulated tower structures would be very much better and more attractive if they could be relocated to a different site requiring the same types of operation when they have completed work at their first site. It is not anticipated that the dismounting and relocation or articulated tower structures will give rise to particular technical problems. The major concern would be the procurement of the relevant specifications on the structural strength and other structural performance characteristics in relation to the new design conditions, represented by water depth, deck payload and the environmental conditions at the site. Those parameters may be different and possible minor modifications to the original structure may also, therefore, be necessary. The cost of the anchoring and lower joint assembly is also a significant part of the total.

If all the design conditions are largely unchanged at the new site, the relocation may be straightforward.

If the conditions are different at the new site, relocation of articulated tower structures may not always be possible. The relocation will need to be subjected to a techno-economic appraisal.

9. STATIC STABILITY

The stability of an articulated tower should be checked, in general terms, under both static and dynamic excitations. The dynamic stability of monolithic single articulated towers under the regular wave excitation was investigated in Chapter 6. This section is, therefore, centred around the static stability of monolithic single articulated tower structures only.

The static stability is considered in three different conditions: intact condition, damaged condition and free floating condition.

9.1 Static Stability in the Intact Condition

The static stability in the intact condition is represented by the static heel under the static loading due to mean wind, steady current and mean wave drift. The static heel, due to the lateral offset of the deck payload from the vertical axis of symmetry is also taken into account. In summarising the main features of the static stability in the intact condition, the following conclusions may be drawn.

The static stability improves rapidly as water depth increases. The stability requirements may be difficult to satisfy in

very shallow waters. The static stability is less affected by the payload in deep waters than in relatively shallow waters. As the payload becomes large, the stability tends to be improved. This is because the restoring stiffness increases with payload.

The static heel, due to the mean wind, steady current and mean wave drift, is of a comparable importance with the magnitude of the dynamic response to waves although they are different in nature in respect to their interaction with the structure. The static heel, due to a steady current which is of the same order as that due to the mean wave drift accounts for about 12% up to 38% of that due to mean wind in extreme conditions.

The static heel due to the lateral offset of the deck payload from the vertical axis is also important. For example, it is easily worked out from Table 8.6, that one metre lateral offset of the deck payload can result in a static tilt of the same order as, or sometimes, over twice as much as, that due to steady current. This is in clear distinction from the conventional fixed platforms.

9.2 Static Stability in the Damaged Condition

The stability is measured by the static heel, due to flooding damage to the structure. Table 8.7 shows the sources of possible hazards to the structure during its lifetime. The probability of occurrence of those hazards during the lifetime of the structure is to be considered in estimating the static stability in the damaged condition. However, lack of data on this aspect prevents further discussion. The worst flooding damage to the buoyancy chamber is assumed to happen as indicated in fig. 3.1 at the junction between

horizontal and vertical bulkheads so that the top four adjacent compartments are flooded.

Based on the above assumptions, the static heel, due to flooding is given by:-

$$\theta_{df} = \frac{480p(q+1)(R_4-R_{4i})(R_4^2-R_{4i}^2+R_4R_{4i})\rho_w g}{\pi\{p(q+1)^2K_\ell-8\pi(R_4^2-R_{4i}^2)\ qz_5+z_4-(q+1)z_1\ \rho_w g\}} \quad \text{(degree)}$$

assuming that the chamber is cylindrical, where R_{4i} is the radius of inner chamber, $R_4 - R_{4i} \geqq 1.5$ according to the DnV Rules [29]; p is the number of vertical bulkheads, $p \geqq 2$; and q is the number of horizontal bulkheads.

The most severe impact, due to the flooding damages to the buoyancy chamber, is obtained by setting $p = 2$ and $q = 1$. A more realistic estimation would be based on $p = 4$ and $q = 1$. It can easily be shown that with $p = 4$ and $q = 1$, that the flooding damage is limited to a negligible extent.

9.3 Static Stability in the Free Floating Condition

The question of static stability arises when the structure, broken at the articulated joint, is freely floating. The free floating stability not only depends on the relative position between the centre of gravity and the centre of buoyancy of the structure but also on the magnitude of the axial force on the articulated joint in the intact condition. Adjustment can be made to the size of the ballast chamber to obtain the free floating stability. The criterion can be formulated mathematically.

When $T_s(z_1) \geq 0$, ie the articulated joint is under hydrostatic compression, $W_\Sigma \geq V_\Sigma$, the structure is stable, if $K_\ell > 0$ and is unstable in the unlikely event of $K_\ell < 0$.

When $T_s(z_1) > 0$, ie $V_\Sigma > W_\Sigma$, if there is a secondary mooring available to prevent the structure from going upwards, the structure will remain stable under $K_\ell > 0$. If there is no secondary mooring available, the structure will go up to such a position that the buoyancy of the immersed part of the structure is equal to the total weight of the structure to form a new equilibrium which is assumed to be in the upright position in an ideal situation for the time being. h_{cg} is unchanged but the distance between the new centre of buoyancy and the joint, denoted as h'_{cb}, is shortened.

1. If $h'_{cb} > h_{cg}$ the new vertical equilibrium is stable.
2. If $h'_{cb} = h_{cg}$ the new vertical equilibrium is critically stable.
3. If $h'_{cb} < h_{cg}$ the new upright equilibrium is also critically stable but the stable equilibrium is either in the oblique position or does not exist.

Conditions such as 2 and 3 are to be avoided in any case. Even if it appears to be in condition 1, the difference of $h'_{cb} - h_{cg}$ should be large enough to ensure a sufficient safety margin not only to allow for the effect of the heaving force but the pitch moment of the horizontal wave force as well.

It is recognised that the amount of tension on the joint, $T_s(z_1) > 0$, is equal to the amount of buoyancy to be lost by the

L2: a distance of z when

$\Rightarrow$ a distance of $\bar{z}_0$ when

Eq. (8.6). $(d - z_i - z_0) \Rightarrow$

$\Rightarrow (d - z_i - \bar{z}_0)$

uplifting of the structure. Assuming that the articulated joint is uplifted by a distance of z when the structure is raised to its new upright equilibrium, $\bar{z}_o$ is given by solving the following equation:-

$$W_\Sigma - \sum_{i=1}^{j} V_{bi} = 0 \tag{8.5}$$

$$\text{where } V_{bi} = \begin{cases} V_i & i<j \\ \rho_w g A_i (d - z_i - z_o) & i=j \end{cases} \tag{8.6}$$

where j is determined by:

$$\sum_{i=1}^{j-1} V_i < W_\Sigma \leqq \sum_{i=1}^{j} V_i$$

Solving equation (8.5) by iteration $\bar{z}_o$ is obtained.

From the above it is clear that the free floating stability is theoretically ensured when $T_s(z_1) = 0.0$, as $K_\ell > 0.0$ always holds in the intact condition. In reality, a certain amount of compression may have to be reserved to compensate for the uplifting effect of the heaving force due to waves in the free floating condition. On the other hand, the free floating stability could also be obtained in some cases even $T_s(z_1) > 0$ so long as $h'_{cb} > h_{cg}$ is sufficiently great. It is easily understood that for a given $T_s(z_1) > 0$, the larger is the diameter of the upper column, the smaller is $h_{cb} - h'_{cb} > 0$.

10. UTILISATION OF THE BUOYANCY CHAMBER

It is shown above that the structural response to wind loading can be very significant when the deck payload is large, especially in shallow waters. However, if the buoyancy chamber is

utilised in this case to accommodate some of the payload machinery which would otherwise be located on board the upper deck, not only could the wind loading be reduced as the result of reduced deck space but also the height of CG will be reduced. The two aspects enhancing each other will result in the reduction of the size of the buoyancy chamber. The dynamic motion response, however, may not be reduced as the mass moment of inertia will also be reduced.

The shear force on the articulated joint, obtained on the basis of constant restoring stiffness, is shown in fig. 8.15. Related results are listed in Table 8.8.

In the particular case examined, the CG is reduced and the total buoyancy needed is reduced by as much as 28%.

The distance between the CB and CG, ie $h_{cb} - h_{cg}$ increases, although both are reduced as the result of partial deck relocation into the buoyancy chamber, ie h_{cg} is reduced more rapidly. The natural frequency is also increased as the result of reduced mass moment of inirtia. Therefore, the angular dynamic response to harmonic waves is increased instead, despite the reduction of wave loading as the result of the reduced buoyancy chamber dimensions.

The shear force on the articulated joint is increased in water depth of 150m, but is reduced dramatically in the water depth of 100m despite the increase of angular dynamic response.

11. CONCLUDING REMARKS

This chapter has concentrated attention on the geometrical

optimisation of monolithic single articulated tower structures. The basic design specifications are assumed to be the water depth, deck payload and environmental conditions. The following conclusions are drawn.

1. In pre-determining the minimum deck clearance, the total of the extreme angular displacement is estimated by equation (8.1) which is largely justified according to the subsequent results obtained.

The deck space required depends directly on the deck payload expected. Owing to lack of data and the empirical relationship, the deck space/deck payload ratio is currently assumed to be between $5m^3/t$ and $10m^3/t$. A deck rectangular, in plan view, is assumed although the option of a circular deck is open.

The dynamic response of the structure to waves is practically independent of the deck dimensions under the condition of zero static axial force on the articulated joint.

The deck dimensions can be determined purely on the basis of minimising the wind loading which means to use a flat deck other than a tall and slender one.

Because of the ragged surface of the deck in reality, C_{dal} is not likely to be under 1.0. A more accurate estimation of the wind loading on the deck, based on a model test, will be justified in real design practices due to the importance of the wind loading on it.

The deck clearance depends on the total of the extreme angular displacement, water depth, extreme wave height and the breadth

of the deck. It varies from about 20m up to 35m, assuming a 30m extreme regular wave.

2. A ballast chamber is considered necessary on the basis of stability requirements and to reduce axial tension on the articulated joint. The impact of the ballast chamber is mainly on the internal sectional forces along the structure, particularly along its lower part, which depend on the dimensions and position of the chamber, the ballasting material density and the wave frequency.

From the practical point of view, it is undesirable to have a larger volume ballast chamber than that necessary to make the static tension on the articulated joint zero. In deep waters, it is preferable to use less ballasting. In shallow waters, light ballasting is desirable for those structures with large payloads. In most other cases, appropriately heavy ballasting is required to reduce the shear force on the articulated joint.

The position of the ballasting should be located as low as possible using dense materials, but materials with a density greater than $2.5t/m^3$ do not offer much advantage. In addition, a flat ballast chamber results in relatively small shear forces on the joint.

3. The length of the lower column depends on the position and the dimensions of the buoyancy chamber. Its diameters should be as low as possible braring in mind the following considerations:-

a. The minimum diameter is thought to be about 7m if it is to provide dry access to the deeply immersed part of the structure down to the articulated joint and contain risers etc.

b. It must have a reasonable reserve margin of structural strength to resist possible immediate structural failure due to overloading and long term fatigue failure due to moderate but persistent cyclic loading and due to those loads imposed during the transit and installation stages.

c. Its diameter should also be large enough to render the low natural frequencies of the first few modes of the FMV motion well above wave frequencies of high energy density to avoid any resonance effect, especially in relatively deep waters.

The use of a large diameter lower column reduces the buoyancy efficiency and increases the structural material consumption. Although it reduces the dynamic response in moderate wave conditions, it worsens the extreme dynamic response to waves. However, the most significant effect of using a large diameter lower column is to increase the sectional forces along the lower part of the structure, particularly the shear force on the articulated joint.

4. The position and dimensions of the buoyancy chamber are not independent of other column dimensions. They affect the structural characteristics, static and dynamic response, and internal sectional forces along the structure, with the shear force on the articulated joint in particular.

Among the parameters defining the dimensions and position of the buoyancy chamber, its volume and submergence depth, L_s, are the most influencial ones. Its diameter/length ratio, α_4, has practically no effect except for those structures with large payloads in shallow waters.

The submergence depth, L_s, varies from 0.1d up to 0.3 d. The minimum submergence depth of the buoyancy chamber is thought to be 15m for an extreme design wave of 30m in height in the North Sea conditions.

Practically, the diameter/length ratio, α_4, of the buoyancy chamber varies from 0.5 up to 1.5. The size of the buoyancy chamber varies in such a region that the static tilt due to extreme mean wind loading varies from 30% to 10% of θ_Σ as given in equation (8.1).

5. The designs in fig. 8.1a,b and c all have weaknesses, which lead to either poor dynamic responbse, huge structural weight or severe loading on the articulated joint. Option 8.1d provides a basic geometry which can be manipulated to give good compromises between the competing design objectives. The upper and lower columns should be as slender as structural and practical considerations will allow.

6. The effect of the structural mass distribution along an articulated tower structure can be examined by varying the equivalent column shell thicknesses, $\bar{t}_i$, of the columns. Increase of $\bar{t}_i$ always achieves improved dynamic response but heavily increases the structural material consumption. Nevertheless, use of minimum structural weight is not always favoured for all the column components from the point of view of reducing the internal sectional forces, especially the shear force on the articulated joint, as well as the dynamic response.

7. The shear force on the articulated joint of an articulated tower can be kept low if:-

a. ballasting material of high density is used;

b. flat ballast chamber is used, ie D_2/L_2 ratio is kept high;

c. the ballast chamber is located as low as possible, preferably right above the articulated joint;

d. light ballasting is used for structures in deep waters and appropriate ballasting is used for structures in shallow waters so that $T_s(z_1) \geq 0.0$;

e. the lower column diameter is as small as possibly allowed;

f. the buoyancy chamber is submerged deeply with small α_4 ratio in deep waters and in shallow waters except for those structures with large payloads, in which case, the buoyancy chamber should be shallowly submerged with large α_4 ratio instead;

g. the size ofathe buoyancy chamber is kept small; and

h. the structural mass per unit length of the upper column is kept high but that of the lower column is kept low.

i. the structural mass per unit length of the buoyancy chamber is kept high except for those structures with large payloads in shallow waters; and

j. In very shallow waters, part of the deck payload is removed into the buoyancy chamber.

8. The deep water limit to the applications of monolithic single articulated tower structures are defined by:

a. minimum natural frequencies of their flexural mode vibration motion,

b. maximum structural weight to give an economic performance, and

c. maximum shear force allowed on the articulated joint.

The lower column diameter is the critical parameter. It is believed that for monolithic single articulated tower structures the deep water limit is 300m to 350m with the total material consumption being 12,000t to 15,000t in such depths. However, their deep water limit could be improved if the overall bending stiffness of the lower column could be increased without enlarging its diameter. Then the shallow water depth limit is not expected to be very much below 100m. In addition, the deep water limit seems very much independent of the deck payload.

9. The shallow water depth limit of monolithic single articulated tower structures depends on their purpose of application which heavily affects the basic design requirements such as the amount of deck payload, economic performance and technical performance, etc. The possible requirements of the technical performance are summarised as:

a. the size of the limiting angle in extreme and operational conditions,

b. maximum horizontal acceleration at the deck level in terms of human response to random vibration motion, and

c. maximum permissible shear force allowed on the articulated joint.

It is difficult to define the shallow water depth limit in absolute terms without specific requirements. The limit is reached automatically when any of the requirements specified cannot be satisfied.

10. The water depth range in which monolithic single articulated tower structures with payloads varying from 500t to 5,000t can be efficiently used is about 100m to 300m. In this range of depths, the angular response and associated accelerations can be kept within a range which will petmit a wide range of operational activities from oil/gas production to single point moorings etc. The shear force on the articulated joint and the structural material consumption are moderate. The process of fabrication, installation, inspection and maintenance is not envisaged to involve any particular difficulties.

11. In all water depths, the dynamic responses to slowly varying wave drift and fluctuating wind, which are more restoring stiffness dependent, are very important compared with that to harmonic waves which is more natural frequency dependent.

12. The buoyancy chamber could be utilised to accommodate some of the production machinery composing part of the deck payload.

13. There exists the possibility of relocating an articulated tower structure, on finishing the operations at one site, to another site. It is envisaged that the overall economic background of the structure would become much more attractive if relocation of the structure were possible for similar applications.

14. The static stability in the intact condition improves as water depth increases. In all water depths the static heel due to mean wind loading is a predominant part of the total static heel. The static heel due to steady current accounts for about 12% up to 38% of that due to mean wind loading. The static heel due to mean wave drift normally is greater than that due to the mean wind loading. Any lateral offset in the centre of gravity of the deck payload can produce a significant heel angle and it is thus necessary to carfully consider the deck layout from this point of view. Even one metre lateral offset can result in a static heel of the same order as, or greater than, that due to current loading in relatively shallow waters.

The static stability in a damaged condition can be ensured by limiting the amount of maximum possible flooding, dividing the buoyancy chamber into smaller compartments using vertical and transverse bulkheads. With two transverse and three or four vertical bulkheads, the flooding damage to the buoyancy chamber can be sufficiently limited.

The static stability in free floating condition, theoretically, is always ensured if zero static tension on the joint is kept, ie $T_s(z_1) = 0.0$. When $T_s(z_1) > 0.0$, the structure may also be statically stable under certain conditions. Preferably, a secondary mooring parallel to the articulated joint should be available in this case to ensure that the structure does not go up to the free floating condition if the design involves $T_s(z_1) > 0.0$. Even if $T_s(z_1) = 0.0$, it may also be necessary to resist the over-turning effect of the pitch moment on the structure.

15. There is a need to carry out a comprehensive study on the economic performance of articulated tower structures with to regard certain important aspects as listed below:-

a. material consumption and fabrication cost,

b. cost of tow-out and installation etc, and

c. operational efficiency and cost, both in the short term - say monthly - and the long term.

Often decisions are centred purely on the economic grounds with regard to the feasibility or preference of offshore structures under consideration. Material consumption taken above as the sole economic factor due to the lack of data might be gravely prejudicial on the judgement of the economic performance of the structure in consideration overall.

LIST OF FIGURES

LIST OF TABLES

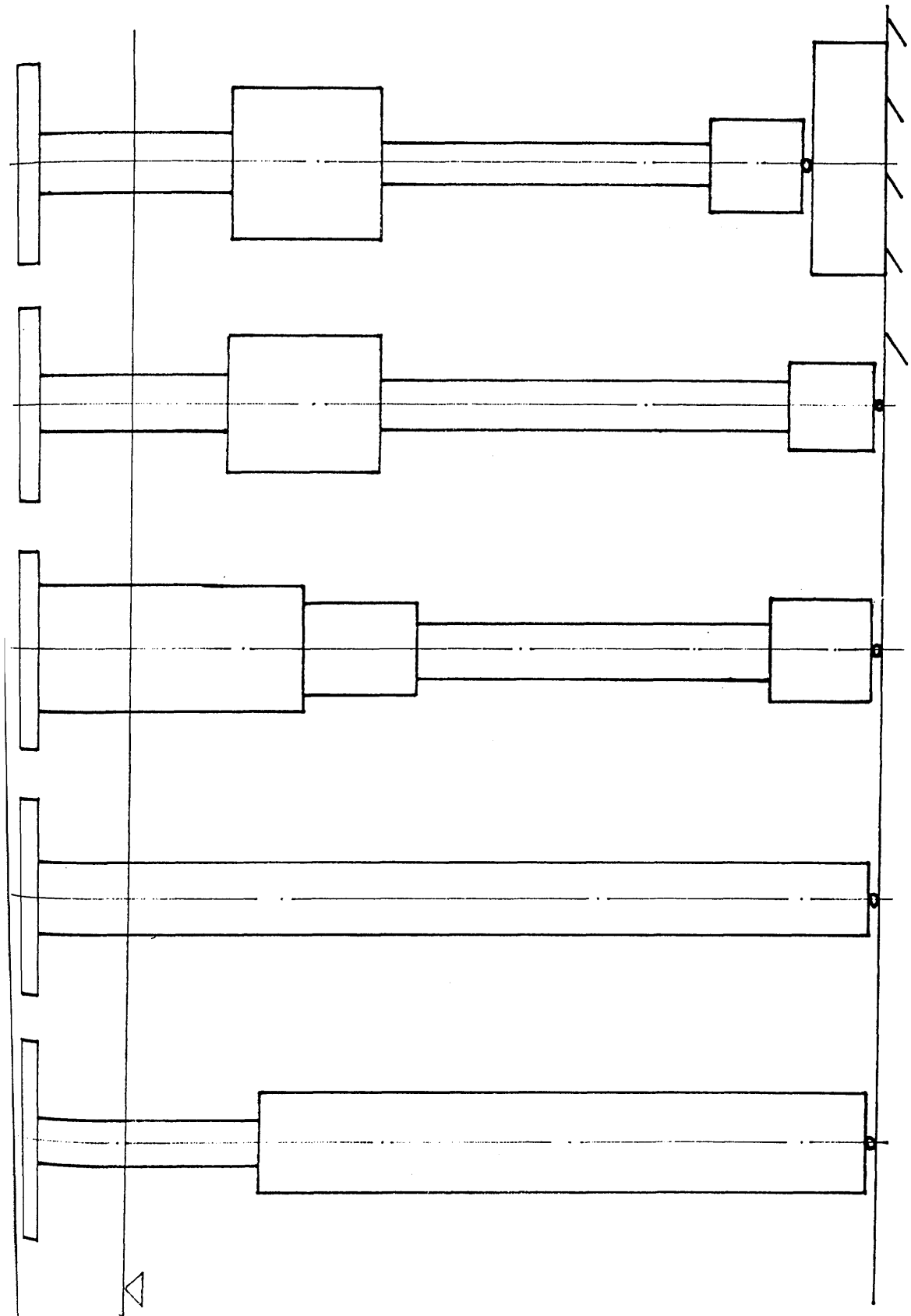

Fig. 8.1 options of possible structural geometry of a monolithic single articulated tower

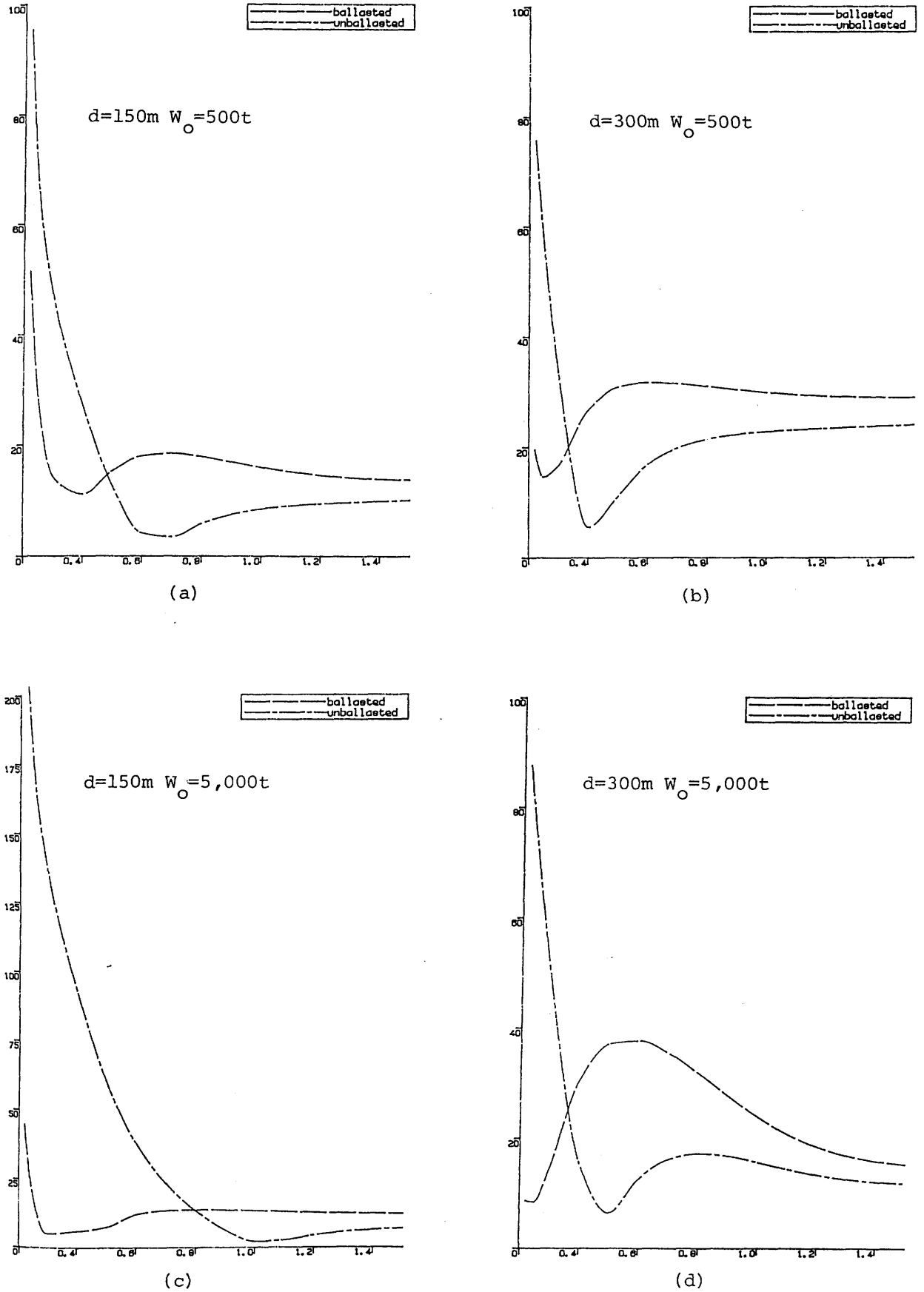

Fig. 8.2 shear force on the articulated joint showing the effect of ballasting (sample structure data from Table 8.3)

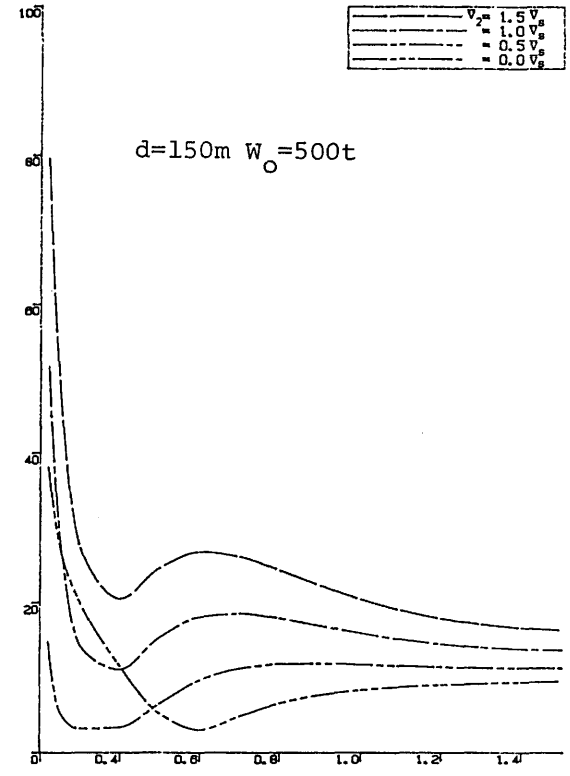

(a)

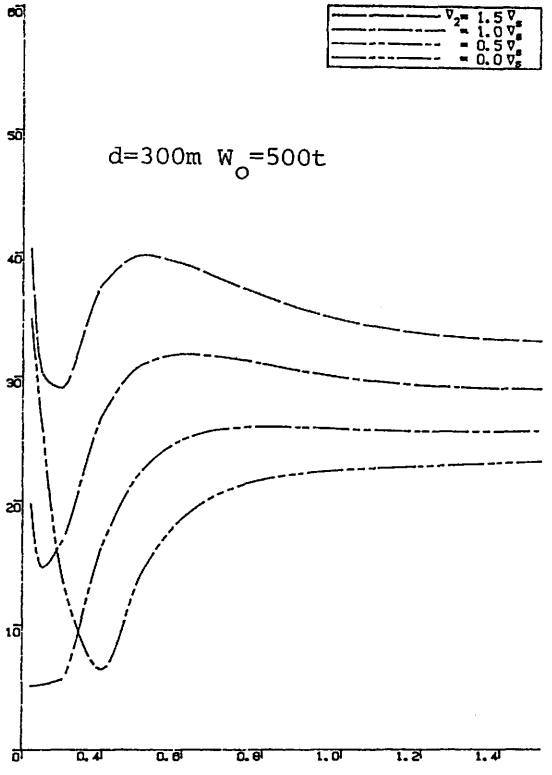

(b)

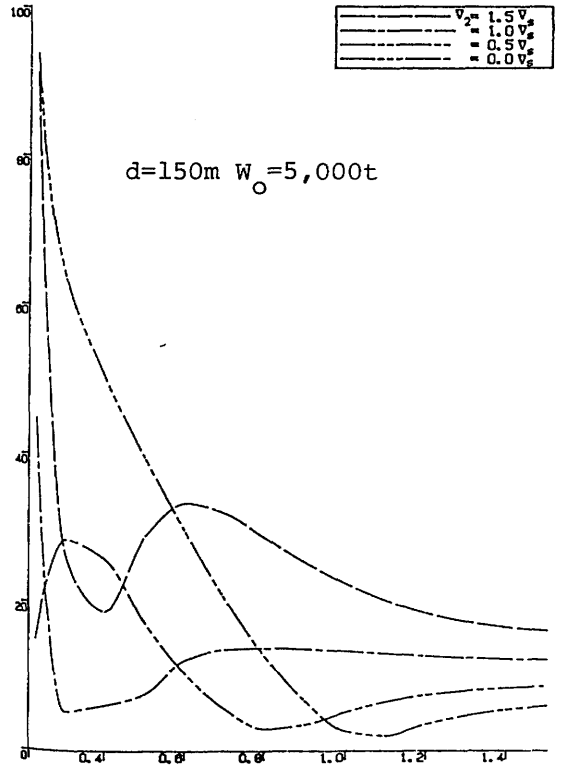

(c)

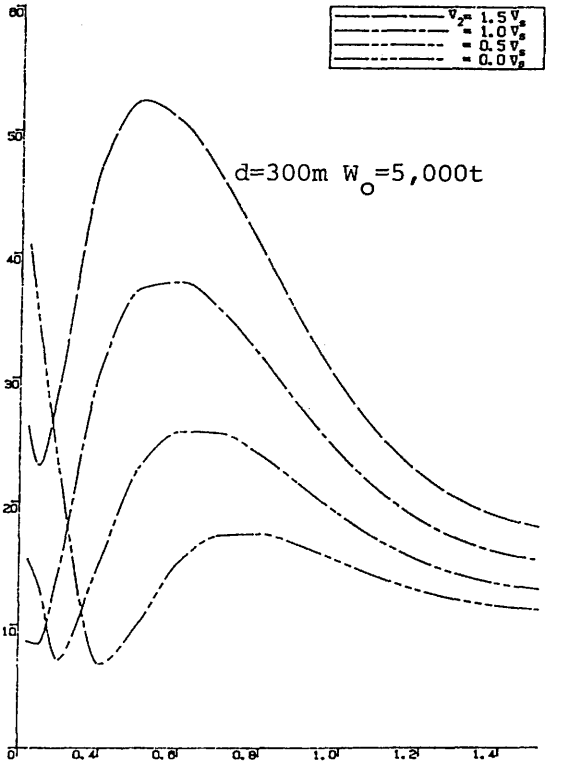

(d)

x : ω rad/s ; y : F_s/H t/m

Fig. 8.3a shear force on the articulated joint showing the effect of varying the amount of ballasting

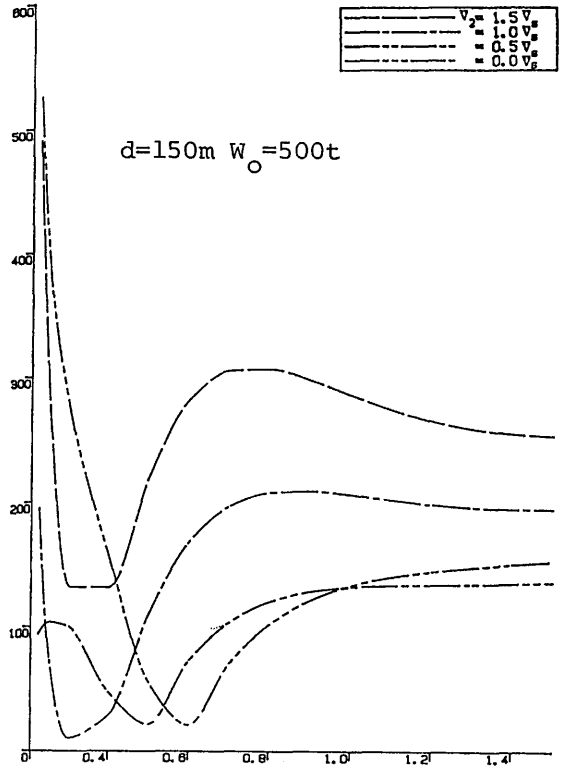

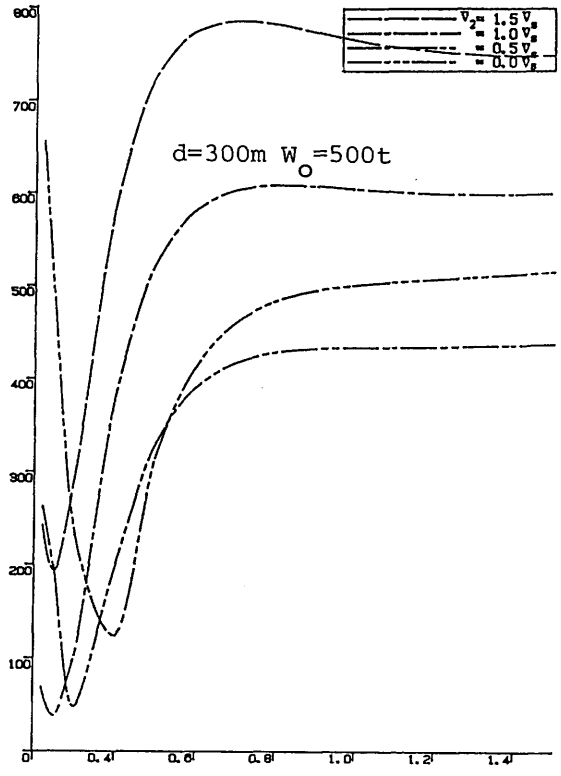

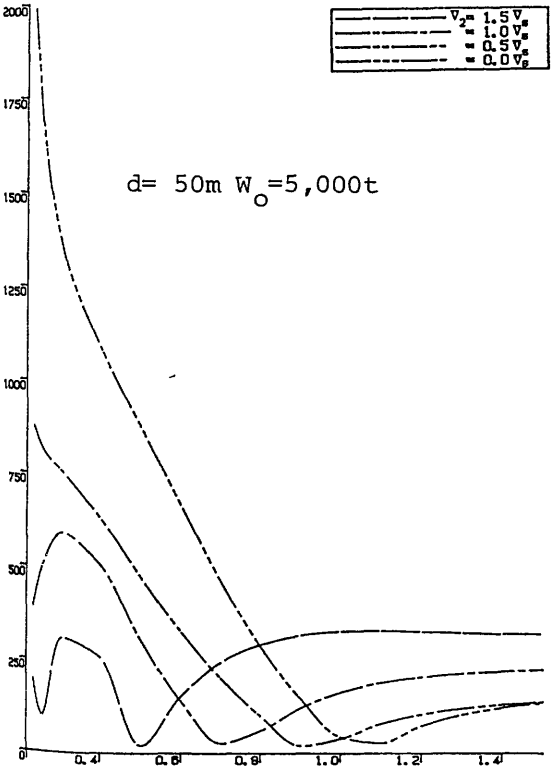

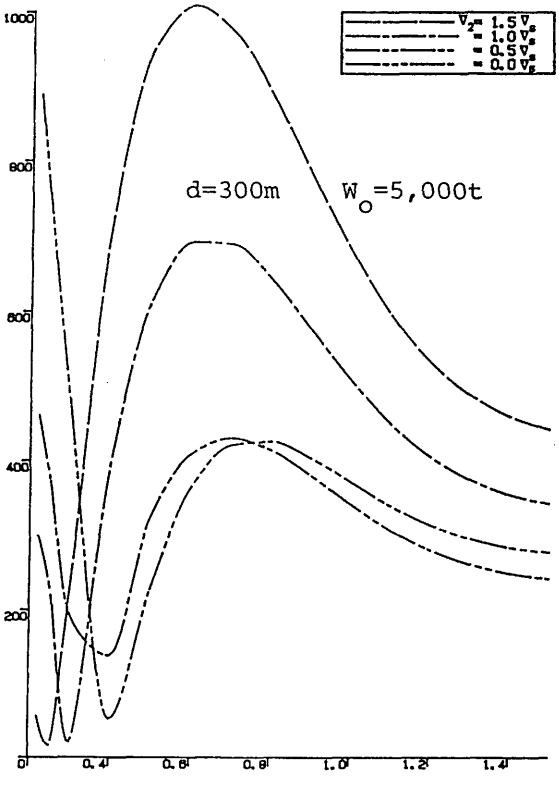

x : ω rad/s ; y : F_s t/m

Fig. 8.3b shear force on the articulated joint showing the effect of varying the amount of ballasting (sample structure in Table 8.3)

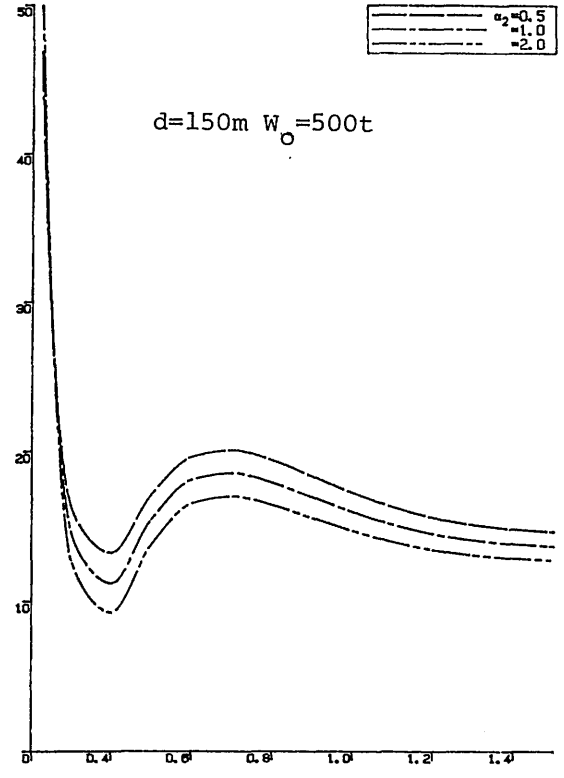

(a)

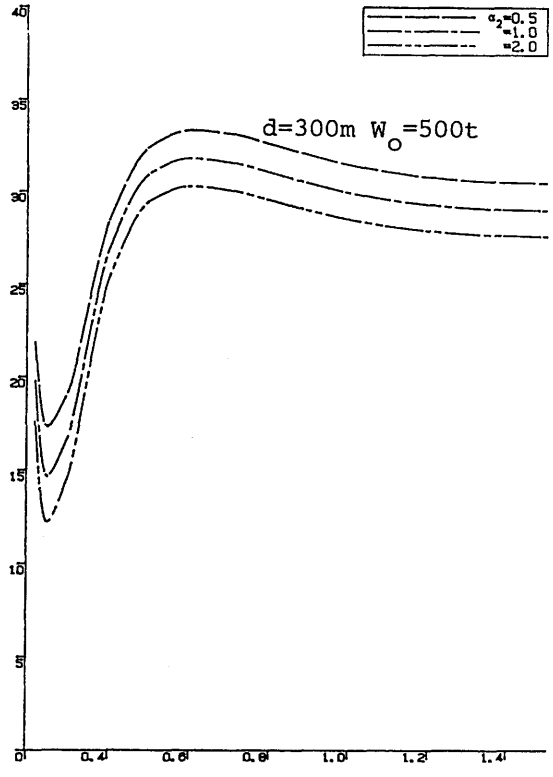

(b)

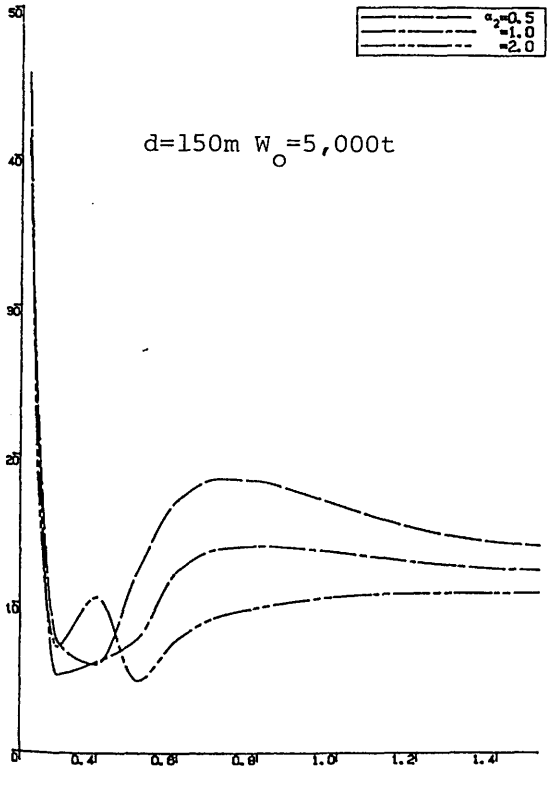

(c)

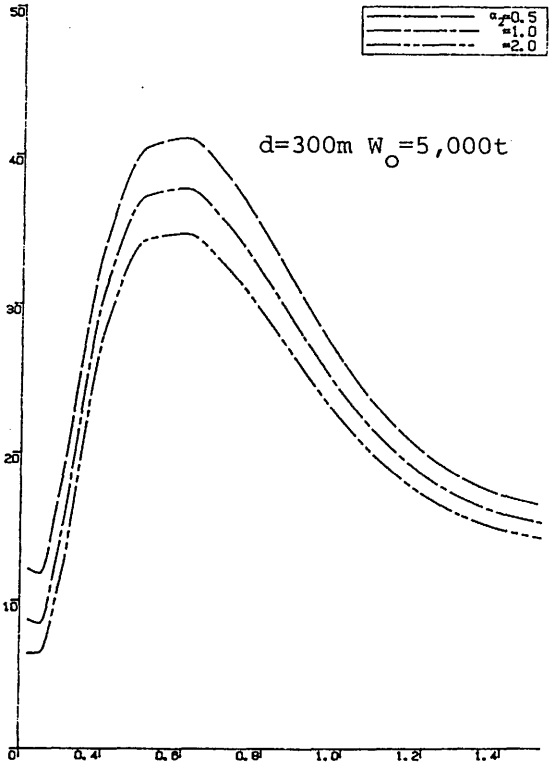

(d)

x : ω rad/s ; y : F_s/H t/m

Fig. 8.4 shear force on the articulated joint showing the effect of varying diameter/length ratio of the ballast chamber

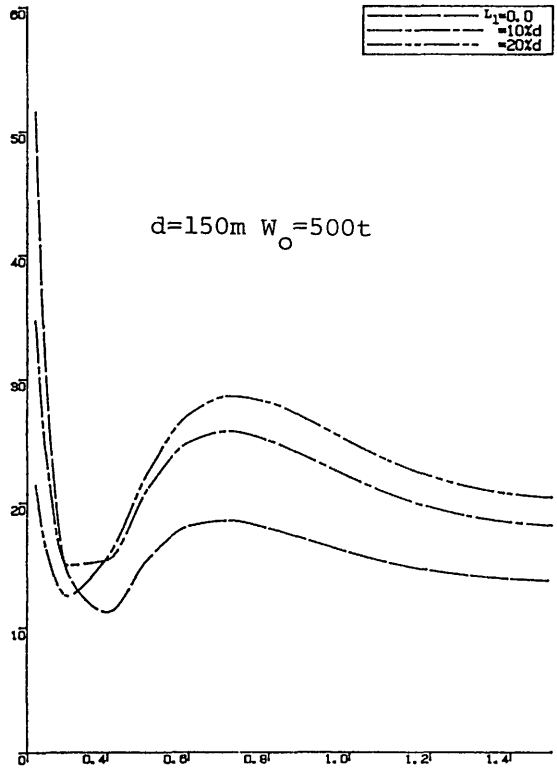

(a)

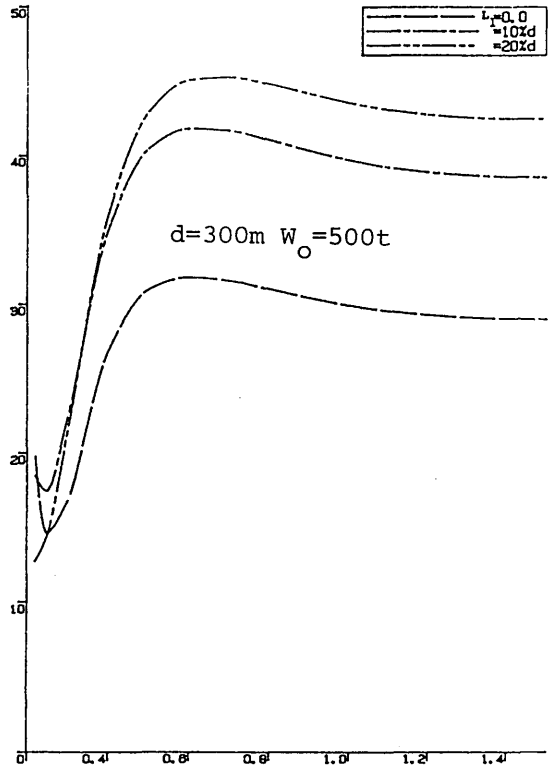

(b)

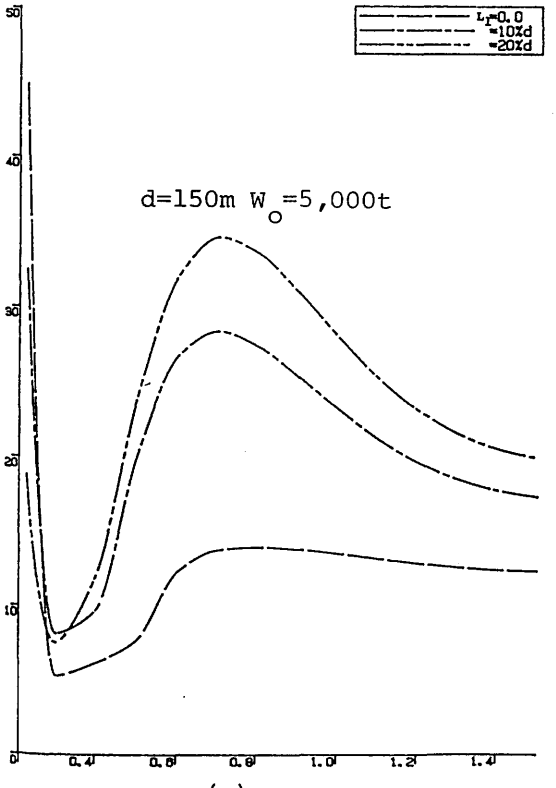

(c)

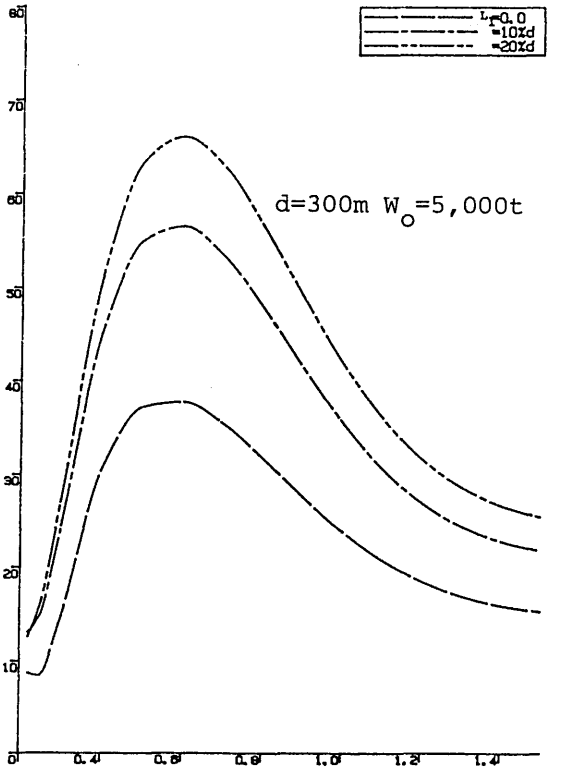

(d)

x : ω rad/s ; y : F_s/H t/m

Fig. 8.5 shear force on the articulated joint showing the effect of varying the position of the ballast chamber

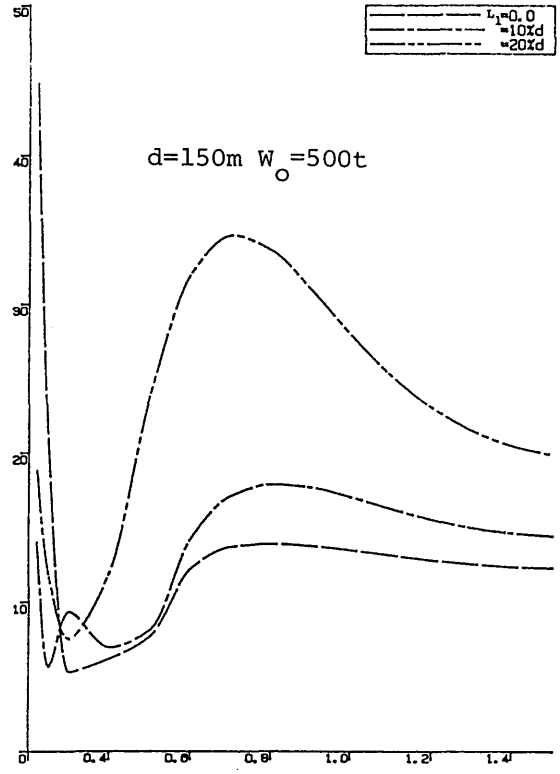

(a)

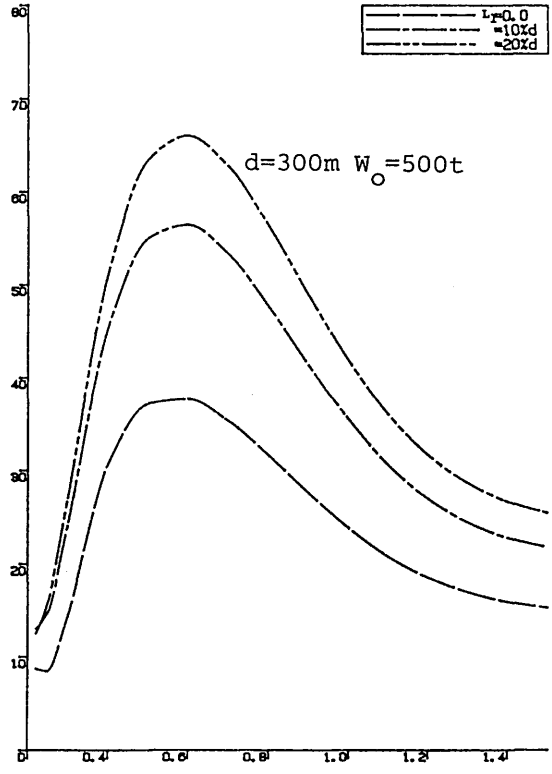

(b)

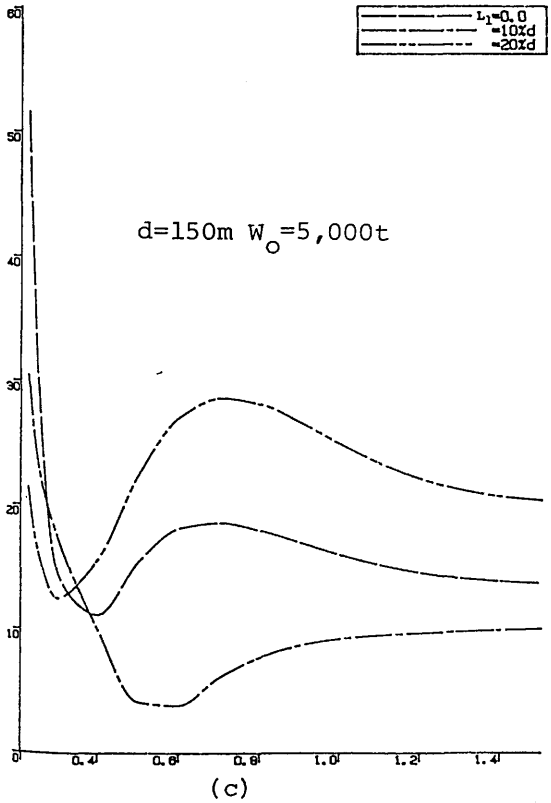

(c)

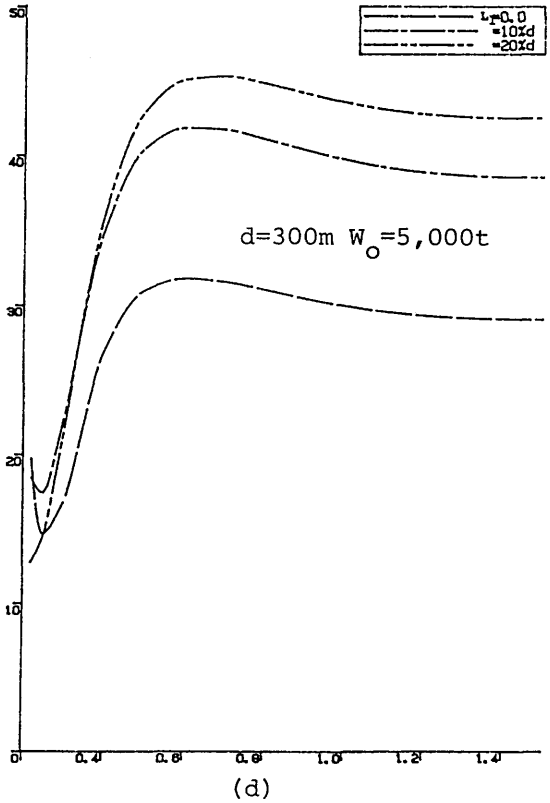

(d)

x : ω rad/s ; y : F_s/H t/m

Fig. 8.6 shear force on the articulated joint showing the effect of varying the position of the ballast chamber

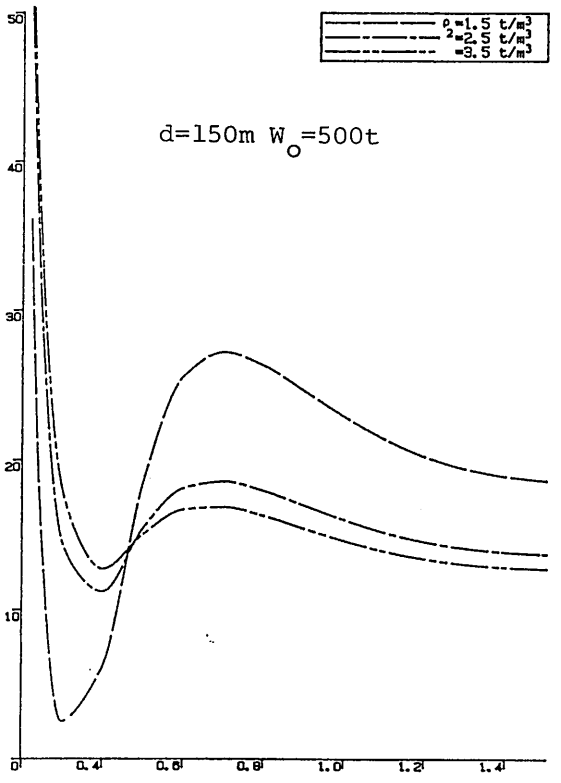

(a)

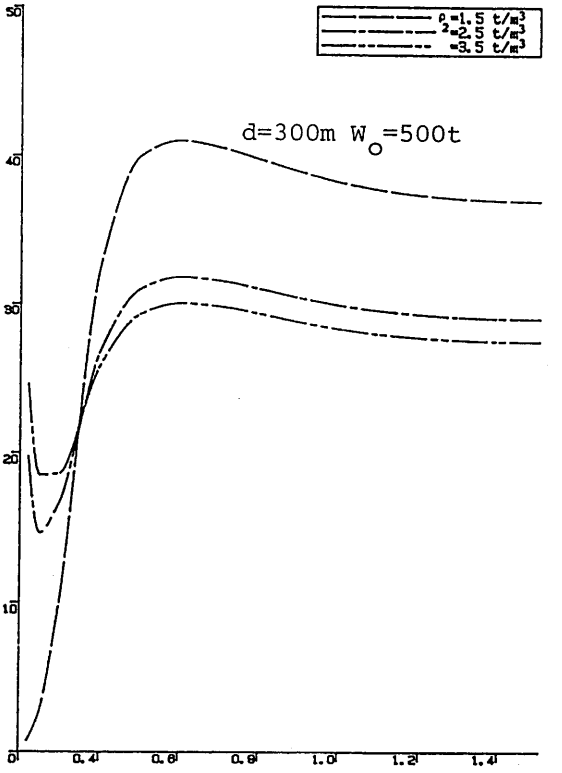

(b)

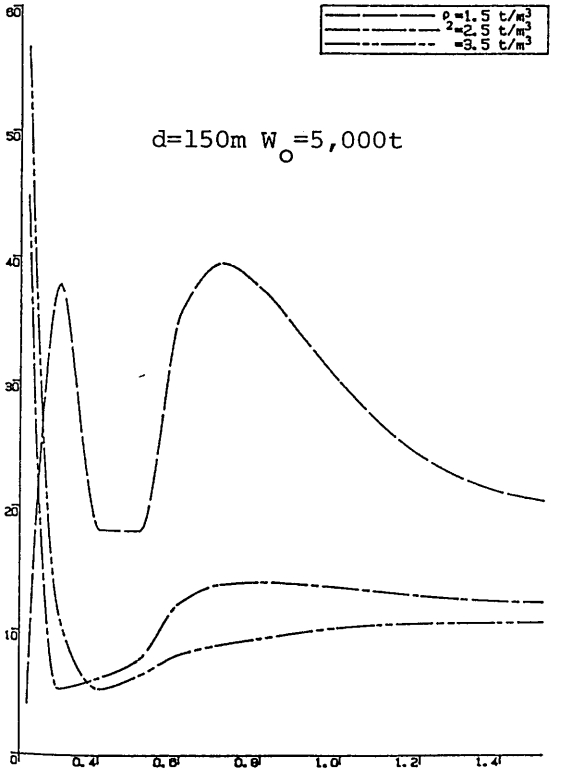

(c)

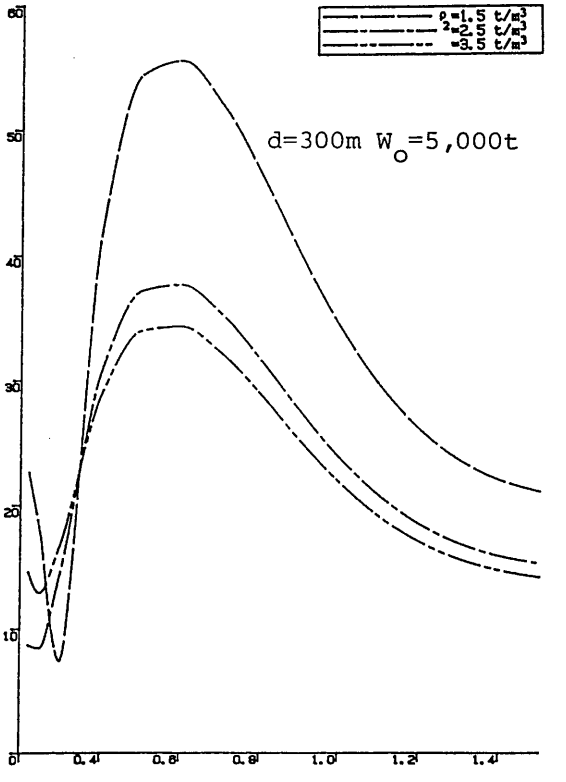

(d)

x : ω rad/s ; y : F_s/H t/m

Fig. 8.7 shear force on the articulated joint showing the effect of varying the ballasting material density

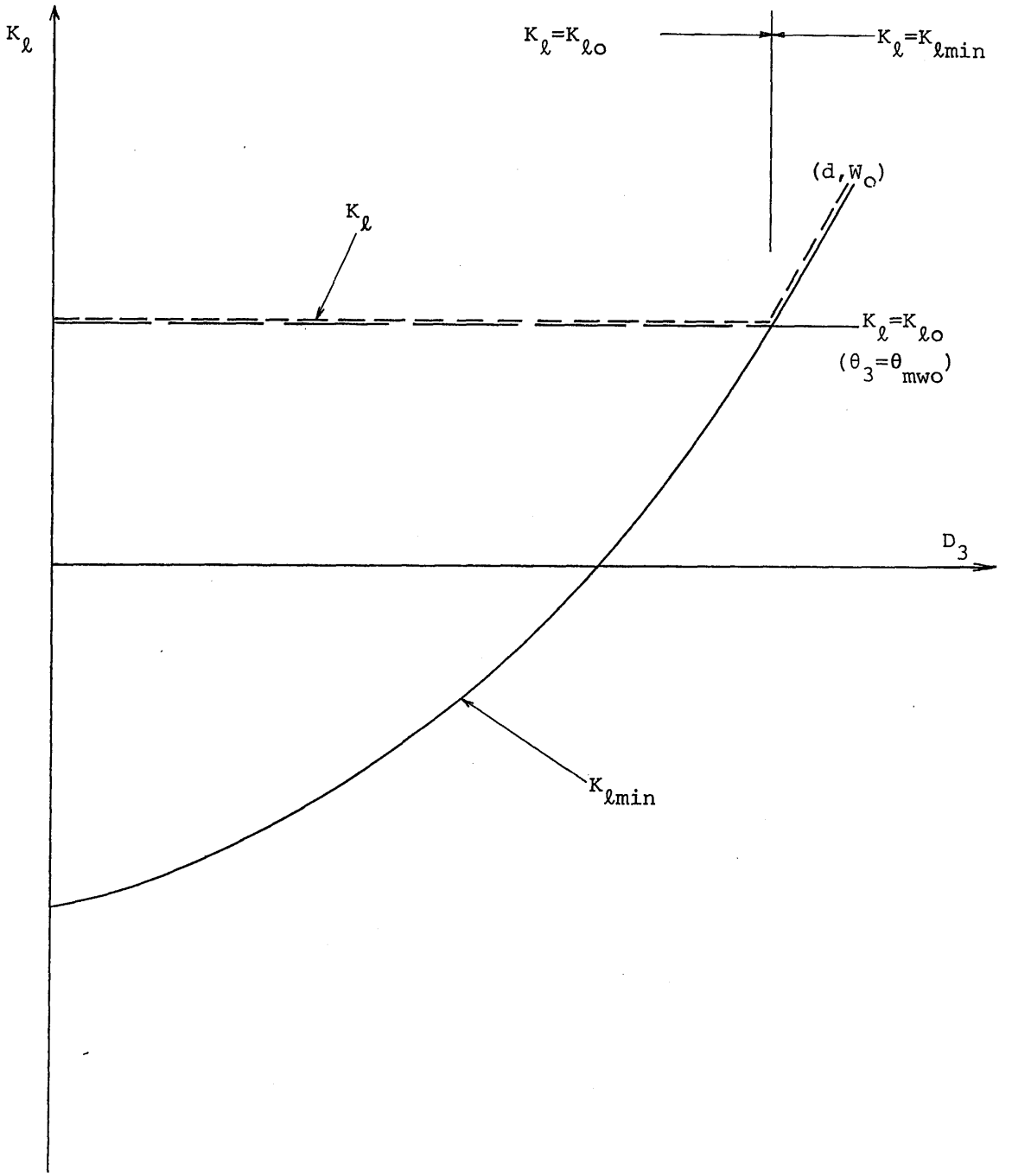

Fig. 8.8 variation of K_ℓ with the lower column diameter

θ_3 : static tilt angle under mean wind loading
θ_{mwo} : specified value of θ_3
K_ℓ : restoring stiffness
$K_{\ell min}$: restoring stiffness calculated according to θ_{mwo}
$K_{\ell o}$: minimum of K_ℓ

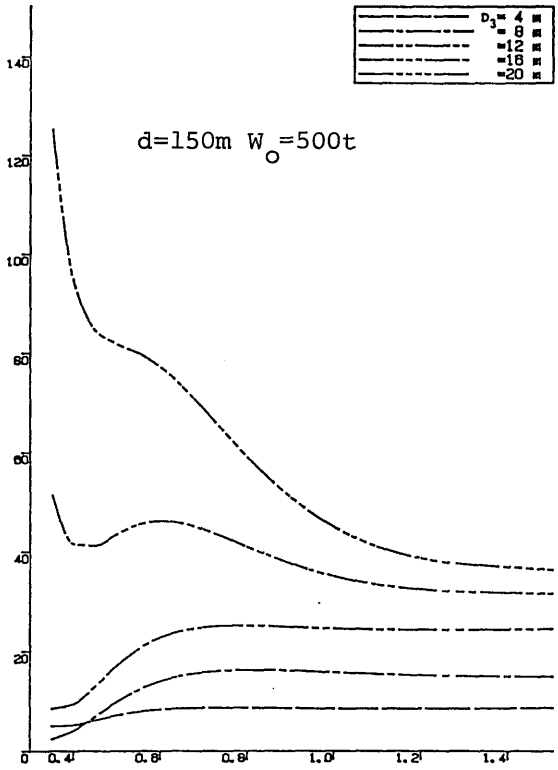

(a)

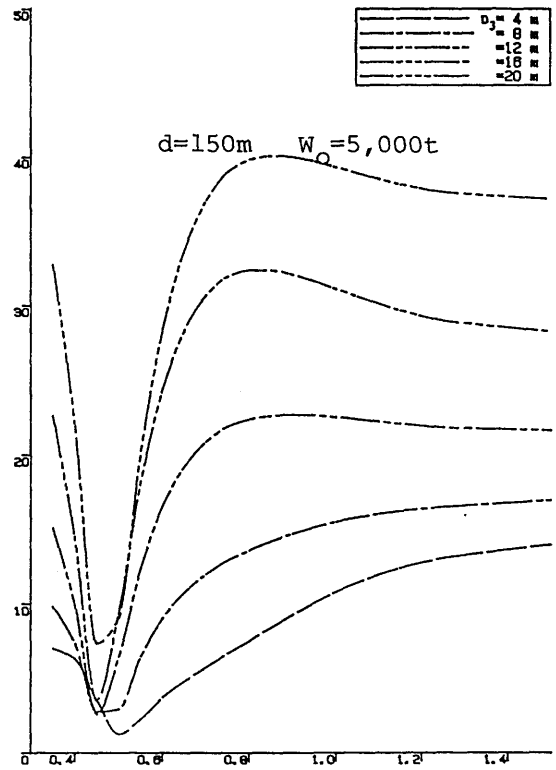

(b)

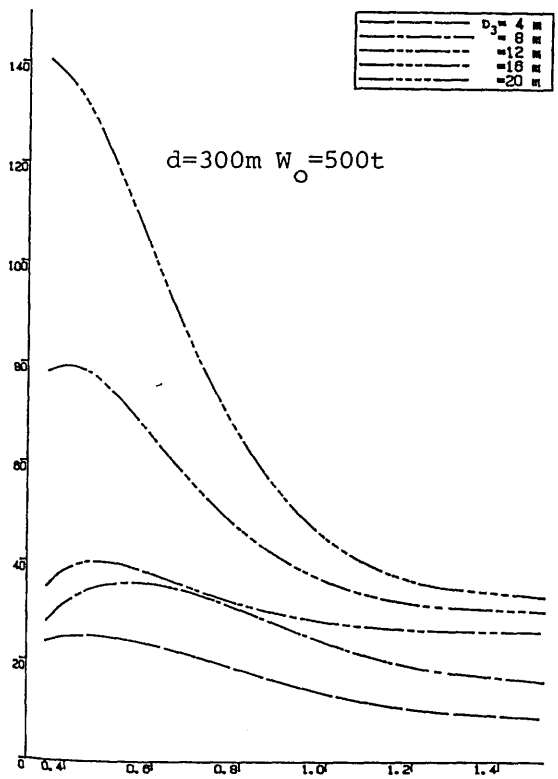

(c)

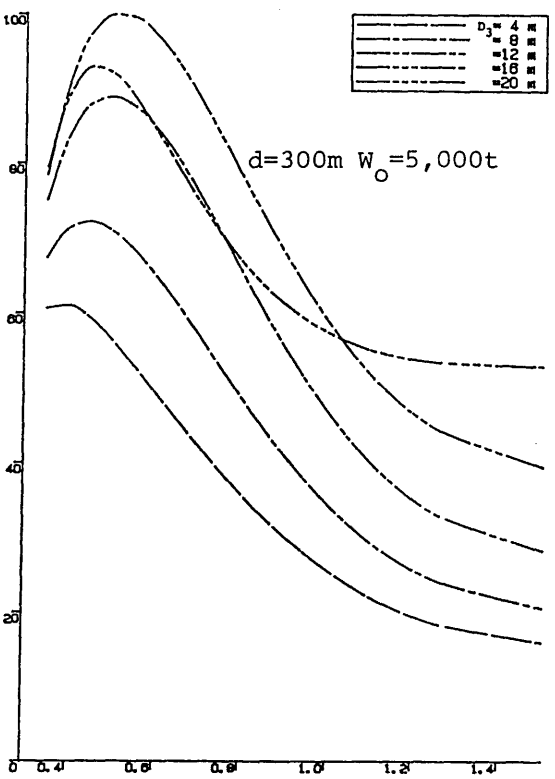

(d)

x : ω rad/s ; y : F_s/H t/m

Fig. 8.9 shear force on the articulated joint showing the effect of varying the lower column diameter (sample structure : Table 8.1)

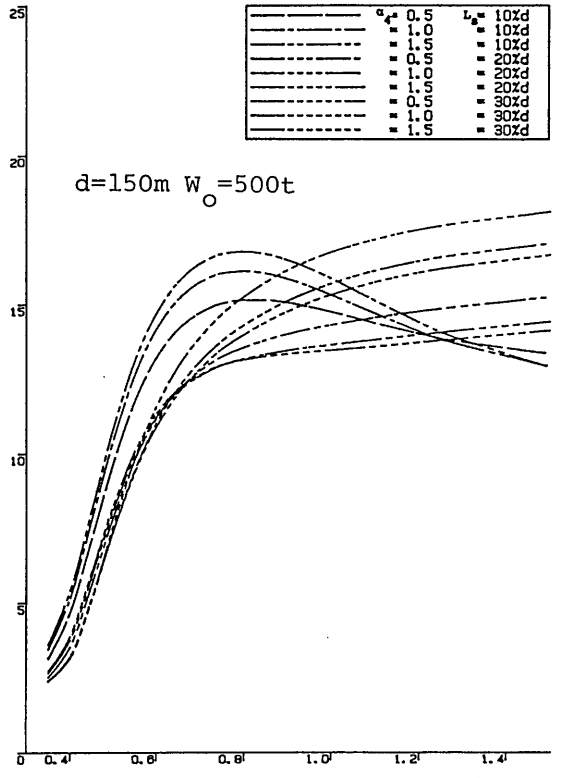

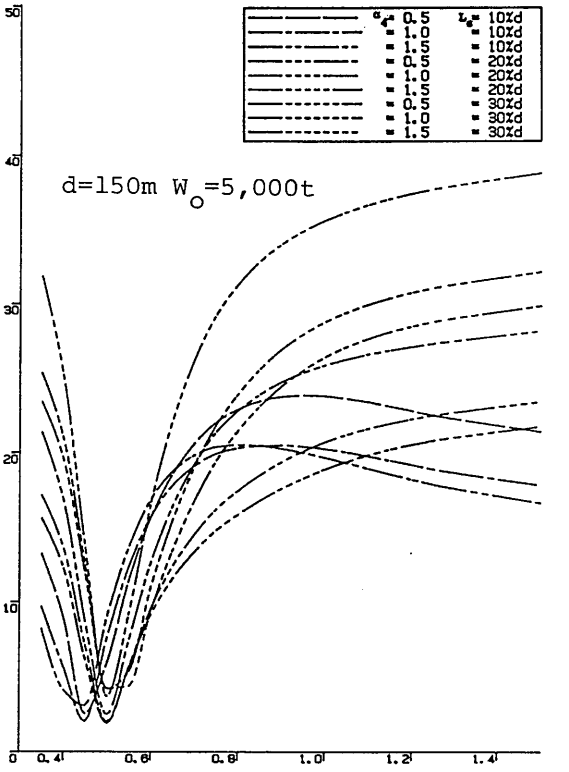

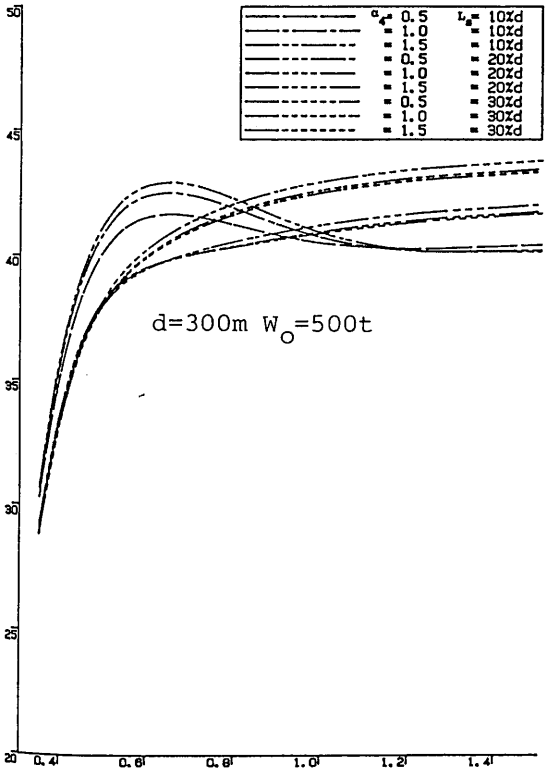

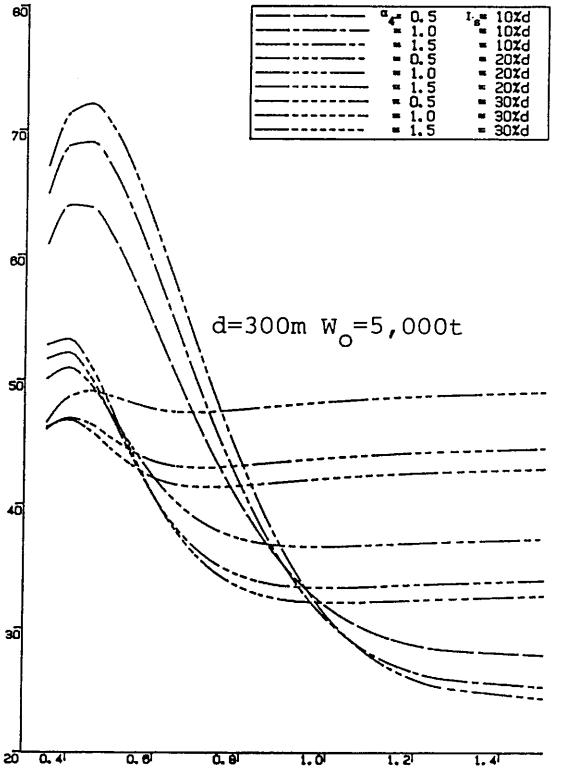

x : ω rad/s ; y : F_s/H t/m

Fig. 8.10 shear force on the articulated joint showing the effect of varying the position and diameter/length ratio of the buoyancy chamber(sample structure data from Table 8.1)

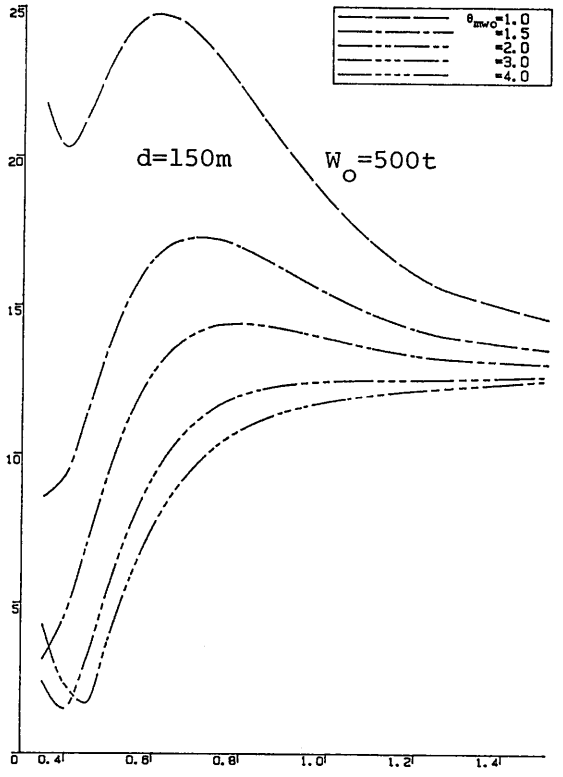

(a)

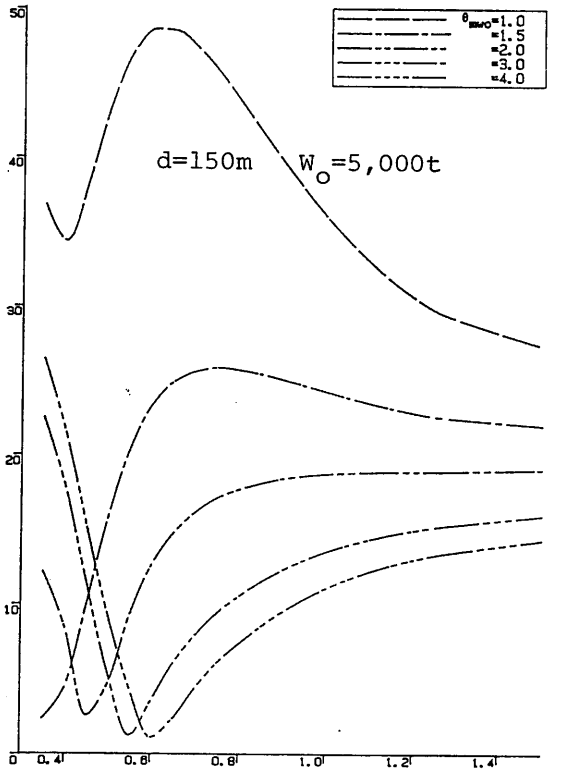

(b)

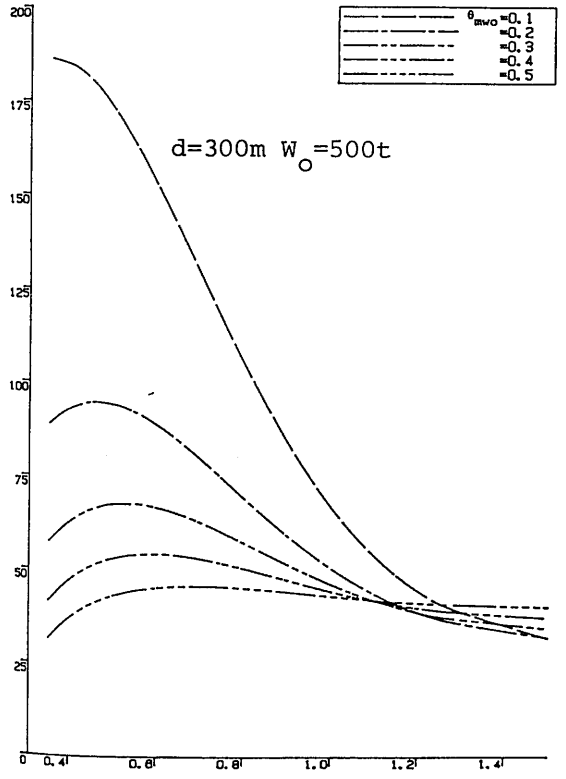

(c)

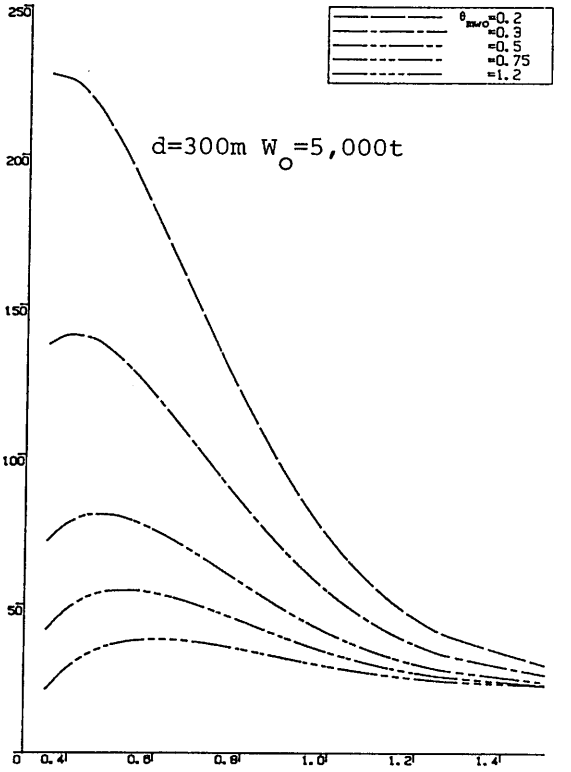

(d)

x : rad/s ; y : F_s/H t/m

Fig. 8.11 shear force on the articulated joint showing the effect of varying the size of the buoyancy chamber (sample structure data from Table 8.1)

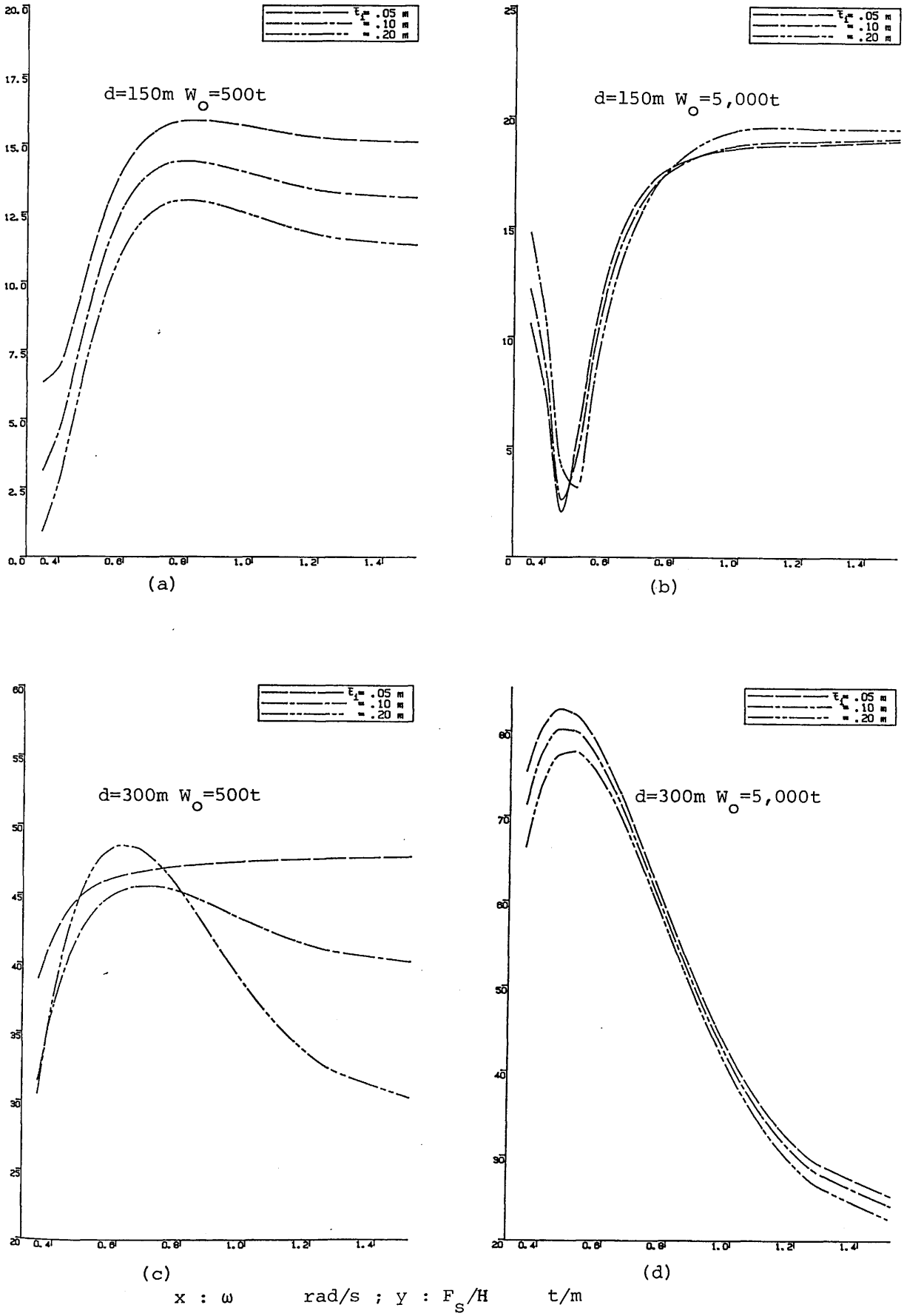

Fig. 8.12 shear force on the articulated joint showing the effect of varying the structural mass distribution (sample structure data from Table 8.1)

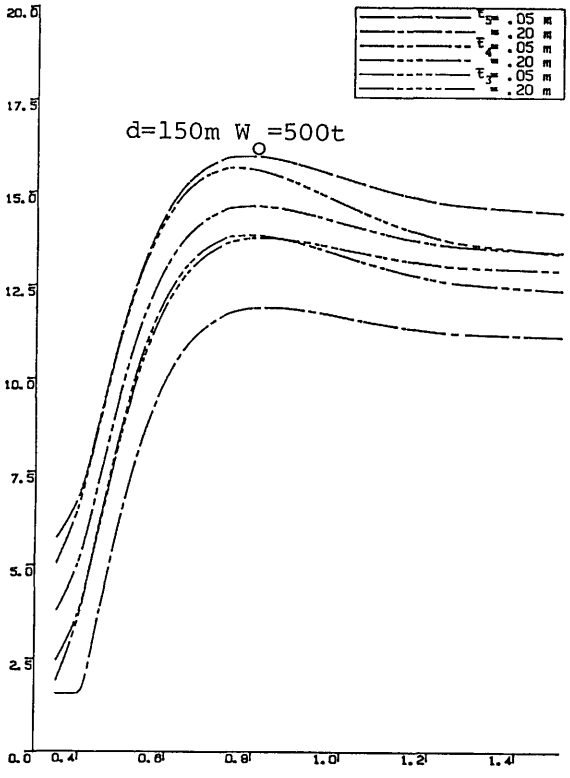

(a)

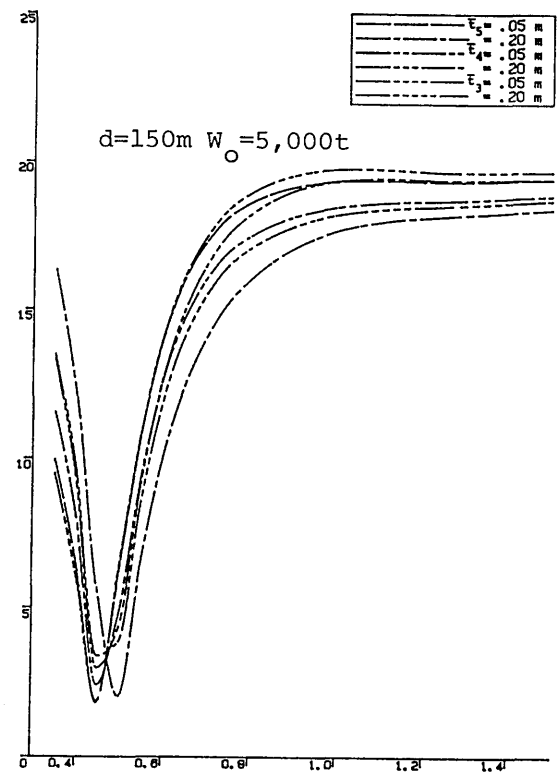

(b)

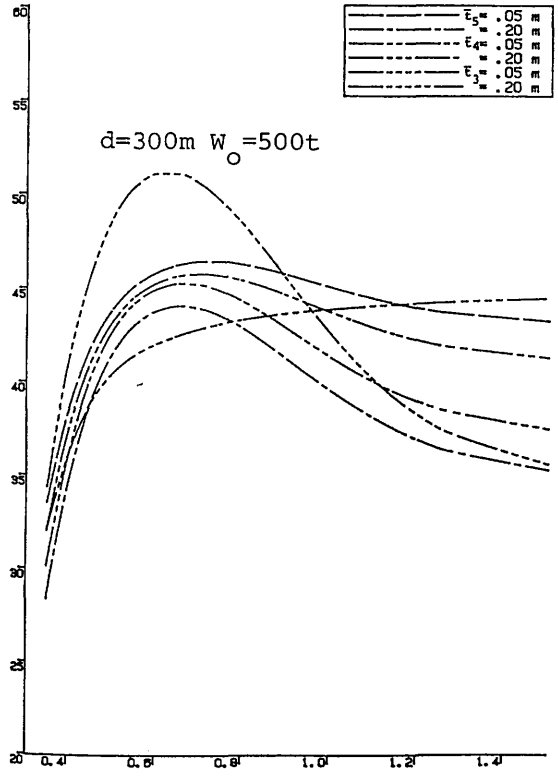

(c)

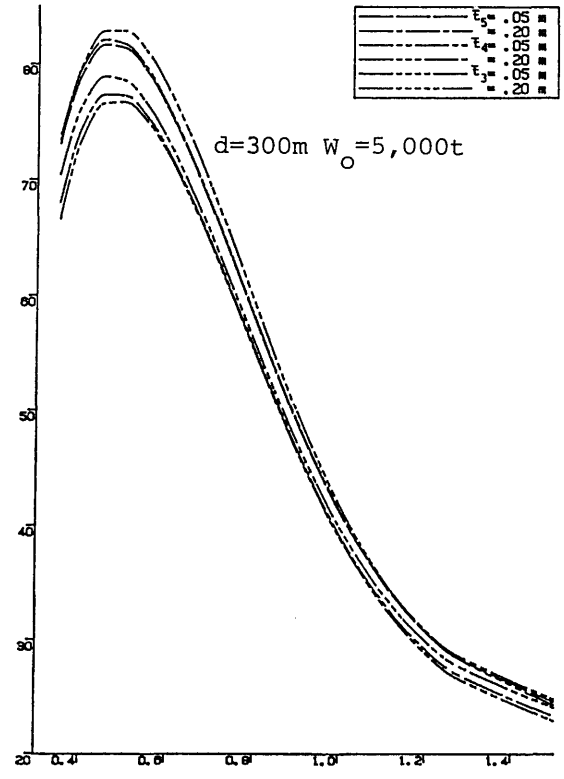

(d)

x : ω rad/s ; y : F_s/H t/m

Fig. 8.13 shear force on the articulated joint showing the effect of varying the structural mass distribution

(sample structure data from Table 8.1)

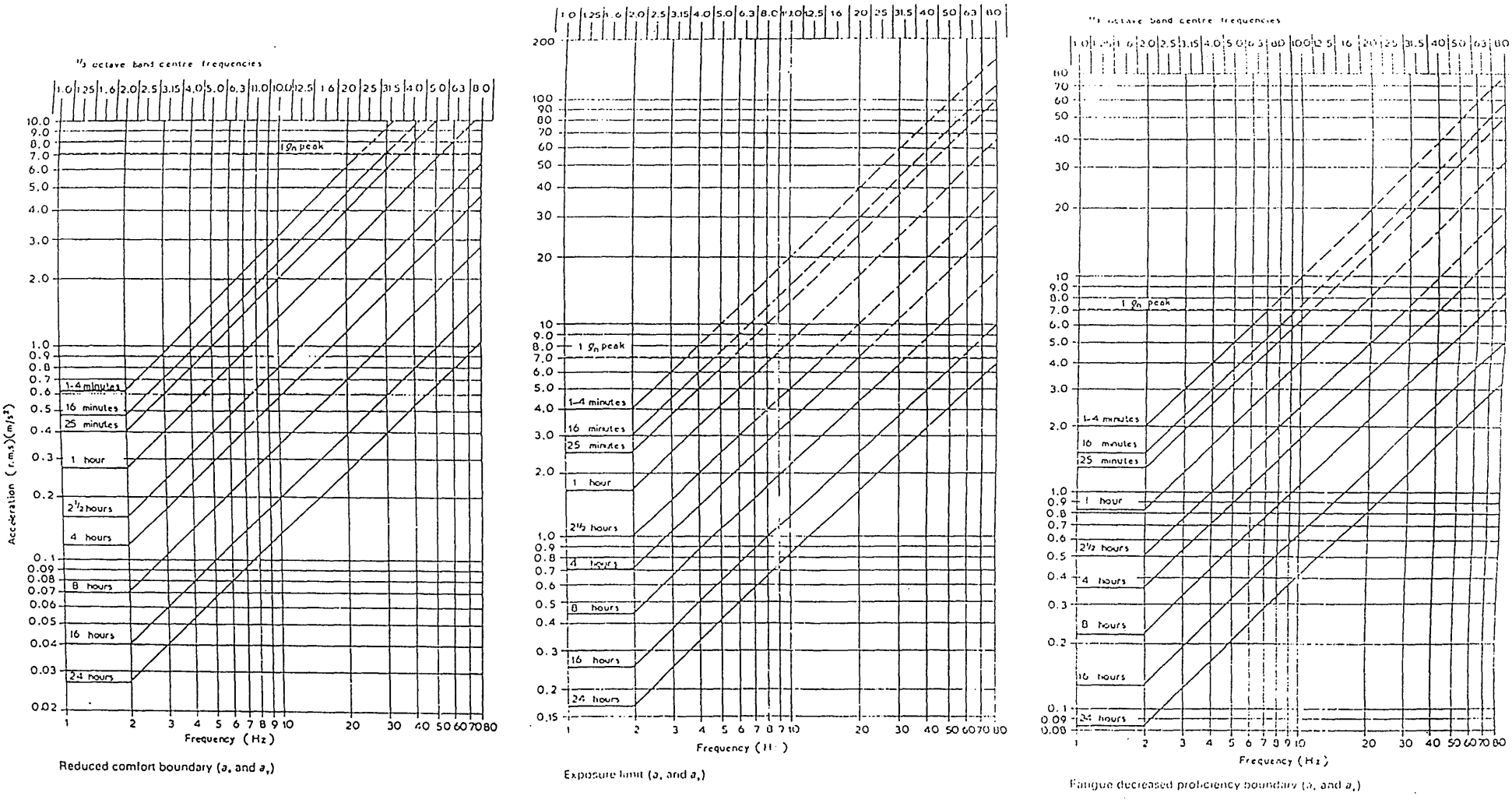

Fig. 8.14 criteria defining the tolerance of human response to random vibrations (ref. 78)

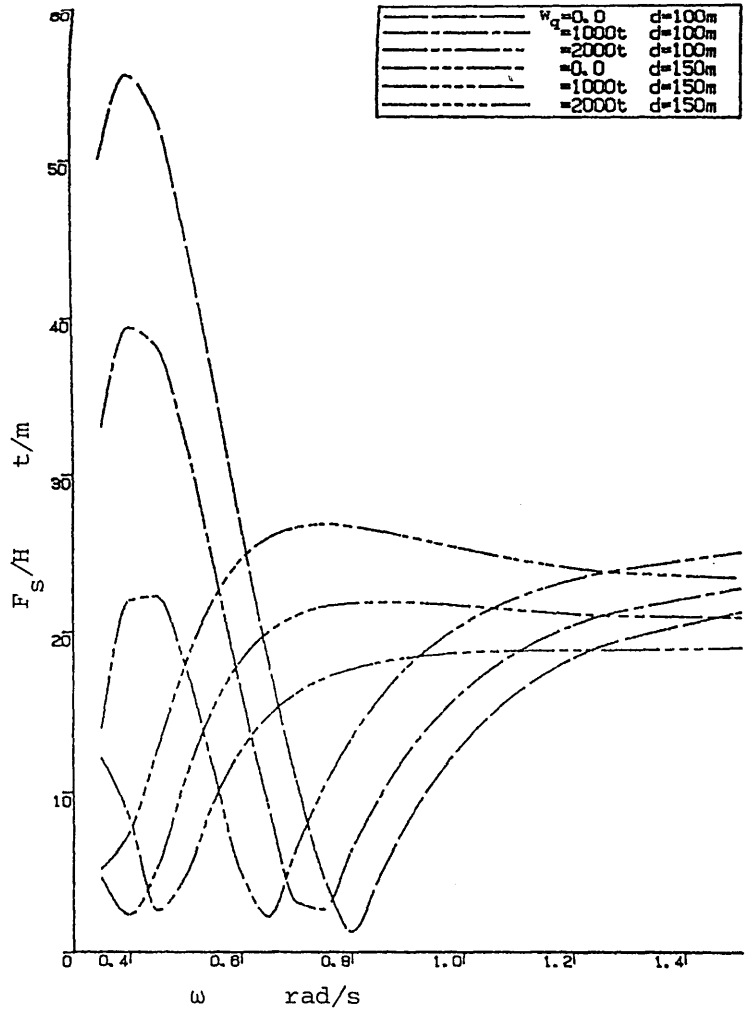

Fig. 8.15 shear force on articulated joint showing the effect of partial deck payload relocation into buoyancy chamber

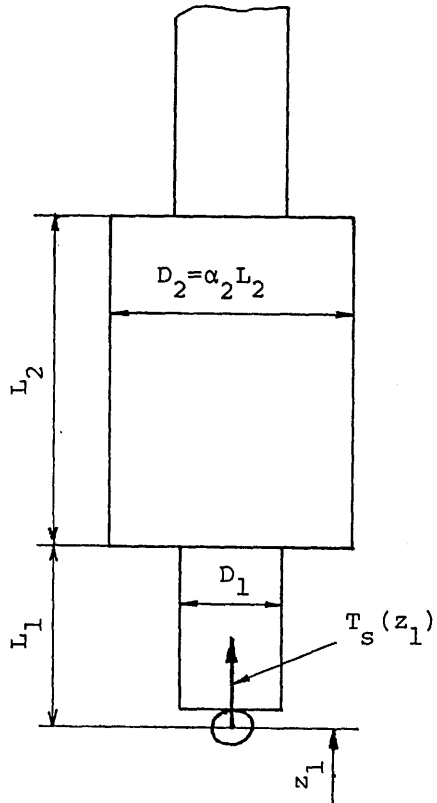

Fig. 8.16 parameters defining the position of the ballast chamber

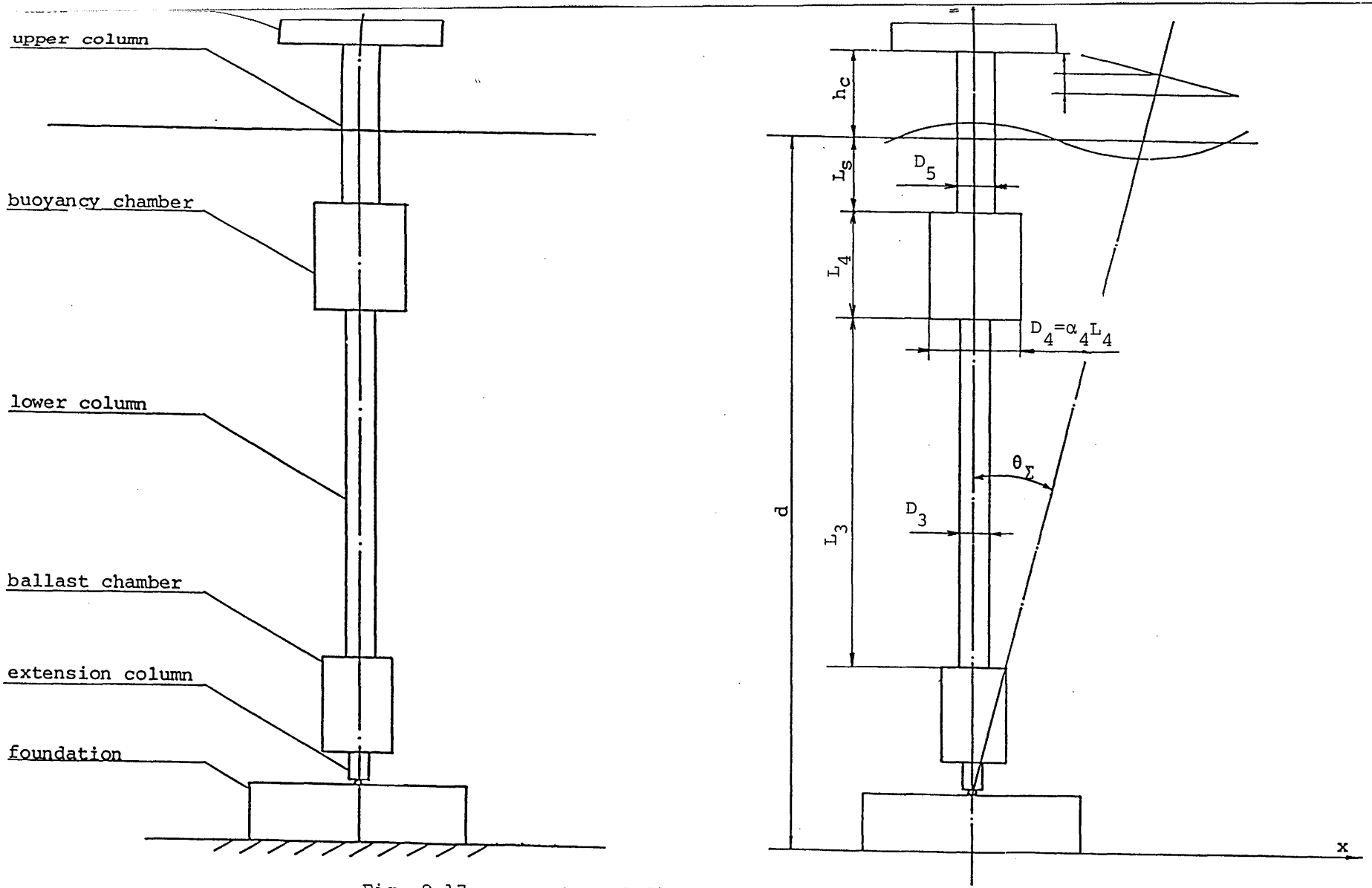

Fig. 8.17 parameters defining the position and dimensions of the buoyancy chamber

Table 8.1 list of four sample structures and relevant parameters used in the present chapter

deck payload (t)	water depth (m)	upper column (m)	buoyancy chamber	lower column (m)	ballast chamber	extension column (m)
(a) 500	150	D = 7.0	D/L=1.0	D = 7.0m	D/L=1.0	D=0.0
(b) 5000	150	10.0	=1.0	=10.0m	=1.0	=0.0
(c) 500	300	7.0	=1.0	=10.0m	=1.0	=0.0
(d) 5000	300	10.0	=1.0	=10.0m	=1.0	=0.0
related conditions:		$\bar{t}$=0.1m	L_s=20m	$T_s(z_1)$=0.		
Waves	deterministic			stochastic		
extreme	H/T=30m/16s			H_s/T_z=16m/16s		
operational	H/T=15m/12s			H_s/T_z=10m/10s		
related conditions:	C_a=2.0	C_d=0.7	H=f(T) (DnV)	Bretschneider spectrum		
wind	mean wind			fluctuating differential wind		
extreme	$\bar{V}_{wsl0}$=48m/s			β=0.09		
operational	$\bar{V}_{wsl0}$=35m/s			β=0.09		
related conditions	Harris spectrum with L=1800m			κ=.0033		
	C_{dal}=1.5		C_{dal}=0.7			
current :as stated in Table 2.2 with C_d=0.7						

Table 8.2 estimated deck clearance in various water depths

D_{Ne} \ d (m)	100	150	200	250	300	350	400
θ_Σ / h_c	20	13.875	9.5	6.875	6.0	5.5	5.0
25	30.30	26.19	23.14	21.45	21.07	20.91	20.69
50	34.95	29.31	25.24	22.97	22.39	22.11	21.79
75	39.60	32.43	27.34	24.48	23.70	23.32	22.88

Table 8.3 sample structure data used in examining the imapct of ballasting

water depth	(m)	150 (a)	300 (b)	150 (c)	300 (d)
Deck					
deck payload	(t)	500	500	5,000	5,000
deck space	(m^3)	5,000	5,000	30,000	30,000
deck heihgt	(m)	6	6	12	12
deck clearance	(m)	24.9	20.5	26.2	21.1
Upper Column					
diametre	(m)	7	7	8	8
equiv. shell thickness	(m)	0.1	0.1	0.1	0.1
Buoyancy Chamber					
diameter	(m)	17.9	10.0	29.0	25.0
length	(m)	17.9	10.0	29.0	25.0
equiv. shell thickness	(m)	0.1	0.1	0.1	0.1
submergence depth L_s	(m)	20.0	20.0	20.0	20.0
Lower column					
diameter	(m)	7.0	10.0	8.0	10.0
equiv. shell thickness	(m)	0.1	0.1	0.1	0.1
Ballast chamber					
daimeter/length		1.0			
size		determined so that $T_s(z_1)=0.0$ with ballasting material of density of $2.5t/m^3$			
equiv. shell thickness	(m)	0.1	0.1	0.1	0.1
Extension Column					
diameter	(m)	7.0	10.0	8.0	10.0
length		0.	0.	0.	0.
equiv. shell thickness	(m)	0.1	0.1	0.1	0.1

Table 8.4 list of the structural characteristics and motion response of the sample structures showing the effect of D_3

iterm	unit	condition	D_3 (m) 4	8	12	16	20	4	8	12	16	20
			(a)					(b)				
V_T	kt		10.2428	11.6961	13.9870	17.6752	26.1382	16.6671	17.9277	19.9334	22.6464	26.1395
W_{Ts}	kt		2.7769	3.2001	3.5914	3.9449	4.6366	3.4837	3.8481	4.1956	4.5186	4.7986
h_{cb}	m		52.4285	47.9548	42.3095	37.1702	37.0611	51.0285	48.7172	45.3716	41.6873	37.9984
h_{cg}	m		28.5039	27.0016	24.7883	22.1734	20.0622	27.4350	26.7825	25.6440	24.3225	22.9549
I_s	$kg.m^2$ x10^{11}		0.2385	0.2444	0.2495	0.2538	0.2866	0.3695	0.3753	0.3816	0.3884	0.3950
I_{ta}	$kg.m^2$ x10^{11}		0.3746	0.3716	0.3594	0.3508	0.5030	0.5767	0.5757	0.5688	0.5555	0.5320
C_{td}	N.m.s x10^{10}		0.0438	0.0448	0.0446	0.0417	0.0466	0.0534	0.0544	0.0546	0.0540	0.0516
K_t	N.m x10^{10}		0.2404	0.2404	0.2404	0.2600	0.4357	0.3857	0.3857	0.3857	0.3857	0.3857
ω_n	rad/s		0.1980	0.1975	0.1987	0.2074	0.2349	0.2019	0.2014	0.2015	0.2021	0.2040
θ_4	degree	extreme	0.3329	0.3409	0.3402	0.2945	0.1950	0.2461	0.2510	0.2530	0.2511	0.2404
θ_3	degree	extreme	1.9979	1.9978	1.9979	1.8471	1.1020	2.0015	2.0014	2.0014	2.0014	2.0016
K_{tmin}	N.m x10^{10}		-0.0696	0.0060	0.1147	0.2600	0.4357	-0.1276	-0.0448	0.0617	0.2033	0.3742
σ_3	degree	operational	0.3512	0.3510	0.3513	0.3265	0.1973	0.3493	0.3491	0.3492	0.3493	0.3497
σ_3	degree	extreme	0.6243	0.6239	0.6248	0.5831	0.3564	0.6221	0.6217	0.6218	0.6223	0.6235
σ_1	degree	operational	0.1843	0.1575	0.1621	0.2305	0.2912	0.1228	0.1191	0.1131	0.1043	0.0911
σ_1	degree	extreme	2.3374	2.4708	5.4702	20.4550	35.1820	1.4643	1.4785	1.5136	1.5724	1.6654
σ_{1x}	m/s^2	operational	0.0987	0.0784	0.0654	0.0793	0.0911	0.0638	0.0610	0.0564	0.0498	0.0400
σ_{1x}	m/s^2	extreme	0.1898	0.1788	0.2642	0.6975	1.2734	0.1300	0.1284	0.1262	0.1233	0.1189
σ_2	degree	operational	0.2311	0.2532	0.2315	0.1938	0.1694	0.2001	0.2107	0.2269	0.2454	0.2581
σ_2	degree	extreme	0.3288	0.3406	0.3046	0.2626	0.2455	0.3517	0.3590	0.3683	0.3793	0.3906
θ_2	degree	operational	0.1284	0.1516	0.1329	0.1029	0.0876	0.1132	0.1221	0.1333	0.1447	0.1529
θ_2	degree	extreme	0.1649	0.1831	0.1636	0.1364	0.1256	0.1815	0.1882	0.1970	0.2071	0.2072
$T_z(z_1)$	kt	ω=0.4 rad/s	0.7819	0.7638	0.6873	0.6713	1.2840	1.4004	1.3918	1.3436	1.2342	1.1615
θ_{Ts}	degree	extreme	2.9947	3.0693	2.9948	2.6872	1.7992	2.9721	2.8055	2.8499	2.8923	2.9067
θ_{Td}	degree	extreme	9.7663	10.2840	22.0567	20.5000	35.2000	6.5175	6.5743	6.7091	6.9323	7.2827
			(c)					(d)				
V_T	kt		20.6708	25.0628	32.0602	46.8638	71.8508	32.7365	36.9192	43.6203	52.7525	71.6175
W_{Ts}	kt		4.4897	5.7666	6.9509	8.3418	10.2069	5.4946	6.7076	7.8676	8.9337	10.2872
h_{cb}	m		112.7074	98.3786	81.7810	73.0693	73.2437	111.8202	102.9187	90.9909	79.0504	73.6024
h_{cg}	m		38.0289	36.7848	33.6319	29.5840	27.6784	35.6825	35.4073	33.8505	31.8026	29.3966
I_s	$kg.m^2$ x10^{11}		1.1069	1.1965	1.2553	1.3633	1.6522	1.5829	1.6746	1.7504	1.8047	1.9498
I_{ta}	$kg.m^2$ x10^{11}		3.7549	3.6796	3.4199	3.9628	5.9964	5.8452	5.7892	5.5832	5.2097	6.0281
C_{td}	N.m.s x10^{10}		0.3811	0.4082	0.4106	0.4197	0.4979	0.4724	0.5000	0.5118	0.5016	0.5079
K_t	N.m x10^{10}		1.5138	1.5139	1.5138	1.9985	3.2106	2.4443	2.4443	2.4443	2.4443	3.1047
ω_n	rad/s		0.1765	0.1762	0.1799	0.1937	0.2049	0.1814	0.1810	0.1826	0.1867	0.1973
θ_4	degree	extreme	0.1537	0.1628	0.1625	0.1218	0.0880	0.1144	0.1208	0.1239	0.1215	0.0942
θ_3	degree	extreme	0.5003	0.5003	0.5003	0.3790	0.2359	0.5001	0.5001	0.5001	0.5001	0.3937
K_{tmin}	N.m x10^{10}		-0.0570	0.3513	1.0378	1.9985	3.2106	-0.1450	0.2778	0.9571	1.9069	3.1047
σ_3	degree	operational	0.0881	0.0881	0.0884	0.0677	0.0424	0.0874	0.0874	0.0875	0.0878	0.0697
σ_3	degree	extreme	0.1549	0.1548	0.1557	0.1201	0.0757	0.1542	0.1541	0.1544	0.1553	0.1239
σ_1	degree	operational	0.0402	0.0266	0.0143	0.0158	0.0170	0.0340	0.0307	0.0257	0.0188	0.0114
σ_1	degree	extreme	0.3927	0.3363	0.3729	0.7305	0.9416	0.3538	0.3377	0.3204	0.3009	0.3102
σ_{1x}	m/s^2	operational	0.0672	0.0423	0.0180	0.0179	0.0182	0.0542	0.0484	0.0396	0.0274	0.0139
σ_{1x}	m/s^2	extreme	0.1234	0.0912	0.0700	0.0975	0.1194	0.1092	0.1009	0.0892	0.0743	0.0592
σ_2	degree	operational	0.0802	0.0888	0.0872	0.0779	0.0704	0.0593	0.0639	0.0712	0.0793	0.0784
σ_2	degree	extreme	0.1246	0.1262	0.1178	0.1092	0.1053	0.1206	0.1220	0.1233	0.1235	0.1191
θ_2	degree	operational	0.0393	0.0498	0.0506	0.0418	0.0364	0.0288	0.0329	0.0381	0.0433	0.0435
θ_2	degree	extreme	0.0555	0.0628	0.0628	0.0561	0.0528	0.0518	0.0547	0.0582	0.0621	0.0628
$T_z(z_1)$	kt	ω=0.4 rad/s	1.9742	1.8038	1.3856	1.4566	2.5365	3.2317	3.0889	2.7501	2.1433	2.3764
θ_{Ts}	degree	extreme	0.8755	0.9139	0.9137	0.7252	0.5351	0.8216	0.8396	0.8567	0.8699	0.7391
θ_{Td}	degree	extreme	1.7606	1.5645	1.6837	2.9933	3.8020	1.6174	1.5629	1.5027	1.4417	1.4185

Table 8.5 list of the characteristics and structural response of sample strucure showing the effect of L_s and $a_4=D_4/L_4$

iterm	unit	condition	a_4	0.5		1.0			1.5		
			L_s/d (%) 10	20	30	10	20	30	10	20	30
						(a)					
V_Σ	kt		10.3977	10.9808	11.7976	10.1862	10.6987	11.3975	10.1032	10.5903	11.2500
$W_{\Sigma s}$	kt		3.6557	3.7258	3.8208	3.5871	3.6432	3.7172	3.5537	3.6039	3.6698
h_{cb}	m		73.3551	69.8777	65.6273	74.1494	70.9641	67.1198	74.3705	71.3016	67.6032
h_{cg}	m		42.8388	40.9782	38.7292	43.0022	41.3062	39.2809	42.9635	41.3409	39.3976
I_s	$kg.m^2$ $x10^{11}$		0.5263	0.5191	0.5125	0.5208	0.5145	0.5086	0.5171	0.5113	0.5058
$I_{\Sigma a}$	$kg.m^2$ $x10^{11}$		0.8181	0.7745	0.7314	0.8243	0.7818	0.7397	0.8251	0.7832	0.7417
$C_{\Sigma d}$	N.m.s $x10^{10}$		0.1427	0.1342	0.1269	0.1407	0.1329	0.1262	0.1388	0.1315	0.1253
K_Σ	N.m $x10^{10}$		0.3113	0.3113	0.3113	0.3112	0.3112	0.3112	0.3112	0.3112	0.3112
ω_n	rad/s		0.1522	0.1551	0.1582	0.1521	0.1550	0.1579	0.1523	0.1551	0.1579
θ_4	degree	extreme	0.4254	0.3779	0.3614	0.4280	0.3806	0.3577	0.4253	0.3801	0.3556
θ_3	degree	extreme	1.9996	2.0010	1.9995	1.9998	2.0012	1.9998	1.9997	2.0011	1.9997
$K_{\Sigma min}$	N.m $x10^{10}$		0.0777	0.0777	0.0777	0.0777	0.0777	0.0777	0.0777	0.0777	0.0777
σ_3	degree	operational	0.3394	0.3412	0.3421	0.3394	0.3411	0.3421	0.3395	0.3412	0.3421
σ_3	degree	extreme	0.5888	0.5929	0.5956	0.5888	0.5927	0.5953	0.5890	0.5928	0.5954
σ_1	degree	operational	0.1661	0.1421	0.1299	0.1771	0.1484	0.1334	0.1823	0.1515	0.1353
σ_1	degree	extreme	2.3630	2.4893	2.6996	2.3799	2.4821	2.6617	2.3984	2.4917	2.6600
σ_{1x}	m/s^2	operational	0.0861	0.0659	0.0574	0.0958	0.0703	0.0596	0.1007	0.0725	0.0607
σ_{1x}	m/s^2	extreme	0.1807	0.1697	0.1690	0.1882	0.1731	0.1697	0.1922	0.1753	0.1707
σ_2	degree	operational	0.2528	0.2501	0.2484	0.2485	0.2452	0.2428	0.2449	0.2413	0.2386
σ_2	degree	extreme	0.3393	0.3359	0.3341	0.3382	0.3343	0.3318	0.3373	0.3332	0.3305
θ_2	degree	operational	0.1498	0.1499	0.1503	0.1458	0.1457	0.1458	0.1432	0.1430	0.1430
θ_2	degree	extreme	0.1808	0.1816	0.1830	0.1783	0.1790	0.1800	0.1768	0.1774	0.1783
$T_z(z_1)$	kt	ω=0.4 rad/s	0.3740	0.3226	0.2842	0.4675	0.4026	0.3528	0.5533	0.4770	0.4180
$\theta_{\Sigma s}$	degree	extreme	3.1486	3.1043	3.0934	3.1412	3.0966	3.0777	3.1325	3.0897	3.0688
$\theta_{\Sigma d}$	degree	extreme	9.8351	10.3235	11.1385	9.8995	10.2948	10.9903	9.9704	10.3313	10.9831
						(b)					
V_Σ	kt		35.2767	35.9935	47.5236	33.0747	36.7243	42.0617	32.3134	35.6515	40.4116
$W_{\Sigma s}$	kt		6.4639	6.8052	7.3213	6.1235	6.3667	6.7064	5.9763	6.1872	6.4751
h_{cb}	m		76.8417	69.5081	61.0251	80.4221	73.8289	66.3859	81.6447	75.3050	68.1939
h_{cg}	m		49.1065	45.0429	40.4359	50.8396	47.1863	43.1237	51.3671	47.8608	43.9829
I_s	$kg.m^2$ $x10^{11}$		2.3464	2.3348	2.3366	2.3270	2.3146	2.3100	2.3143	2.3028	2.2977
$I_{\Sigma a}$	$kg.m^2$ $x10^{11}$		2.8726	2.6508	2.4437	2.9615	2.7403	2.5267	2.9918	2.7728	2.5602
$C_{\Sigma d}$	N.m.s $x10^{10}$		0.2584	0.2312	0.2087	0.2565	0.2311	0.2097	0.2521	0.2284	0.2082
K_Σ	N.m $x10^{10}$		0.9595	0.9596	0.9596	0.9596	0.9596	0.9596	0.9595	0.9596	0.9596
ω_n	rad/s		0.1356	0.1387	0.1417	0.1347	0.1378	0.1409	0.1345	0.1375	0.1405
θ_4	degree	extreme	0.2365	0.2002	0.1882	0.2452	0.1994	0.1829	0.2464	0.1998	0.1802
θ_3	degree	extreme	1.9991	2.0011	2.0011	1.9991	2.0012	2.0011	1.9992	2.0012	2.0012
$K_{\Sigma min}$	N.m $x10^{10}$		-0.3923	-0.3923	-0.3923	-0.3923	-0.3923	-0.3923	-0.3923	-0.3923	-0.3923
σ_3	degree	operational	0.3228	0.3252	0.3268	0.3223	0.3247	0.3263	0.3222	0.3245	0.3262
σ_3	degree	extreme	0.5544	0.5595	0.5633	0.5532	0.5583	0.5622	0.5529	0.5579	0.5619
σ_1	degree	operational	0.1136	0.0901	0.0778	0.1289	0.0981	0.0815	0.1370	0.1026	0.0840
σ_1	degree	extreme	1.4933	1.5548	1.6976	1.4926	1.5168	1.6106	1.5012	1.5115	1.5878
σ_{1x}	m/s^2	operational	0.0577	0.0392	0.0310	0.0702	0.0446	0.0334	0.0775	0.0477	0.0349
σ_{1x}	m/s^2	extreme	0.1260	0.1137	0.1117	0.1354	0.1170	0.1106	0.1410	0.1195	0.1112
σ_2	degree	operational	0.2356	0.2330	0.2322	0.2196	0.2157	0.2128	0.2089	0.2048	0.2015
σ_2	degree	extreme	0.3648	0.3700	0.3780	0.3640	0.3631	0.3660	0.3615	0.3597	0.3611
θ_2	degree	operational	0.1368	0.1374	0.1392	0.1276	0.1275	0.1280	0.1221	0.1218	0.1219
θ_2	degree	extreme	0.1978	0.2019	0.2091	0.1916	0.1944	0.1988	0.1882	0.1915	0.1942
$T_z(z_1)$	kt	ω=0.4 rad/s	2.2744	2.0651	1.9572	2.8036	2.5040	2.3021	3.2913	2.9260	2.6674
$\theta_{\Sigma s}$	degree	extreme	3.0377	3.0078	3.0246	3.0116	2.9770	2.9781	2.9992	2.9658	2.9570
$\theta_{\Sigma d}$	degree	extreme	6.5363	6.7906	7.3125	6.5316	6.6263	6.9789	6.5605	6.6033	6.6803

(Table 8.5 continued)

			(c)							
V_L	kt		34.1566	34.5122	34.9881	34.0814	34.4147	34.8569	34.0495	34.3749	34.8050
W_{Ls}	kt		8.8269	8.8628	8.9099	8.8029	8.8338	8.8739	8.7893	8.8178	8.8547
h_{cb}	m		121.4187	120.3059	118.8544	121.5238	120.4716	119.1111	121.5373	120.5069	119.1820
h_{cg}	m		51.9211	51.5238	51.0078	51.8729	51.4954	51.0098	51.8229	51.4520	50.9783
I_s	kg.m^2 x10^{11}		3.4044	3.3880	3.3721	3.3950	3.3795	3.3646	3.3878	3.3731	3.3590
I_{La}	kg.m^2 x10^{11}		8.3565	8.2361	8.1159	8.3661	8.2468	8.1280	8.3656	8.2473	8.1297
C_{Ld}	N.m.s x10^{10}		0.5302	0.5220	0.5149	0.5285	0.5208	0.5140	0.5269	0.5195	0.5131
K_L	N.m x10^{10}		2.3280	2.3280	2.3280	2.3279	2.3280	2.3280	2.3279	2.3279	2.3280
ω_n	rad/s		0.1407	0.1415	0.1424	0.1407	0.1415	0.1423	0.1407	0.1415	0.1423
θ_4	degree	extreme	0.1881	0.1848	0.1879	0.1892	0.1844	0.1874	0.1894	0.1841	0.1871
θ_3	degree	extreme	0.4998	0.5000	0.4973	0.4998	0.5000	0.4973	0.4998	0.5001	0.4973
K_{Lmin}	N.m x10^{10}		1.9911	1.9911	1.9911	1.9911	1.9911	1.9911	1.9911	1.9911	1.9911
σ_3	degree	operational	0.0851	0.0852	0.0847	0.0851	0.0852	0.0847	0.0851	0.0852	0.0847
σ_3	degree	extreme	0.1466	0.1469	0.1461	0.1466	0.1469	0.1461	0.1466	0.1469	0.1461
σ_1	degree	operational	0.0198	0.0179	0.0171	0.0204	0.0182	0.0173	0.0206	0.0183	0.0173
σ_1	degree	extreme	0.3157	0.3106	0.3099	0.3181	0.3121	0.3107	0.3193	0.3129	0.3113
σ_{1x}	m/s^2	operational	0.0316	0.0281	0.0271	0.0327	0.0285	0.0272	0.0331	0.0287	0.0273
σ_{1x}	m/s^2	extreme	0.0762	0.0720	0.0704	0.0775	0.0726	0.0707	0.0781	0.0730	0.0709
σ_2	degree	operational	0.0925	0.0919	0.0914	0.0923	0.0916	0.0911	0.0920	0.0913	0.0908
σ_2	degree	extreme	0.1251	0.1242	0.1235	0.1252	0.1242	0.1235	0.1252	0.1242	0.1235
θ_2	degree	operational	0.0537	0.0538	0.0538	0.0535	0.0535	0.0535	0.0533	0.0533	0.0533
θ_2	degree	extreme	0.0655	0.0656	0.0657	0.0654	0.0654	0.0655	0.0653	0.0653	0.0654
$T_z(z_1)$	kt	ω=0.4 rad/s	0.2329	0.1593	0.1104	0.2964	0.2025	0.1403	0.3508	0.2398	0.1663
θ_{Ls}	degree	extreme	0.9501	0.9472	0.9510	0.9508	0.9460	0.9494	0.9506	0.9453	0.9487
θ_{Ld}	degree	extreme	1.4795	1.4047	1.4568	1.4878	1.4665	1.4595	1.4919	1.4692	1.4615
			(d)							
V_L	kt		74.8331	82.3786	93.1117	72.3476	78.9644	88.0786	71.3961	77.6939	86.2732
W_{Ls}	kt		11.8221	12.2713	12.8837	11.3348	11.6902	12.1608	11.1035	11.4216	11.8387
h_{cb}	m		147.8332	135.9928	122.6155	151.1393	140.0125	127.5526	152.2793	141.4250	129.3048
h_{cg}	m		58.7208	55.0426	50.9964	58.9654	55.5625	51.8411	58.8788	55.5939	52.0090
I_s	kg.m^2 x10^{11}		9.6680	9.5062	9.3737	9.4963	9.3581	9.2434	9.3902	9.2665	9.1643
I_{La}	kg.m^2 x10^{11}		24.6311	22.6190	20.6320	25.0630	23.0925	21.1429	25.1957	23.2483	21.3210
C_{Ld}	N.m.s x10^{10}		0.8349	0.7484	0.6755	0.8074	0.7307	0.6656	0.7858	0.7154	0.6555
K_L	N.m x10^{10}		6.5396	6.5396	6.5396	6.5395	6.5395	6.5395	6.5394	6.5395	6.5395
ω_n	rad/s		0.1381	0.1427	0.1476	0.1376	0.1420	0.1467	0.1375	0.1418	0.1465
θ_4	degree	extreme	0.0880	0.0834	0.0813	0.0872	0.0806	0.0785	0.0871	0.0791	0.0770
θ_3	degree	extreme	0.5000	0.4994	0.5008	0.5000	0.4994	0.5008	0.5000	0.4994	0.5008
K_{Lmin}	N.m x10^{10}		0.6062	0.6062	0.6062	0.6062	0.6062	0.6062	0.6062	0.6062	0.6062
σ_3	degree	operational	0.0824	0.0828	0.0838	0.0823	0.0827	0.0837	0.0823	0.0827	0.0837
σ_3	degree	extreme	0.1417	0.1429	0.1450	0.1415	0.1426	0.1447	0.1415	0.1426	0.1447
σ_1	degree	operational	0.0185	0.0108	0.0077	0.0221	0.0123	0.0084	0.0241	0.0132	0.0088
σ_1	degree	extreme	0.2940	0.2712	0.2737	0.3110	0.2794	0.2741	0.3200	0.2846	0.2762
σ_{1x}	m/s^2	operational	0.0242	0.0123	0.0086	0.0308	0.0143	0.0093	0.0345	0.0154	0.0097
σ_{1x}	m/s^2	extreme	0.0719	0.0543	0.0476	0.0811	0.0585	0.0494	0.0860	0.0607	0.0504
σ_2	degree	operational	0.0719	0.0683	0.0563	0.0661	0.0628	0.0600	0.0624	0.0594	0.0568
σ_2	degree	extreme	0.1208	0.1162	0.1126	0.1207	0.1156	0.1116	0.1201	0.1148	0.1106
θ_2	degree	operational	0.0382	0.0380	0.0378	0.0353	0.0350	0.0347	0.0336	0.0333	0.0330
θ_2	degree	extreme	0.0582	0.0587	0.0594	0.0565	0.0568	0.0573	0.0554	0.0556	0.0560
$T_z(z_1)$	kt	ω=0.4 rad/s	3.4238	2.4005	1.7308	4.4171	3.0816	2.2019	5.2640	3.6670	2.6128
θ_{Ls}	degree	extreme	0.8208	0.8182	0.8197	0.8132	0.8078	0.8077	0.8087	0.8015	0.8010
θ_{Ld}	degree	extreme	1.3920	1.3113	1.3183	1.4495	1.3372	1.3177	1.4797	1.3536	1.3234

Table 8.6 list of the structural characteristics and motion response showing the effect of variation of the buoyancy chamber size

item	unit	condition	θ_{mwo}= 1.0	1.5	(a) 2.0	3.0	4.0	1.0	1.5	(b) 2.0	3.0	4.0
V_t	kt		15.3519	11.9846	10.3416	8.7277	7.9324	51.6894	39.8489	34.1573	28.6361	25.9469
W_{ts}	kt		4.0993	3.7775	3.6043	3.4171	3.3148	7.2817	6.5677	6.1967	5.8128	5.6146
h_{cb}	m		75.6739	74.3518	73.1473	71.2362	69.8310	77.5063	78.0796	78.3086	78.4200	.4200
h_{cg}	m		34.3249	39.0478	42.4650	47.0079	49.8448	39.6456	45.3405	49.6643	55.6455	59.5395
I_s	$kg.m^2$ $x10^{11}$		0.5698	0.5366	0.5187	0.4989	0.4877	2.4642	2.3679	2.3223	2.2777	2.2555
I_{ta}	$kg.m^2$ $x10^{11}$		1.2721	0.9653	0.8101	0.6523	0.5718	4.2769	3.3494	2.8872	2.4252	2.1941
C_{td}	N.m.s $x10^{10}$		0.1636	0.1473	0.1380	0.1272	0.1208	0.2905	0.2628	0.2476	0.2311	0.2222
K_t	N.m $x10^{10}$		0.6226	0.4150	0.3112	0.2075	0.1556	1.9192	1.2794	0.9596	0.6397	0.4797
ω_n	rad/s		0.1838	0.1662	0.1530	0.1342	0.1212	0.1687	0.1496	0.1357	0.1166	0.1038
θ_4	degree	extreme	0.2374	0.3255	0.4099	0.5717	0.7278	0.1282	0.1777	0.2259	0.3205	0.4139
θ_3	degree	extreme	1.0002	1.5005	2.0007	3.0013	4.0022	1.0004	1.5006	2.0009	3.0016	4.0023
K_{tmin}	N.m $x10^{10}$		0.0777	0.0777	0.0777	0.0777	0.0777	-0.3923	-0.3923	-0.3923	-0.3923	-0.3923
σ_3	degree	operational	0.1758	0.2593	0.3401	0.4951	0.6427	0.1694	0.2480	0.3234	0.4658	0.5996
σ_3	degree	extreme	0.3104	0.4534	0.5903	0.8496	1.0937	0.2966	0.4296	0.5554	0.7904	1.0089
σ_1	degree	operational	0.2369	0.1920	0.1654	0.1353	0.1186	0.1676	0.1348	0.1164	0.0967	0.0864
σ_1	degree	extreme	6.2882	3.3922	2.4057	1.6649	1.3587	3.9603	2.0315	1.4934	1.0689	0.8886
σ_{1x}	m/s^2	operational	0.1103	0.0946	0.0846	0.0724	0.0652	0.0777	0.0660	0.0589	0.0510	0.0466
σ_{1x}	m/s^2	extreme	0.3271	0.2251	0.1813	0.1404	0.1205	0.2262	0.1566	0.1274	0.1002	0.0873
σ_2	degree	operational	0.1966	0.2240	0.2473	0.2887	0.3266	0.1567	0.1896	0.2182	0.2690	0.3150
σ_2	degree	extreme	0.2787	0.3079	0.3367	0.3931	0.4479	0.2903	0.3273	0.3634	0.4333	0.5003
θ_2	degree	operational	0.1006	0.1238	0.1457	0.1875	0.2277	0.0829	0.1057	0.1275	0.1703	0.2124
θ_2	degree	extreme	0.1337	0.1563	0.1785	0.2222	0.2653	0.1394	0.1659	0.1924	0.2456	0.2988
$T_z(z_1)$	kt	ω=0.4 rad/s	1.1054	0.6664	0.4441	0.2173	0.1007	4.7202	3.3650	2.6931	2.0235	1.6891
θ_{ts}	degree	extreme	1.7722	2.4507	3.1239	4.4605	7.7890	1.6858	2.3413	2.9955	4.3042	5.6091
θ_{td}	degree	extreme	25.2080	13.7448	9.9994	7.6401	7.2032	15.9279	8.4083	6.5370	5.5929	5.7376

item	unit	condition	θ_{mwo}= 0.1	0.2	(c) 0.3	0.4	0.5	0.2	0.3	(d) 0.5	0.75	1.2
V_t	kt		101.0288	58.4170	44.7217	37.9915	33.9877	144.1574	102.6359	70.5238	54.9263	43.4799
W_{ts}	kt		12.7927	10.5274	9.6413	9.1389	8.7941	14.7337	12.8753	11.2345	10.3254	9.5743
h_{cb}	m		154.3732	144.0324	135.1839	127.9055	121.8242	160.4104	158.6145	154.5928	150.1361	144.1022
h_{cg}	m		36.8816	42.4380	46.7149	49.8007	51.9813	44.7607	50.3252	60.0357	69.1999	80.2028
I_s	$kg.m^2$ $x10^{11}$		5.4735	4.3025	3.8522	3.5894	3.4002	11.4104	10.3843	9.5459	9.0980	8.7286
I_{ta}	$kg.m^2$ $x10^{11}$		37.1273	19.3720	13.3530	10.2880	8.4059	55.3731	38.9322	25.7231	19.0669	14.0237
C_{td}	N.m.s $x10^{10}$		0.9770	0.7439	0.6418	0.5786	0.5314	1.1692	0.9978	0.8356	0.7393	0.6544
K_t	N.m $x10^{10}$		11.6403	5.8200	3.8800	2.9099	2.3279	16.3491	10.8993	6.5396	4.3596	2.7247
ω_n	rad/s		0.1653	0.1568	0.1502	0.1448	0.1404	0.1565	0.1487	0.1362	0.1244	0.1094
θ_4	degreen	extreme	0.0628	0.1028	0.1375	0.1678	0.1938	0.0508	0.0676	0.0988	0.1355	0.1970
θ_3	degree	extreme	0.1000	0.1999	0.2999	0.3999	0.4998	0.2001	0.3001	0.5002	0.7503	1.2005
K_{tmin}	N.m $x10^{10}$		1.9911	1.9911	1.9911	1.9911	1.9911	0.6062	0.6062	0.6062	0.6062	0.6062
σ_3	degree	operational	0.0176	0.0348	0.0518	0.0685	0.0850	0.0339	0.0503	0.0821	0.1204	0.1856
σ_3	degree	extreme	0.0308	0.0606	0.0898	0.1183	0.1465	0.0589	0.0871	0.1411	0.2052	0.3134
σ_1	degree	operational	0.0448	0.0386	0.0322	0.0265	0.0217	0.0371	0.0340	0.0284	0.0234	0.0179
σ_1	degree	extreme	0.8990	0.5774	0.4554	0.3773	0.3216	0.5739	0.4548	0.3293	0.2502	0.1810
σ_{1x}	m/s^2	operational	0.0641	0.0589	0.0510	0.0432	0.0358	0.0532	0.0506	0.0444	0.0380	0.0302
σ_{1x}	m/s^2	extreme	0.1732	0.1390	0.1148	0.0958	0.0805	0.1385	0.1203	0.0955	0.0766	0.0577
σ_2	degree	operational	0.0541	0.0709	0.0812	0.0880	0.0926	0.0463	0.0547	0.0673	0.0792	0.0960
σ_2	degree	extreme	0.1114	0.1164	0.1197	0.1227	0.1256	0.1103	0.1151	0.1227	0.1316	0.148 0
θ_2	degree	operational	0.0245	0.0341	0.0417	0.0480	0.0535	0.0219	0.0268	0.0354	0.0450	0.0607
θ_2	degree	extreme	0.0437	0.0502	0.0577	0.0607	0.0654	0.0441	0.0484	0.0564	0.0657	0.0820
$T_z(z_1)$	kt	ω=0.4 rad/s	7.9130	3.3416	1.7270	0.8779	0.3373	12.4504	8.3670	5.0007	3.2598	1.9086
θ_{ts}	degree	extreme	0.3376	0.5036	0.6810	0.8106	0.9554	0.4272	0.5612	0.8244	1.1483	1.7250
θ_{td}	degree	extreme	3.6279	2.3685	1.9174	1.6560	1.5002	2.3495	1.9086	1.5147	1.3973	1.5640

Table 8.7 list of the structural characteristics and motion response of the sample structures showing the mass distribution along the structure by varying the column thicknesses

iterm	unit	condition	$\bar{t}$ (m) $\bar{t}_i$=0.05	$\bar{t}_i$=0.10 i=3,4,5	$\bar{t}_i$=0.20	$\bar{t}_5$=.05	$\bar{t}_5$=.20	$\bar{t}_4$=0.05	$\bar{t}_4$=0.20	$\bar{t}_3$=.05	$\bar{t}_3$=.20
						(a)					
V_Σ	kt		9.2350	10.3416	13.0787	9.7186	11.5922	10.0235	11.1442	10.1051	10.7747
$W_{\Sigma s}$	kt		2.0152	3.6043	7.2455	3.1498	4.5040	3.2945	4.3882	2.7191	5.3459
h_{cb}	m		65.2072	73.1473	85.4758	70.8550	76.8673	71.6895	76.4196	69.3377	80.0708
h_{cg}	m		30.8465	42.4650	61.2188	38.2078	49.4973	40.0321	47.9492	37.9397	50.6235
I_s	kg.m^2 x10^{11}		0.3309	0.5187	0.9554	0.4193	0.7157	0.4723	0.6344	0.4680	0.6130
$I_{\ell a}$	kg.m^2 x10^{11}		0.6213	0.8101	1.2428	0.7289	0.9698	0.7645	0.9241	0.7403	0.9422
$C_{\ell d}$	N.m.s x10^{10}		0.1247	0.1380	0.1622	0.1326	0.1476	0.1350	0.1449	0.1333	0.1460
K_ℓ	N.m x10^{10}		0.3112	0.3112	0.3112	0.3112	0.3112	0.3112	0.3112	0.3112	0.3113
ω_n	rad/s		0.1808	0.1530	0.1190	0.1646	0.1359	0.1586	0.1413	0.1605	0.1415
θ_4	degree	extreme	0.3752	0.4099	0.4700	0.3959	0.4345	0.4022	0.4277	0.3981	0.4300
θ_3	degree	extreme	2.0007	2.0007	2.0006	2.0007	2.0008	2.0007	2.0006	2.0009	2.0005
$K_{\ell min}$	N.m x10^{10}		0.1937	0.0777	-0.1656	0.1322	-0.0316	0.0847	0.0638	0.1327	-0.0365
σ_3	degree	operational	0.3508	0.3401	0.3196	0.3451	0.3311	0.3426	0.3342	0.3435	0.3342
σ_3	degree	extreme	0.6182	0.5903	0.5432	0.6030	0.5687	0.5966	0.5759	0.5987	0.5761
σ_1	degree	operational	0.2208	0.1654	0.1211	0.1903	0.1359	0.1750	0.1477	0.1740	0.1538
σ_1	degree	extreme	4.9185	2.4057	1.2984	3.2461	1.6541	2.7428	1.8856	2.8162	1.9539
σ_{1x}	m/s^2	operational	0.1100	0.0846	0.0620	0.0965	0.0698	0.0892	0.0758	0.0886	0.0789
σ_{1x}	m/s^2	extreme	0.2895	0.1813	0.1180	0.2218	0.1392	0.1974	0.1541	0.1988	0.1600
σ_2	degree	operational	0.2187	0.2473	0.3033	0.2362	0.2682	0.2407	0.2633	0.2365	0.2665
σ_2	degree	extreme	0.2836	0.3367	0.4516	0.3147	0.3792	0.3240	0.3680	0.3169	0.3734
θ_2	degree	operational	0.1218	0.1457	0.1951	0.1355	0.1651	0.1401	0.1595	0.1374	0.1610
θ_2	degree	extreme	0.1437	0.1785	0.2579	0.1632	0.2083	0.1700	0.1996	0.1660	0.2020
$T_z(z_1)$	kt	ω=0.4 rad/s	0.1782	0.4441	1.0482	0.3291	0.6694	0.3798	0.6043	0.3474	0.6262
$\theta_{\Sigma s}$	degree	extreme	2.9500	3.1239	3.5016	3.0487	3.2677	3.0822	3.2261	3.0621	3.3280
$\theta_{\Sigma d}$	degree	extreme	19.8612	10.0000	5.9125	13.2664	7.1591	11.3023	8.0225	11.5861	8.2840
						(b)					
V_Σ	kt		31.9873	34.1573	39.0635	33.1574	36.1704	33.1496	36.4388	33.9445	34.5662
$W_{\Sigma s}$	kt		3.6668	6.1967	11.7417	5.5656	7.4573	5.2480	8.3525	5.2074	8.1707
h_{cb}	m		75.5582	78.3086	83.0447	77.7009	79.3948	77.3407	80.2701	77.2371	80.3991
h_{cg}	m		44.9709	49.6643	57.9987	48.1927	52.3440	47.8256	53.4197	48.4126	52.0942
I_s	kg.m^2 x10^{11}		2.0103	2.3223	3.0051	2.1805	2.6056	2.1927	2.6129	2.2766	2.4114
$I_{\ell a}$	kg.m^2 x10^{11}		2.5926	2.8872	3.5293	2.7777	3.1053	2.7618	3.1684	2.8231	3.0130
$C_{\ell d}$	N.m.s x10^{10}		0.2371	0.2476	0.2687	0.2438	0.2550	0.2432	0.2571	0.2453	0.2519
K_ℓ	N.m x10^{10}		0.9596	0.9596	0.9596	0.9596	0.9596	0.9596	0.9595	0.9596	0.9595
ω_n	rad/s		0.1444	0.1357	0.1212	0.1391	0.1296	0.1392	0.1288	0.1372	0.1330
θ_4	degree	extreme	0.2185	0.2259	0.2403	0.2232	0.2311	0.2228	0.2325	0.2244	0.2288
θ_3	degree	extreme	2.0009	2.0009	2.0009	2.0009	2.0009	2.0009	2.0009	2.0009	2.0009
$K_{\ell min}$	N.m x10^{10}		-0.2248	-0.3923	-0.7495	-0.3120	-0.5539	-0.3782	-0.4204	-0.3182	-0.5495
σ_3	degree	operational	0.3281	0.3234	0.3139	0.3253	0.3196	0.3253	0.3191	0.3242	0.3218
σ_3	degree	extreme	0.5666	0.5554	0.5342	0.5599	0.5469	0.5600	0.5458	0.5573	0.5517
σ_1	degree	operational	0.1258	0.1164	0.1027	0.1210	0.1087	0.1199	0.1099	0.1171	0.1151
σ_1	degree	extreme	1.7518	1.4934	1.1926	1.5973	1.3333	1.5846	1.3389	1.5227	1.4423
σ_{1x}	m/s^2	operational	0.0638	0.0589	0.0517	0.0613	0.0550	0.0607	0.0555	0.0593	0.0582
σ_{1x}	m/s^2	extreme	0.1421	0.1274	0.1081	0.1339	0.1170	0.1327	0.1179	0.1289	0.1248
σ_2	degree	operational	0.2096	0.2182	0.2354	0.2152	0.2241	0.2145	0.2262	0.2164	0.2218
σ_2	degree	extreme	0.3367	0.3634	0.4202	0.3536	0.3828	0.3520	0.3889	0.3577	0.3745
θ_2	degree	operational	0.1194	0.1275	0.1444	0.1254	0.1336	0.1241	0.1351	0.1259	0.1307
θ_2	degree	extreme	0.1753	0.1924	0.2296	0.1859	0.2054	0.1851	0.2089	0.1889	0.1993
$T_z(z_1)$	kt	ω=0.4 rad/s	2.2798	2.6931	3.5950	2.5375	3.0031	2.5164	3.0895	2.6058	2.8643
$\theta_{\Sigma s}$	degree	extreme	2.9197	2.9955	3.1587	2.9668	3.0526	2.9632	3.0681	2.980	3.0260
$\theta_{\Sigma d}$	degree	extreme	7.4867	2.6708	5.4907	6.9165	5.9747	6.8684	5.9890	6.6419	6.3559

(Table 8.7 continued)

			(c)							
V_Σ	kt		33.8481	33.9877	38.0078	33.3330	35.2912	33.7004	34.7316	33.4755	35.4206
$W_{\Sigma s}$	kt		5.0791	8.7941	17.1580	8.2269	9.9142	8.5101	9.5326	5.6683	14.7996
h_{cb}	m		110.7034	121.8242	148.3821	119.1477	126.7881	120.5626	124.9912	111.7614	140.3808
h_{cg}	m		33.9453	51.9813	85.9297	47.9333	59.5260	50.1270	56.6454	39.3033	73.3663
I_s	$kg.m^2 \times 10^{11}$		1.9306	3.4002	6.9192	2.9013	4.3863	3.1891	3.9453	2.4681	5.0369
$I_{\Sigma a}$	$kg.m^2 \times 10^{11}$		7.2799	8.4059	12.4844	7.9484	9.3054	8.1957	8.9483	7.2787	10.7077
C_{td}	$N.m.s \times 10^{10}$		0.4941	0.5314	0.6253	0.5178	0.5553	0.5253	0.5461	0.4941	0.5882
K_Σ	$N.m \times 10^{10}$		2.5479	2.3279	2.3279	2.3279	2.3279	2.3278	2.3279	2.3787	2.3279
ω_n	rad/s		0.1663	0.1404	0.1095	0.1465	0.1304	0.1430	0.1344	0.1562	0.1216
θ_4	degree	extreme	0.1647	0.1938	0.2237	0.1890	0.2021	0.1917	0.1990	0.1764	0.2125
θ_3	degree	extreme	0.4567	0.4998	0.4999	0.4998	0.4998	0.4999	0.4998	0.4892	0.4999
$K_{\Sigma min}$	$N.m \times 10^{10}$		2.5479	1.9911	0.8621	2.1298	1.7136	2.0223	1.9287	2.3787	1.2053
σ_3	degree	operational	0.0805	0.0850	0.0795	0.0859	0.0835	0.0854	0.0841	0.0852	0.0820
σ_3	degree	extreme	0.1408	0.1465	0.1343	0.1485	0.1429	0.1473	0.1444	0.1481	0.1395
σ_1	degree	operational	0.0265	0.0217	0.0190	0.0225	0.0202	0.0220	0.0209	0.0226	0.0210
σ_1	degree	extreme	0.6849	0.3216	0.1957	0.3706	0.2610	0.3402	0.2841	0.4603	0.2403
σ_{1x}	m/s^2	operational	0.0421	0.0358	0.0317	0.0371	0.0337	0.0363	0.0348	0.0365	0.0349
σ_{1x}	m/s^2	extreme	0.1224	0.0805	0.0606	0.0876	0.0708	0.0832	0.0749	0.0961	0.0698
σ_2	degree	operational	0.0841	0.0926	0.1039	0.0911	0.0952	0.0919	0.0943	0.0863	0.1002
σ_2	degree	extreme	0.1101	0.1256	0.1556	0.1221	0.1323	0.1240	0.1298	0.1142	0.1436
θ_2	degree	operational	0.0450	0.0535	0.0664	0.0518	0.0567	0.0527	0.0554	0.0481	0.0610
θ_2	degree	extreme	0.0543	0.0654	0.0871	0.0628	0.0703	0.0642	0.0684	0.0580	0.0776
$T_z(z_1)$	kt	ω=0.4 rad/s	0.0072	0.3373	1.4868	0.2012	0.5983	0.2752	0.4955	0.0076	0.9944
$\theta_{\Sigma s}$	degree	extreme	0.8386	0.9554	1.0721	0.9402	0.9833	0.9485	0.9726	0.8976	1.0229
$\theta_{\Sigma d}$	degree	extreme	2.8314	1.5002	1.1352	1.6700	1.3026	1.5639	1.9874	1.2511	
			(d)							
V_Σ	kt		67.9318	70.5238	76.3339	69.8420	71.8895	69.1085	73.6526	69.9688	71.5992
$W_{\Sigma s}$	kt		6.6946	11.2345	20.9171	10.6944	12.3142	9.8639	14.2690	8.5504	16.5863
h_{cb}	m		147.9054	154.5928	167.1892	153.7711	156.1835	152.5254	158.8601	150.8924	161.7756
h_{cg}	m		49.7406	60.0357	79.8301	58.2908	63.4223	56.0319	68.3202	55.5849	68.6398
I_s	$kg.m^2 \times 10^{11}$		7.4939	9.5459	14.0295	9.0676	10.5022	8.5925	11.6443	8.8893	10.8329
$I_{\Sigma a}$	$kg.m^2 \times 10^{11}$		23.4701	25.7231	30.5912	25.3041	26.5600	24.7869	27.7843	24.7909	27.5594
C_{td}	$N.m.s \times 10^{10}$		0.8043	0.8356	0.8992	0.8299	0.8469	0.8228	0.8631	0.8228	0.8602
K_Σ	$N.m \times 10^{10}$		6.5395	6.5396	6.5396	6.5396	6.5395	6.5395	6.5395	6.5395	6.5395
ω_n	rad/s		0.1453	0.1362	0.1211	0.1379	0.1328	0.1400	0.1288	0.1393	0.1305
θ_4	degree	extreme	0.0962	0.0988	0.1041	0.0983	0.0998	0.0979	0.1011	0.0978	0.1008
θ_3	degree	extreme	0.5002	0.5002	0.5002	0.5002	0.5002	0.5002	0.5002	0.5002	0.5002
$K_{\Sigma min}$	$N.m \times 10^{10}$		1.1708	0.6062	-0.5437	0.7477	0.3229	0.6376	0.5434	0.9987	-0.1928
σ_3	degree	operational	0.0834	0.0821	0.0796	0.0824	0.0816	0.0827	0.0810	0.0826	0.0813
σ_3	degree	extreme	0.1441	0.1411	0.1355	0.1417	0.1399	0.1424	0.1385	0.1422	0.1391
σ_1	degree	operational	0.0318	0.0284	0.0237	0.0292	0.0271	0.0299	0.0258	0.0293	0.0278
σ_1	degree	extreme	0.4032	0.3293	0.2467	0.3430	0.3055	0.3584	0.2823	0.3495	0.2981
σ_{1x}	m/s^2	operational	0.0495	0.0444	0.0371	0.0455	0.0424	0.0466	0.0404	0.0457	0.0421
σ_{1x}	m/s^2	extreme	0.1104	0.0955	0.0766	0.0985	0.0902	0.1017	0.0849	0.0995	0.0891
σ_2	degree	operational	0.0669	0.0673	0.0685	0.0673	0.0674	0.0672	0.0677	0.0670	0.0679
σ_2	degree	extreme	0.1178	0.1227	0.1336	0.1219	0.1244	0.1207	0.1272	0.1205	0.1271
θ_2	degree	operational	0.0338	0.0354	0.0388	0.0351	0.0360	0.0347	0.0369	0.0348	0.0367
θ_2	degree	extreme	0.0524	0.0564	0.0649	0.0556	0.0579	0.0547	0.0601	0.0548	0.0595
$T_z(z_1)$	kt	ω=0.4 rad/s	4.4166	5.0007	6.2508	4.8923	5.2169	4.7584	5.5321	4.7597	5.4737
$\theta_{\Sigma s}$	degree	extreme	0.8058	0.8244	0.8637	0.8207	0.8314	0.8165	0.8415	0.8170	0.8388
$\theta_{\Sigma d}$	degree	extreme	1.7763	1.5147	1.2462	1.5625	1.4332	1.6164	1.3568	1.5844	1.4106

Table 8.8 Source of hazards

Accident loads	Structural failure	System failures
Collisions	Design faults	Ballast system
Groundings	Fabrication faults	etc
Helicopter crash	etc	
Dropped objects		
Explosions		
Fires		
etc		

Abnormal environment	Hydrocarbon release
Heavy weather	Gas blow-out
Waves (e.g. lack of air gap)	Oil Blow-out
Wind	etc
Icing	
etc	
Earthquake	
Soil	
Tsunamis	
etc	

Table 8.9 list of the structural characteristics and motion response showing the effect of deck payload relocation $z_q = z_5 - 15.0$m

iterm	unit	condition W_q = 5000t / W_q^o = 0.0	4000t / 1000t	3000t / 2000t	5000t / 0.0	4000t / 1000t	3000t / 2000t
			d=100m			d=150m	
V_Σ	kt	37.4671	33.5903	29.8416	34.1573	31.9032	29.6715
$W_{\Sigma s}$	kt	5.5336	5.2969	5.0590	6.1967	6.0524	5.9046
h_{cb}	m	48.7286	48.7398	48.6486	78.3086	77.2013	75.8733
h_{cg}	m	35.2415	33.6956	31.7143	49.6643	46.5327	42.8979
I_s	$kg.m^2 \times 10^{11}$	1.2450	1.0419	0.8394	2.3223	1.9705	1.6181
$I_{\ell a}$	$kg.m^2 \times 10^{11}$	1.1570	1.0456	0.9343	2.8872	2.6528	2.4169
K_ℓ	N.m x10	0.4956	0.4956	0.4956	0.9596	0.9596	0.9596
ω_e^n	rad/s	0.1436	0.1541	0.1672	0.1357	0.1441	0.1542
θ_4	degree extreme	0.2667	0.2579	0.2487	0.2259	0.2200	0.2136
θ_4^3	degree extreme	3.0008	3.0008	3.0007	2.0009	2.0008	2.0009
$K_{\ell min}$	$N.m \times 10^{10}$	-0.4768	-0.3464	-0.2190	-0.3923	-0.2226	-0.0539
σ_3	degree operational	0.4864	0.4939	0.5018	0.3234	0.3280	0.3329
σ_3	degree extreme	0.8394	0.8577	0.8780	0.5554	0.5662	0.5781
σ_1	degree operational	0.3241	0.3682	0.4360	0.1164	0.1300	0.1492
σ_1	degree extreme	5.1164	6.5950	10.9002	1.4934	1.7988	2.3355
σ_{1x}	m/s^2 operational	0.0860	0.0977	0.1152	0.0589	0.0658	0.0753
σ_{1x}	m/s^2 extreme	0.2177	0.2589	0.3390	0.1274	0.1464	0.1757
σ_2	degree operational	0.3876	0.3697	0.3511	0.2182	0.2121	0.2058
σ_2	degree extreme	0.6978	0.6409	0.5836	0.3634	0.3429	0.3222
θ_2	degree operational	0.2271	0.2111	0.1947	0.1275	0.1208	0.1138
θ_2	degree extreme	0.3724	0.3368	0.3013	0.1924	0.1783	0.1641
$T_z(z_1)$	kt ω=0.4 rad/s	3.3350	2.8557	2.3820	2.6931	2.3588	2.0226
θ_z	degree extreme	4.7563	4.6051	4.4539	2.9955	2.9332	2.8700
$\theta_{\Sigma s}$	degree extreme	20.9262	26.7254	43.8035	6.5370	7.6669	9.7098
$\theta_{\Sigma d}$							

CHAPTER 9

THE DESIGN OF SINGLE ARTICULATED TOWERS - HYBRID FORM

1. INTRODUCTION

This Chapter deals with the design issues of hybrid single articulated towers (HATs) and compares their design with the design of single articulated towers of a monolithic structural form MAT).

From the investigations into the design aspects of MATs in Chapter 8, the problems with their application can be identified as follows:-

a. Low natural frequencies of FMV motion, significant consumption of structural material weight and large magnitude internal sectional forces, especially on the articulated joint, associated with the use of large diameter lower column in deep waters.

b. Bad static stability or large magnitude dynamic motion response in shallow waters.

c. Significant heaving force on the articulated joint.

HATs eliminate some of the above problems by using lattice structures to replace the large diameter single columns of MATs as lattice structures normally are expected to have greater structural strength and are stiffer and lighter. Structurally, risers can still be accommodated within the frame columns of the lattices.

The disadvantages foreseen, accompanied with the use of trussed structures, are that additional torsional loading will be induced on the articulated joint and that the possibility of dry access to the buoyancy chamber and/or the lower part of the structure for maintenance and inspection purposes is eliminated. On the other hand, a HAT may be much more difficult to install as the lattice often does not have enough buoyancy to support its weight. Built-in buoyancy may have to be incorporated into the main frames of the lattice to avoid such difficulties. Furthermore, the weld joints where the high stress concentration occurs, could give rise to fracture problems due to fatigue as the structural response is dynamic in the case of articulated tower structures. The trussed structure has proved to be reliable in conventional fixed jacket platforms where the structural response is largely of a static nature to the dynamic excitation. Nevertheless, the structural strength of a lattice has to be checked, in design practice, according to relevant codes [79], against the possible structural failures such as excessive yielding, buckling and brittle fracture etc of the structural members. In the present study, the structural strength calculation of the HATs is omitted since it is assumed to follow the normal principles of jacket structures. It is shown below, that the sectional forces on the lattice are smaller in magnitude compared with the sectional forces on the conventional fixed jacket structures.

In the event of a hybrid structure, the heaving force will become more pronounced on the structure than that on a monolithic structure as the exposed area on the hybrid structure, mainly on the top and on the bottom of the buoyancy chamber, is enlarged. It was realised that this could be a serious problem and consideration was given as to how it might be overcome by a redesign of the buoyancy

chamber.

The Use of a frustrum buoyancy chamber is shown in Section 9 to be very effective in reducing the heaving force, even with a small taper angle. This is due to the effect of the decay of the wave kinematics below the surface. The surge force on it and the centre of buoyancy/gravity remain very much unaffected. Since the fabrication of such a large volume frustrum chamber engenders little extra difficulty, it is clearly preferable.

2. MODELLING OF THE LATTICE STRUCTURE

The modelling of a MAT needs to be modified where appropriate for the HATs. Therefore, the modelling of a lattice is dealt with first. The lattice of a HAT replacing the upper/lower column of a MAT is referred to as the upper/lower lattice, respectively. The co-ordinates system is set up such that the origin is at seabed, the x axis coincides with the direction of wave propagation; the z axis coincides with the vertical axis of the structure and points positive upwards and the y axis is determined by the right-hand principle., as shown in fig. 9.1. A lattice structure is detailed in Table 9.1. Based on one bay of a lattice, modelling of the lattice is carried out as listed in Table 9.2.

In calculating the structural mass of a lattice, β_m ($\beta_m > 1$), defined as the ratio between the total mass of the lattice and that of its bracings is defined in Table 9.2a. It indicates the importance of the structural mass of the bracings in comparison with the structural mass of the main frames for a given lattice.

The contribution of the bracings is neglected in calculating the second moment of inertia of the solid cross sectional area of the lattice about axis y' through the geometrical centre of the cross section. The mass moment of inertia of a lattice is approximated by considering its total mass evenly distributed on the centre line along its length although it can be calculated exactly without much difficulty.

Using the wave loading program developed by Incecik [80] based on Morison's equation given in equation (2.14) or its linearised form, the wave loading on each member of a lattice is calculated. Summarising the wave loading on the individual members of the lattice yields the total wave loading. In addition, this computer program has been modified to calculate the wind and current loading, first and second moment of inertia of added hydrodynamic mass and linearised viscous damping. The wave loading due to wave drift forces has been neglected as it is difficult to estimate for a lattice structure.

There is no doubt that the bracings of a lattice are of importance functionally as they maintain the integrity, rigidity and structural strength of the lattice. It is, however, easily understood that if the contribution of the bracings to the structural weight, buoyancy, mass moment of inertia and external loading of the lattice were small compared with the contribution of the main frames the bracings could be neglected in the dynamic/static response analysis of HATs, which would make the analysis much simpler without much sacrifice to the accuracy. Preliminary investigation was conducted under the following conditions that $r_i = r_j$ and $t_{ri} = t_{rj}$, $i,j \geq 7$, ie the radius and the shell thickness of all the bracing cylinders are the same. The conclusion drawn is that the contributions increase with

r_7/r_6 and t_{r7}/t_{r6} ratios as expected and are very important, even when these two ratios are fairly low. Therefore, the presence of the bracings on the lattice structures is accounted for in the following, with $r_i = r_j$ and $t_{ri} = t_{rj}$, $i,j \geq 7$ specified.

3. THE WATER DEPTH CAPACITY OF HATs

Based on the finite element procedure described in Chapter 4, the natural frequencies of FMV motion of HATs were calculated by computer program MONO.FLEXURE. It was modified so that when the elemental matrices are formed in the program for the elements making up the lattice, the formulation of the structural mass, added hydrodynamic mass, buoyancy and sectional bending stiffness of the lattice in Section 2 are used instead of those of the single column which is replaced by the lattice. There are three types of hybrid articulated towers, as shown in fig. 1.2.

3.1. Water Depth Capacity of Type I HATs

From Chapter 4, the water depth capacity of a MAT primarily depends on the overall stiffness of the lower column. Use of an upper lattice to replace the upper column of the MAT is not expected to affect the water depth capacity of the structure substantially. Although the lattice is lighter, the weight saving is not very significant in deep waters for the type I HATs as the length of the upler lattice is limited. Therefore, for a MAT and type I HAT having the same payload and total structural weight, the water depth capacity of the HAT will not be considerably greater.

3.2. Water Depth Capacity of Type II and III HATs

Since the upper lattice does not greatly affect the water depth capacity, type II and III HATs are expected to have roughly the same water depth capacity. The parameters influencing the water depth capacity of type II and III HATs may include the number of main frames, n_f, the radius and shell thickness of the main frames, r_6 and t_{r6}, the radii and shell thicknesses of the bracing cylinders, r_7 and t_{r7} and the circumferential radius on which the main frames are located, r_5. Results of a parametrical study show that ω_1 depends mainly on r_5. Other parameters have a significant effect on ω_1 only in shallow waters.

In addition, ω_1, obtained when $n_f = 4$ is only marginally greater than ω_1, when $n_f = 3$. Therefore, there is no real advantage of using 4 leg lattices over 3 leg lattices as far as the FMV motion is concerned. Instead, the reduction of the structural weight achieved using a 4 leg lattice is less significant than that when using a 3 leg lattice.

If the maximum dimension of the cross section of the lower lattice is taken to be the dimensions of the cross section of the buoyancy chamber, then the water depth capacity of HATs is around 450m, as is seen in Table 9.3 where the condition $D_4 \geqq r_5 + r_6$ is observed. The total structure weight is 4500 tonnes. However, if the dimension of the cross section of the lower lattice is allowed to increase beyond the cross sectional dimension of the buoyancy chamber, the water depth capacity may well be increased.

There are two options for the buoyancy chamber to be

connected with the lattice structure. The first one is to keep the buoyancy chamber integrated and locate it on the lattice which is rather like the arrangement of the buoyancy chamber on a guyed tower. The second option is to have a buoyancy chamber associated with each main frame of the lattice, ie the built-in chambers on the main frames are used as the buoyancy chamber. A sketch of the scheme is shown in fig. 9.2.

By allowing the radius of the cross section of the lower lattice to vary between r_5 = 20m and r_5 = 45m and keeping ω_1 around 1.0 rad/s, the water depth capacity can vary from 550m up to 750m for both type II and III HATs (Table 9.4) which is about twice as great as the water depth capacity of MATs as shown in Chapter 4. The water depth capacity is limited purely by the natural frequencies of the FMV motion. Up to 750m, the structural weight is not critical as it is in the case of MATs.

When d varies from 550m up to 750m, the total structural weight of the type II and III HATs varies from 5000 to 6200 tonnes and from 4200 tonnes to 5200 tonnes, respectively. Compared with the structural weight of MATs in water depths of 300m to 350m, the weight saving may amount up to 8000 tonnes. Similar percentage savings in buoyancy are achieved. Also, the structural weight and total buoyancy of type II and III HATs are very insensitive to the variation of water depth and increases very slowly as the water depth increases.

The natural frequency of the second FMV motion tends to become critical in water depths above 550m. It varies from ω_2 = 2.2 rad/s to 3.5 rad/s.

The dimensions of the lower lattice are small compared with conventional fixed jacket platforms. This is due to the fact that the sectional forces along the length of both types of HATs are very small compared with those along fixed jacket platforms. In the present case the external wave loading is only partially transferred into the structure, whereas it is transferred completely into a conventional fixed jacket platform.

In spite of the reduced structural weight of the type II and III HATs, there may be difficulties associated with their float-out and installation in very deep waters. Considerations have to be given to the design of the lattice sections of these two types of hybrid articulated tower structures.

3.3. Avoiding Local Resonant Vibration due to Vortex Shedding

Apart from avoiding overall flexural vibration of a hybrid articulated tower, it is necessary to avoid failure of individual members on a lattice structure due to vortex induced local resonant vibration. This is done by separating the vortex shedding frequency and the natural frequency of the flexural mode vibration of individual members. The vortex shedding frequency is given by the Strouhal number, defined in equation (2.19).

Using finite element analysis, the natural frequency of the first flexural mode vibration of a uniform beam cylinder of 30m long, 0.25m in diameter and 0.025m in wall thickness, with the added hydrodynamic mass coefficient $C_m = 1.0$ and with two ends of the beam clamped, is $\omega_1 = 305$ rad/s. This is typical of the extremely slender and soft bracings in lattice structures used in hybrid articulated

towers. A frequency of 305 rad/s is far away from any vortex shedding frequency.

4. CRITERIA OF COMPARISON

If the type I, II or III HATs are compared with their equivalent MATs, it is essential to arrive at an equivalent datum on which the comparative studies can be carried out.

4.1. Conditions of Equivalence

The conditions of equivalence between a lattice and a single column can be defined in two different ways: to achieve the same cross sectional structural strength under generalised loading, or the same vibration rigidity. As the columns of the MATs and the lattice of the HATs are under general loading, interacting with the geometrical dimensions of the structures. The structural strength requirements for the columns as well as for the lattice are very complex and cannot be defined in a simple mathematical form. If the assumption is made that the sectional bending strength is of the major concern, the structural strength requirements may well be simplified merely to achieve the same $(\bar{RI}_x)$ ratio.

On the other hand, if the same structural rigidity conditions are simplified to the same sectional bending stiffness conditions for the column and the lattice, the equivalent radius of the single column to a given lattice and the structural weight ratio between the equivalent single column and the lattice are calculated in Table 9.5.

It is noticed that the above two equivalence conditions are

grossly simplified. This is due to the omission of the actual bending moment in condition I and, what is more, due to the assumption of predominant bending strength requirements and the use of the same sectional bending stiffness in condition II. More rational equivalence conditions could be used.

Condition I is more likely to apply to the upper column than to the lower column, especially in deep waters and condition II, to the lower column. The radius of the equivalent single column obtained under condition I is normally smaller than the radius of the equivalent single column under condition II. Therefore, condition II may be applied to both lower and upper columns.

Comparative studies could also be carried out under other equivalent conditions such as to achieve the same static heel due to current and mean wind for the HAT and equivalent MAT.

In carrying out the comparative studies, certain typical structures are chosen. The relevant data of the sample structures are listed in Table 9.6.

4.2 Ground of Comparative Studies

Under conditions I or II, comparative studies of HATs against the equivalent MATs can be performed in the following aspects:

a. distribution of the external loadings with that of the wave loading and inertia loading, in particular,

b. characteristics of the structures,

c. static and dynamic response, and

d. distribution of the internal sectional forces.

The formulation of the structural response of HATs to the environmental excitations can be carried out in the same way as that of MATs, the formulae for the response analysis of MATs being modified where appropriate.

The computer program for the analysis of HATs so obtained, is also directly applicable to MATs. This is done by setting $r_j = 0$, $j = 5,...10$ and $r_{11} = R_i = \frac{D_i}{2}$ and $t_{r11} = \bar{t}_i$ with D_i defined for a MAT as in fig. 1.1.

5. DISTRIBUTION OF THE EXTERNAL LOADINGS

Use of a lattice to replace an equivalent single column of large diameter reduces the wave loading attraction. Therefore, the total loading is reduced on HATs compared with their equivalent MATs. Again, the significance of the reduction is frequency dependent.

The wave loading reduction using the upper lattice is important especially at relatively high wave frequencies, while the wave loading reduction using a lower lattice is only important at low frequencies, the significance increasing with water depth. More reduction is achieved by combining the upper and lower lattices. Therefore, the wave loading on the equivalent MAT is, as expected, the greatest and the wave loading on the type III HAT is the smallest at all frequencies (fig. 9.5). As for the type I and II HATs, the relative magnitude of the wave loading depends on wave frequency. In the low frequency range, say $\omega < 0.6$ rad/s, the wave loading on the

type I HAT is greater. This is because in this low frequency range, the wave penetration is deep.

Above ω = 1.0 rad/s, the wave loading on the type I and III HATs decreases much more rapidly due to the use of the upper lattice.

The total inertia loading is greater than the wave loading above the resonance frequency, especially for the type I HAT and the equivalent MAT. The inertia loading of the equivalent MAT is also the greatest. When compared with the type II and III HATs, the increase of the wave loading and the inertia loading on the MAT may be as much as 30% and 40%, respectively, at certain frequencies within $\omega \in$ (0.2,1.0) rad/s.

For the type II and III HATs, the inertia loading of the buoyancy chamber composes the predominant part of the total inertia loading. For the type I HAT and the equivalent MATs, the inertia loading of the buoyancy chamber and that of the lower column are the two major components.

The inertia loading on the part of the structure above SECTION 3, is much more important for the type II and III HATs than for the type I HAT and the equivalent MAT.

6. CHARACTERISTICS OF THE SAMPLE STRUCTURES

Certain characteristics of the sample structures in Table 9.6 are also listed in Table 9.7, which gives the mass moment of inertia, damping and the restoring stiffness.

The use of a lattice also reduces the mass moment of inertia, particularly that of the added hydrodynamic mass, restoring stiffness and natural frequency. This is because the use of lattices results in a much greater reduction of buoyancy than the reduction of structural weight. Such changes in the upper lattice are significant only in shallow waters. The effects of the lower lattice, on the other hand, are significant at all water depths, especially in deep waters. The variation (increase or decrease) rates of these characteristics with water depth are reduced by the use of lattices, or in other words, the use of lattices makes these characteristics less sensitive to water depth variation.

The viscous damping of the type I HAT and the equivalent MAT is greater than the viscous damping of the type II HATs but their damping ratios are smaller because of their much greater mass moment of inertia.

7. STATIC RESPONSE OF THE MODEL STRUCTURES

The static tilt angle of the four structures due to mean wind loading and steady current loading is also listed in Table 9.7. It is calculated according to the design environmental conditions.

a. The tilt angles of the type I HAT and the equivalent MAT are very similar and much less than the tilt angles of the type II and III HATs, which are nearly equal.

b. The total tilt angles of all the four structures decreases with water depth although those of the type II and III HATs decreases much more slowly than those of the other two structures.

c. The static tilt angles of the type I HAT and the equivalent MAT due to current loading decrease with water depth while those of the type II and III HATs somehow increase with water depth slightly. This is because the increase of the current loading on the type II and III HATs may exceed the increase of their restoring stiffness with water depth.

d. The type II and III HATs have much greater static tilt angle under the mean wind loading and steady current loading than the type I HAT and the equivalent MAT. Consequently, if the static angles are to be kept the same for all the four structures, the size of the buoyancy chamber of the type II and III HATs has to be increased.

8. DYNAMIC RESPONSE OF THE MODEL STRUCTURES

The dynamic response due to harmonic waves and fluctuating wind is calculated. The calculated dynamic response due to harmonic waves includes angular response, horizontal deck acceleration and the internal sectional forces. The rms angular response and deck acceleration due to random waves are also calculated corresponding to the extreme condition and the operational condition. Only the angular dynamic response due to fluctuating wind is calculated and is represented in the form of rms.

The response pattern of the HATs is similar to that of the equivalent MAT, ie it is single-peaked at the resonant frequency and decreases monotonically above the resonant frequency (fig. 9.6). Apart from the difference in resonant frequencies, the resonant response of

these structures is very different because of the viscous damping effect. Above the resonance, the responses of the type I HAT and the equivalent MAT are largely the same but have a greater dynamic response in the low frequency region than the responses of the type II and III HATs ($0.2 < \omega$ with ω_r = 0.5, 0.4 and 0.3 rad/s when d = 150m, 300m and 450m, respectively, in figs 9.5 and 9.6. In particular, the types I and II HATs have the greatest and smallest response, respectively, in this region so that they also give the greatest and smallest rms angular displacement when T_z is large. In a high frequency region ($\omega > \omega_r$), however, it is the type II HAT and the MAT having large diameter upper columns that have the greater dynamic response. The above response pattern can be more clearly seen in fig. 9.7.

The internal sectional shear force and bending moment on different sections along the model structures are plotted finally in figs. 9.7 to 9.9 in the form of RAO.

Water depth, deck payload and wave frequency are the main factors influencing the effect of using lattices on the distribution of the internal sectional forces. At low wave frequencies in general, use of lattices, especially the lower lattice, reduces the internal sectional shear force and bending moment along the bottom part of the structure. The effect is particularly significant on the shear force on the articulated joint. The sectional forces along the top part of the structure are increased instead. In mild wave conditions, on the other hand, the opposite may happen.

Under the extreme waves, the dynamic responses of the type II and III HATs will be much less than the responses of the type I HAT as

well as the equivalent MAT. Under operational waves, their responses are generally worse.

From the structural strength point of view, the sectional forces in different wave frequency ranges affects the structural strength in different ways. The strength of the type II and III HATs against the immediate structural failure due to overloading will be improved at all the sections of practical concern, especially at SECTIONS 1 and 2, the ends of the lower lattice. The structural strength of the articulated joint will be greatly improved, especially in deep water which will certainly contribute to the deep water applications of the type II and III HATs. Deep water applications of those two structures will also be favoured by the fact that the fatigue strength of the lower lattice may also be greatly improved in comparison with the lower columns of the type I HAT and the MAT.

The random angular response of the sample hybrid structures to the random wind is more pronounced than the response of the monolithic structure to the random wind. Again, the type II HAT has the greatest response and the type I HAT has the lowest. The difference is about 30%, 100% and 170% in a water depth of of 150m, 300m and 450m, respectively, decreasing as the size of the buoyancy chamber increases. In addition, the response of the type III HAT is only marginally less than the response of the type II HAT and the response of the MAT is also only marginally less than the response of the type I HAT. This is because the restoring stiffnesses of the type II and III HATs are not very different from each other and increase far more gradually with water depth than the restoring stiffnesses of the other two structures.

The response of the structure to wind gust spectra is equally important as is the response to random waves. As far as the water depth is concerned, the response of all the four structures to random waves and to random wind decreases with water depth. However, the variation of the size of the buoyancy chamber has an entirely different effect on the response to random waves and on the response to random wind. This is because the response to random wind is more restoring stiffness dependent and is of an almost quasi-static nature, while the response to random waves is very much natural frequency dependent, or in other words, it is of a largely dynamic nature.

9. REDUCTION OF THE HEAVING FORCE

The possible reduction of the heaving force on the buoyancy chamber by modifying the shape of the chamber from a cylinder to a frustrum was discussed earlier in Chapter 3. The importance of the reduction is demonstrated here under the conditions that they have the same volume and height. A sketch is shown in fig. 3.2 where C_p is the height of the centre of the buoyancy of the frustrum buoyancy chamber from the bottom of the chamber. In calculating the heaving force the following simplifications are made, ie the existence of the related structures on top and at the bottom of the buoyancy chamber is neglected so that the chamber is regarded as a closed body in isolation. In addition, the drag force is neglected.

In the case of the buoyancy chamber being connected with the upper and lower lattice, the first simplification should be practically viable as the existence of the lattice structures is expected to have little effect on the heaving force exerted on the buoyancy chamber. The second simplification should be reasonably

accurate apart from very low frequencies. Since the wave frequencies of significance are within $\omega \in (0.3,0.8)$ rad/s, the present results in this frequency range should be indicative of the trends to be expected.

Typical results are obtained as shown in fig. 9.10. They are the wave frequency dependent heaving forces on the frustrum buoyancy chamber and on the cylinder buoyancy of the same volume and height, respectively. Figure 9.10b shows the ratio between the heaving forces on the frustrum chamber and that on the cylindrical chamber. In particular, the resultant heaving force is given, deduced similarly to equation (2.12), as:-

$$F_{1v}(z,t) = \{\frac{\pi D_4^2}{4}\left[P_w(z) - P_w(z_5)\right] + \frac{\pi D_4^3}{8}\left[p_v(z_5) + p_v(z_4)\right]\}\cos\omega t$$

for the cylindrical buoyancy chambers, and

$$F_{iv}(z,t) = \left[\frac{\Pi}{4}\left(D_{41}^2 P_w(z_4) - D_{40}^2 P_w(z_5)\right) + \frac{\Pi}{8}\left(D_{41}^3 p_v(z_4) + D_{40}^2 p_v(z_5)\right)\right.$$

$$\left. + \left(P_s(z_5) - P_s(z_4)\right) + \left(P_t(z_5) - P_t(z_4)\right)\right]\cos\omega t$$

for the heaving force on the frustrum buoyancy chamber, respectively.

$P_w(z)$ and $P_v(z)$ are defined in equations (2.7) and (2.13), respectively. $P_s(z)$ and $P_t(z)$ are currently given as:-

$$P_s(z) = \frac{\pi\rho_w g\, H\tan\beta_1}{k\cosh kd}\left\{\left[\frac{D_{40}}{2} + (d - z - L_2)\tan\beta_1\right]\sinh kz - \frac{\tan\beta_1}{k}\cosh kz\right\}$$

$$P_t(z) = \frac{\rho_w g C_{mv} H \tan\beta_1}{8k^2 \cosh kd} \left[k^2 D_{41}^2 \sinh kz - 4kD_{41}(kz\sinh kz - \cosh kz)\tan\beta_1 \right.$$

$$\left. + 4[(2 + k^2z^2)\sinh kz - 2kz\cosh kz]\tan^2\beta_1 \right]$$

In long waves the pressure decreases with the distance below the water surface very slowly. The resultant heaving force is small and is negative. But for the frustrum chamber, the resultant heaving force can not only be positive but also be significant even with a small taper angle due to the large difference between the cross sectional areas of the bottom and top surfaces. Increase of the taper angle β_1 (fig. 3.2), increases the severity of the heaving force on a frustrum buoyancy chamber at very low frequencies.

If the taper angle is appropriately chosen, the reduction of the heaving force, using a frustrum buoyancy chamber, can be achieved at all the frequencies of practical concern which can be taken as 0.35 rad/s upwards. This is seen from fig. 9.10b. In fact, it can be chosen so that the zero crossing point is about 0.35 rad/s (T = 18s), leading to a significant reduction between 30% and 100%.

In addition, it is found that the zero heaving force wave frequency mainly depends on β_1. In achieving the balance between avoiding the large amplitude low frequency heaving force on the frustrum buoyancy chamber and obtaining the maximum reduction of heaving force, the taper angle β_1 is seen to be between 3^0 and 9^0 practically, according to fig. 9.10b, in the leading wave frequency range $\omega \in$ (0.3, 0.7) rad/s.

10. DECK PAYLOAD CAPACITY OF THE HYBRID STRUCTURES

The above discussion is centred on the comparisons between the hybrid structures and the monolithic structure in water depths not less than 150m. As for the comparison of the deck payload capacity, it should be carried out in deep waters as well as in shallow waters. The deck payload mainly affects static stability, motion response and structural strength.

Hybrid structures, especially the type II and III ones are likely to have greater deck payload capacity apart from greater water depth capacity above water depth of 150m. This is primarily due to the fact that they have much greater structural strength and yet their material consumption is considerably lower. Increase of water depth results in more efficient allocation of buoyancy as far as the type II and III hybrid structures are concerned. But in shallower waters, their deck payload is not expected to differ very much from monolithic structures as their static and dynamic responses are not very different.

In deeper waters, only the applications of hybrid structures is likely to be feasible. As the deck payload variation has little effect on the rigidity of hybrid structures, in terms of the natural frequencies of the flexural mode vibration motion, it is likely that the deck payload capacity of the hybrid structures in such water depths will be governed by the shear force on the articulated joint and/or the motion response. Any problems associated with the malfunction or failure of the articulated joint in deep waters will be potentially serious. Therefore, the design of the articulated joint in deep waters in the case of large deck payloads may involve particular

difficulties with regard to the considerations of long term inspection and maintenance although the shear force on the joint may not increase with water depth. In addition, the limitations on the maximum horizontal deviation of the structures at the deck level may also impose restrictions on the deep water applications of hybrid structures with large deck payloads. This is because the horizontal movement of the structures at the deck level does not necessarily always decrease with the increase of water depth, although the angular displacement decreases, in general.

11. CONCLUDING REMARKS

Single articulated tower structures can be of three different structural forms, using lattice structures to replace the large diameter single columns of articulated tower structures of monolithic form. They can be used to avoid some of the shortcomings of single monolithic articulated tower structures, associated with its functional and economical performance.

In particular, single hybrid articulated tower structures have been studied on comparative grounds against an equivalent monolithic articulated tower. Brief conclusions are drawn below.

1. The immediate advantage of hybrid structures over monolithic structures is that they are light and stiff.

The water depth capacity depends mainly on the rigidity of the lower column/lattice. The water depth capacity of the type I hybrid articulated towers is not markedly different from that of the single monolithic articulated towers. Type II and III hybrid

articulated tower structures have roughly the same water depth capacity. The rigidity of the lower lattice depends mainly on the main frame spacing of the lattice parameter r_5. Assuming that the minimum natural frequency is no less than 1.0 rad/s, the water depth capacity of the type II and III hybrid structures is around 400m to 450m if the cross sectional dimensions of the lower lattice is not to be greater than the cross dimension of the buoyancy chamber. In such water depths r_5 is of the order of 15m. If the cross sectional dimensions of the lower lattice is to increase further to 30m to 50m, the water depth capacity can be increased up to 550m to 750m.

The structural weight of the type II hybrid structures increases with water depth very slowly. Even in a water depth of 750m, the total structural weight is of the order of 5500 to 7000 tonnes, showing significant weight saving as well as buoyancy saving.

2. Use of lattice structures also affects the external loading on hybrid structures, structural motion, and distribution of the of the internal sectional forces along hybrid structures.

The weight and buoyancy saving achieved using hybrid structures, reduce the shear force on the articulated joint of hybrid structures as well as the internal sectional forces along the bottom part of the structure. This may improve their deep water application performance in the long term. But the sectional forces on the top half of the structure may be greatly increased.

Such savings also tend to penalise their angular motion responses in most cases except in extreme waves. Therefore, they show little advantage over monolithic structures in very shallow waters

from a motion point of view although significant material weight can be saved. In addition, the static tilt of the type II and III hybrid structures can be significant even in deep waters.

3. It is desirable for all the types of articulated tower structures to use a frustrum buoyancy chamber when the deck payload is large. This is mainly aimed at reducing the time varying large amplitude heaving force exerted mostly on the top and bottom surfaces of the chamber, due to its shallow submergence. It is demonstrated that this is very effective, even with a small taper angle of 3^{o} to 5^{o}.

The taper angle of the frustrum can be adjusted most favourably so that the heaving force in the wave frequency range of specific concern can be minimised.

LIST OF FIGURES

LIST OF TABLES

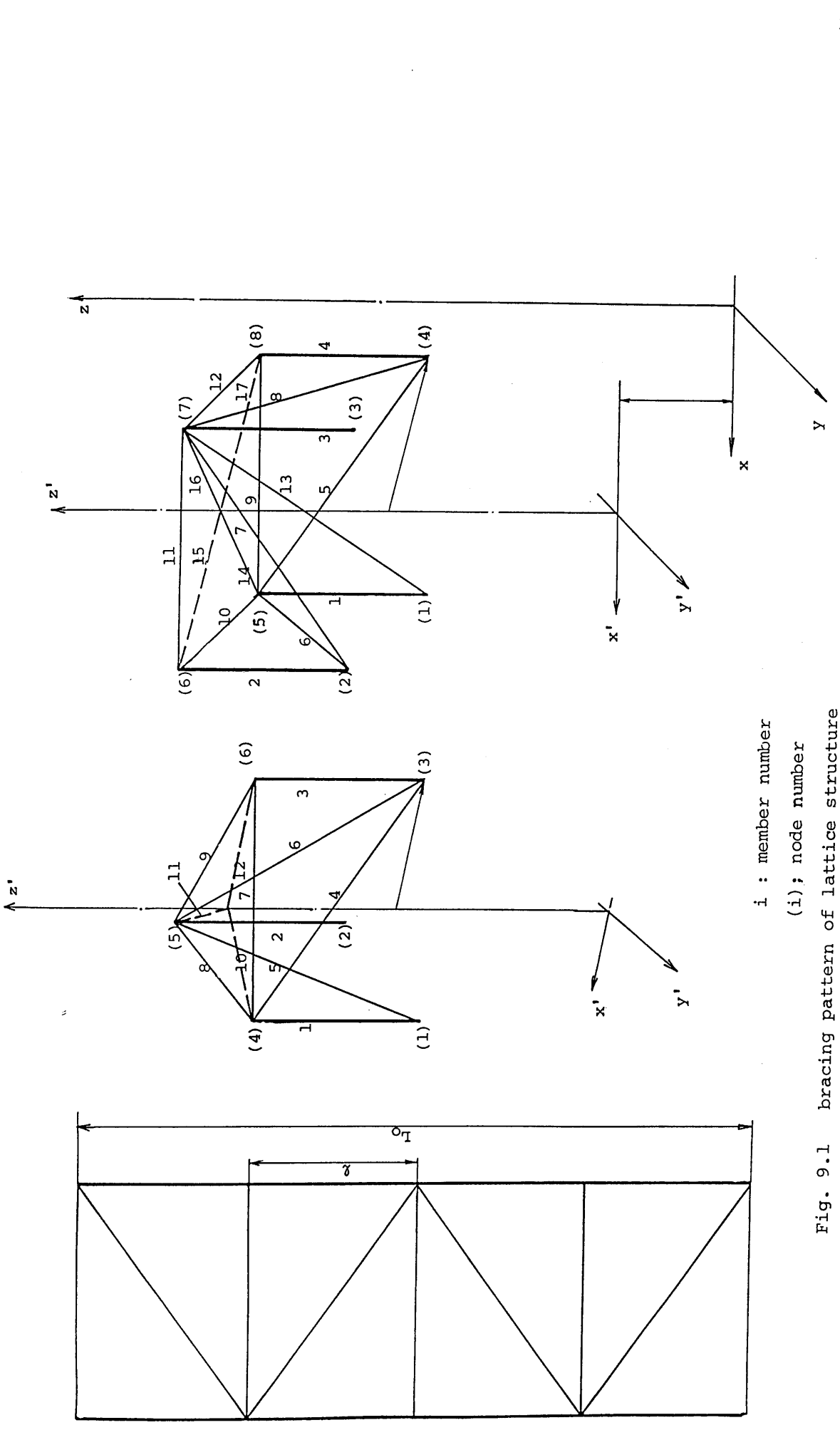

i : member number

(i) ; node number

Fig. 9.1 bracing pattern of lattice structure

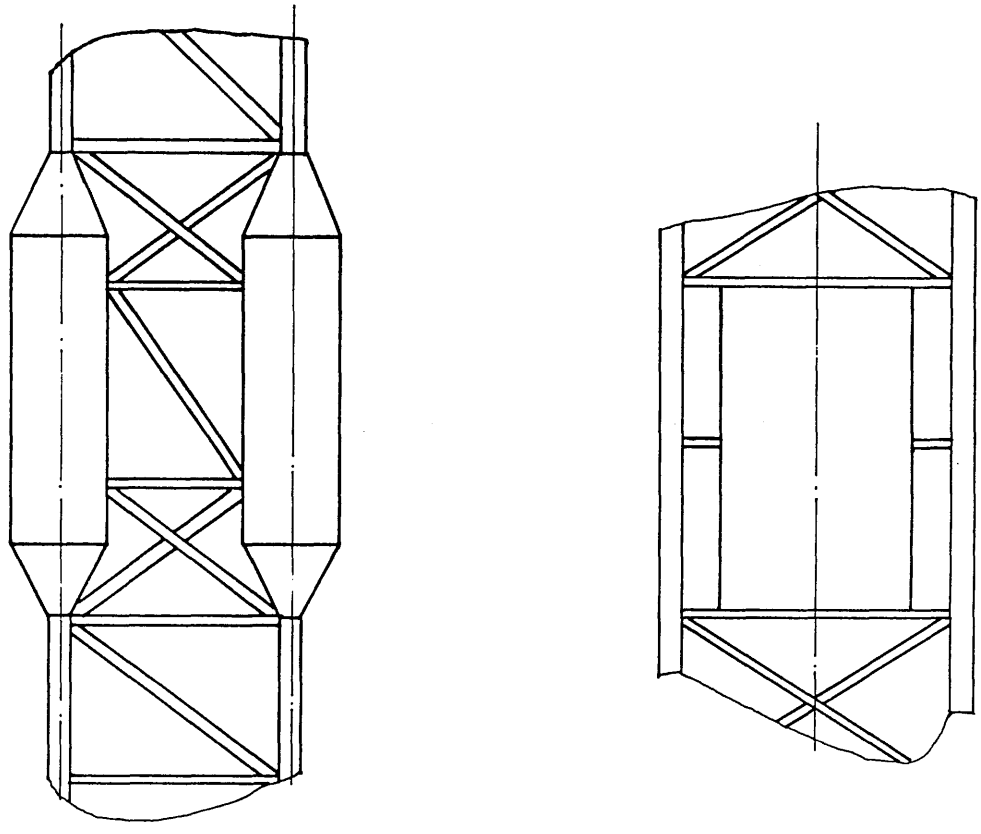

Fig. 9.2 mounting of the buoyancy chamber on the lattice structure

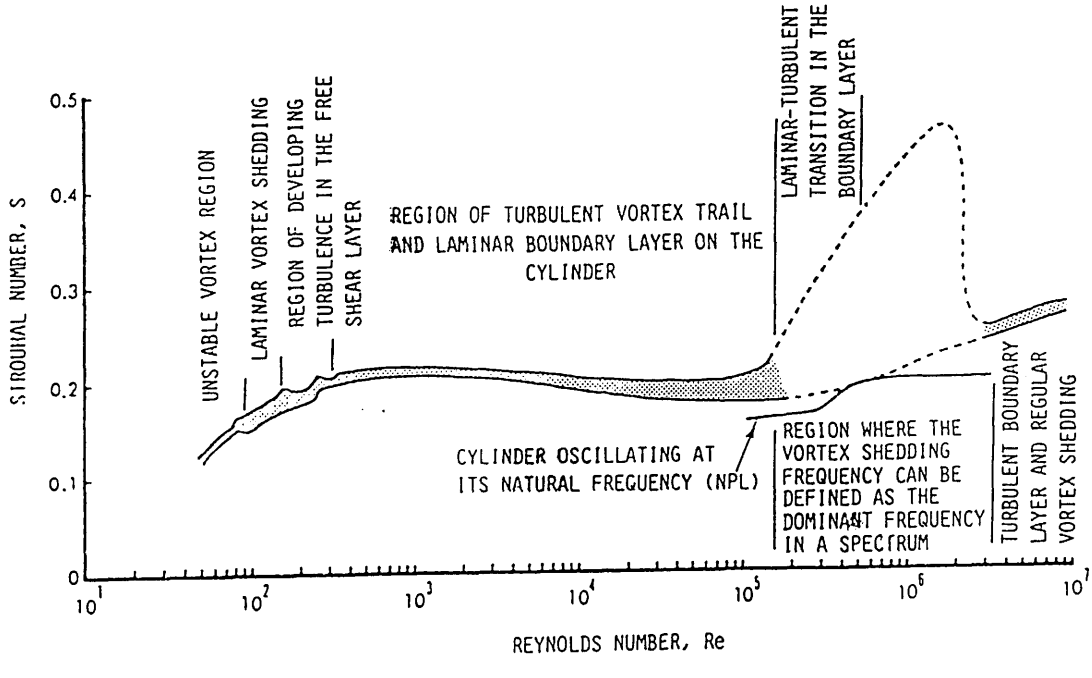

Fig. 9.3 Strouhal-Reynolds number relationship for circular cylinders (from ref. 81)

x : ω rad/s ; y ; MP/H t.m/m

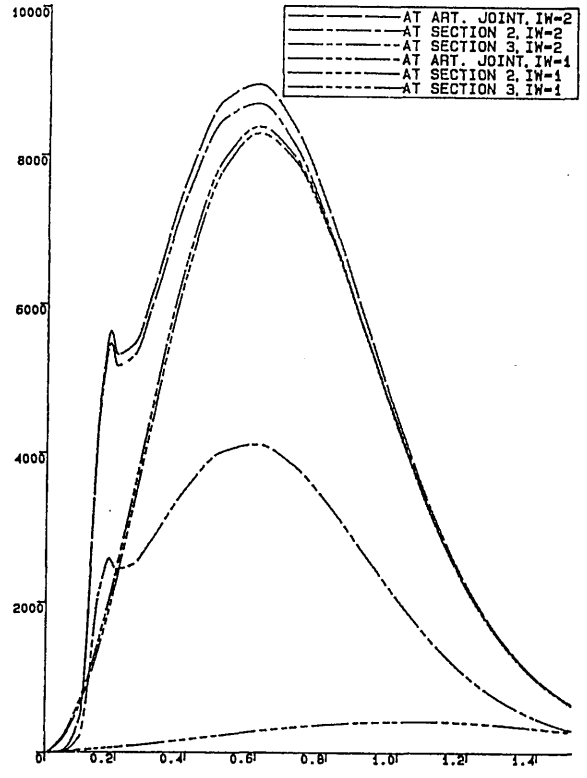

type III HAT

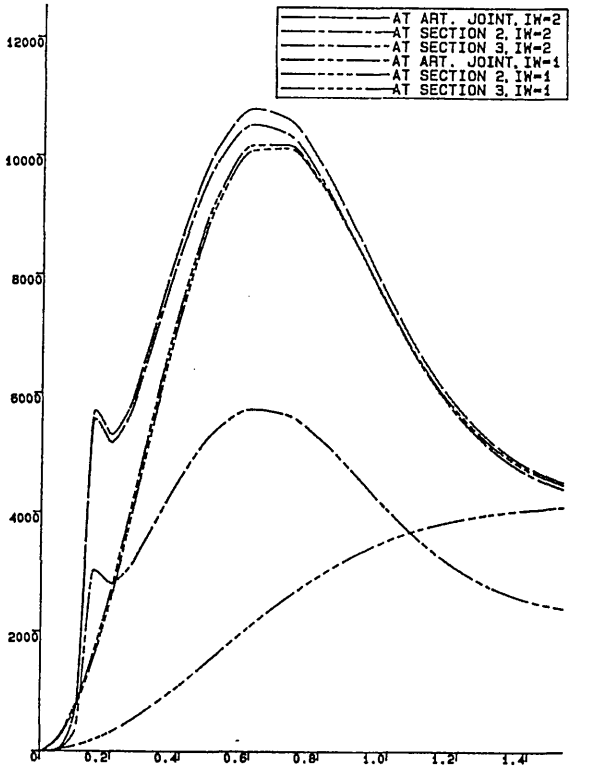

type II HAT

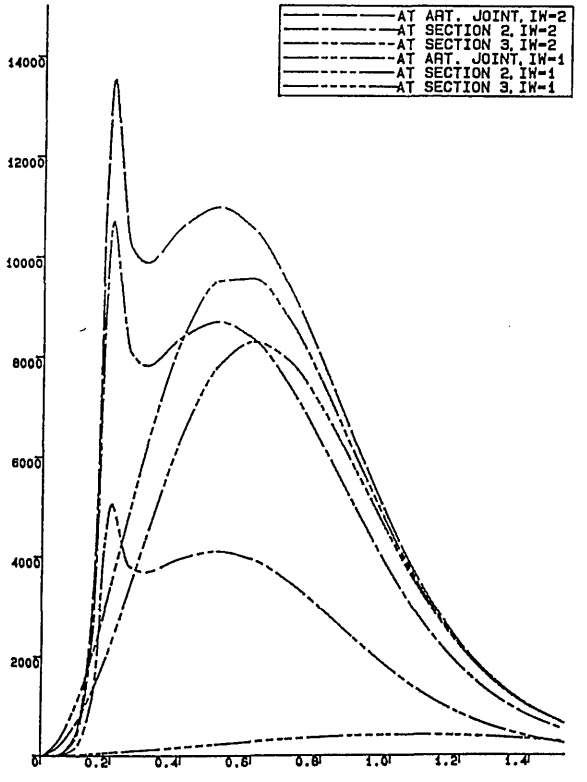

type I HAT

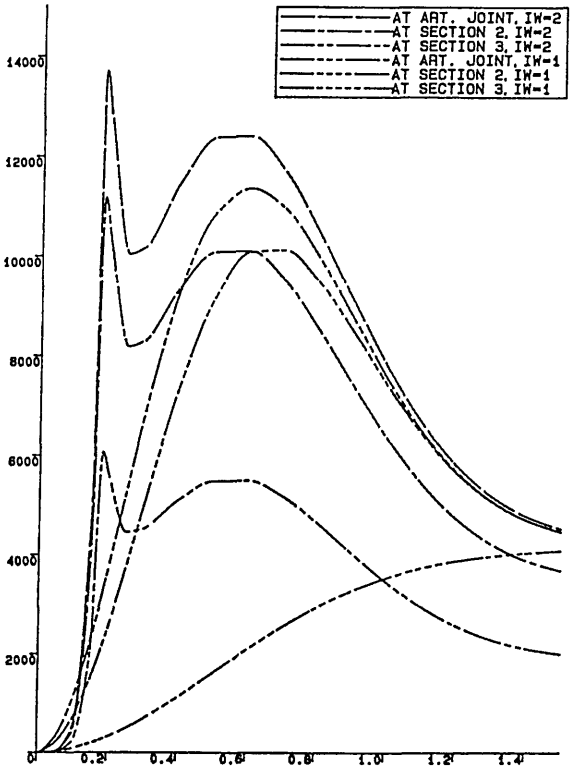

equiv. MAT

(a) d=150m

Fig. 9.4 distribution of the pitch moment of wave and mass inertia forces (MP represents the pitch moments)

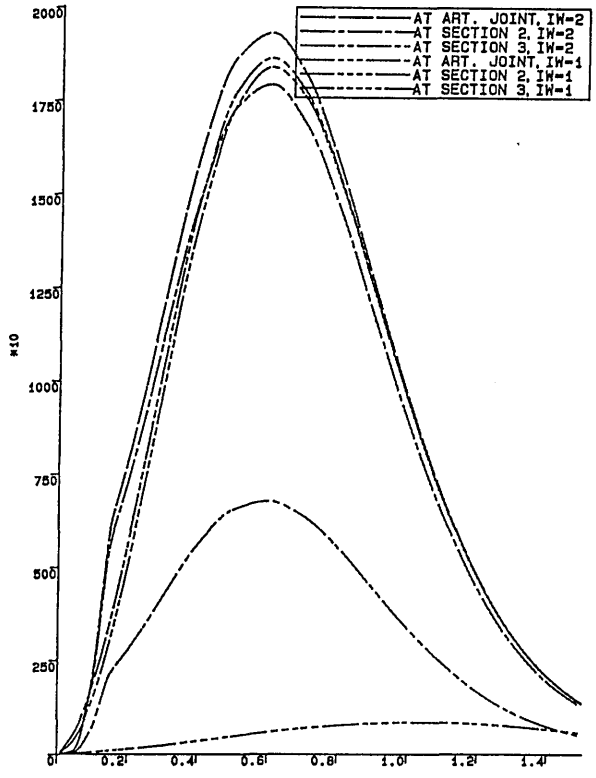

type III HAT

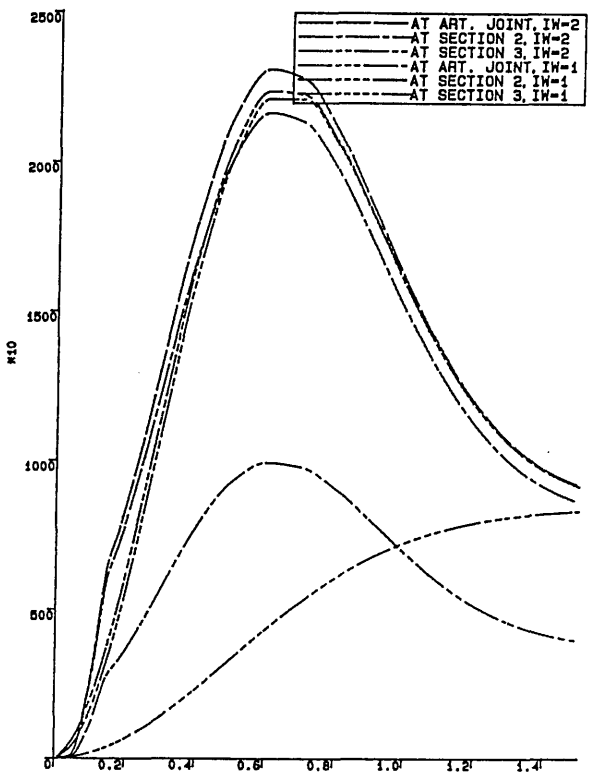

type II HAT

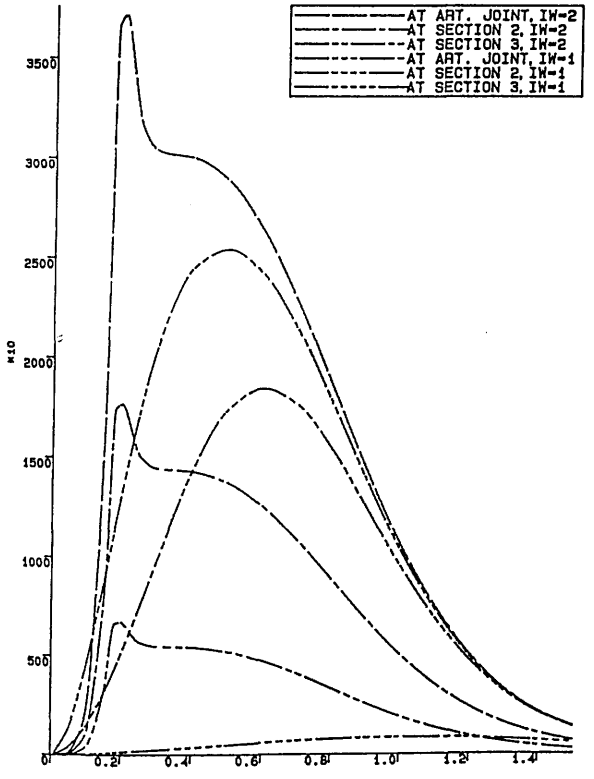

type I HAT

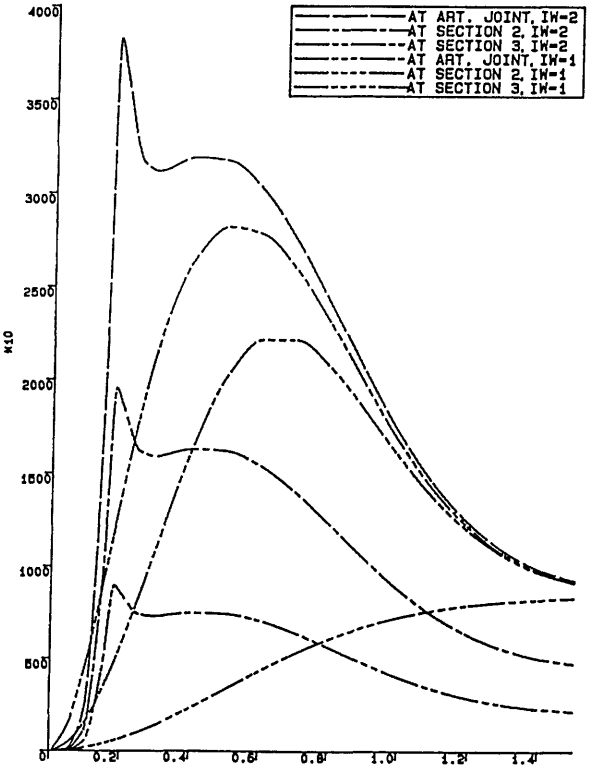

equiv. MAT

(b) d=300m

(Fig. 9.4 contd)

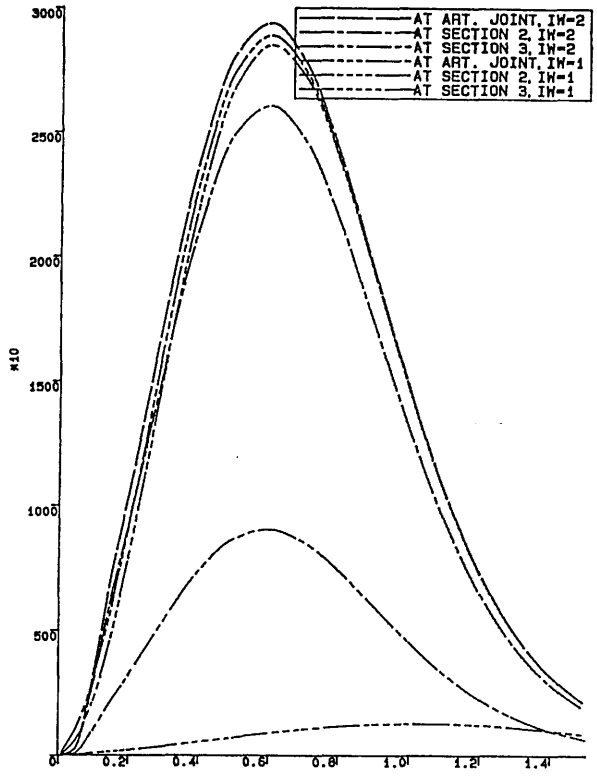

type III HAT

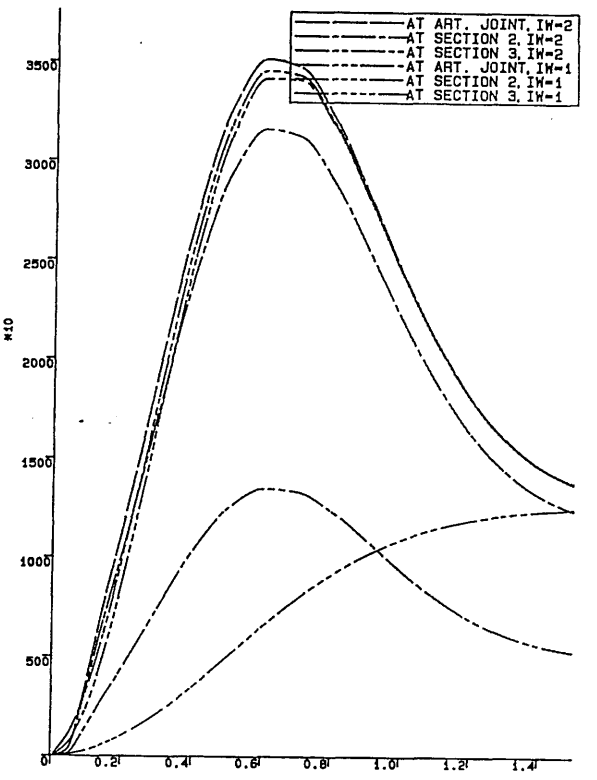

type II HAT

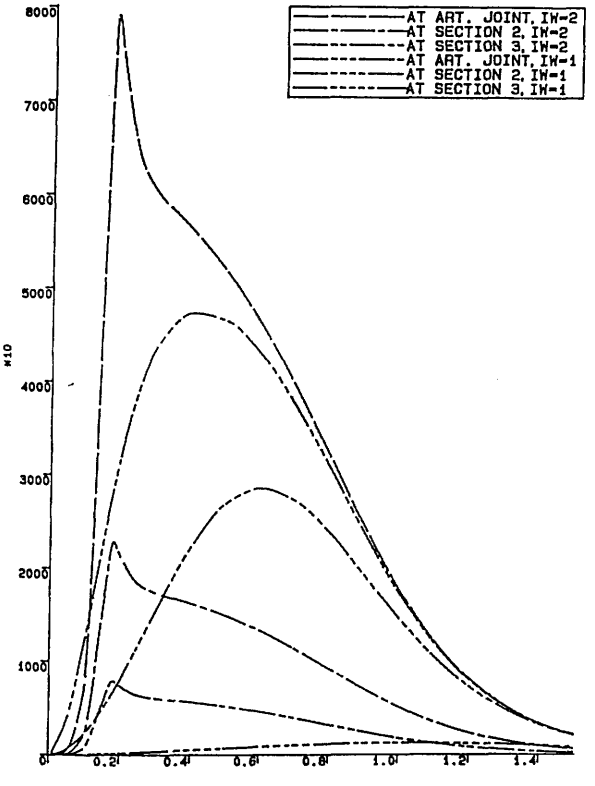

type I HAT

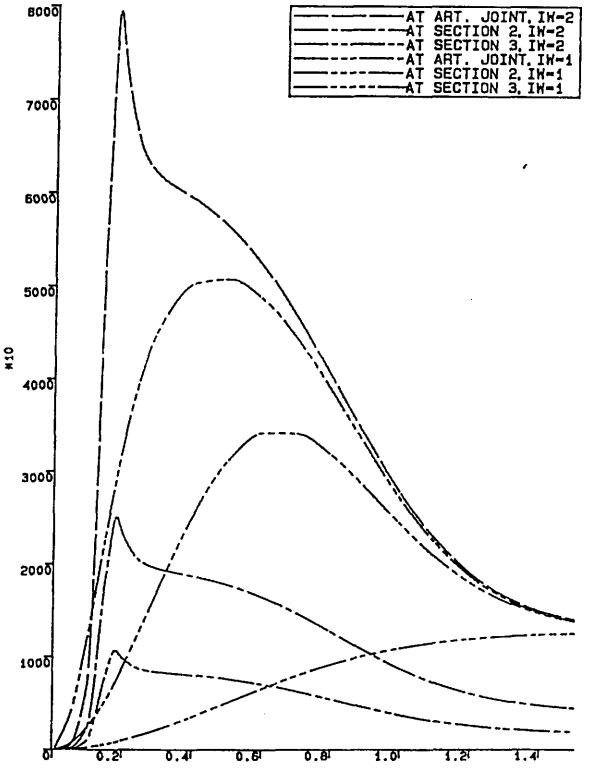

equiv. MAT

(c) d=450m

(Fig. 9.4 contd)

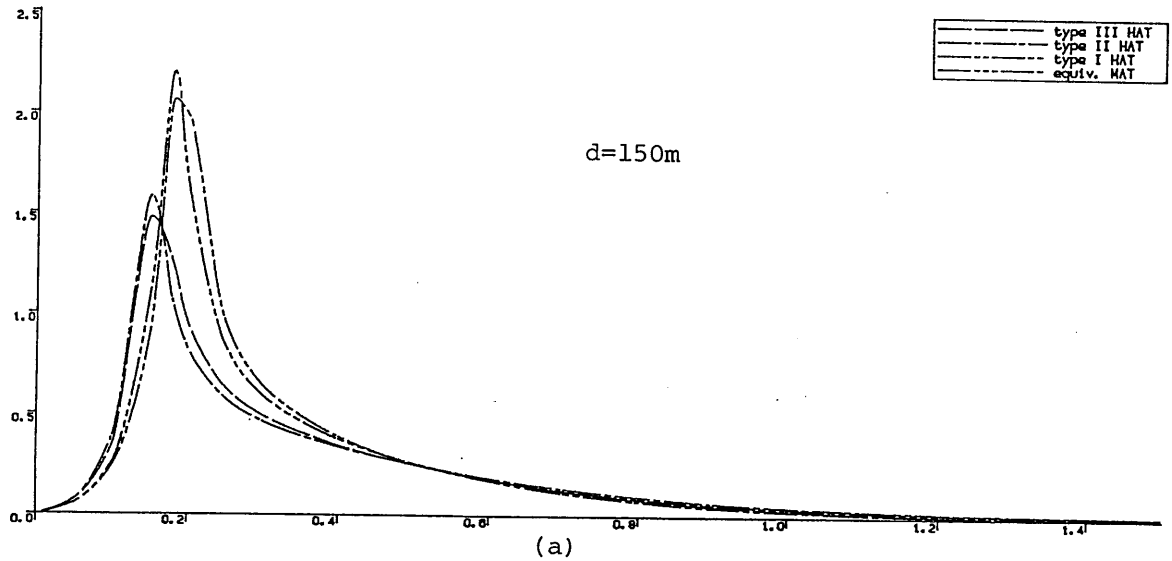

(a)

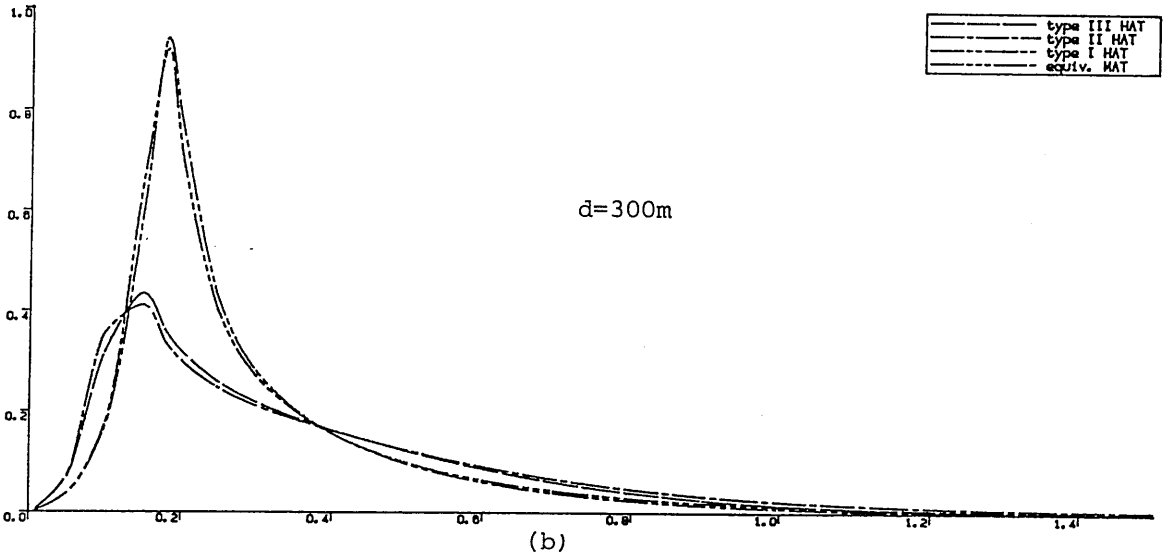

(b)

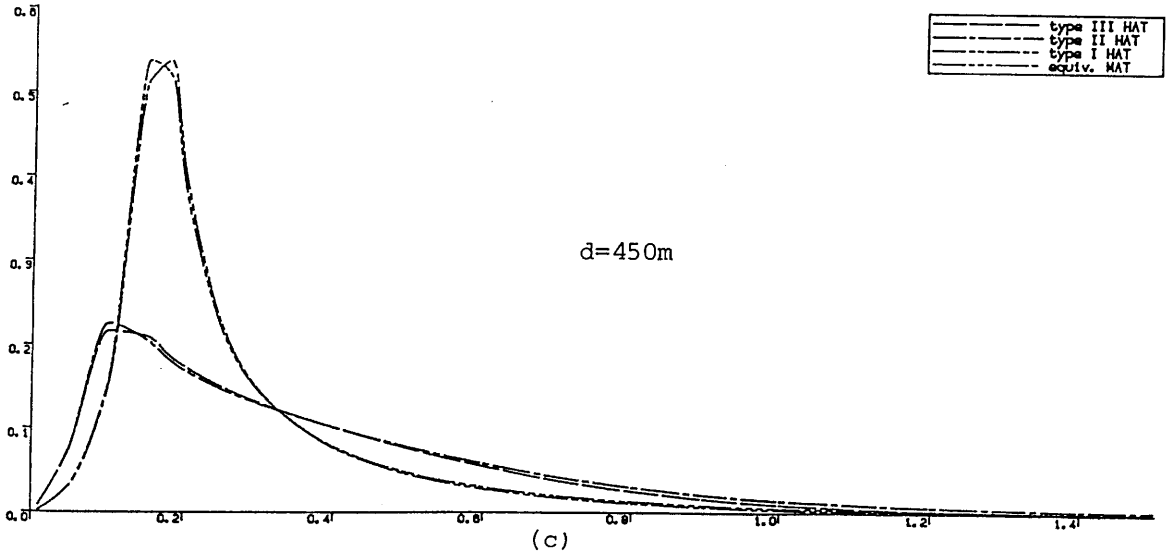

(c)

x : ω rad/s ; y : θ/H degree/m

Fig. 9.5 RAO of angular displacement

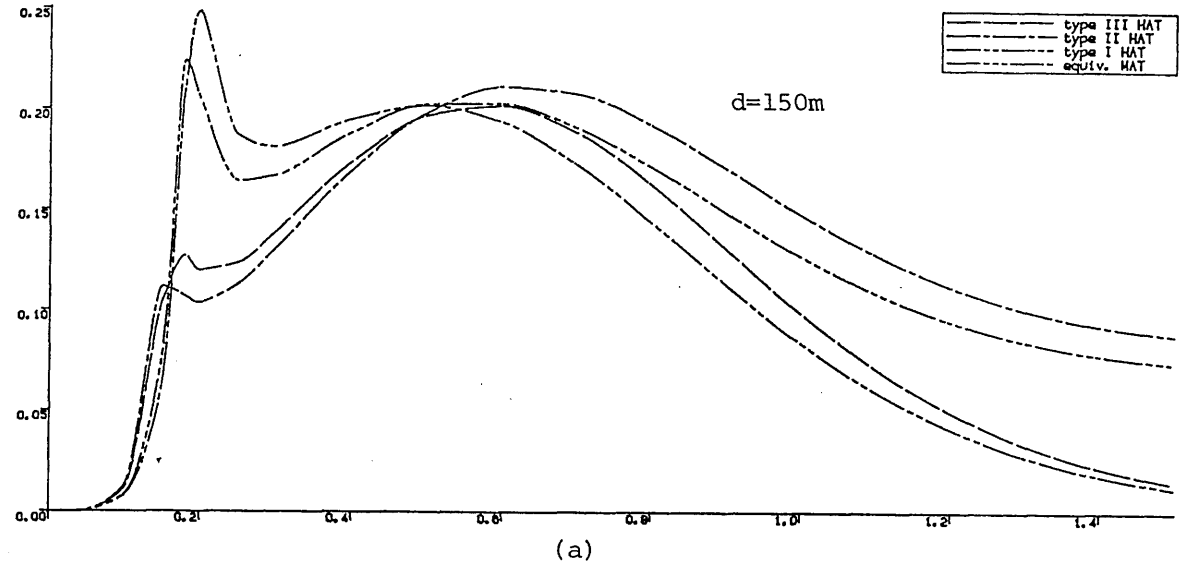

(a)

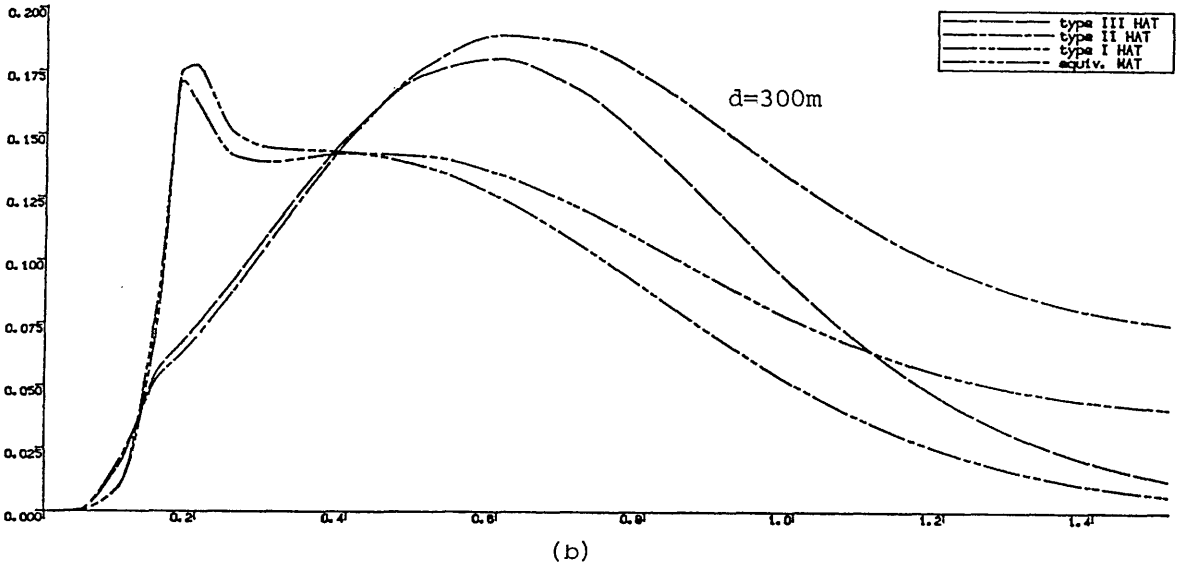

(b)

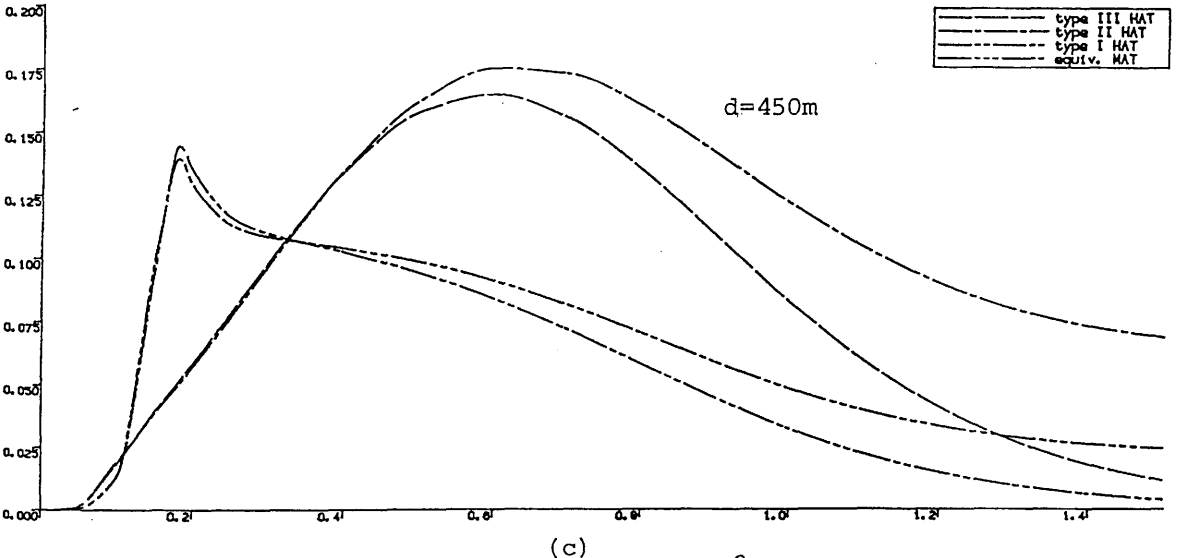

(c)

x : ω rad/s ; y : a_x/H $m/s^2/m$

Fig. 9.6 RAO of the horizontal acceleration at middle deck level

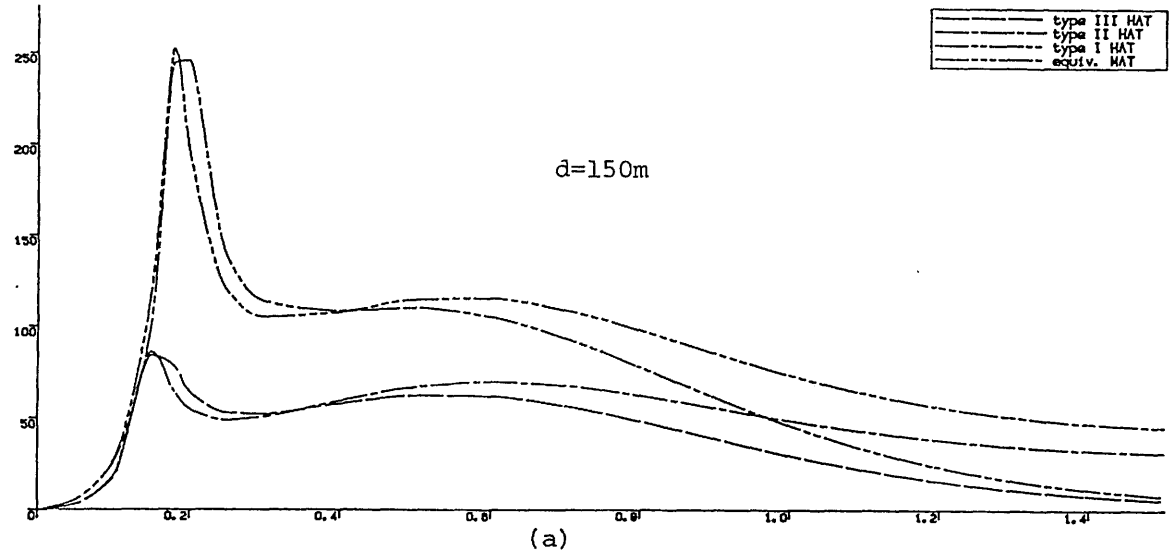

(a)

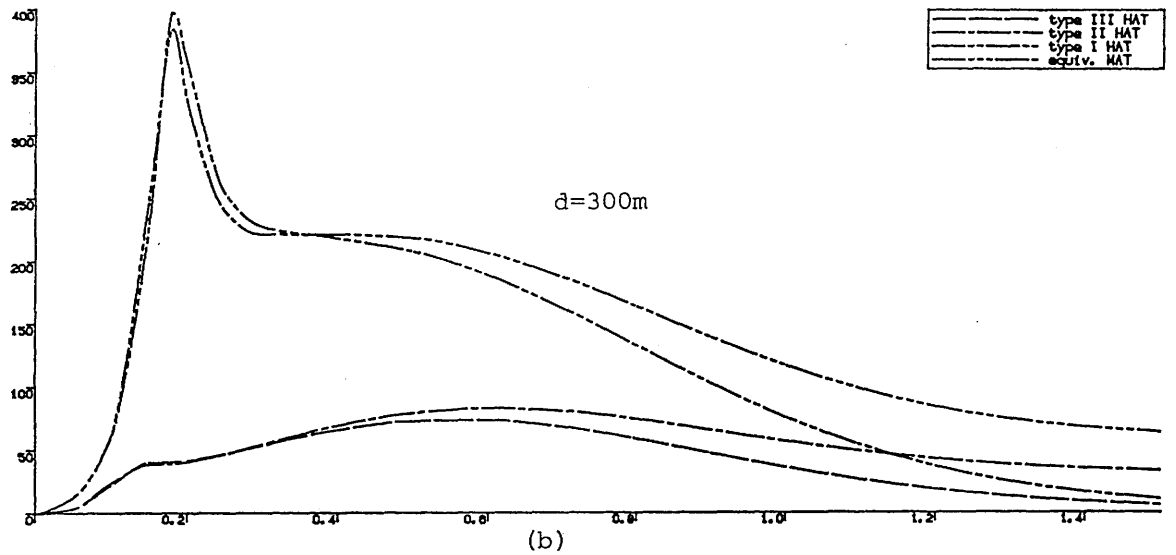

(b)

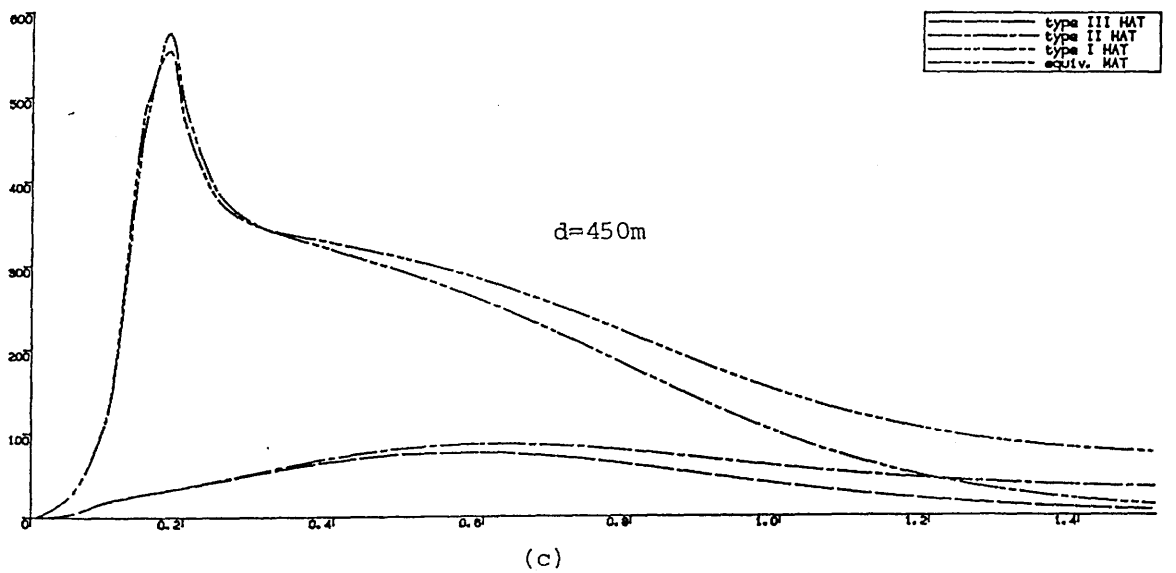

(c)

x : ω rad/s ; y : F_s/H t/m

Fig. 9.7 RAO of the shear force on the articulated joint

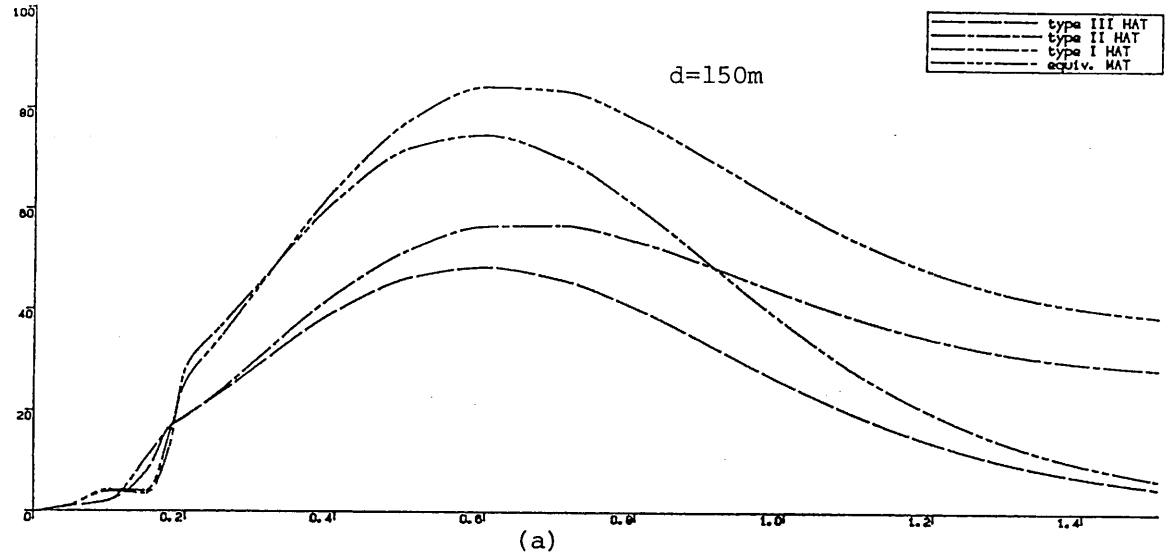

(a)

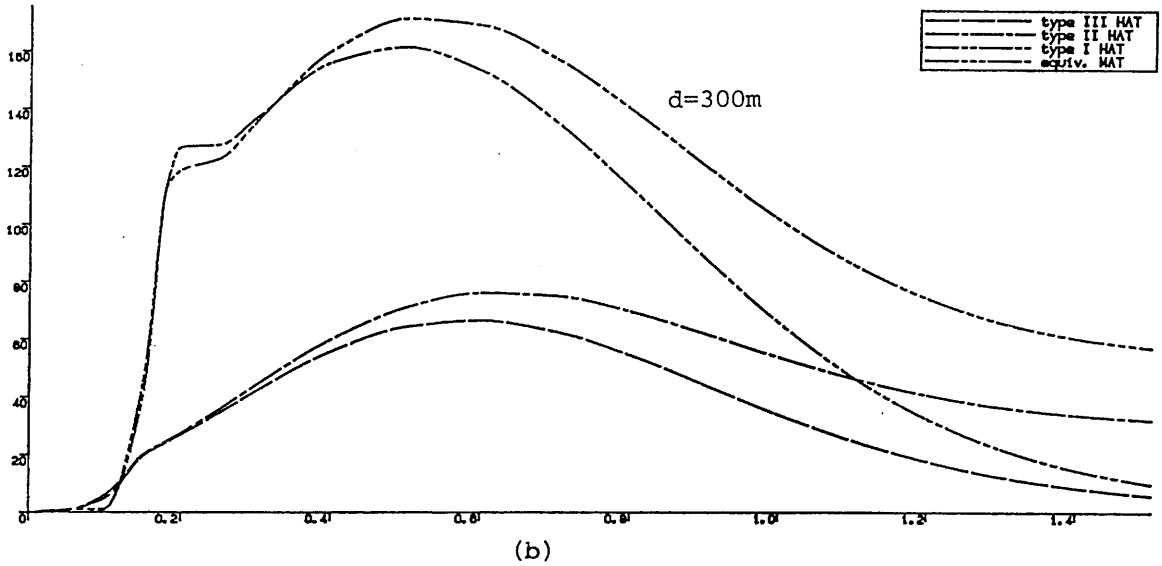

(b)

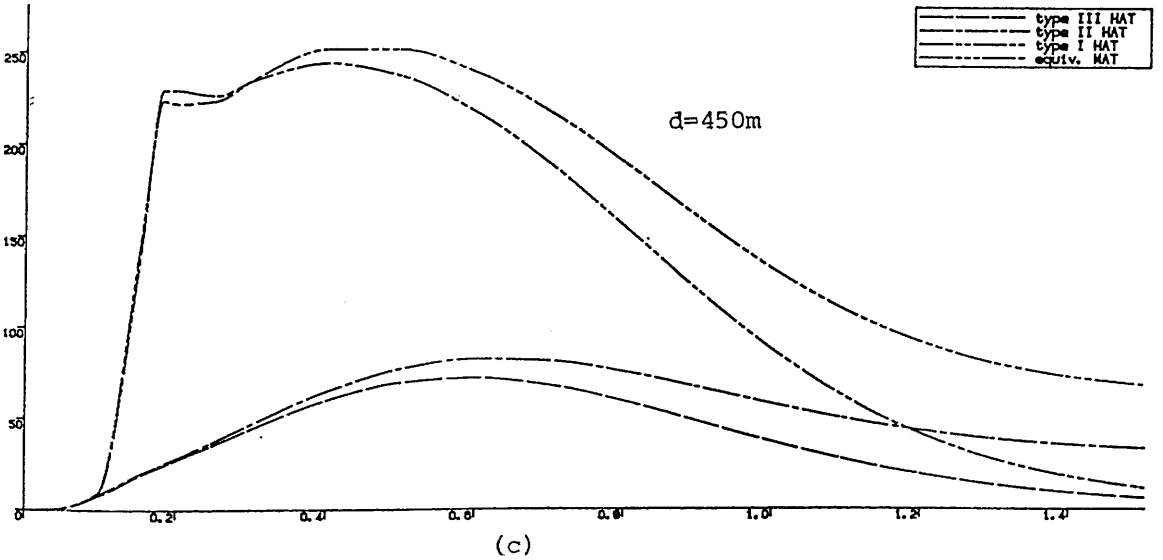

(c)

x : ω rad/s ; y : F_S/H t/m

Fig. 9.8 RAO of the internal sectional shear force on SECTION 1

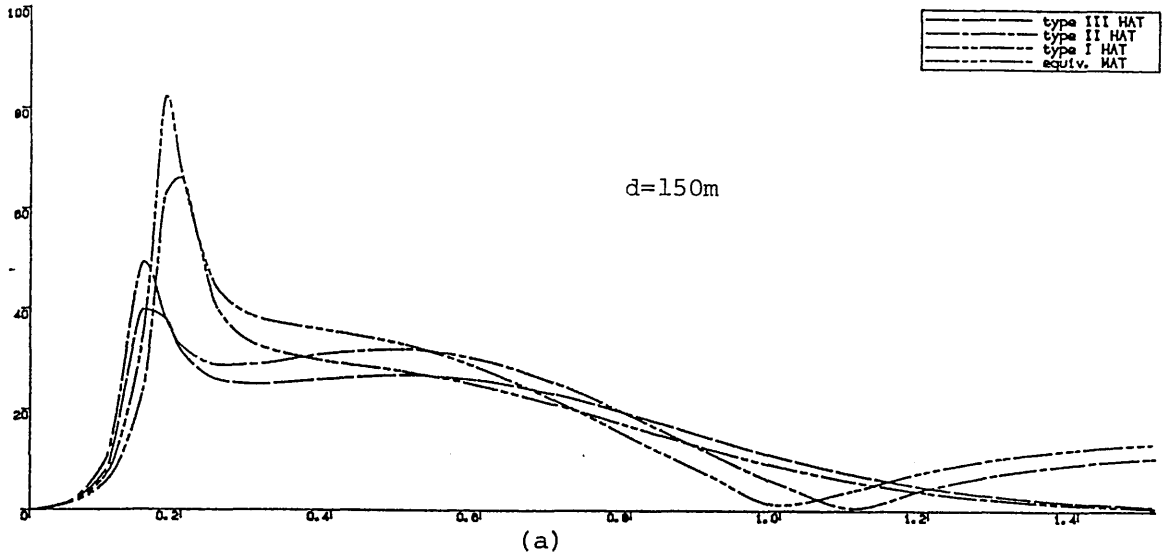

(a)

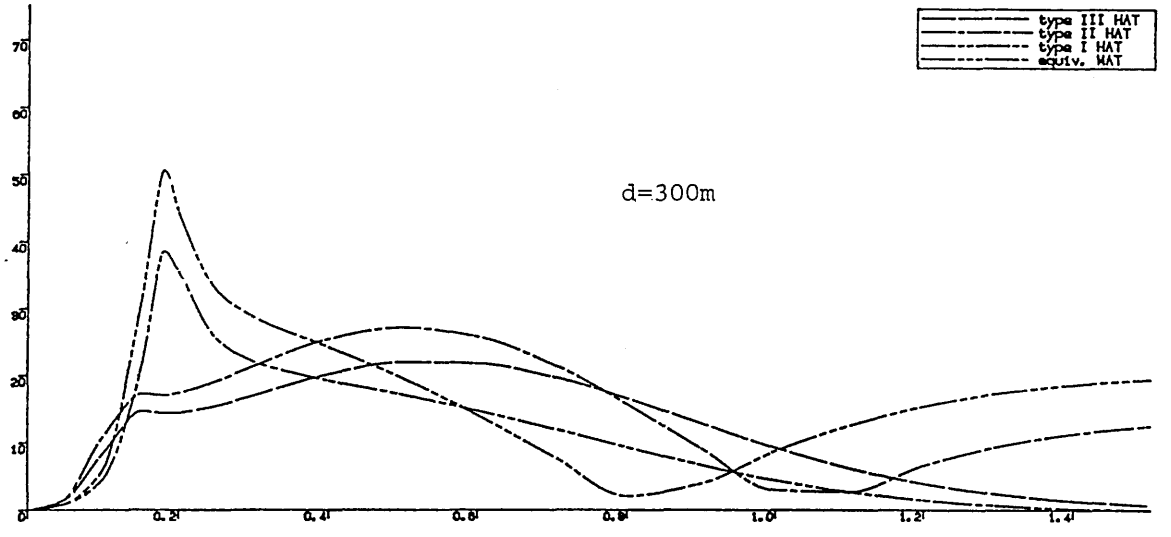

(b)

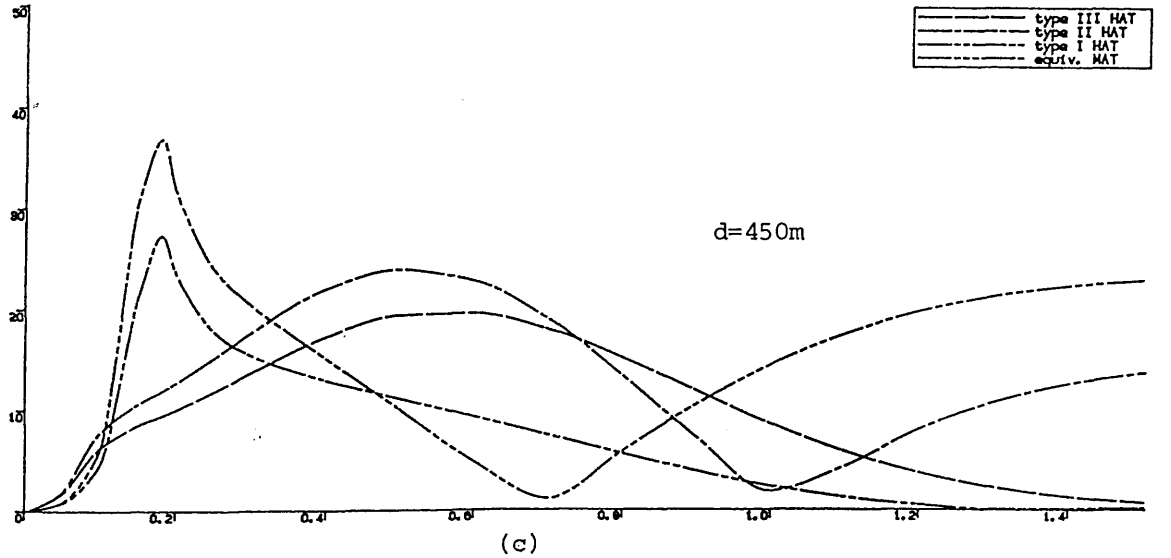

(c)

x : ω rad/s ; y : F_S/H t/m

Fig. 9.9 RAO of the internal sectional shear force on SECTION 3

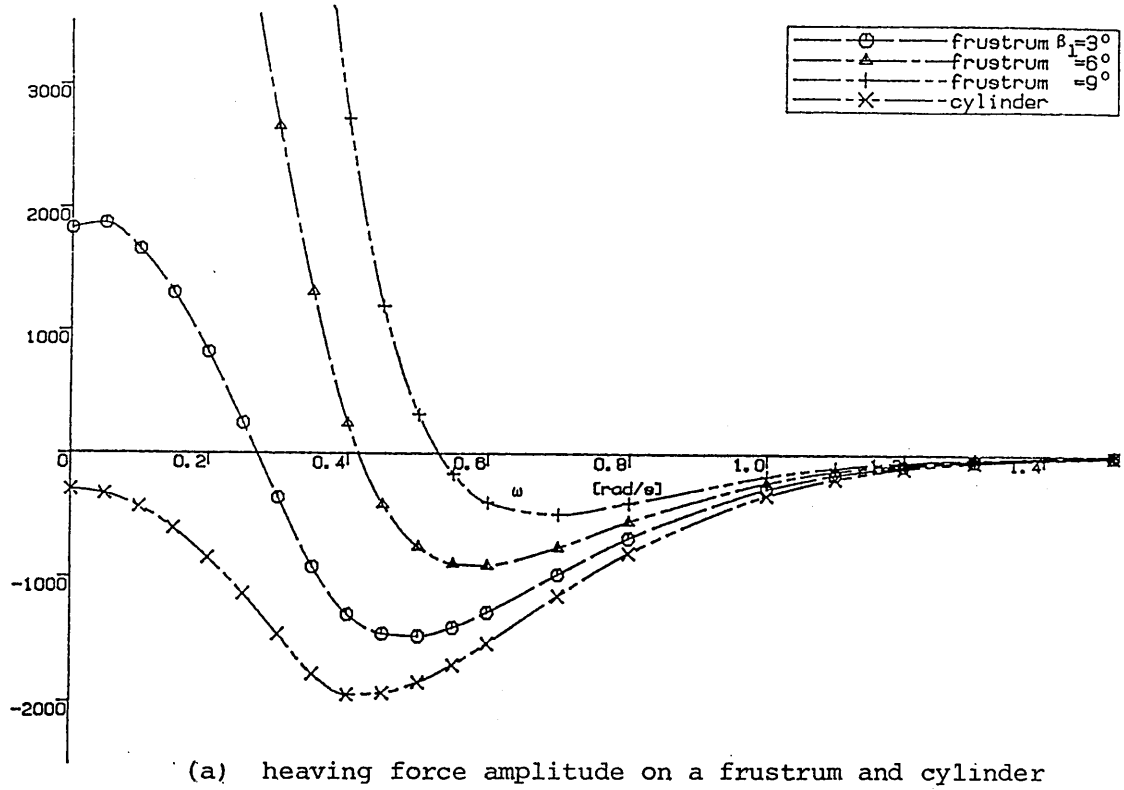

(a) heaving force amplitude on a frustrum and cylinder buoyancy chamber of the same volume and height

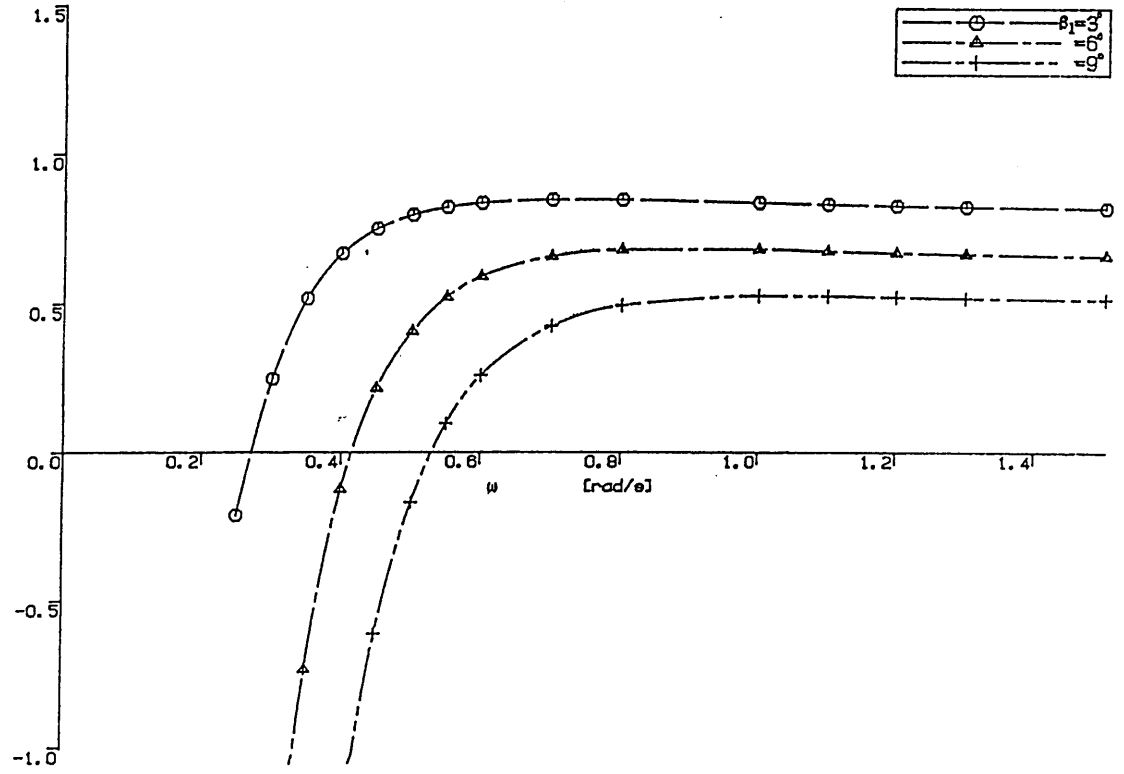

(b) ratio between the heaving force on a frustrum buoyancy chamber and the heaving force on a cylinder buoyancy chamber of the same volume and height

Fig. 9.10 heaving force on a isolated buoyancy chamber submerged in waves

Table 9.1 Details of a Lattice Structure

(a) Details of a Lattice

Lattice length : L_o from z_i to z_{i+1} replacing the ith single column of MAT

No of bays divided : $$n_b = \begin{cases} \text{Integer}(R_\ell) & \text{if } R_\ell - \text{Integer}(R_\ell) < 0.5 \\ \text{Integer}(R_\ell) + 1 & \text{Otherwise} \end{cases} \quad (9.1)$$

$$R_\ell = \frac{L_o}{2r_5}$$

No of main frames : $n_f = 3,4$

(b) Details of a Single Bay of the Lattice

Geometrical parameter	Member No $n_f=3$	Geometrical Relationship	Member No $n_f=4$	Geometrical Relationship	Notes
ℓ_6, r_6, t_6	1 2 3	$\ell_6=L_o/n_b=\ell$	1 2 3 4	$\ell_6=L_o/n_b$	main frames
ℓ_8, r_8, t_{r8}	4 5 6	$\ell_8=\sqrt{\ell^2+\ell_7^2}$	5 6 7 8	$\ell_8=\sqrt{\ell^2+\ell_7^2}$	lateral diagonal bracings
ℓ_7, r_7, t_{r7}	7 8 9	$\ell_7=2r_5\sin\frac{\pi}{n_f}$	9 10 11 12	$\ell_7=2r_5\sin\frac{\pi}{n_f}$	horizontal lateral bracing
ℓ_9, r_9, t_{r9}	10 11 12	$\ell_9=r_5$	14 15 16 17	$\ell_9=r_5$	horizontal diagonal bracing
$\ell_{10}, r_{10}, t_{r10}$			13	$\ell_{12}=\sqrt{\ell_6^2+2\ell_7^2}$	spatial diagonal bracing
$\ell_{11}, r_{11}, t_{r11}$	13	$\ell_{11}=\ell_6$	18	$\ell_{11}=\ell_6$	riser
n_t = 9 without riser n_t = 13 with riser			n_t = 15 without riser n = 18 with riser		

Table 9.2 Modelling of a Lattice Structure

(a) Structural Mass

main frames (j=6) :
lateral diagonal bracings (j=7) : $m_j = 2\pi r_j t_{rj} \rho_s n_f \ell_j$ (j=6,7,8)
horizontal lateral bracings (j=8) :

horizontal diagonal bracings : $m_9 = \begin{cases} 2\pi r_9 t_{r9} \rho_s n_f \ell_9 & \text{with risers} \\ 2\pi(n_f-3) n_f r_9 t_{r9} \rho_s \ell_9 & \text{otherwise} \end{cases}$

spatial diagonal bracings : $m_{10} = 2\pi(n_f-3) r_{10} t_{r10} \rho_s \ell_{10}$

risers : $m_{11} = \begin{cases} 0.0 & \text{with risers} \\ 2\pi r_{11} t_{r11} \rho_s \ell_{11} & \text{otherwise} \end{cases}$

total mass of one bay : $M_b = \sum_{j=t}^{11} m_j = \beta_m m_b$ (9.2)

total mass of the lattice : $m_i = n_b m_6$ (9.3)

(b) Buoyancy

buoyancy components : $V_{bj} = m_j \frac{r_j \rho_w}{2 t_{rj} \rho_s}$ (j=6,7,8,9,10,11)

total buoyancy of one bay : $V_b = \sum_{j=6}^{11} V_b$ (9.4)

total buoyancy of the lattice : $V_i = n_b V_b$ (9.5)

(c) Sectional Bending Stiffness

second moment of inertia of the cross section : $I_x = I_y = \pi n_f r_6 t_{r6} (r_6^2 + r_6^2)$
(neglecting the contributions from the bracings)

(d) Mass Moment of Inertia (approximated)

Approximated first and second moment of inertia of structural mass about y'-axis

$$I_s^{(i)} = \frac{M_i}{3L_o} [(z_{i+1} - z_o)^3 - (z_i - z_o^3)], \quad \bar{I}_s^{(i)} = \frac{M_i}{2L_o} [(z_{i+1} - z_o)^2 - (z_i - z_o)^2]$$

(e) Stiffness (approximated)

for $\bar{K}_\ell^{(i)}$ and $K_\ell^{(i)}$, substituting $m_s(z)$ and $m_a(z)$ as given by:-

$$m_s(z) = \frac{M_i}{L_o}, \text{ and } m_a(z) = \frac{V_i}{L_o}$$

into the appropriate equations in Table 5.1

Table 9.3 list of ω_1 (in rad/s) indicating the water depth capacity of type II HATs when r_5 is limited by D_4

V_4 (m)	D_4 (m)	r_5 \ d (m)	400	450
10,000	23.2	10.5	1.26	1.03
15,000	26.8	12.5	1.50	1.23

deck : W_o=3,000t V_0=30,000m^3 h_c=25m n_d=4

U.C. : D_5=10.0m $\bar{t}_5$=0.1m L_s=30m

B.C. : $\bar{t}_4$=0.1m

L.L. : r_6=0.75m $\bar{t}_{r6}$=0.025m r_j=0.15m $\bar{t}_{rj}$=0.01m j=7,8,9,10

Ba.C. : α_2=1.0 $\bar{t}_2$=0.1m ρ_2=2.5t/m^3 $T_s(z_1)$=0.0

E.C. : L_1=0.0

Table 9.4 water depth capacity of hybrid articulated tower structures

(a) list of ω_1 (in rad/s) indicating the water depth capacity of type II HATs when the buoyancy chamber is disintegrated

lattice dimensions (m)	d (m)	ω_1 (rad/s)	ω_2 (rad/s)	$W_{\Sigma s}$ (tonnes)	V_Σ (tonnes)
r_5=20 r_6=0.75 t_{r6}=0.025 r_j=0.15 t_{rj}=0.01 j=7,8,9,10	550	1.05	2.96	5,295	17,957
	600	.925	2.66	5,446	18,345
r_5=25 r_6=0.75 t_{r6}=0.025 r_j=0.15 t_{rj}=0.01 j=7,8,9,10	550	1.29	3.49	5,301	17,962
	600	1.13	3.18	5,456	18,355
r_5=45 r_6=0.75 t_{r6}=0.025 r_j=0.25 t_{rj}=0.01 j=7,8,9,10	750	1.30	3.83	6,197	20,364

deck : W_o=5,000t h_c=21.5m V_o=30,000m^3 n_d=4

U.C. : D_5=9.0m $\bar{t}_5$=0.09m L_s=30m

B.C. : V_4=10,000t α_4=1.0 $\bar{t}_4$=0.15m

Ba.C. : α_2=1.0 $\bar{t}_2$=0.1m ρ_2=2.5t/m^3 $T_s(z_1)$=0.0

E.C. : D_1=0.0 L_1=0.0

(b) list of ω_1 (in rad/s) indicating the water depth capacity of type III HATs when the buoyancy chamber is disintegrated

lower lattice dimensions (m)	d (m)	ω_1 (rad/s)	ω_2 (rad/s)	$W_{\Sigma s}$ (tonnes)	V_Σ (tonnes)
r_5=20 r_6=0.75 t_{r6}=0.025 r_j=0.15 t_{rj}=0.01 j=7,8,9,10	550	1.03	2.35	4,260	15,495
	600	.893	2.19	4,431	15,872
r_5=25 r_6=0.75 t_{r6}=0.025 r_j=0.15 t_{rj}=0.01 j=7,8,9,10	550	1.21	2.61	4,267	15,501
	600	1.09	2.43	4,441	15,881
r_5=45 r_6=0.75 t_{r6}=0.025 r_j=0.25 t_{rj}=0.01 j=7,8,9,10	750	1.27	2.62	5,227	17,857

Deck : W_o=5,000t V_o=30,000m^3 h_c=21.5m n_d=4

U.L. : r_5=10m r_6=0.5m $\bar{t}_{r6}$=0.02m r_j=0.1m $\bar{t}_{rj}$=0.01m j=7,8,9,10

B.C. : V_4=10,000t α_4=1.0 $\bar{t}_4$=0.15m L_s=30m

Ba.C. : α_2=1.0 $\bar{t}_2$=0.1m ρ_2=2.5t/m^3 $T_s(z_1)$=0.0

E.C. : L_1=0.0

Table 9.5 Conditions of Equivalence Between a Lattice and a Single Column

Condition I

bending strength condition : $(\bar{R}/I_x)_{column} = (\bar{R}/I_x)_{lattice}$

R is the characteristic cross sectional radius

equivalent single column radius : $R = \left[\frac{n_f r_6 t_{r6} (1+\alpha_r)^2}{t} \right]^{1/2}$, $\alpha_r = \frac{r_5}{r_6}$

structural weight ratio between the equivalent column and lattice : $\gamma_w = \left[\frac{(1+\alpha_r^2)\bar{t}^2}{n_f \beta_m t \; t_{r6}(1+\alpha_r)} \right]^{1/2}$

Condition II

bending stiffness condition : $(EI_x)_{column} = (EI_x)_{lattice}$

equivalent single column radius : $R = \left[\frac{n_f r_6 t_{r6} (1+\alpha_r^2)}{t} \right]^{1/3}$

structural weight ratio between the equivalent column and lattice : $\gamma_w = \left[\frac{(1+\alpha_r^2)\bar{t}^3}{n_f^2 \beta_m^3 t \; t_{r6}^2} \right]^{1/3}$

Table 9.6 geometrical dimensions of the sample HATs and their equivalent MATs used in Chapter 9

component		type I HAT	type II HAT	type III HAT	equivalent MAT
Deck		W_o=1,000t V_o=10,000m^3 n_d=2			
U.C.		R_5=2.653m $\bar{t}_5$=0.075m t_5=0.035m			
U.L.		r_5=7.0m r_6=0.5m t_{r6}=0.025m r_j=0.15m t_{rj}=0.015m j=7,8,9,10			
B.C.		α_4=1.0 $\bar{t}_4$=0.1m L_s=20m			
L.L.	d=150m (a)	r_5=7.0m	r_6=0.5m t_{r6}=0.025m r_j=0.15m t_{rj}=0.015m j=7,8,9,10		
	d=300m (b)	r_5=10.0m			
	d=450m (c)	r_5=13.0m			
L.C.	d=150m (a)	R_3=3.751m	$\bar{t}_3$=0.09m t_3=0.035m		
	d=300m (b)	R_3=4.7537m			
	d=450m (c)	R_3=5.66m			
Ba.C.		α_2=1.0 ρ_2=2.5t/m^3 $\bar{t}_2$=0.12m $T_s(z_1)$=0.0			
E.C.		L_1=0.0 (z_1=0.0)			

related conditions:

C_a=2.0

C_d=1.0 for lattice structures and C_d=0.7 otherwise

Table 9.7 static response,dynamic response and characteristics of the articulated tower structures in Table 9.6

d (m)	150		300		450	
W_0/V_4 (t/t)	.25	.125	.25	.125	.25	.125
static tilt angle(in degrees) due to mean wind loading						
type III HAT	4.18	1.42	2.75	1.02	2.32	.886
type II HAT	4.14	1.42	2.72	1.02	2.29	.892
type I HAT	2.37	1.16	.689	.496	.295	.250
equiv. Mat	2.37	1.17	.696	.502	.300	.254
static tilt angle(in degrees) due to steady current loading						
type III HAT	.653	.26	.64	.268	.7028	.30
type II HAT	.6074	.248	.579	.257	.659	.289
type I HAT	.384	.218	.188	.151	.123	.112
equiv. MAT	.362	.208	.181	.146	.12	.11
angular dynamic response (r.m.s. in degrees) due to random wind loading						
type III HAT	.8475	.4935	.3057	.1963	.1688	.1137
type II HAT	.8655	.5094	.3104	.2103	.171	.1162
type I HAT	.6639	.4453	.1600	.1314	.0624	.0561
equiv. MAT	.683	.4603	.1644	.1353	.0642	.0577
angular dynamic response(r.m.s. in degrees) due to random waves loading						
type III HAT	.377	.527	.183	.233	.115	.145
type II HAT	.391	.52	.191	.234	.122	.147
type I HAT	.373	.504	.136	.175	.064	.0825
equiv. MAT	.385	.5	.143	.179	.0684	.0856
angular dynamic response(r.m.s. in degrees) due to random wave loading						
type III HAT	2.560	6.51	1.07	1.72	.635	.911
type II HAT	2.36	5.57	1.03	1.6	.625	.878
type I HAT	3.76	7.74	1.62	2.04	.857	.977
equiv. MAT	3.38	6.47	1.53	1.84	.838	.953
horizontal deck acceleration(r.m.s. in m/s^2) due to random wave loading						
type III HAT	.69	1.54	.561	.831	.493	.678
type II HAT	.658	1.33	.551	.791	.494	.661
type I HAT	.902	1.78	.702	.878	.531	.613
equiv. MAT	.831	1.52	.677	.842	.525	.469

	150		300		450	
	.25	.125	.25	.125	.25	.125
second moment of inertia of the total structural mass (ballasting material included) about the articulated joint(in kg.m $*10^{11}$)						
type III HAT	.4746	.5404	1.882	2.179	4.381	5.098
type II HAT	.5547	.6202	2.19	2.487	5.029	5.746
type I HAT	.5488	.6102	3.046	3.302	9.829	10.4
equiv. MAT	.6288	.6898	3.354	3.61	10.48	11.05
second moment of inertia of the total added hydrodynamic mass about articulated joint(in kg.m $*10^{11}$)						
type III HAT	.6166	1.168	3.169	6.017	7.789	14.83
type II HAT	.6948	1.246	3.504	6.353	8.652	15.59
type I HAT	.8227	1.352	7.428	10.07	31.53	37.73
equiv. MAT	.9008	1.43	7.764	10.41	32.3	38.5
restoring stiffness(in N.m $*10^{10}$)						
type III HAT	.1897	.5594	.5266	1.423	.8758	2.298
type II HAT	.1944	.5647	.541	1.438	.9076	2.33
type I HAT	.3338	.6835	2.101	2.918	6.892	8.141
equiv. MAT	.339	.689	2.116	2.934	6.925	8.175
natural frequency of RBMV motion(in rad/s)						
type III HAT	.132	.181	.102	.132	.0845	.107
type II HAT	.125	.174	.0975	.128	.0815	.104
type I HAT	.156	.187	.142	.148	.129	.130
equiv. MAT	.149	.18	.138	.145	.127	.128
total structural mass(excluding the mass of the ballasting material in tonnes)						
type III HAT	1,560	2,374	1,957	2,761	2,333	3,145
type II HAT	1,880	2,700	2,274	3,082	2,634	3,450
type I HAT	3,223	3,837	7,430	7,970	13,023	13,500
equiv. MAT	3,551	4,178	7,760	8,294	13,334	13,807
total buoyancy (in tonnes)						
type III HAT	6,000	12,600	6,480	13,000	6,940	13,500
type II HAT	6,290	12,800	6,770	13,300	7,250	13,800
type I HAT	12,500	18,200	31,500	37,500	65,300	71,200
equiv. MAT	12,300,	18,500	31,800	37,800	65,600	71,500

CHAPTER 10

CONCLUDING REMARKS

1. INTRODUCTION

Attention throughout the present work has been centred around single articulated tower structures, including monolithic arrangements composed of several columns of varying diameter and hybrid ones composed of columns and lattices. Detailed conclusions are drawn at the end of each chapter. This chapter abstracts some of the important conclusions and overall conclusions are drawn. Recommendations for further research are outlined.

2. CONCLUSIONS

1. Articulated tower structures have many potential uses in the offshore oil industry. The basic design specifications of an articulated tower are the water depth, deck payload and environmental conditions. Existing applications of articulated tower structures, together with limited theoretical and experimental studies have, to a large extent, demonstrated the feasibility of their use in relatively shallow waters as flare stacks, production platforms, mooring towers for floating productions and offloading systems.

2. Indirect optimisation has been performed based on parametric studies of design variables, including those parameters defining the environmental conditions and those defining the geometrical dimensions of the structure. With regard to the uncertainty in modelling the

environmental conditions and the structure-environment interaction, it is particularly important from the point of view of practical design to show the effect of those parameters when they vary over a wide range. From the studies of those parameters defining the environmental conditions, some of the unique features of articulated tower structures in comparison with conventional fixed offshore structures are seen to include:

a. Sensitivity of angular dynamic response and internal sectional shear force and bending moment to wave frequency and to the selection of C_a, C_d etc.

b. The importance of the second order wave loading, wind loading and current loading with respect to the first order wave loading.

3. With regard to the relative column dimensions there are several options of structural geometry available. It is concluded that designs with a definite buoyancy chamber located in the middle and immersed below the wave trough level are preferable.

4. Reduction of wind loading is the predominant factor in the deck design. The deck space and the deck height should be as small as possible for a given payload. There is little data available on the relationship between the deck space and deck payload. A ratio of $5m^3/t$ to $10m^3/t$ between the deck space and deck payload is used with the maximum deck space limited to $30,000m^3$. The deck shape also deserves careful consideration but low flat shapes are preferable. In addition, the layout of the deck payload should be worked out very carefully to reduce the lateral offset of the payload gravity centre.

5. The upper column diameter is determined primarily by the

structural strength considerations. Its minimum diameter is thought to be about 7m if it is to provide a dry access to the buoyancy chamber. The lower column diameter is determined also by structural strength considerations in shallow waters, but by flexural mode vibration motion in deep waters.

6. The position and dimensions of the buoyancy chamber, related to the dimensions of other columns, are the most influencial geometrical parameters. The minimum submergence depth of the buoyancy chamber is about 15m in North Sea conditions. Its size can be estimated such that the static tilt due to mean wind loading on the deck is between 10% and 30% of the total of the extreme tilt angle, as estimated by equation (8.1). Specifically, its size can be changed to achieve the required total of the static and dynamic angular responses. Its diameter/length ratio is only important in the case of large payload structures in shallow waters.

The buoyancy chamber can be utilised to accommodate some of the machinery which would otherwise be located on the deck. In addition, using a frustrum buoyancy chamber in place of a cylindrical one is advantageous in terms of reducing the heaving force on it and therefore on the articulated joint.

7. The static stability in the intact condition is represented by the static tilt due to mean wind, steady current, mean wave drift and lateral offset of the deck payload. Among these, the static tilt due to wind loading forms the major part of the total static tilt. The static tilt due to current accounts to 10% to 40% of that due to mean wind, while that due to the lateral offset of the deck payload and that due to mean wave drift are of the same order as, or higher than,

that due to current. The extreme of the total maximum angular displacement under combined wave, wind and current can be estimated by equation (8.1) under the assumed North Sea conditions at present.

The static stability in the damaged condition is related to the flooding damage to the buoyancy chamber but the flooding can be effectively eliminated by dividing the buoyancy chamber into smaller compartments using an inner chamber together with vertical and transverse bulkheads.

If the possibility of structural failure or malfunction of an articulated joint is envisaged, the static stability in the free floating condition must be considered. Basically, it is required that in the free floating condition, the structure be at least statically stable. This primarily results in the use of the ballast chamber which is also aimed at lowering the centre of gravity and reducing the forces on the articulated joint.

Secondary mooring is desirable to ensure the free floating stability of the whole structure in case of failure or malfunction of the articulated joint. Because of the severe loading on the articulated joint and the difficulties involved in its inspection and maintenance, the articulated joint is among the most vulnerable parts of the whole structure. Various ways of reducing the forces on on the articulated joint have been outlined in Chapter 8.

8. The structural strength of large diameter thin shell cylinders, either unstiffened or stiffened, under general loading, ie axial compression/tension, shear, bending, torsion and external pressure, has been calculated according to DnV Rules which although

very comprehensive are not very accurate in some cases. The computerised design codes provide a convenient means of assessing the structural strength of articulated tower structures. It is true in most cases that stringer stiffened cylinders have less structural weight than ring frame stiffened ones. Therefore, stringer stiffened cylinders are to be used from the point of view of reducing the structural material consumption. However, examination of the effect of structural mass distribution along the structure indicates that minimum structural weight is not always desirable as far as reducing structural motion and internal sectional forces are concerned.

9. There exists a possibility that an articulated tower structure could be relocated, on finishing the operations at one site, to another site. In doing so, the overall economic background could be greatly improved but relocation is not likely to be always feasible, or straightforward. The pull-out and the reinstallation in the same depth of water is not expected to give rise to any particular difficulties. The major consideration involved includes satisfaction of the new requirements on:-

a. The basic design specifications: deck payload, water depth and environment.

b. Motion response characteristics.

c. Structural strength at the articulated joint and other critical sections along the structure.

10. The linear dynamic response analysis of monolithic single articulated tower structures is valid in waves. This has been confirmed both through time domain simulation and model testing. In terms of the structural motion response, the non-linear effect is

insignificant. The time saving in design, in using frequency domain analysis rather than time domain analysis is readily recognised.

In addition, the Mathiew type dynamic instability is related to the non-linear effect due to the interaction between the heaving force and pitch moment. However, it is theoretically and experimentally demonstrated that the dynamic motion response is stable.

11. In addition, the parametric studies revealed some of the shortcomings and limitations of monolithic single articulated tower structures. These include bad structural motion in shallow waters, rapid decrease of the natural frequencies of flexural mode vibration motion in deep waters and increasingly significant shear force on the articulated joint.

The shallow water application of an articulated tower structure is likely to be limited by constraints on the static and/or dynamic response. The minimum water depth depends on the maximum motion response allowed, the environmental conditions and the deck payload.

In order to avoid flexural mode vibration motion, increasing water depth results in an increase of the lower column diameter. Consequently, the structural material consumption increases very rapidly while the buoyancy efficiency decreases. If the minimum natural frequency is specified to be about 1.0 rad/s, the maximum water depth for the application of single articulated tower structures is around 300m to 350m.This ensures negligibly small flexural mode vibration motion.

12. Hybrid articulated tower structures can avoid some of these shortcomings or achieve certain compromises. Hybrid articulated towers structures utilise lattices and can be of three different forms. The immediate advantages are threefold: an increase of overall bending stiffness and structural strength, an increase of buoyancy efficiency and, a reduction of structural material consumption. The structural motion response may not always be improved and even penalised slightly in some cases. Nevertheless, the reduction of the internal sectional forces, especially the shear force on the articulated joint, is significant. Hybrid articulated towers, particularly the type I and II hybrid structures, are preferable in deep waters in which their advantages become greatly pronounced.

The potential difficulties involved in the application of hybrid structures mainly in deep waters are expected to rise from:-

a. The installation of those structures owing to the use of the lattices.

b. The structural strength of the articulated joint to resist the torsional loading exerted on the lattice sections.

c. The inspection and maintenance of the articulated joint.

The appropriate procedure of dealing with such difficulties has to be worked out in designing hybrid structures.

3. FURTHER STUDIES

On finishing the present work, a need is constantly felt for further studies on the following aspects which are relevant to the present study.

1. Model testing or full scale measurement on wind loading on the above water part, especially on the deck structure, is desirable for accurate and reliable assessment of the wind loading and wind loading induced structural response. This should be directed towards obtaining design data on the wind drag coefficient, wind velocity and profile together with wind induced structural response.

2. A more rational estimation of the environmental loadings needs to be established with regard to the directionality and coincidence, both in direction and occurrence, of winds, waves and current both in the short term and in the long term. The present assumptions of probability of once in 100 years in occurrence, coincidence in occurrence as well as in direction between wind, wave and current may well be far too conservative.

3. Detailed case studies of functional performance on the grounds of more rational modelling of design and operational conditions should be carried out. The corresponding economic performance with regard to the cost of fabrication, commissioning and installation, and operational efficiency and cost, together with cost of inspection and maintenance should also be studied.

4. Systematic and comprehensive model testing with varying model geometrical dimensions under combined action of wind, waves and current, measuring motion response, shear force bending moment along the structure and the wave drift effect should also be carried out to investigate the effect of their combination on the behaviour of the model structure. More importantly, full scale measurements over a meaningfully representative period of operation could validate the above theoretical predictions and model tests.

5. Finally, comparative studies between different concepts on the ground of their functional and economic performances should also be undertaken to select the best solution for specific circumstances.

APPENDIX 1

INTERNAL SECTIONAL FORCES ALONG AN ARTICULATED TOWER STRUCTURE IN WAVES

The sectional shear force and the sectional bending moment are obtained, referring to the column segment in fig. 2.1, undergoing plane motion subjected to the forces as shown in the figure as:

a. Shear Force

$$F_{s1}^{(i)} = F_{i}^{(i)} + F_{c}^{(i)} + F_{k}^{(i)} - F_{\ell d}^{(i)} - F_{\ell i}^{(i)} + F_{s2}^{(i)} \qquad \text{(A1.1)}$$

b. Bending Moment

$$M_{b2}^{(i)} = M_{i}^{(i)} + M_{c}^{(i)} + M_{k}^{(i)} - M_{\ell d}^{(i)} - M_{\ell i}^{(i)} + M_{b2}^{(i)} - F_{s1}^{(i)} (z_{1i} - z_{1}) + F_{s2}^{(i)} (z_{2i} - z_{1}) \Big|_{z_o = z_1} \qquad \text{(A1.2)}$$

where the left-hand side terms of equations (A1.1) and (A1.2) are the sectional shear force at section $z = z_{1i}$ and bending moment at section $z = z_{2i}$, respectively; the first to fifth terms at the right-hand of the equations correspond to the force on the column segment due to inertia and added inertia, damping, restoring stiffness and the wave force of inertia part and linearised drag part, respectively. In the above two equations the sectional shear force bending moment (referred to as the sectional forces in a general sense in the following) at section $z = z_{1i}$ and $z = z_{2i}$ are both unknown. To avoid the sectional forces at $z = z_{1i}$, section $z = z_{2i}$ is taken as the top of the deck at which the sectional shear force is zero (neglecting the wind drag), ie $z_{2i} = z_{N_e+1}$. Therefore, equation (A1.1) can be re-written, according to equation (5.17), as:-

$$F_{s1}(z,t) = F_i + F_c + F_k - F_{\ell d} - F_{\ell i} \tag{A1.3}$$

where

$$F_i = \left[SumI_s^{(i)} \Big|_{z=z} + SumI_{\ell a}^{(i)} \Big|_{z=z} \right] [- e\omega^2 \sin(\omega t + \phi)] \tag{A1.4}$$

$$F_c = SumC_{\ell d}^{(i)} \Big|_{z=z} e\omega\cos(\omega t + \phi) \tag{A1.5}$$

$$F_k = SumK_{\ell}^{(i)} \Big|_{z=z} e\sin(\omega t + \phi) \tag{A1.6}$$

$$F_{\ell d} = SumF_{\ell d}^{(i)} \Big|_{z=z} \tag{A1.7}$$

$$F_{\ell i} = SumF_{\ell i}^{(i)} \Big|_{z=z} \tag{A1.8}$$

These are obtained by combining Tables 5.1 and 5.2.

In addition, set:-

$$F_i = X_1 \sin(\omega t + \phi)$$

$$F_c = X_2 \cos(\omega t + \phi)$$

$$F_k = X_3 \cos(\omega t + \phi)$$

$$F_{\ell d} = X_4 \cos\omega t$$

and $$F_{\ell i} = X_5 \sin\omega t$$

and simply denote:-

$$F_{s1}(z,t) \text{ as } F_s(z,t) = F_s \sin(\omega t + \phi_s) \tag{A1.9}$$

then:-

$$F_s = \left[[(x_1 + x_3)\sin\Phi + x_2\cos\Phi - x_4]^2 + [(x_1 + x_3)\cos\Phi - x_2\sin\Phi - x_5]^2 \right]^{1/2} \quad \text{(A1.10)}$$

$$\Phi_s = \tan^{-1} \frac{(x_1 + x_3)\sin\Phi + x_2\cos\Phi - x_4}{(x_1 + x_3)\cos\Phi - x_2\sin\Phi - x_5} \quad \text{(A1.11)}$$

where $F_s = F_s(z,\omega)$ is the amplitude of sectional shear force $F_s(z,t)$.

The RAO of $F_s(z,t)$ is obtained as:-

$$G_s(\omega) = \frac{F_s(z,\omega)}{H} \quad \text{(A1.12)}$$

Therefore, $S_s(\omega) = G_s(\omega) S_\eta(\omega)$ (A1.13)

gives the response spectrum of the internal sectional shear force on section z = z, and:-

$$\sigma_s^2 = \int_0^\infty S_s(\omega)\, d\omega \quad \text{(A1.14)}$$

yields the rms shear force on section z = z.

Once the sectional shear force is known, the sectional bending moment can be calculated. In doing so, let $z_{1i} = z_1$ and $z_{2i} = z$ in equation (5.17), so that equation (A1.2) can be written as:-

$$M_{b2} = M_i + M_c + M_k - M_{\ell d} - M_{\ell i} + F(z,t)(z - z_1) \quad \text{(A1.15)}$$

where

$$M_i = \left[\text{SumI}_s^{(i)}\Big|_{z=z_1,z_o=z} - \text{SumI}_s^{(i)}\Big|_{z=z,z_o=z_1} + \text{SumI}_{\ell a}^{(i)}\Big|_{z=z_1,z_o=z_1} - \text{SumI}_{\ell a}^{(i)}\Big|_{z=z,z_o=z_1}\right][-e\omega^2\sin(\omega t+\phi)] = y_1\sin(\omega t+\phi) \quad \text{(A1.16)}$$

$$M_c = \left[\text{SumC}_{\ell d}^{(i)}\Big|_{z=z_1,z_o=z_1} - \text{SumC}_{\ell d}^{(i)}\Big|_{z=z,z_o=z_1}\right] e\omega\cos(\omega t+\phi) \quad \text{(A1.17)}$$

$$= y_2\cos(\omega t+\phi)$$

$$M_k = \left[\text{Sumk}_{\ell}^{(i)}\Big|_{z=z_1,z_o=z_1} - \text{SumK}_{\ell}^{(i)}\Big|_{z=z,z_o=z_1}\right] e\sin(\omega t+\phi) \quad \text{(A1.18)}$$

$$= y_3\sin(\omega t+\phi)$$

$$M_{\ell d} = \left[\text{SumM}_{\ell d}^{(i)}\Big|_{z=z_1,z_o=z_1} - \text{SumK}_{\ell}^{(i)}\Big|_{z=z,z_o=z_1}\right] \quad \text{(A1.19)}$$

$$= y_4\cos(\omega t+\phi)$$

$$M_{\ell i} = \left[\text{SumM}_{\ell i}^{(i)}\Big|_{z=z_1,z_o=z_1} - \text{SumM}_{\ell i}^{(i)}\Big|_{z=z,z_o=z_1}\right] \quad \text{(A1.20)}$$

$$= y_5\sin(\omega t+\phi)$$

Simply denote:-

$$M_{b2} = M_b(z,t) = M_b\sin(\omega t+\phi_b) \quad \text{(A1.21)}$$

Then:-

$$M_b = \left[[(y_1+y_3)\sin\phi + y_2\cos\phi - y_4 + F_s\sin\phi_s]^2 + [(y_1+y_3)\cos\phi - y_2\sin\phi - y_5 + F_s\cos\phi_s]^2\right]^{1/2} \quad \text{(A1.22)}$$

and

$$\phi_b = \tan^{-1}\left[\frac{(y_1+y_3)\sin\phi + y_2\cos\phi - y_4 + F_s\sin\phi_s}{(y_1+y_3)\cos\phi - y_2\sin\phi - y_5 + F_s\cos\phi_s}\right] \quad \text{(A1.23)}$$

Similarly, the RAO of $M_b(z,t)$ is:-

$$G_b(\omega) = \frac{M_b}{H} \tag{A1.24}$$

and the rms of the sectional bending moment is obtained from its spectrum:-

$$S_b(\omega) = G_b^2(\omega) S_\eta(\omega) \tag{A1.25}$$

REFERENCES

1. BELLON de CHASSY, C, FRANKHOUSER, H S and PICARD, J, 'Various Uses for the Articulated Column ELFOCEAN, a New Concept', OTC 1392, 1971.

2. SHULTZ, A R, 'Single Point Mooring Systems for Floating Process Plant', Modular And Barge Mounted Process Plants Symp, American Institute of Chemical Engineers National Meeting, Anaheim, California, 7-10 June, 1982.

3. 'THE CHALLENGE OFFSHORE', Shell Briefing Service, 1 Nov, 1983.

4. MARKS, V E, 'Future Small Oilfield Development', SPE 12988, 1984.

5. WAY, C R, 'The Fundamental Issues in Future Development Concepts (100 to 250 meters Water Depth)', SPE 12987, 1984.

6. FJELD SVEIN, 'Deepwater Platforms Problem Areas', EUR 234, 1980.

7. SMITH, J R and TAYLOR, R S, 'The Development of Articulated Buoyancy Column Systems as an Aid to Economic Offshore Production', EUR 266, European Offshore Petroleum Conference and Exhibition, Oct, 1980.

8. SNOWDEN, D P, 'Floating Production Systems for North Sea Marginal Fields', OTC 4819, 1984.

9. OFFSHORE ENGINEER, p9-10, Jan 1976; p9, Feb 1976; p69-74, Sep 1977; p11, Feb 1979; p9-11, Mar 1979; p132-134, Apr 1984; p15-17, Sep 1984.

10. CONAT, 'Articulated Offshore Systems', CONAT Presentation, London, 2 June, 1981.

11. SPIDSOE, N and BRATHAUG, H P, 'Measured Motion of a North Sea Articulated Loading Platform', 1-11, OTC 4639, 1983.

12. KIRK, C L, 'Response of Articulated Towers to Waves and Current', OTC 2798, 1977.

13. KIRK C L and JAIN, R K, 'The Dynamic Response of Double Articulated Offshore Loading Structure to Non-colinear Waves and Current', Applied Mechanical Engineers Conf, Yale University, 1977.

14. KIRK, C L, 'Dynamic Response of Articulated Platforms in Random Seas', Paper C1, International Conference on Flow Induced Vibrations in Fluid Engineering, Reading, England, Sep, 1982.

15. CHAKRABARTI, K S, 'Transverse Motion of an Articulated Tower', Jour of Waterway, Port, Coastal and Ocean Division, Feb, 1980.

16. EATOCK-TAYLOR, R, DRAKE, K R and DUNCAN, P E, 'The Dynamics of a Flexible Articulated Column in Waves', Engineering Structures, Vol 5, July, 1983.

17. DRAKE, K R, EATOCK-TAYLOR, R and MATSUI, T, 'The Drift of an Articulated Column in Regular Waves', Departmental Report, Department of Mechanical Engineering, University College, London, Oct, 1982.

18. BISHOP, R E D and PRICE, W G, 'On the Relationship between 'Dry Modes' and 'Wet Modes' in the Theory of Ship Response' Jour Sound Vibration, Vol 45, 1976.

19. PORANSKI, P F, 'The First Yoke Mooring for a VLCC in the Open Ocean', OTC 3564, 1979.

20. EYKHOUT, F, 'An Integrated Floating Production Storage and Offloading System-SALS in 380ft Water Depth', OTC 3142, 1978.

21. O'NEIL, D A, 'A Unique Approach to the Offshore Gas Disposal Problem: Castellon 'SALS' Production Facilities', OTC 3447, 1979.

22. EATOCK-TAYLOR, R and TUNG, S M, 'Mean Drift Forces on an Articulated Column in a Wave Tank', Proc, Royal Society, London, A394, 1984.

23. BURY, M R C, WALSH, S R and WARREN, J G, 'Model Investigation of an Articulated Column Structure', Offshore Structures, The Use of Physical Models in Their Design, edited by ARMER, G S T and GARAS, F K, Lancaster Construction Press,1981

24. SNOWDEN, J G, WARREN, J G and BURY, M R C, 'The Development of Hydrodynamic Analysis for Articulated Column-based Floating Production Systems', Behaviour of Offshore Structures, pp545-551, 1985.

25. NAESS, ARVID, 'Loads and Motions of an Articulated Loading Platform with Moored Tanker', OTC 3841, 1980.

26. DUMAZY, CHRISTIAN and LETURQ, MITHEL, 'Behaviour of a Floating Vessel/Articulated Column System', OTC 4547, 1983.

27. SCHELLIN, T E and KOCH, T, 'Calculated Dynamic Response of an Articulated Tower in Waves, Comparison with Model Tests', Germaniser Lloyd Report,Hamburg,Germany,1982

28. PINKSTER, J A, 'Low Frequency Phenomena Associated with Vessels Moored at Sea', Society of Petroleum Engineering of AIME, Paper No 4837, 1974.

29. DnV, 'Rules for the Design, Construction and Inspection of Offshore Structures, Oslo, 1977. Reprinted with corrections, 1981.

30. CARTER, J H T, 'Evolutionary Developments Advancing the Floating Production, Storage and Offloading Concepts', OTC 4273, 1982.

31. BURNS, G E, 'Buoyant Towers for Phase I Development of Garoupe Field', OTC 2828, 1977.

32. HOGBEN, N, 'Fluid Loading of Offshore Structures, a State of Art Appraisal: Wave Loads', RINA, 1974.

33. SARPKAYA, T and ISAACSON, M, 'Mechanics of Wave Forces on Offshore Structures', Van Nostrand Reinhold Conference, 1981.

34. MILLER, N S, 'Effects of Geometry and Dimensions on Natural Heaving Period in Semi-submersibles and Tethered Buoyant Platforms - Some Design Considerations', Lecture notes for a course held at the Department of Naval Architecture and Ocean Engineering, University of Glasgow, 26-30 Sep, 1977.

35. WADE, B G and DWYER, M, 'On the Application of Morison's Equation to Fixed Offshore Platforms', OTC 2723, 1976.

36. BORGMAN, L E, 'Computation of the Ocean Wave Forces on Inclined Cylinders', Jour of Geophysics, Res, Trans Amer, Geophysical Union, Vol 37, pp885-888, 1958.

37. CHAKRABARTI, S K, et al, 'Wave Forces on a Randomly Orientated Tube', OTC 2190, 1975.

38. SARPKAYA, T, et al, 'Hydrodynamic Interference of Two Cylinders in Harmonic Flow, OTC 3775, 1980.

39. HSU, F H and BLENKARN, K A, 'Analysis of Peak Mooring Forces Caused by Slow Vessel Drift Oscillations in Random Seas', OTC 1159, 1970.

40. REMERY, G F M and HERMANS, A J, 'The Slow Drift Oscillations of Moored Objects in Random Seas', OTC 1500, 1971.

41. PINKSTER, J A, 'Low Frequency Second Order Wave Exciting Force on Floating Structures', Netherlands Ship Model Basin, Report No 650, 1980.

42. STANDING, R G, DACUNHA, N M C and MATTERN, R B, 'Mean Wave Drift Forces: Theory and experiment', NMI Report, R124 OT-R-8175, 1981.

43. KIRK, C L and ETOK, E U, 'Dynamic Response of Tethered Production Platform in a Random Sea State', BOSS, Paper No 57, 1979.

44. TUNG, C C and HUANG, N E, 'Interactions between Waves and Currents and Their Influence on Fluid Forces', BOSS, Vol 1, pp129-143, Trondheim, 1976.

45. DnV, 'Rules for the Design, Construction and Inspection of Offshore Structures', Appendix A - Environmental conditions, 1977. Reprinted with corrections, 1979.

46. RULE CASE COMMITTEE(b), 'A short Description of the Basic Loading Problem', Paper No 05/RVH, 4 June, 1982 ABS,New York

47. VALIDAKIS, J, et al, 'Computer Program and Background Study of Wave Spectra', Department of Naval Architecture and Ocean Engineering, University of Glasgow, Report No NAOE-84-56, 1984.

48. McGREGOR, R C, FAULKNER, D and MILLER, N S, 'Towards an Improved Definition of Offshore Environmental Loading for Platform Design', Oceanography,1984

49. BRITISH STANDARD INSTITUTION, 'Code of Basic Data for the Design of Buildings',Part Two - Wind Loads , Cp3:Chapter V:Part 2:1972

50. HUSLID, J M and GUDMESTAD, O T, et al, 'Alternative Deep Water Concepts for Northern North Sea Extreme Conditions', BOSS, 1982.

51. DnV, 'Rules for Classification of Mobile Offshore Units', Rule proposal RP-SD-16-82 Rev 5, Aug, 1983.

52. BRITISH SHIP RESEARCH ASSOCIATION, 'A Critical Evaluation of the Data on Wave Force Coefficients', BSRA contract Report No W.278, 1976.

53. HOGBEN, N and MILLER, B L, et al, 'Estimation of Fluid Loading on Offshore Structures', NMI Report No R11,OT-R-7614, 1977.

54. LLOYD'S REGISTER OF SHIPPING, 'Rules for Construction and Classification of Mobile Offshore Units', 1972.

55. DnV, 'Rules for the Design, Construction and Inspection of Offshore Structures', Appendix B, 1977.

56. BUREAU VERITAS, 'Rules and Regulations for the Construction and Classification of Offshore Platforms', 1975.

57. SHAW, T, 'Mechanics of Wave-Induced Forces on Cylinders', Symp on the Mechanics of Wave-Induced Forces on Cylinders, Fearon Pitman Publishers Inc.,1979

58. DET NORSKE VERITAS, 'Rules for the Design, Construction andInspection of Offshore Structures', Appendix C - Steel Structures, 1977. Reprinted with corrections, 1981.

59. NELDER, J A and MEAD, R, 'Simplex Minimisation', Computer Jour, Vol 7, 1964.

60. NAG FILE: E04CCF, NAG FORTRAN Library Routine Document, Mark II, Vol 3, University Computing Services, University of Glasgow.

61. PAVIANA, D and HILMMELBLAU, D M, 'Constrained Nonlinear Optimisation by Heuristic Programming', Optimisation Res, Vol 17, 1969.

62. OCEAN INDUSTRY, Sep, 1982, May, 1983 and Sep, 1983.

63. BS5500, 'Unfired Fusion Welded Pressure Vessels', Issue No 2, Section 3, Jan, 1982.

64. RULES CASE COMMITTEE (CONOCO/ABS Rule Case Committee), 'Model Code for Structural Design of Tension Leg Platforms (Draft), Nov, 1983. ABS, New York

65. DAS, P K and FRIEZE, P A, 'Weight Optimisation of Ring and Orthogonally Stiffened Cylinders, Preliminary Report', Report No NAOE-82-07, Department of Naval Architecture and Ocean Engineering, University of Glasgow, 1982.

66. BAZLUR, RAHMAN, 'A computer Program for the Structural Design of Circular Caissan, Circular Column Type Semi-submersibles', Final Year Project 1982-83, Department of Naval Architecture and Ocean Engineering, University of Glasgow, 1983.

67. WILDE, D J, 'Optimum Seeking Method', Prentice-Hill Inc, Englewood Cliffs, New Jersey, 1962.

68. FORTRAN, Mark II, Vol 4, F02AEF, Computer Services, University of Glasgow.

69. CLOUGH, K W, 'Dynamics of Structures', McGraw-Hill, 1975.

70. CHAKRABARTI, S K, 'Steady Drift Force on Vertical Cylinder-Viscous versus Potential', Applied Ocean Research, No 2, Vol 6, pp73-82, 1984.

71. EATOCK-TAYLOR, R and DRAKE, K R, 'Design Considerations of Articulated Columns', Offshore Engineering Group, International Symp on Development in Floating Production Systems, RINA, Mar, 1984.

72. DALLY, J W and RILEY, W F, 'Experimental Stress Analysis', 2nd Edition, McGraw-Hill Kogakusha Ltd, Date unknown.

73. McDOWALL, E J, 'A Study on the Problems of Wave Generation in a Tank', Final Year Project, Department of Naval Architecture and Ocean Engineering, University of Glasgow, 1979/1980.

74. BATHE, J K and WILSON, E L, 'Numerical Methods in Finite Element Analysis', Prentice-Hill Ico, 1976.

75. NAGF ROUTINE, 'Routine D02BBF, Vol 2, Computer Centre, University of Glasgow.

76. RAINEY, R C T, 'The Dynamics of Tethered Platforms', Trans. RINA, pp58-80, 1979

77. ABRAMOWITZ, M and STEGUN, I A, 'Handbook of Mathematical Functions', National Bureau of Standards, Washington DC, 1964.

78. BRITISH STANDARDS INSTITUTION, Paper No DD32, 1974.

79. DnV RULES, 'Classification Notes, Strength Analysis of Main Structures of Self Elevating Units', Note No 31, DnV, Norway, 1984.

80. INCECIK, A, 'Design Aspects of the Hydrodynamic and Structural Loading on Floating Offshore Platforms under Wave Excitation', Thesis supmitted for the degree of doctor of philosophy in the Department of Naval Architecture and Ocean Engineering, University of Glasgow, 1982.

81. LIEHNARD, J H, 'Synopsis of Lift, Drag and Vortex Frequency Data for Rigid Circular Cylinders', Bulletin 300, College of Engineering Research Division, Washington State University., 1966.

82. Blagoveshchensky, S N , 'Theory of Ship Motion' ,Dover ,1962